2023 COASTAL MASTER PLAN

HABITAT SUITABILITY INDEX MODEL IMPROVEMENTS

ATTACHMENT D5

REPORT: VERSION 03
DATE: NOVEMBER 2022
PREPARED BY: DAVID C. LINDQUIST, SHAYE E. SABLE, LAURA D'ACUNTO, ANN C. HIJUELOS, ERIK I. JOHNSON, SUMMER R. M. LANGLOIS, NICOLE L. MICHEL, LINDSAY NAKASHIMA, ANN M. O'CONNELL, KATIE PERCY & ELIZABETH M. ROBINSON

COASTAL PROTECTION AND
RESTORATION AUTHORITY
150 TERRACE AVENUE
BATON ROUGE, LA 70802
WWW.COASTAL.LA.GOV

COASTAL PROTECTION AND RESTORATION AUTHORITY

This document was developed in support of the 2023 Coastal Master Plan being prepared by the Coastal Protection and Restoration Authority (CPRA). CPRA was established by the Louisiana Legislature in response to Hurricanes Katrina and Rita through Act 8 of the First Extraordinary Session of 2005. Act 8 of the First Extraordinary Session of 2005 expanded the membership, duties, and responsibilities of CPRA and charged the new authority to develop and implement a comprehensive coastal protection plan, consisting of a master plan (revised every six years) and annual plans. CPRA's mandate is to develop, implement, and enforce a comprehensive coastal protection and restoration master plan.

CITATION

Lindquist, D. C., Sable, S. E., D'Acunto, L., Hijuelos, A. C., Johnson, E. I., Langlois, S. R. M., Michel, N. L., Nakashima, L., O'Connell, A. M., Percy, K., & Robinson, E. M. (2022). 2023 Coastal Master Plan: Attachment D5: Habitat Suitability Index Model Improvements. Version 3. (p. 194). Baton Rouge, Louisiana: Coastal Protection and Restoration Authority.

ACKNOWLEDGEMENTS

This document was developed as part of a broader Model Improvement Plan in support of the 2023 Coastal Master Plan under the guidance of the Modeling Decision Team:

- Coastal Protection and Restoration Authority (CPRA) of Louisiana – Elizabeth Jarrell (formerly CPRA), Stuart Brown, Ashley Cobb, Catherine Fitzpatrick (formerly CPRA), Krista Jankowski, David Lindquist, Sam Martin, and Eric White
- University of New Orleans – Denise Reed

The following experts were responsible for the preparation of this document:

- David C. Lindquist – CPRA
- Shaye E. Sable – Dynamic Solutions, LLC
- Laura D'Acunto – United States Geological Survey (USGS), Wetland and Aquatic Research Center
- Ann C. Hijuelos – USGS, Wetland and Aquatic Research Center
- Erik I. Johnson – Audubon Louisiana
- Summer R. M. Langlois – CPRA
- Nicole L. Michel – Audubon Louisiana
- Lindsay Nakashima – Audubon Louisiana
- Ann M. O'Connell – University of New Orleans
- Katie Percy – Audubon Louisiana
- Elizabeth M. Robinson – Louisiana State University (LSU) AgCenter

The authors would like to thank the following for their assistance in this effort:

- The Louisiana Department of Wildlife and Fisheries (LDWF), specifically the Office of Fisheries and the Wildlife Diversity Program, for providing data used in the development of the models.
- Brady Carter (LDWF), Robert Dobbs (LDWF), Wim Kimmerer (San Francisco State University), Megan La Peyre (USGS, Louisiana Fish and Wildlife Cooperative Research Unit), Claire Lay (Abt Associates), Paul Leberg (University of Louisiana at Lafayette), Nicole Lorenz (LDWF), Tom Minello (National Marine Fisheries Service), Robert Romaire (LSU AgCenter), Michael Seymour (LDWF), Nick Smith (Ducks Unlimited), Tom Soniat (University of New Orleans), Philip Stouffer (LSU AgCenter), Sabrina Taylor (LSU AgCenter), Hardin Waddle (USGS, Wetland and Aquatic Research Center), and Stefan Woltmann (Austin Peay State University) for providing valuable input throughout the model improvement and development process.

Any use of trade, firm, or product names is for descriptive purposes only and does not imply endorsement by the U.S. Government. The term recommendation used within this report refers to suggestions and options for improving habitat suitability models based on best available science and peer-reviewed literature. The term is not used to imply management or policy changes.

EXECUTIVE SUMMARY

Habitat suitability index (HSI) models were developed for the 2023 Coastal Master Plan to evaluate the potential effects of coastal restoration and protection projects on habitat for key coastal fish, shellfish, and wildlife species. These species included: eastern oyster, brown shrimp, white shrimp, blue crab, crayfish, gulf menhaden, spotted seatrout, largemouth bass, American alligator, gadwall, mottled duck, brown pelican, seaside sparrow, and bald eagle. Most of these species were included in the 2017 Coastal Master Plan analyses, and the HSI models from that effort were refined and improved following the recommendations described in the technical memorandum: *2023 Coastal Master Plan Habitat Suitability Index Model Improvement Recommendations* (Sable et al., 2019). In addition to model improvements, HSI models were created for seaside sparrow and bald eagle, both of which are new species for the master plan analyses.

For the HSI models that are primarily literature-based, literature reviews were conducted for recent studies that could be used to improve the suitability index (SI) relationships that compose the models. As a result of this review, modifications were made to the salinity-related SIs of the oyster model including: expanding the time period used for salinity effects to spawning; adjusting the range of suitable annual average salinity to be more representative of Louisiana populations; and making oyster's minimum salinity tolerance temperature dependent. In addition, a new SI was incorporated in the oyster HSI model that accounts for the effects of sediment deposition on oysters. The crayfish HSI model was improved by adjusting the time periods used for the SIs that describe the hydrology required for the crayfish life cycle, and the soil characteristics SI that was part of the 2017 crayfish model was removed because soil conditions do not appear to be limiting for crayfish burrow construction in coastal Louisiana. The other literature-based HSI models from the 2017 Coastal Master Plan, i.e., American alligator, gadwall, mottled duck, and brown pelican, were unchanged, with the exception of a small adjustment made to the suitability of forested wetlands for gadwall. Lastly, a literature-based HSI model was created for seaside sparrow that consists of SIs related to vegetated habitat type, marsh vegetation coverage, and marsh elevation.

Statistical-based HSI models were developed for brown shrimp (both small and large juvenile stages), white shrimp (small and large juvenile stages), blue crab (juvenile stage), gulf menhaden (juvenile and adult stages), spotted seatrout (juvenile and adult stages), largemouth bass, and bald eagle. The bald eagle HSI model was developed from a bald eagle nest probability of occurrence model that related nest occurrence from survey data with land cover type. The resulting model showed that combinations of forested wetlands, flotant marsh, and open water habitats were most suitable for nesting bald eagles. The 2023 fish, shrimp, and blue crab HSI models were developed using new approaches for the formulation of the water quality and structural habitat SIs that compose the models. For the 2017 models, the water quality SI was derived using only generalized linear mixed models (GLMMs) to

estimate the relationship between salinity, water temperature, and species' catch. For the 2023 models, however, multiple GLMMs and generalized additive models (GAMMs) were created for each species or life stage. These alternative models were compared and a single model that performed well statistically and was ecologically reasonable was selected for the species' water quality SI. The structural habitat SI was developed using a meta-analysis of published literature to estimate the relative importance of various estuarine habitats to the fish and shellfish species. The results of this analysis were then used to modify the 2017 structural habitat SI relationship to account for the added habitat value of submerged aquatic vegetation and oyster reefs, which are also important habitats for juvenile fish and shellfish. Similar to the 2017 fish, shrimp, and blue crab models, the water quality and structural habitat SIs were then combined to create the 2023 HSI models.

The 2023 Coastal Master Plan HSI models were integrated with the Integrated Compartment Model (and are referred to as ICM-HSIs) and tested using environmental output from the 2017 Coastal Master Plan future without action scenario. The tests showed that, in general, the models produced reasonable representations of species' habitat distribution. Furthermore, the improvements made to the oyster, crayfish, fish, shrimp, and blue crab HSI models generally yielded more realistic results compared to the 2017 HSI models.

TABLE OF CONTENTS

LIST OF TABLES

LIST OF FIGURES

LIST OF ABBREVIATIONS

CPRA ..... COASTAL PROTECTION AND RESTORATION AUTHORITY
CPUE ..... CATCH PER UNIT EFFORT
GAMM ..... GENERALIZED ADDITIVE MIXED MODEL
GLMM ..... GENERALIZED LINEAR MIXED MODEL
HSI ..... HABITAT SUITABILITY INDEX
ICM ..... INTEGRATED COMPARTMENT MODEL
LDWF ..... LOUISIANA DEPARTMENT OF WILDLIFE AND FISHERIES
PPT ..... PARTS PER THOUSAND
SAV ..... SUBMERGED AQUATIC VEGETATION
SI ..... SUITABILITY INDEX
TL ..... TOTAL LENGTH
USFWS ..... UNITED STATES FISH AND WILDLIFE SERVICE
USGS ..... UNITED STATES GEOLOGICAL SURVEY

1.0 INTRODUCTION

Habitat suitability index (HSI) modeling has a long history in water resource and restoration planning for predicting the effects of management actions on fish and wildlife habitat (United States Fish and Wildlife Service [USFWS], 1981). HSI models consist of functions, called suitability indices (SI), that relate key environmental variables to the quality or suitability of a habitat for a species. These SIs are developed using species life history information along with presence-absence or relative abundance data collected over a range of environmental conditions. The indices are standardized to a 0 to 1 scale (with 1 representing the most suitable condition), and then combined to produce an HSI score that represents the capacity of a habitat to support a species. Although HSI models are often criticized because they only quantify habitat conditions, which may not directly correlate to species abundance (Weber et al., 2016), they remain a practical and tractable way to assess changes in habitat quality for species.

Habitat suitability index models have been used in Louisiana's Coastal Master Plan modeling efforts to evaluate the potential effects of coastal restoration and protection projects on habitat for key coastal fish, shellfish, and wildlife species. For the 2012 Coastal Master Plan, the HSI models consisted of SIs developed using published literature and best professional judgement of species-habitat relationships (Nyman et al., 2013). For the 2017 Coastal Master Plan, suggested improvements to the HSI models included using statistical analyses of empirical datasets to estimate the species-habitat relationships (Rose & Sable, 2013). Such an approach would allow for more defensible and rigorous HSI functions to be developed. Consequently, the brown shrimp, white shrimp, blue crab, gulf menhaden, bay anchovy, spotted seatrout, and largemouth bass HSI models included water quality SIs that statistically relate species catch-per-unit-effort (CPUE) data with corresponding salinity and water temperature measurements collected by the Louisiana Department of Wildlife and Fisheries (LDWF). This water quality SI was then combined with a literature-based structural habitat SI, and in some cases a chlorophyll a SI, to form the HSI model for each fish, shrimp, and crab species. Other species' 2017 HSI models continued to be literature based because of the lack of suitable datasets from which statistical relationships could be derived. These models were improved and refined by incorporating new ecological knowledge from the literature. The improved 2017 HSI models were then integrated with the 2017 Coastal Master Plan's Integrated Compartment Model (ICM), and thus are a subroutine of the larger model called ICM-HSI (but hereafter referred to as just HSI). The ICM-HSI uses output from the other ICM subroutines and calculates an annual suitability score for each 500 m x 500 m vegetation subroutine grid cell (note: a 480 m x 480 m grid cell size will be used for HSI calculations in the 2023 Coastal Master Plan). A complete description of the 2017 models can be found in the 2017 Coastal Master Plan appendices, Attachments C3-6 to C3-19, located at: https://coastal.la.gov/our-plan/2017-coastal-master-plan/.

Recommendations for HSI model improvement were solicited following the 2017 Coastal Master Plan, and further investigated in the technical memorandum: 2023 Coastal Master Plan Habitat Suitability Index Model Improvement Recommendations (Sable et al., 2019). The final recommendations from that effort included continuing the improvement and refinement of the literature-based HSI models by incorporating new ecological knowledge from recent literature. For the fish, shrimp, and blue crab HSI models, a meta-analysis approach was proposed that would improve the structural habitat SI by using empirical data from published studies to estimate the relative importance of aquatic habitats to each species. In addition, a new modeling approach was recommended for selecting the best and most appropriate statistical models to use for the 2023 water quality SIs. Methods to detect and resolve statistical issues and improve model fit were also proposed for the water quality SI analyses. The recommendations also included an updated list of species to be included in the master plan analyses (Table 1). The species selected cover a range of taxonomic groups, life histories, trophic levels, and habitats, and include two new species, seaside sparrow and bald eagle.

The purpose of this report is to document the methods used to refine, improve, and develop the HSI models for the 2023 Coastal Master Plan, following the recommendations detailed in Sable et al. (2019). The HSI models are categorized herein as those that are primarily literature-based, including eastern oyster, crayfish, American alligator, gadwall, mottled duck, brown pelican, and seaside sparrow, and those that are primarily statistical-based, including brown shrimp, white shrimp, blue crab, gulf menhaden, spotted seatrout, largemouth bass, and bald eagle. For the pre-existing literature-based HSI models, this report focuses on changes made to the previous version of the models and the rationale for the changes. For the other HSI models, i.e., seaside sparrow, bald eagle, and the fishes, shrimps, and blue crab, the methods used in model development are summarized in the main body of this report with further detail provided as attachments. The full HSI model for all species except gulf menhaden, spotted seatrout, and blue crab are presented here, and all models are available at: https://github.com/CPRA-MP/.

Table 1. Species included in the 2023 Coastal Master Plan HSI analyses, their ecological or economic significance, and the source of the HSI model used for the model improvement effort. x = separate HSI models for the small and large juvenile life stages were developed. y = separate HSI models for juvenile and adult life stages were developed.

SPECIES	SPECIES SIGNIFICANCE	MODEL SOURCE
EASTERN OYSTER (*CRASSOSTREA VIRGINICA*)	• ESTUARINE, SEDENTARY, PLANKTIVOROUS MOLLUSK • PROVIDES VALUABLE ECOSYSTEM SERVICES • SUPPORTS IMPORTANT COMMERCIAL FISHERIES	2012 COASTAL MASTER PLAN

SPECIES	SPECIES SIGNIFICANCE	MODEL SOURCE
BROWN SHRIMP [X] (*FARFANTEPENAEUS AZTECUS*)	• BENTHIC CRUSTACEAN THAT USES ESTUARIES AS JUVENILE NURSERY HABITAT • SUPPORTS IMPORTANT COMMERCIAL FISHERIES	2017 COASTAL MASTER PLAN
WHITE SHRIMP [X] (*LITOPENAEUS SETIFERUS*)	• BENTHIC CRUSTACEAN THAT USES ESTUARIES AS JUVENILE NURSERY HABITAT • SUPPORTS IMPORTANT COMMERCIAL FISHERIES	2017 COASTAL MASTER PLAN
BLUE CRAB (*CALLINECTES SAPIDUS*)	• BENTHIC CRUSTACEAN FOUND IN ESTUARINE HABITATS THROUGHOUT MOST OF ITS LIFE CYCLE • SUPPORTS IMPORTANT COMMERCIAL FISHERIES	2017 COASTAL MASTER PLAN
CRAYFISH (*PROCAMBARUS CLARKII* AND *P. ZONANGULUS*)	• BENTHIC CRUSTACEAN PRIMARILY ASSOCIATED WITH FRESHWATER HABITATS • SUPPORTS IMPORTANT COMMERCIAL FISHERIES	2017 COASTAL MASTER PLAN
GULF MENHADEN [Y] (*BREVOORTIA PATRONUS*)	• PLANKTIVOROUS FISH THAT USES ESTUARIES AS JUVENILE NURSERY HABITAT • SUPPORTS IMPORTANT COMMERCIAL FISHERIES	2017 COASTAL MASTER PLAN
SPOTTED SEATROUT [Y] (*CYNOSCION NEBULOSUS*)	• PREDATORY FISH FOUND IN ESTUARINE HABITATS THROUGHOUT MOST OF ITS LIFE CYCLE • POPULAR RECREATIONAL FISHERY SPECIES	2017 COASTAL MASTER PLAN
LARGEMOUTH BASS (*MICROPTERUS SALMOIDES*)	• PREDATORY FISH PRIMARILY ASSOCIATED WITH FRESHWATER HABITATS • POPULAR RECREATIONAL FISHERY SPECIES	2017 COASTAL MASTER PLAN
AMERICAN ALLIGATOR (*ALLIGATOR MISSISSIPPIENSIS*)	• UPPER TROPHIC LEVEL REPTILE PRIMARILY ASSOCIATED WITH FRESHWATER HABITATS • COMMERCIALLY-HARVESTED SPECIES	2017 COASTAL MASTER PLAN
GADWALL (*ANAS STREPERA*)	• MIGRATORY WATERFOWL THAT USES ESTUARIES AS WINTERING HABITAT • POPULAR RECREATIONALLY-HUNTED SPECIES	2017 COASTAL MASTER PLAN
MOTTLED DUCK (*ANAS FULVIGULA*)	• WATERFOWL THAT IS YEAR-ROUND RESIDENT OF ESTUARIES • STATE-IDENTIFIED SPECIES OF CONSERVATION NEED	2017 COASTAL MASTER PLAN

SPECIES	SPECIES SIGNIFICANCE	MODEL SOURCE
BROWN PELICAN (*PELECANUS OCCIDENTALIS*)	• UPPER TROPHIC LEVEL COASTAL SEABIRD THAT NESTS PRIMARILY ON COASTAL ISLANDS • STATE-IDENTIFIED SPECIES OF CONSERVATION NEED	2017 COASTAL MASTER PLAN
SEASIDE SPARROW (*AMMOSPIZA MARITIMA FISHERI*)	• YEAR-ROUND RESIDENT OF VEGETATED MARSH HABITATS • STATE-IDENTIFIED SPECIES OF CONSERVATION NEED	NEW MODEL
BALD EAGLE (*HALIAEETUS L. LEUCOCEPHALUS*)	• UPPER TROPHIC LEVEL RAPTOR THAT NESTS PRIMARILY IN WOODED, FRESHWATER HABITATS • STATE-IDENTIFIED SPECIES OF CONSERVATION NEED	NEW MODEL

2.0 LITERATURE-BASED MODELS

The literature-based HSI models for the 2023 Coastal Master Plan include those for eastern oyster, crayfish, American alligator, gadwall, mottled duck, brown pelican, and seaside sparrow. Except for seaside sparrow, HSI models for these species were also included in the 2017 Coastal Master Plan. To improve the 2017 models, literature reviews were conducted for recent research on these species that could be used to refine the existing SIs or develop new SIs. The review particularly focused on locating research pertaining to the areas of potential model improvement identified by the 2017 HSI model developers. The model developers, and other subject matter experts, were consulted to provide guidance on relevant research and input on possible model changes.

2.1 EASTERN OYSTER

The existing eastern oyster HSI model had not been updated since its development for the 2012 Coastal Master Plan (Soniat, 2012; Master Plan Appendix D13 located at: https://coastal.la.gov/our-plan/2012-coastal-masterplan/cmp-appendices/). Since then, much research has been conducted on the effects of environmental variables, such as salinity and water temperature, on oyster populations. This research was used to modify the three salinity-based SIs in the oyster HSI model. In the previous model, the "mean salinity during the spawning season" SI defined the spawning season as May through September (Soniat, 2012). This time period is considered too narrow and misses significant reproduction by oysters based on field data collected over the past decade (Casas et al., 2015). Furthermore, LDWF monitoring data show that spat recruitment remains high and actually peaks in November (Dr. Megan La Peyre, USGS, written communication, 4/17/2019). Consequently, for the 2023 oyster HSI model, the time period used for this SI was expanded to April through November. The suitability relationship used for the index, though, was unchanged.

The "minimum monthly salinity" SI, which takes into account the effects of freshwater inflow events on oysters, consisted of a single relationship covering the entire year in the previous model (Soniat, 2012). However, the tolerance of oysters to the inflow events is dependent on water temperature. Laboratory experiments and field studies have shown that oysters can survive several months in salinities less than 3 parts per thousand (ppt) at low water temperatures (<25°C), whereas during warmer periods low salinities negatively impact spawning, recruitment, growth, and survival (La Peyre et al., 2013; Rybovich et al., 2016; Lowe et al., 2017). Denapolis (2018) used two minimum salinity relationships in a modified HSI model to account for this temperature-salinity interaction, one for cool months (October through March) and one for warm months (April through September). These relationships were incorporated into the 2023 HSI model with slight modifications. The suitability at 5 ppt was increased in accordance with the aforementioned research showing oyster survivability at low

salinities. The range of optimal salinities was expanded to 8 to 10 ppt, rather than a peak at 8 ppt, because there are no data to support maximum survival at 8 ppt. Lastly, the suitability of salinities greater than 20 ppt was set to 0.001, rather than 0.0, because oysters can exist at these higher salinities, though survivability is low due to predation and disease.

The relationship used for the SI "mean annual salinity" was modified to better reflect conditions suitable for oysters in Louisiana. The previous relationship gave relatively high suitabilities to salinities above 20 ppt (Soniat, 2012). This may reflect suitable conditions for oysters elsewhere in the Gulf of Mexico or along the Atlantic Coast but does not accurately reflect conditions in Louisiana estuaries, where high rates of mortality from predation and disease occur at salinities greater than 15-20 ppt (Lowe et al., 2017). Therefore, suitabilities were reduced at mean annual salinities greater than 15 ppt, and suitability was set to 0.001 at salinities above 25 ppt.

In addition to the modifications to existing SIs, several new SIs were considered for inclusion in the 2023 oyster HSI model. A suitability index for water temperature was explored because 32˚C is considered a threshold for oyster feeding and mortality (La Peyre et al., 2013; Rybovich et al., 2016). However, this was determined to be unnecessary because water temperatures greater than 32°C do not occur often, and the "minimum monthly salinity" relationships implicitly account for some of the mechanisms that affect oysters at summer temperatures. Suitability indices for dissolved oxygen and bottom type were also considered but not included because the ICM does not provide suitable output for these parameters. An SI describing the effects of sediment deposition on oysters is included in the 2023 HSI model, because high levels of sediment deposition over time (>40-60 mm per year) can interfere with metabolic processes, bury oyster beds, and result in oyster mortality (Colden & Lipcius, 2015). This new SI is appropriate for larger oyster life stages (i.e., seed and sack-sized oysters). Oyster spat, by comparison, are less tolerant of sedimentation, particularly during settlement (Thomsen & McGlatthery, 2006), but there was a lack of data with which to determine precise tolerance levels for spat. The 2023 oyster HSI model is used to calculate the annual habitat suitability score of each model cell for post-settlement life stages of eastern oyster in coastal Louisiana. The model equation is: $HSI = (SI_1 \times SI_2 \times SI_3 \times SI_4 \times SI_5 \times SI_6)^{1/6}$.

SI_1 = Percent of cell covered by cultch (V_1). This SI remains in the model to allow for assessments of impacts to current oyster grounds. For the 2023 Coastal Master Plan analyses, SI_1 will be set to 1.0 to provide estimates of future oyster habitat suitability independent of current cultch conditions.

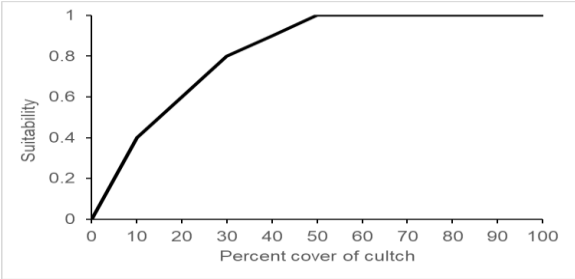

$SI_1 = 0.04*V_1$, when $V_1 \leq 10\%$
$(0.02*V_1) + 0.2$, when $10 < V_1 \leq 30$
$(0.01*V_1) + 0.5$, when $30 < V_1 \leq 50$
1.0, when $V_1 > 50$

Figure 1. Suitability relationship for oyster SI_1, percent cultch.

SI_2 = Mean salinity during the spawning season, April through November (V_2):

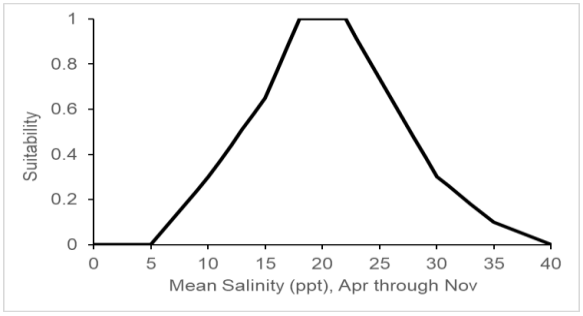

$SI_2 = 0.0$, when $V_2 < 5$ ppt
$(0.06*V_2) - 0.3$, when $5 \leq V_2 < 10$
$(0.07*V_2) - 0.4$, when $10 \leq V_2 < 15$
$(0.1167*V_2) - 1.1$, when $15 \leq V_2 < 18$
1.0, when $18 \leq V_2 < 22$
$(-0.0875*V_2) + 2.925$, when $22 \leq V_2 < 30$
$(-0.04*V_2) + 1.5$, when $30 \leq V_2 < 35$
$(-0.02*V_2) + 0.8$, when $35 \leq V_2 < 40$

Figure 2. Suitability relationship for oyster SI_2, mean salinity during spawning season.

SI_3 = Minimum monthly mean salinity (V_3). Two relationships are used: one for cool months, October through March, and one for warm months, April through September. The SI is derived by calculating the suitability of the lowest monthly mean salinity for each of the two time periods using the relationships described below; then the overall SI is calculated using the equation: $SI_3 = (SI_3 \text{ cool} \times SI_3 \text{ warm})^{1/2}$.

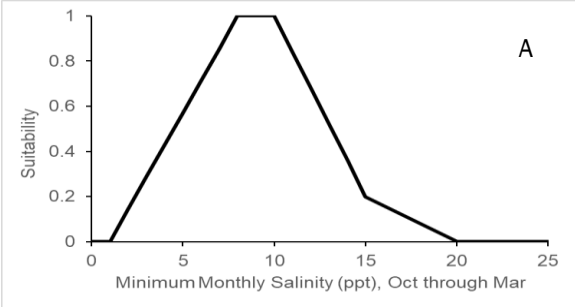

$SI_{3\ cool}$ = 0.0, when $V_3 \leq 1$ ppt
$(0.1429*V_3) - 0.1429$, when $1 < V_3 < 8$
1.0, when $8 \leq V_3 < 10$
$(-0.16*V_3) + 2.6$, when $10 \leq V_3 < 15$
$(-0.04*V_3) + 0.8$, when $15 \leq V_3 < 20$
0.001, when $V_3 \geq 20$

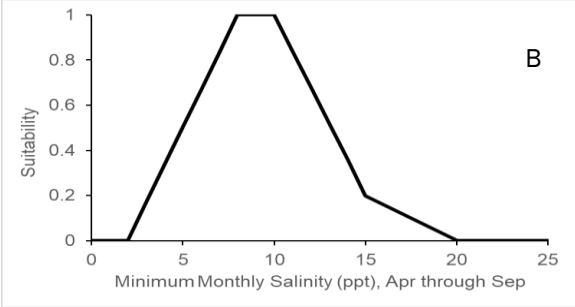

$SI_{3\ warm}$ = 0.0, when $V_3 \leq 2$ ppt
$(0.1668*V_3) - 0.33$, when $2 < V_3 < 8$
1.0, when $8 \leq V_3 < 10$
$(-0.16*V_3) + 2.6$, when $10 \leq V_3 < 15$
$(-0.04*V_3) + 0.8$, when $15 \leq V_3 < 20$
0.001, when $V_3 \geq 20$

Figure 3. Suitability relationship for oyster SI_3, minimum monthly salinity, for A) cool months and B) warm months.

SI_4 = Mean annual salinity (V_4):

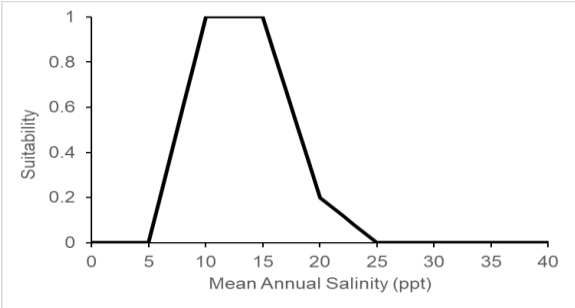

SI_4 = 0.0, when $V_4 < 5$ ppt
$(0.2*V_4) - 1.0$, when $5 \leq V_4 < 10$
1.0, when $10 \leq V_4 < 15$
$(-0.16*V_4) + 3.4$, when $15 \leq V_4 < 20$
$(-0.04*V_4) + 1.0$, when $20 \leq V_4 < 25$
0.001, when $V_3 \geq 25$

Figure 4. Suitability relationship for oyster SI_4, mean annual salinity.

SI_5 = Percent of cell covered by land (V_5). This SI is included to restrict the oyster HSI output to model cells that are primarily open water habitat (Soniat, 2012).

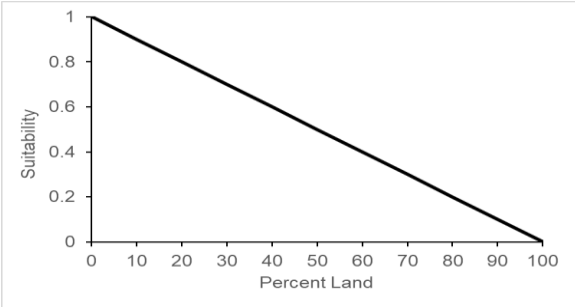

$SI_5 = (-0.01*V_5) + 1.0$

Figure 5. Suitability relationship for oyster SI_5, percent land.

SI_6 = Cumulative sediment deposition (V_6). The annual amount of sediment deposition for the open water parts of a cell is calculated by summing mean monthly sediment deposition, then the SI is derived using the suitability relationship described below.

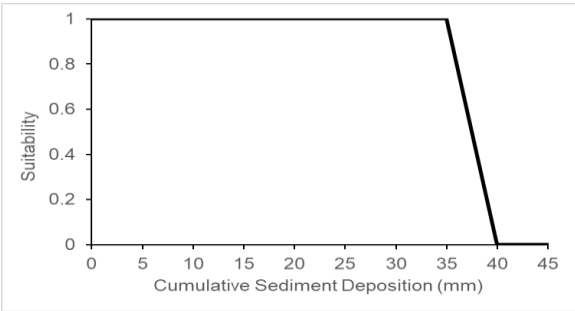

$SI_6 = 1.0$, when $V_6 < 35$ mm
$(-0.2*V_6) + 8.0$, when $35 \leq V_6 < 40$
0.0, when $V_6 \geq 40$

Figure 6. Suitability relationship for oyster SI_6, sediment deposition.

2.2 CRAYFISH

Recommended improvements to the 2017 crayfish HSI model included making adjustments to the time periods used for the two SIs that describe the hydrology required for the crayfish life cycle (Romaire, 2017). One SI described suitable water depths for the high-water season, which was defined as October through June; and the other described suitable water depths for the low-water season, which was defined as July through September. The time periods used for these seasons, however, did not accurately reflect the patterns of high and low waters observed in the 2017 ICM simulations. In particular, the July through September time period often coincided with peak water levels in many swamp areas and only captured the beginning of water level recession (Figure 7). Therefore, for the 2023 crayfish HSI model, the time period for the low-water season was changed to

September through December, and the time period for the high-water season was changed to January through August. These periods of wetland flooding and drying are generally consistent with that seen for the Atchafalaya Basin swamp, which supports large populations of crayfish (Hupp et al., 2008; Bonvillain, 2012).

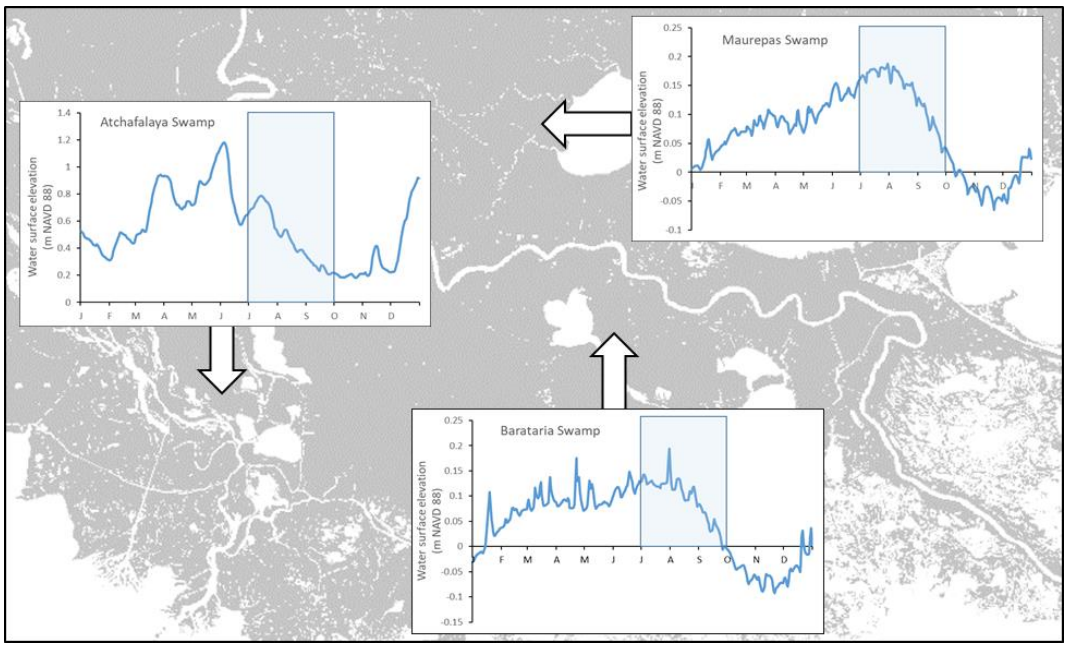

Figure 7. Daily water surface elevations for year 4 of the 2017 Coastal Master Plan ICM simulation for select swamp model compartments. The blue box indicates the time period used for the low-water season suitability index of the 2017 crayfish HSI model.

The 2017 crayfish HSI model also included a SI related to the soil characteristics required for crayfish burrow construction. This index, which was based on the percentage of sand in the soil, did not help differentiate crayfish habitat because sand content simulated by the ICM was almost always optimal. As an alternative, Romaire (2017) suggested an index based on the soil classification system used in the United States Department of Agriculture Soil Surveys published for each Louisiana parish. The soil classes for each coastal parish were evaluated for sand content and other possible unfavorable soil characteristics for crayfish burrowing, such as permeability or available water capacity (a measure of the soil's capacity to hold water). Soils with a high percentage of sand (>50% by weight), rapid permeability (>6.0 inches per hour), and low available water capacity (<0.10 inch per inch) were found on barrier islands, cheniers, fastlands, and in marshes near the Gulf. These areas are either outside the ICM domain or would not be considered suitable crayfish habitat due to high salinities or unfavorable hydrology (i.e. they do not flood regularly). Otherwise, it appears that the soils present in

Louisiana's coastal wetlands are highly suitable for crayfish burrow construction. Consequently, the 2023 crayfish HSI model does not include a soil SI.

Except for these changes, the 2023 crayfish HSI model is the same as the 2017 model (Romaire, 2017). The HSI model is comprised of three component indices that describe suitable water conditions (SI_1 and SI_2), vegetated habitat types (SI_3), and conditions needed for reproduction (SI_4). The model is used to calculate the annual habitat suitability score of each model cell for all life stages of crayfish. The model equation is: $HSI = (SI_1 \times SI_{2\ \text{Dec through Jul}})^{1/6} \times (SI_3)^{1/3} \times (SI_{4\ \text{Aug through Nov}})^{1/3}$.

SI_1 = Mean annual salinity (V_1):

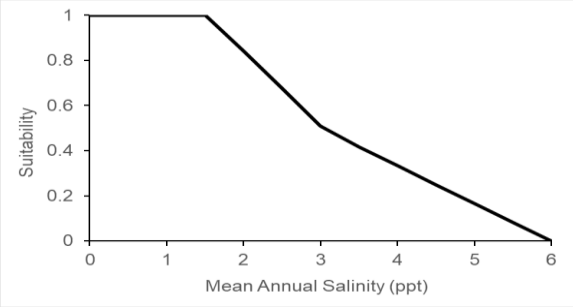

$SI_1 = 1$, when $V_1 \leq 1.5$ ppt
$1.5 - (0.333 * V_1)$, when $1.5 < V_1 \leq 3.0$
$1.0 - (0.167 * V_1)$, when $3.0 < V_1 \leq 6.0$
0.0, when $V_1 > 6.0$

Figure 8. Suitability relationship for crayfish SI_1, mean annual salinity.

SI_2 = Mean water depth from January through August (V_2):

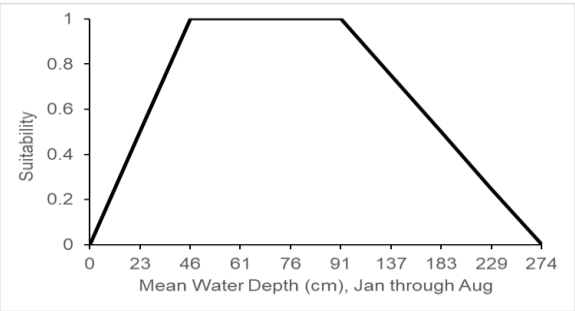

$SI_2 = 0.0$, when $V_2 \leq 0$ or > 274 cm
$0.02174 * V_2$, when $0 < V_2 \leq 46$
1.0, when $46 < V_2 \leq 91$
$1.5 - (0.00547 * V_2)$, when $91 < V_2 \leq 274$

Figure 9. Suitability relationship for crayfish SI_2, water depth January to August.

SI_3 = Proportion of cell covered by habitat types (V_3):

$SI_3 = [(1.0 \times V_{3a}) + (0.85 \times V_{3b}) + (0.75 \times V_{3c}) + (0.6 \times V_{3d}) + (0.2 \times V_{3e}) + (0.0 \times V_{3f}) + (0.0 \times V_{3g})]$
Where: V_{3a} = the proportion of a model cell that is swamp or bottomland hardwood

V_{3b} = the proportion of a model cell that is fresh marsh
V_{3c} = the proportion of a model cell that is open water
V_{3d} = the proportion of a model cell that is intermediate marsh
V_{3e} = the proportion of a model cell that is brackish marsh
V_{3f} = the proportion of a model cell that is saline marsh
V_{3g} = the proportion of a model cell that is bare ground

SI_4 = Mean water depth from September through December (V_4):

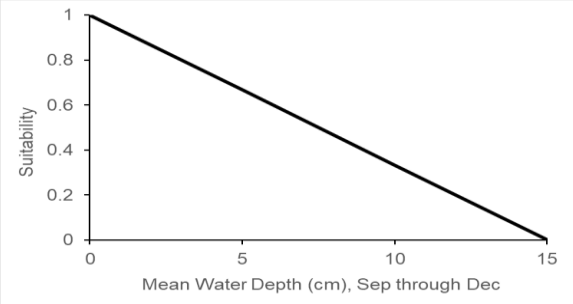

SI_4 = 0.0, when V_4 > 15 cm
1.0 – (0.06667*V_4), when $V_4 \leq 15$
1.0, when $V_4 \leq 0$

Figure 10. Suitability relationship for crayfish SI_4, water depth September to December.

2.3 AMERICAN ALLIGATOR

A review of recent research did not yield any new information that could be used to improve the 2017 alligator HSI model. Consideration was given to modifying the "Salinity" and "Habitat type" SIs by increasing suitability of saline habitats, based on a recent study by Nifong and Silliman (2017) that showed frequent utilization of such habitats in Georgia. However, the previous HSI model was developed to consider whether the entire alligator life cycle could be supported by a habitat; and although alligators may periodically utilize saline habitats, they usually have lower body condition and are unable to successfully reproduce in these habitats (Dr. Hardin Waddle, USGS, written communication, 2/18/2020). Therefore, the "Salinity" and "Habitat type" SIs were unchanged, and the 2023 alligator HSI model is the same as the 2017 model (Waddle, 2017). The model is used to calculate the annual habitat suitability score of a model cell for alligator in coastal Louisiana, and takes into account factors important for nesting, foraging, physiology, and predator avoidance. The model equation is: $HSI = (SI_1 \times SI_2 \times SI_3 \times SI_4 \times SI_5)^{1/5}$.

SI_1 = Percent of cell that is open water (V_1):

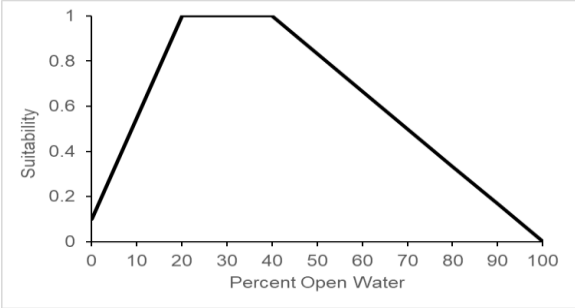

SI_1 = ((4.5*V_1)/100) + 0.1, when V_1 < 20%
1.0, when 20 ≤ V_1 ≤ 40
((-1.667*V_1/100) + 1.667, when V_1 > 40

Figure 11. Suitability relationship for alligator SI_1, percent open water.

SI_2 = Mean annual water depth relative to the marsh surface (V_2):

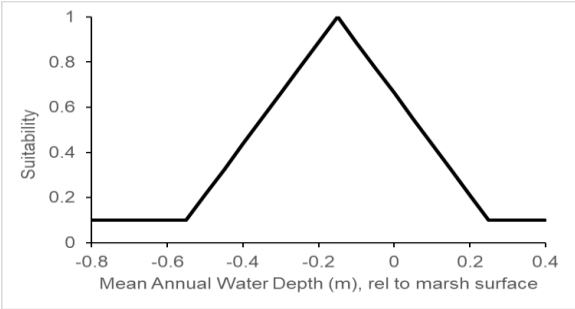

SI_2 = 0.1, when V_2 ≤ -0.55 or ≥ 0.25 m
(2.25*V_2) + 1.3375, when -0.55 < V_2 < -0.15
1.0, when V_2 = -0.15
(-2.25*V_2) + 0.6625, when -0.15 < V_2 < 0.25

Figure 12. Suitability relationship for alligator SI_2, water depth relative to marsh surface.

SI_3 = Proportion of cell covered by habitat types (V_3). Habitat types other than swamp, fresh marsh, intermediate marsh, and brackish marsh are given a suitability score of 0.0.

SI_3 = [(0.551 x V_{3a}) + (0.713 x V_{3b}) + (1.0 x V_{3c}) + (0.408 x V_{3d})]
Where: V_{3a} = the proportion of a model cell that is swamp forest
V_{3b} = the proportion of a model cell that is fresh marsh
V_{3c} = the proportion of a model cell that is intermediate marsh
V_{3d} = the proportion of a model cell that is brackish marsh

SI_4 = Edge (V_4). This SI is based on output produced from the ICM-Morphology subroutine, which scales estimated edge such that the median value has an SI value of 0.5 and values at the 90th

percentile and above have a value of 1.0.

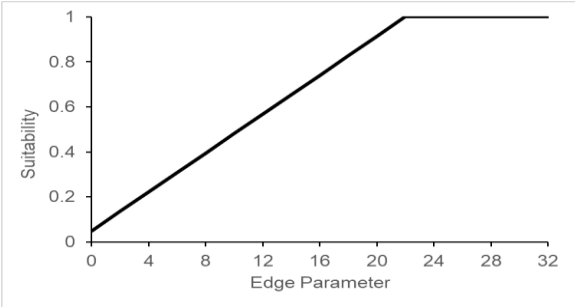

$SI_4 = 0.05 + (0.95*(V_4/22.0)$, when $0 \leq V_4 \leq 22$
1.0, when $V_4 > 22$

Figure 13. Suitability relationship for alligator SI_4, edge.

SI_5 = Mean annual salinity (V_5):

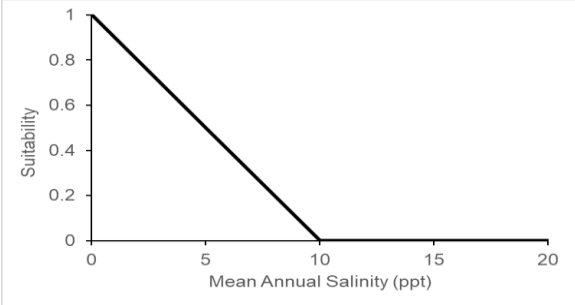

$SI_5 = (-0.1*V_5) + 1.0$, when $0 \leq V_5 \leq 10$ ppt
0.0, when $V_5 > 10$

Figure 14. Suitability relationship for alligator SI_5, mean annual salinity.

2.4 GADWALL

One of the recommended improvements to the 2017 gadwall HSI model was to incorporate more data and research on gadwall use of forested wetlands (Leberg, 2017a). Because of a lack of empirical data, the 2017 model assumed a suitability score of 0.25 for both swamp forests and bottomland hardwood forests. However, recent field surveys conducted by Hucks (2017) found that gadwall rarely used forested wetland habitats. Therefore, for the 2023 gadwall HSI model, the suitability score for swamp forests and bottomland hardwood forests in the "vegetative habitat type" SI was lowered from 0.25 to 0.05 based on the recommendation of the 2017 HSI model developer (Dr. Paul Leberg, University of Louisiana at Lafayette, oral communication, 3/2/2020). Otherwise, the 2023 gadwall HSI model is the same as the 2017 model (Leberg, 2017a). The model is used to calculate the annual habitat suitability score of a model cell for gadwall wintering in coastal Louisiana from October through

April. The model equation is: $HSI = (SI_1 \times SI_2 \times SI_3)^{1/3}$.

SI_1 = Proportion of cell covered by habitat types and associated open water (V_1). When there is no emergent vegetation in a cell, the cell should be assigned to one of following habitat types based on average annual salinity: fresh marsh <1.5 ppt; intermediate marsh ≥ 1.5 to < 4.5 ppt; brackish marsh ≥ 4.5 to < 9.5 ppt; and saline marsh ≥ 9.5 ppt.

$SI_1 = [(0.68 \times V_{1a}) + (1.0 \times V_{1b}) + (0.5 \times V_{1c}) + (0.09 \times V_{1d}) + (0.05 \times V_{1e}) + (0.0 \times V_{1f})]$

Where: V_{1a} = the proportion of a model cell that is fresh attached or fresh floating marsh

V_{1b} = the proportion of a model cell that is intermediate marsh

V_{1c} = the proportion of a model cell that is brackish marsh

V_{1d} = the proportion of a model cell that is saline marsh

V_{1e} = the proportion of a model cell that is swamp or bottomland hardwood

V_{1f} = the proportion of a model cell that is non-wetland habitat

SI_2 = Proportion of cell with submerged aquatic vegetation (SAV) (V_2):

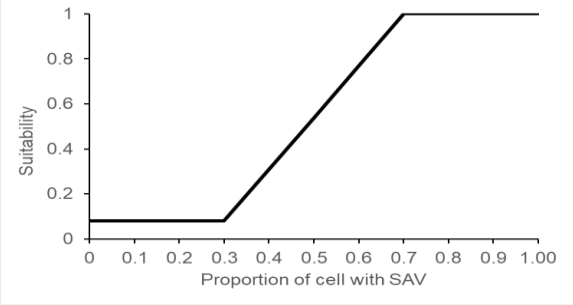

SI_2 = 0.08, when V_2 <0.30

(2.3*V_2) – 0.61, when 0.30 ≤ V_2 <0.70

1.0, when V_2 ≥0.70

Figure 15. Suitability relationship for gadwall SI_2, percent SAV.

SI_3 = Mean water depths from October through April (V_3). This SI is derived by calculating the mean water depth for each 30-meter pixel of a model cell, estimating the proportion of the model cell covered by each depth category, then plugging these estimates into the following equation:

$SI_3 = [(0.05*V_{3a}) + (0.15*V_{3b}) + (0.35*V_{3c}) + (0.60*V_{3d}) + (0.83*V_{3e}) + (1.0*V_{3f}) + (0.86*V_{3g}) + (0.61*V_{3h}) + (0.37*V_{3i}) + (0.20*V_{3j}) + (0.10*V_{3k}) + (0.05*V_{3l})]$

Where: V_{3a} = the proportion of cell with mean water depth ≤ 4 cm

V_{3b} = the proportion of cell with mean water depth >4 to ≤ 8

V_{3c} = the proportion of cell with mean water depth >8 to ≤ 12

V_{3d} = the proportion of cell with mean water depth >12 to ≤ 18

V_{3e} = the proportion of cell with mean water depth >18 to ≤ 22

V_{3f} = the proportion of cell with mean water depth >22 to ≤ 28
V_{3g} = the proportion of cell with mean water depth >28 to ≤ 32
V_{3h} = the proportion of cell with mean water depth >32 to ≤ 36
V_{3i} = the proportion of cell with mean water depth >36 to ≤ 40
V_{3j} = the proportion of cell with mean water depth >40 to ≤ 44
V_{3k} = the proportion of cell with mean water depth >44 to ≤ 78
V_{3l} = the proportion of cell with mean water depth >78 to ≤ 150

2.5 MOTTLED DUCK

A review of recent research and literature did not yield any information that could be used to improve or modify the 2017 mottled duck HSI model. Therefore, the 2023 mottled duck HSI model is the same as the 2017 model (Leberg, 2017b). The model is used to calculate the annual habitat suitability score of a model cell for post-fledgling juvenile and adult mottled duck in coastal Louisiana. Nesting habitat is not considered by the model because nesting occurs in non-wetland habitats that are not simulated by the ICM. The model equation is: $HSI = (SI_1 \times SI_2 \times SI_3 \times SI_4)^{1/4}$.

SI_1 = Proportion of cell covered by habitat types and associated open water (V_1). When there is no emergent vegetation in a cell, the cell should be assigned to one of following habitat types based on average annual salinity: fresh marsh <1.5 ppt; intermediate marsh ≥ 1.5 to < 4.5 ppt; brackish marsh ≥ 4.5 to < 9.5 ppt; and saline marsh ≥ 9.5 ppt.

$SI_1 = [(1.0 \times V_{1a}) + (0.67 \times V_{1b}) + (0.55 \times V_{1c}) + (0.23 \times V_{1d}) + (0.0 \times V_{1e}) + (0.0 \times V_{1f})]$
Where: V_{1a} = the proportion of a model cell that is fresh attached or fresh floating marsh
V_{1b} = the proportion of a model cell that is intermediate marsh
V_{1c} = the proportion of a model cell that is brackish marsh
V_{1d} = the proportion of a model cell that is saline marsh
V_{1e} = the proportion of a model cell that is swamp or bottomland hardwood
V_{1f} = the proportion of a model cell that is non-wetland habitat

SI_2 = Proportion of cell that is emergent marsh (V_2):

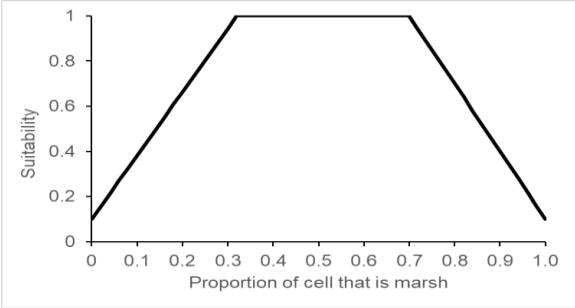

SI_2 = $(2.81*V_2) + 0.1$, when $V_2 < 0.32$
1.0, when $0.32 \leq V_2 \leq 0.70$
$(-3.0*V_2) + 3.1$, when $V_2 > 0.70$

Figure 16. Suitability relationship for mottled duck SI_2, percent marsh.

SI_3 = Mean annual water depth. This SI is derived by calculating the mean water depth for each 30-meter pixel of a model cell, estimating the proportion of the model cell covered by each depth category, then plugging these estimates into the following equation:

$SI_3 = [(0.6*V_{3a}) + (1.0*V_{3b}) + (0.83*V_{3c}) + (0.57*V_{3d}) + (0.35*V_{3e}) + (0.22*V_{3f}) + (0.09*V_{3g}) + (0.0*V_{3h})]$

Where: V_{3a} = the proportion of cell with mean water depth ≥0 to ≤ 8 cm
V_{3b} = the proportion of cell with mean water depth >8 to ≤ 30
V_{3c} = the proportion of cell with mean water depth >30 to ≤ 36
V_{3d} = the proportion of cell with mean water depth >36 to ≤ 42
V_{3e} = the proportion of cell with mean water depth >42 to ≤ 46
V_{3f} = the proportion of cell with mean water depth >46 to ≤ 50
V_{3g} = the proportion of cell with mean water depth >50 to ≤ 56
V_{3h} = the proportion of cell with mean water depth >56

SI_4 = Mean salinity during brood rearing, April through July:

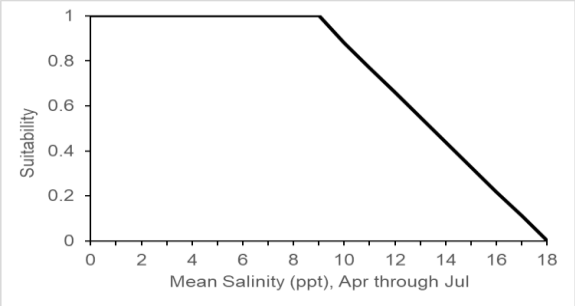

SI_4 = 1.0, when $V_4 \leq 9$ ppt
(-0.11*V_4) + 1.98, when $9 < V_4 \leq 18$
0.0, when $V_4 > 18$

Figure 17. Suitability relationship for mottled duck SI_4, mean salinity April to July.

2.6 BROWN PELICAN

The most relevant recent research on brown pelican nesting habitat requirements was from the RESTORE Act, Center of Excellence-funded project: *Assessment of coastal island restoration practices for the creation of brown pelican nesting habitat* (https://thewaterinstitute.org/la-coe/funded-research). This project assessed the effects of various environmental, ecological, and island geomorphological factors on the nesting success of pelicans on Louisiana's barrier islands. Results suggest that island elevation is an important factor in pelican nesting success (Dr. Paul Leberg, University of Louisiana at Lafayette, oral communication, 3/2/2020). In addition, results from the project could be used to refine the "Distance to the mainland or large islands" SI. Unfortunately, data and analyses from the project were not available in time to make model improvements for the 2023 Coastal Master Plan; therefore, these improvements should be considered for the next master plan modeling effort. The 2023 brown pelican HSI model is the same as the 2017 model (Leberg, 2017c). The model is used to calculate the annual habitat suitability score of a model cell for nesting brown pelican. The model equation is: $HSI = (SI_1 \times SI_2 \times SI_3 \times SI_4 \times SI_5 \times SI_6)^{1/6}$.

SI_1 = Area of island including the cell of interest (V_1). This SI only considers small islands to be suitable for nesting pelicans. Small islands are defined as contiguous model cells comprising a land mass less than 200 hectares in area that is surrounded by cells that are 100% open water.

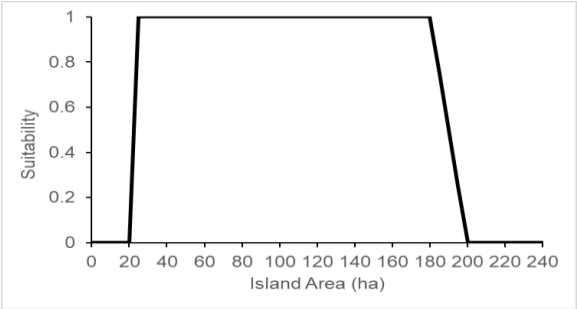

SI_1 = 0.0, when V_1 < 25 or >200 ha
1.0, when 25 ≤ V_1 ≤ 180
10 – (0.05*V_1), when 180< V_1 ≤ 200

Figure 18. Suitability relationship for brown pelican SI_1, island area.

SI_2 = Distance to the mainland or large island (V_2). This SI is the minimum distance from the center of the contiguous cells comprising a small island, including the focal cell, to the center of any cell containing land that does not meet the definition of a small island as described for SI_1.

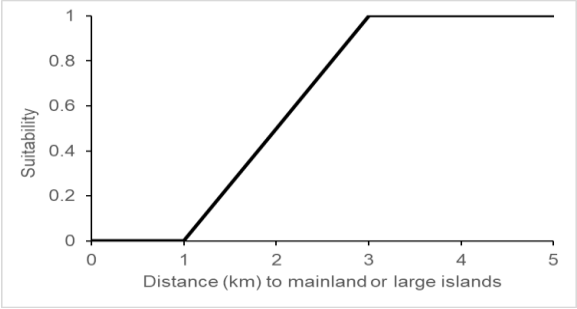

SI_2 = 0.0, when V_2 <1.0 km
(0.5*V_2) – 0.5, when 1.0 ≤ V_2 <3.0
1.0, when V_2 ≥ 3.0

Figure 19. Suitability relationship for brown pelican SI_2, distance to mainland.

SI_3 = Proportion of cell with black mangrove, *Avicennia germinans*, and/or marsh elder, *Iva frutescens* (V_3):

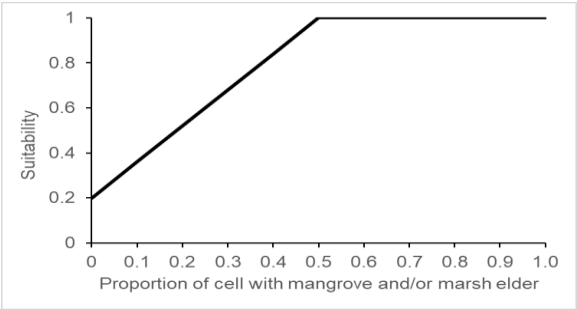

SI_3 = 0.2, when V_3 = 0.0
(1.6*V_3) + 0.2, when 0.0< V_3 <0.5
1.0, when V_3 ≥ 0.5

Figure 20. Suitability relationship for brown pelican SI3, percent mangrove and/or marsh elder.

SI_4 = Distance to human activity (V_4). This SI is the minimum distance from the edge of a human activity area to the edge of the contiguous cells forming the island containing the focal cell.

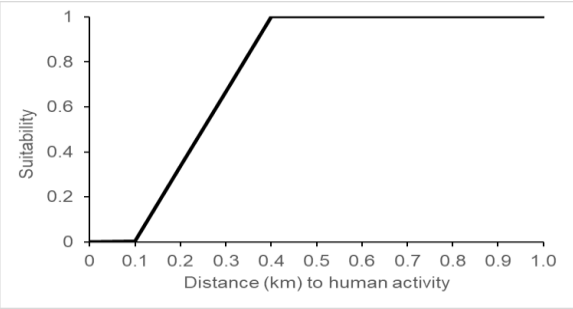

SI_4 = 0.0, when V_4 <0.1 km
(3.33*V_4) – 0.33, when 0.1 ≤ V_4 <0.4
1.0, when V_4 ≥ 0.4

Figure 21. Suitability relationship for brown pelican SI_4, distance to human activity.

SI_5 = Mean gulf menhaden HSI score (V_5). This SI is the mean menhaden HSI score of cells within a 20 km radius of a cell where SI_1 >0.0.

SI_5 = 1.667*V_5, when V_5 <0.60
1.0, when V_5 ≥ 0.60

Figure 22. Suitability relationship for brown pelican SI_5, menhaden HSI score.

SI_6 = Dominant habitat type in cell. Saline marsh receives a score of 1.0, whereas other habitat types receive a score of 0.0.

2.7 SEASIDE SPARROW

Seaside sparrow was included in the 2023 Coastal Master Plan HSI analyses to increase the diversity of bird species and bird habitats represented. Furthermore, because it is a marsh dependent species,

seaside sparrow will likely be sensitive to future marsh loss due to erosion and sea level rise (National Audubon Society, 2014). To evaluate the effects of future landscape changes on seaside sparrow, an HSI model was developed using published literature to identify important environmental variables and formulate SIs describing the effects of these variables on sparrow habitat utilization. Model development focused on incorporating variables for which the ICM could supply input data. Further information of seaside sparrow life history, the model development process, and the SIs included in the model can be found in Attachment 1.

The resulting HSI model for seaside sparrow includes three SIs: habitat type, emergent vegetation coverage, and marsh elevation. Habitat type is included in the model because seaside sparrow abundance has been shown to vary among emergent marsh types in Louisiana and elsewhere along the northern Gulf of Mexico. Emergent vegetation coverage is included because dense vegetation reduces the risk of predation on sparrow nests. Similarly, marsh elevation is included because nests built in higher elevation marshes are less prone to loss from flooding. Therefore, the HSI model is most applicable for calculating the annual habitat suitability score of a model cell for nesting seaside sparrows in coastal Louisiana. The model equation is: $HSI = (SI_1 \times SI_2 \times SI_3)^{1/3}$.

SI_1 = Proportion of model cell covered by habitat types (V_1). Habitat types other than intermediate marsh, brackish marsh, and saline marsh are given a suitability score of 0.0.

$SI_1 = [(1.0 \times V_{1a}) + (0.7 \times V_{1b}) + (0.3 \times V_{1c})]$
Where: V_{1a} = the proportion of a model cell that is saline marsh
V_{1b} = the proportion of a model cell that is brackish marsh
V_{1c} = the proportion of a model cell that is intermediate marsh

SI_2 = Percent of model cell covered by wetland vegetation (V_2). This SI is the ratio of vegetated marsh to non-vegetated habitat (i.e., open water, bare ground, etc.) in a model cell.

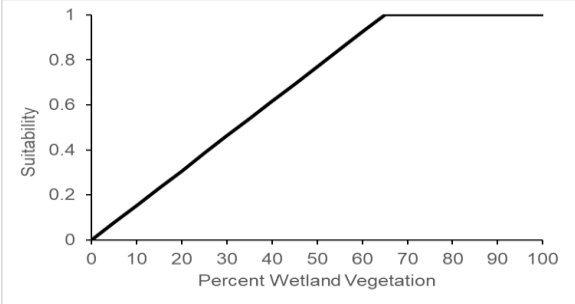

$SI_2 = 0.0154 * V_2$, when $V_2 < 65\%$
1.0, when $V_2 \geq 65$

Figure 23. Suitability relationship for seaside sparrow SI_2, percent wetland.

SI_3 = Mean elevation of marsh relative to mean annual water level (V_3).

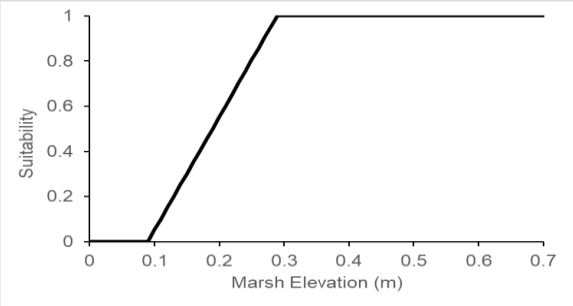

SI_3 = 0.0, when $V_3 \leq 0.09$ m
(5.025*V_3) – 0.452, when $0.09 < V_3 < 0.285$
1.0, when $V_3 \geq 0.285$

Figure 24. Suitability relationship for seaside sparrow SI_3, marsh elevation.

3.0 STATISTICAL-BASED MODELS

The statistical-based HSI models for the 2023 Coastal Master Plan include those for brown shrimp (small and large juvenile stages), white shrimp (small and large juvenile stages), blue crab (juvenile stage), gulf menhaden (juvenile and adult stages), spotted seatrout (juvenile and adult stages), largemouth bass, and bald eagle. The 2023 fish, shrimp, and blue crab HSI models are replacements for the 2017 versions of these models because recent data and a new modeling approach were used in their development. The bald eagle HSI model is new for the 2023 Coastal Master Plan and was developed by adapting a bald eagle nest probability of occurrence model created by Audubon Louisiana.

3.1 BALD EAGLE

Similar to seaside sparrow, bald eagle was included in the 2023 Coastal Master Plan HSI analyses to increase the diversity of bird species and bird habitats represented. Bald eagles are generally associated with palustrine forested wetlands and typically nest in large, mature trees (Buehler, 2020); therefore, they are considered representative of upper estuary habitat. In Louisiana, forested wetlands are being impacted by saltwater intrusion and other stressors, and future sea level rise is expected to have large negative effects on these habitats and consequently bald eagle populations. Therefore, an HSI model was developed to evaluate the effects of future landscape changes on nesting bald eagle habitat. Details of bald eagle life history and HSI model development can be found in Attachment 2.

The bald eagle HSI model was based on a statistical model that relates bald eagle nest probability of occurrence with land cover type. Nest data from coastwide aerial surveys conducted by LDWF during the 2014-2015 breeding season were summarized by a grid of 36 km^2 cells. This cell size was selected following a comparison of models constructed using various estimates of nesting eagle home ranges and core use areas (Smith et al., 2017; Buehler, 2020). Using 2014 land cover data, the percent cover of nine land cover classes: agriculture, developed and upland, forested wetland, flotant marsh, fresh marsh, intermediate marsh, brackish marsh, saline marsh, and open water was also calculated for each 36 km^2 cell. Cells with >95% open water were excluded from the analyses. The relationship between land cover class and nest probability of occurrence across the cells was then modeled using boosted regression trees. Because boosted regression trees use an iterative machine learning algorithm, each model produces slightly different results. Therefore, the analysis was run for 1,000 iterations and model parameters were averaged across all iterations. The effect of the land cover classes on nest occurrence was evaluated by calculating the relative importance of each land cover predictor to the model. In addition, the probability of nest occurrence for each land cover class was plotted across a range of possible percent cover values (with all other land cover classes held to

their average) to visually assess the trend. The results showed that forested wetland, flotant marsh, and open water explained the most variation in the model and had the greatest effect on nest occurrence (Figure 25). Fresh marsh, intermediate marsh, and developed and upland classes had minor effects on nest occurrence and each explained between 1 and 3.5% of the variation.

The nesting bald eagle HSI model was created using the modeled relationships between probability of nest occurrence and the six land cover classes: forested wetland, flotant marsh, fresh marsh, intermediate marsh, open water, and developed and upland. An SI was created for each land cover class by fitting various functions to scaled versions of the relationships shown in Figure 25. Coefficients from the best fitting function were used to develop equations that represent the SI for each land cover class (see following descriptions of each SI). For the final HSI model equation, each SI was weighted by raising the SI to the power of the relative importance of that land cover class. The six weighted SIs were multiplied, then raised by the sum of the six relative importance measures to calculate a geometric mean of the six SIs. The resulting equation is: $HSI = ((SI_1)^{0.0104} \times (SI_2)^{0.3715} \times (SI_3)^{0.4743} \times (SI_4)^{0.0330} \times (SI_5)^{0.0353} \times (SI_6)^{0.0669})^{0.991}$. The model excludes cells that are >95% open water, thus these cells are assigned an HSI score of 0. The HSI model is applicable for calculating the annual habitat suitability score of a cell for adult bald eagle nesting in coastal Louisiana.

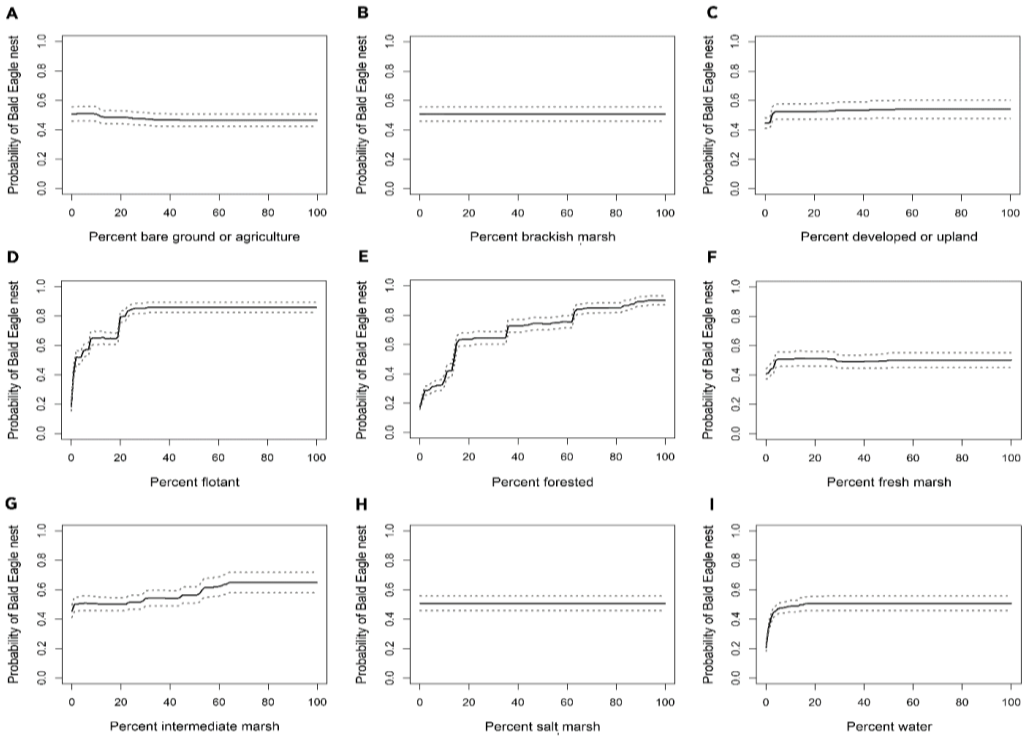

Figure 25. Marginal effects of land cover classes on probability of bald eagle nest occurrence, with 95% confidence intervals for: (A) bare ground or agriculture, (B) brackish marsh, (C) developed or upland, (D) flotant, (E) forested wetland, (F) fresh marsh, (G).

SI_1 = Percent of cell covered by developed and upland (V_1). If there is no developed land or upland in a cell, an SI_1 score of 0.01 is assigned. Otherwise, the SI is calculated using a natural log function:

$$SI_1 = 0.408 + 0.142x \ln V_1$$

SI_2 = Percent of cell covered by flotant marsh (V_2). The SI is calculated using a quartic function:

$$SI_2 = 0.282 + 0.047xV_2 - 1.105e^{-3}xV_2{}^2 + 1.101e^{-5}xV_2{}^3 - 3.967e^{-8}xV_2{}^4$$

SI_3 = Percent of cell covered by forested wetland (V_3). The SI is calculated using a quartic function:

$$SI_3 = 0.015 + 0.048xV_3 - 1.178e^{-3}xV_3{}^2 + 1.366e^{-5}xV_3{}^3 - 5.673e^{-8}xV_3{}^4$$

SI_4 = Percent of cell covered by fresh marsh (V_4). The SI is calculated using a quartic function:

$$SI_4 = 0.370 + 0.070xV_4 - 2.655e^{-3}xV_4{}^2 + 3.691e^{-5}xV_4{}^3 - 1.701e^{-7}xV_4{}^4$$

SI_5 = Percent of cell covered by intermediate marsh (V_5). The SI is calculated using a cubic function:

$$SI_5 = 0.263 - 9.406e^{-3}xV_5 + 5.432e^{-4}xV_5^{\,2} - 3.817e^{-6}xV_5^{\,3}$$

SI_6 = Percent of cell covered by open water (V_6). If there is no open water in a cell, an SI_1 score of 0.01 is assigned. Otherwise, the SI is calculated using an inverse function:

$$SI_6 = 0.985 - 0.105x(1/V_6)$$

3.2 FISH, SHRIMP, AND BLUE CRAB

The 2023 fish, shrimp, and blue crab HSI models consist of two SIs: a water quality SI, which describes the suitability of varying salinity and water temperature to the species or life stage; and a structural habitat SI, which describes the suitability of aquatic habitat composition. The 2017 models also included a chlorophyll SI to account for the effects of planktonic prey and primary productivity on habitat quality for gulf menhaden and largemouth bass. However, the chlorophyll SIs were removed from the models because the 2023 Coastal Master Plan ICM does not provide chlorophyll output. Turbidity was also removed from the largemouth bass water quality SI because inconsistencies and uncertainties in the measurement units reported in the dataset prevented the development of a reliable turbidity-CPUE relationship. The following summarizes the development of the water quality and structural habitat SIs; further detail may be found in Attachments 3 and 4, respectively.

Water Quality Suitability Index

A new modeling approach was implemented for the development of the water quality SIs, based on feedback received about the 2017 HSI models. The water quality SIs included in the 2017 fish, shrimp, and blue crab HSIs were developed using only generalized linear mixed models (GLMMs). However, several other statistical modeling approaches are available, and it was recommended that these approaches be investigated for the development of the water quality SIs (Callaway et al., 2017). As a result, Sable et al. (2019) re-evaluated the modeling approach and identified three components to improve the model development and selection process: 1) detect and resolve data and statistical issues, 2) identify and implement alternative models, and 3) evaluate model fit and performance. This more rigorous approach was implemented for the 2023 Coastal Master Plan, with the goal to compare alternative water quality models and select the best for use in the water quality SIs.

The water quality models were based on statistical analyses of datasets collected by LDWF's long-term fisheries independent monitoring programs. These programs use a variety of gear types to target different species and life stages. Because of this, only data from the gear type that most efficiently collected the species or life stage of interest were used in the subsequent analyses: seine data were used for small juvenile brown shrimp, small juvenile white shrimp, juvenile blue crab, juvenile gulf

menhaden, and juvenile spotted seatrout; 16-foot trawl data were used for large juvenile brown shrimp and large juvenile white shrimp; gillnet data were used for adult gulf menhaden and adult spotted seatrout; and electrofishing data were used for largemouth bass. The datasets for each gear type were subset by the months of highest catch for each species or life stage so that models were developed for when they were present in the estuaries. The datasets were then examined for outliers and other statistical issues, and randomly partitioned across all years of the datasets, with 70% of the data being used for model training and 30% used for model validation.

Using the model training data, two types of statistical models were created for each species or life stage to estimate the effect that water temperature and salinity had on catch-per-unit-effort (CPUE). These models were GLMMs and generalized additive mixed models (GAMMs), which were recommended because they allow for non-linear relationships between the response and predictor. The GLMMs and GAMMs were developed using four different error distributions, i.e., Gaussian, Poisson, zero-inflated Poisson, and negative binomial, so that a total of eight alternative water quality models were created for each species or life stage. The response variable in these models was CPUE, except for the Gaussian models where CPUE was transformed to natural log + 1 to meet that model's assumption of normal distribution. Predictor variables for the models were water temperature, salinity, and Julian date; however, the GLMMs also included the interaction between water temperature and salinity. Random effects were included in the models to account for the occurrence of repeated samples within the same month and year in the dataset.

A number of criteria were used to select the best water quality model of the eight alternatives to use for a species or life stage. Plots of the modeled relationships between CPUE and each individual predictor variable, and heat maps showing the combined effect of salinity and temperature on CPUE, were examined to determine if the relationships were ecologically reasonable. In addition, several different performance metrics were calculated during model training, including R-squared, root mean squared error, and (for GAMMs) the amount of deviance explained, to assess the fit of the model to the observed data and the amount of variance explained by the model. Performance metrics were also calculated during model validation to assess how accurately the model predicted CPUE of a pseudo-independent dataset. In most cases the metrics were similar among models, so the model considered the most ecologically reasonable relative to the other models was usually the one selected (see Attachment 3). As a result of this process, GAMM-Gaussian models were determined to be the best fit statistically and ecologically for blue crab, gulf menhaden, and spotted seatrout, whereas GLMMs were the best fit for brown shrimp, white shrimp, and largemouth bass.

The selected water quality model was then converted into a water quality SI for use in the HSI model for the species or life stage. To do this, a model equation was generated with random effects set at zero and Julian date set to its average value. The equation was then standardized to a 0 to 1 scale by dividing by the maximum predicted CPUE, which was determined by running the model through all

combinations of salinity and water temperature across the ranges observed in the dataset. Therefore, the salinities and water temperatures in which the species or life stage were most commonly collected are considered to be the most suitable. These salinity and water temperature ranges are dictated by numerous factors including physiological tolerances, prey availability, mortality, and seasonal movements, and should not be interpreted as optimums for specific biological processes, such as growth or reproduction.

The water quality SI for selected GLMMs is a linear equation that can be used to calculate the water quality suitability score and is provided in this report for the appropriate species or life stage. However, because the GAMM equations are large and complex, they were converted into a "look-up table" that provides the suitability scores for combinations of salinity and water temperature. These look-up tables are not included in this report but are available at: https://github.com/CPRA-MP/.

Structural Habitat Suitability Index

The approach used to develop the structural habitat SI for juvenile fish, shrimp, and blue crab was also improved for the 2023 Coastal Master Plan. For the 2017 HSI models, the SI was represented by a single relationship that was used to describe the suitability of marsh-to-open water ratios simulated for each model cell (Figure 26). This relationship was based on research conducted by Minello and Rozas (2002) and reflects the observed increase in juvenile fish, shrimp, and crab densities in fragmented marshes with a large amount of marsh edge nursery habitat. However, the relationship does not take into account the effects of other estuarine habitats, such as submerged aquatic vegetation (SAV) or oyster reefs, that are also important nursery habitats for juvenile fish and shellfish.

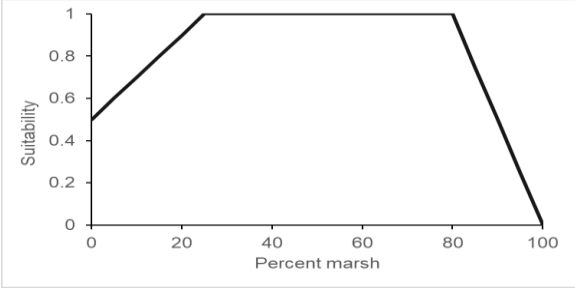

Figure 26. Structural habitat SI relationship used in the 2017 juvenile fish, shrimp, and blue crab HSI models.

The relative value of estuarine habitats to fish and shellfish was determined using a meta-analysis approach similar to that used by Minello (1999) and Minello et al. (2003). A total of 36 studies were identified (primarily from Louisiana and Texas) that compared juvenile fish and shellfish abundances among different habitats. The habitats of interest included: marsh edge (defined as vegetated marsh within 1 meter of the marsh-water interface); marsh interior (vegetated marsh >1 m from the marsh

edge); shallow non-vegetated water bottoms (open waters within 5 m of the marsh edge or with water depths <1 m); deep non-vegetated water bottoms (open waters >5 m from the marsh edge or with water depths >1 m); SAV; and oyster reefs. Species catch data within each study were averaged for each habitat and time period sampled. The habitat averages were then standardized to a 0 to 1 scale by dividing by the maximum habitat average for each time period within the study. The standardized scores were then averaged across studies for each habitat and converted into a suitability score by using a constant multiplier to bring the maximum habitat suitability score to a value of 1.0 for each species (see Attachment 4).

The suitability scores were then used to modify the 2017 structural habitat SI relationship (Figure 26) to better reflect the relative value of the estuarine habitats to juvenile fish, shrimp, and blue crab. Specifically, the y-intercept of the relationship, which represents model cells of 100% open water, was lowered for all species, except gulf menhaden, in accordance with the low suitability scores calculated for open water habitats (deep non-vegetated water bottom scores were used because this category best reflects open water habitats in the ICM). The remainder of the relationship was unchanged because the 25-80% marsh landscape configuration was still considered optimal for juveniles as it contains the maximum amount of valuable marsh edge habitat (Minello & Rozas, 2002). The resulting modified relationship was termed the "baseline relationship" for each species (Figure 27a and 27b), and was used for most model cells. Additional relationships were developed to account for the added habitat value of SAV and oyster reef occurring in open water cells. Thus, the y-intercepts of the baseline relationship were increased in accordance with the higher suitability scores for these habitats (Figure 27c and 27d). The SAV relationship was used when SAV coverage comprised ≥20% of a model cell, with this threshold value subjectively chosen based on the ICM SAV output data distribution. The oyster reef relationship was used when the average decadal oyster HSI score for a model cell was ≥0.50. Oyster HSI score was used as a proxy for oyster reef habitat because the ICM does not simulate changes in reef (i.e., cultch) coverage. Model tests showed that areas of existing oyster reefs and oyster production had HSI scores ≥0.50; therefore it was assumed that cells with such high suitability scores would continue to support oyster reef habitat throughout the ICM simulations. An average decadal value was used to prevent interannual variability in oyster HSI scores from causing large swings in reef habitat availability (i.e. reef would remain even if HSI scores were occasionally lowered).

The meta-analysis approach was not used to develop updated structural habitat SIs for larger juvenile shrimp, adult gulf menhaden, adult spotted seatrout, and largemouth bass. Compared to the juvenile stages, there were fewer studies available that investigated habitat selection for the older life stages and bass. Furthermore, estuarine distribution and movement of older life stages is driven more by prey availability, water quality conditions, and spawning considerations than by the occurrence of particular structural habitats (Gulf States Marine Fisheries Commission, 2001; Gulf States Marine Fisheries Commission, 2015). However, a structural habitat relationship was needed to place the HSI results in the proper geographic context. Therefore, the 2017 structural habitat SIs for the older life stages and largemouth bass were re-used for the 2023 Coastal Master Plan (Figures 28-30).

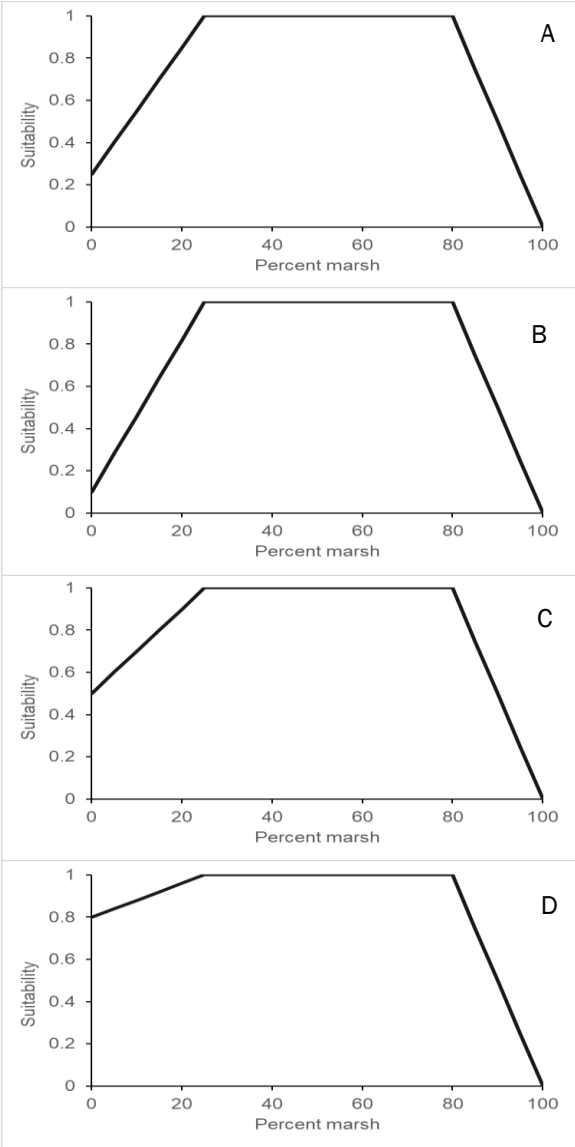

$SI_2 = (0.03*V_2) + 0.25$, when $V_2 < 25$
1.0, when $25 \leq V_2 \leq 80$
$5.0 - (0.05*V_2)$, when $V_2 > 80$

$SI_2 = (0.036*V_2) + 0.1$, when $V_2 < 25$
1.0, when $25 \leq V_2 \leq 80$
$5.0 - (0.05*V_2)$, when $V_2 > 80$

$SI_2 = (0.02*V_2) + 0.5$, when $V_2 < 25$
1.0, when $25 \leq V_2 \leq 80$
$5.0 - (0.05*V_2)$, when $V_2 > 80$

$SI_2 = (0.008*V_2) + 0.8$, when $V_2 < 25$
1.0, when $25 \leq V_2 \leq 80$
$5.0 - (0.05*V_2)$, when $V_2 > 80$

Figure 27. Structural habitat SI relationships for small juvenile shrimp, blue crab, and juvenile fish. A) shrimp and crab baseline relationship, B) spotted seatrout baseline relationship, C) gulf menhaden baseline relationship, and shrimp and crab relationship for cells with oyster HSI scores ≥0.5, and D) shrimp, crab, and spotted seatrout relationship for cells with SAV coverage ≥20%.

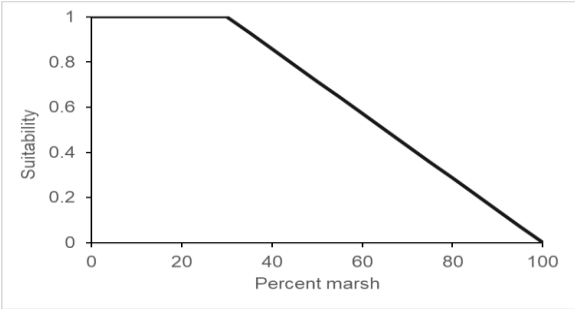

SI_2 = 1.0, when $V_2 \leq 30$
1.43 - (0.0143*V_2), when $V_2 > 30$

Figure 28. Structural habitat SI relationship for larger juvenile brown shrimp, larger juvenile white shrimp, and adult gulf menhaden.

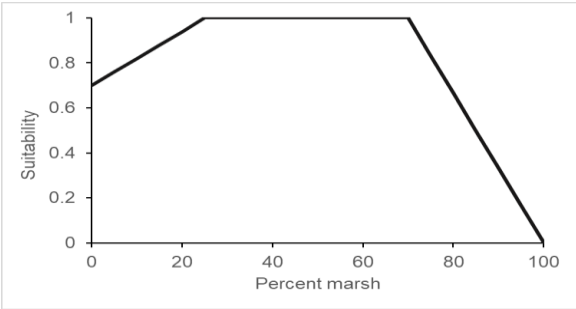

SI_2 = (0.012*V_2) + 0.7, when $V_2 < 25$
1.0, when $25 \leq V_2 \leq 70$
3.33 - (0.0333*V_2), when $V_2 > 70$

Figure 29. Structural habitat SI relationship for adult spotted seatrout.

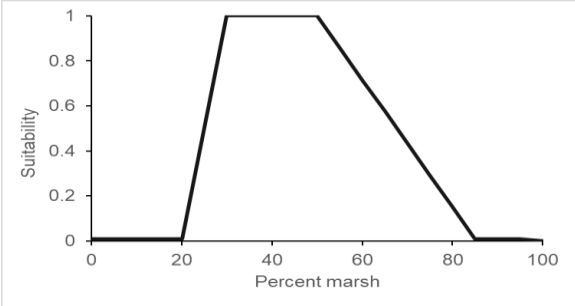

SI_2 = 0.01, when $V_2 < 20$
(0.099*V_2) - 1.997, when $20 \leq V_2 < 30$
1.0, when $30 \leq V_2 < 50$
(-0.0283*V_2) + 2.414, when $50 \leq V_2 < 85$
0.01, when $85 \leq V_2 < 100$
0.0, when V_2 = 100

Figure 30. Structural habitat SI relationship for largemouth bass.

Small Juvenile Brown Shrimp HSI model

This HSI model is applicable to small juvenile brown shrimp (median total length (TL) = 53 mm) that have recently settled to estuaries and are most common between April and July. The model equation is HSI = $(SI_1 \times SI_2)^{1/2}$, where SI_1 is the water quality suitability index and SI_2 is the structural habitat

suitability index. The water quality SI is based on the GLMM-Gaussian model, which is represented by the equation below and depicted in Figure 31, and uses average salinity and water temperature from April through July as model input. The "baseline" structural habitat SI is shown in Figure 27a, but where model cells have an average decadal oyster HSI score ≥0.50 or SAV coverage ≥20% the SI relationships shown in Figures 27c or 27d, respectively, should be used instead.

$$SI_1 = \frac{e^{1.97+1.23(S_{SI})+1.66(T_{SI})-1.07(S_{SI}{}^2)-1.53(T_{SI}{}^2)-0.12(S_{SI}*T_{SI})} - 1}{12.50}$$

Where,

$$S_{SI} = \frac{Salinity \ -7.94}{7.07} \qquad S_{SI}{}^2 = \frac{(Salinity * Salinity) - 112.91}{165.81}$$

$$T_{SI} = \frac{Temperature \ -26.87}{3.73} \qquad T_{SI}{}^2 = \frac{(Temperature * Temperature) - 735.69}{191.54}$$

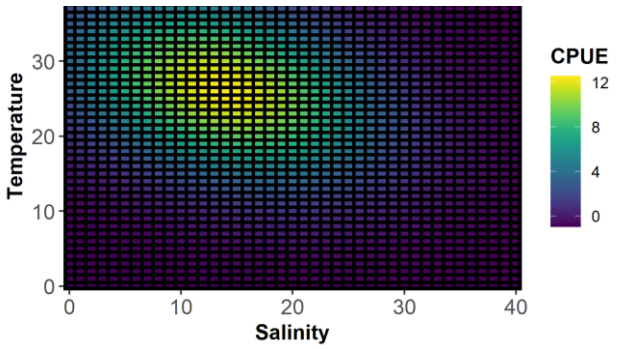

Figure 31. GLMM-Gaussian predicted response of small juvenile brown shrimp CPUE to salinity (ppt) and water temperature (°C).

Large Juvenile Brown Shrimp HSI model

This HSI model is applicable to larger juvenile/sub-adult brown shrimp (median TL = 72 mm) that occur in deeper parts of the estuarine basins primarily between April and July. The model equation is HSI = $(SI_1 \times SI_2)^{1/2}$, where SI_1 is the water quality suitability index and SI_2 is the structural habitat suitability index. The water quality SI is based on the GLMM-Gaussian model, which is represented by the equation below and depicted in Figure 32, and uses average salinity and water temperature from April through July as model input. The structural habitat SI is shown in Figure 28.

$$SI_1 = \frac{e^{2.68+1.54(S_{SI})+0.86(T_{SI})-1.51(S_{SI}{}^2)-0.72(T_{SI}{}^2)-0.18(S_{SI}*T_{SI})} - 1}{24.61}$$

Where,

$$S_{SI} = \frac{Salinity \ -10.97}{8.03} \qquad {S_{SI}}^2 = \frac{(Salinity * Salinity) - 184.85}{216.00}$$

$$T_{SI} = \frac{Temperature \ -26.64}{3.73} \qquad {T_{SI}}^2 = \frac{(Temperature * Temperature) - 723.40}{189.05}$$

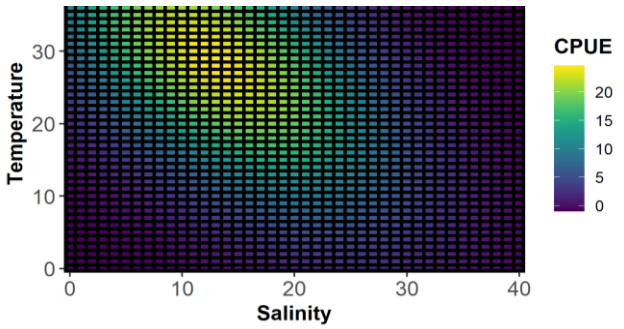

Figure 32. GLMM-Gaussian predicted response of large juvenile brown shrimp CPUE to salinity (ppt) and water temperature (°C).

Small Juvenile White Shrimp HSI model

This HSI model is applicable to small juvenile white shrimp (median total length (TL) = 43 mm) that have recently settled to estuaries and are most common between June and December. The model equation is HSI = $(SI_1 \times SI_2)^{1/2}$, where SI_1 is the water quality suitability index and SI_2 is the structural habitat suitability index. The water quality SI is based on the GLMM-Gaussian model, which is represented by the equation below and depicted in Figure 33, and uses average salinity and water temperature from June through December as model input. The "baseline" structural habitat SI is shown in Figure 27a, but where model cells have an average decadal oyster HSI score ≥0.50 or SAV coverage ≥20% the SI relationships shown in Figures 27c or 27d, respectively, should be used instead.

$$SI_1 = \frac{e^{1.63+0.61(S_{SI})+1.69(T_{SI})-0.54({S_{SI}}^2)-2.02({T_{SI}}^2)-0.08(S_{SI}*T_{SI})} - 1}{10.05}$$

Where,

$$S_{SI} = \frac{Salinity \ -10.69}{7.72} \qquad {S_{SI}}^2 = \frac{(Salinity * Salinity) - 173.92}{208.18}$$

$$T_{SI} = \frac{Temperature \ -24.39}{6.33} \qquad {T_{SI}}^2 = \frac{(Temperature * Temperature) - 635.09}{283.81}$$

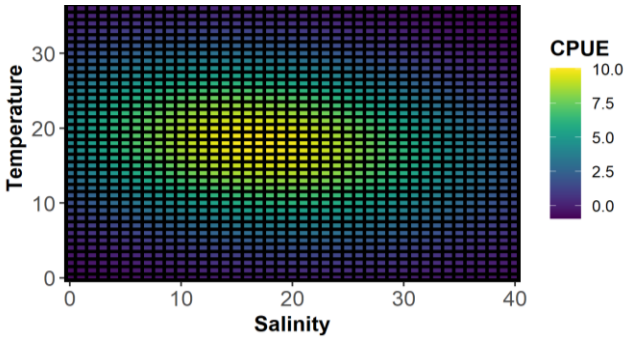

Figure 33. GLMM-Gaussian predicted response of small juvenile white shrimp CPUE to salinity (ppt) and water temperature (°C).

Large Juvenile White Shrimp HSI model

This HSI model is applicable to larger juvenile/sub-adult white shrimp (median TL = 82 mm) that occur in deeper parts of the estuarine basins throughout the year. The model equation is HSI = $(SI_1 \times SI_2)^{1/2}$, where SI_1 is the water quality suitability index and SI_2 is the structural habitat suitability index. The water quality SI is based on the GLMM-Gaussian model, which is represented by the equation below and depicted in Figure 34, and uses average salinity and water temperature over the entire year as model input. The structural habitat SI is shown in Figure 28.

$$SI_1 = \frac{e^{1.57+0.08(S_{SI})+1.00(T_{SI})-0.40({S_{SI}}^2)-1.27({T_{SI}}^2)-0.244(S_{SI}*T_{SI})} - 1}{6.83}$$

Where,

$$S_{SI} = \frac{Salinity \ -12.89}{8.41} \qquad {S_{SI}}^2 = \frac{(Salinity * Salinity) - 236.98}{249.53}$$

$$T_{SI} = \frac{Temperature \ -23.20}{6.46} \qquad {T_{SI}}^2 = \frac{(Temperature * Temperature) - 579.80}{278.79}$$

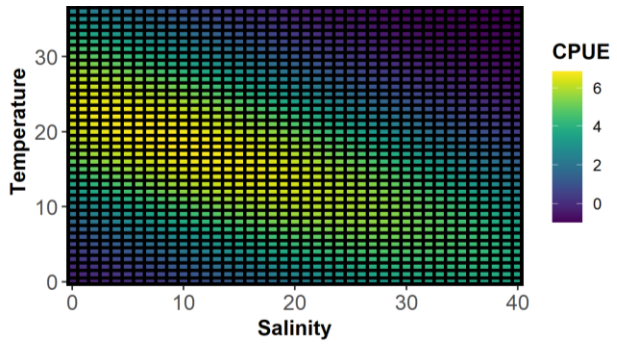

Figure 34. GLMM-Gaussian predicted response of large juvenile white shrimp CPUE to salinity (ppt) and water temperature (°C).

Juvenile Blue Crab HSI model

This HSI model is applicable to juvenile blue crab (carapace width <60 mm) that have recently settled to estuaries and are common throughout the year (note: there were insufficient data to develop a model for adult crabs). The model equation is HSI = $(SI_1 \times SI_2)^{1/2}$, where SI_1 is the water quality suitability index and SI_2 is the structural habitat suitability index. The water quality SI is based on the GAMM-Gaussian model, which is depicted in Figure 35, and uses average salinity and water temperature over the entire year as model input. The look-up table *seine_bluecrab_gamm_table_dec1* provides the suitability scores for salinity and water temperature combinations, and can be found at https://github.com/CPRA-MP/. The "baseline" structural habitat SI is shown in Figure 27a, but where cells have an average decadal oyster HSI score ≥0.50 or SAV coverage ≥20% the SI relationships shown in Figures 27c or 27d, respectively, should be used instead.

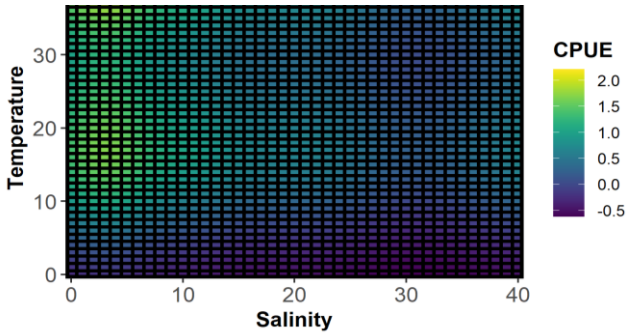

Figure 35. GAMM-Gaussian predicted response of juvenile blue crab CPUE to salinity (ppt) and water temperature (°C).

Juvenile Gulf Menhaden HSI model

This HSI model is applicable to juvenile gulf menhaden (median TL = 35 mm) that have recently settled to estuaries and are most common between January and August. The model equation is HSI = $(SI_1 \times SI_2)^{1/2}$, where SI_1 is the water quality suitability index and SI_2 is the structural habitat suitability index. The water quality SI is based on the GAMM-Gaussian model, which is depicted in Figure 36, and uses average salinity and water temperature from January through August as model input. The look-up table *seine_gulfmenhaden_gamm_table_dec1* provides the suitability scores for salinity and water temperature combinations, and can be found at https://github.com/CPRA-MP/. The structural habitat SI is shown in Figure 27c. Although the meta-analysis indicated that juvenile gulf menhaden are most prevalent over shallow non-vegetated water bottoms, these habitats primarily occur in association with marshes. Therefore, the structural habitat SI for juvenile gulf menhaden is similar to the other juvenile species, with optimum habitat conditions occurring where marsh comprises between 25-80% of a model cell, though the y-intercept is higher for menhaden due to the greater suitability of open waters.

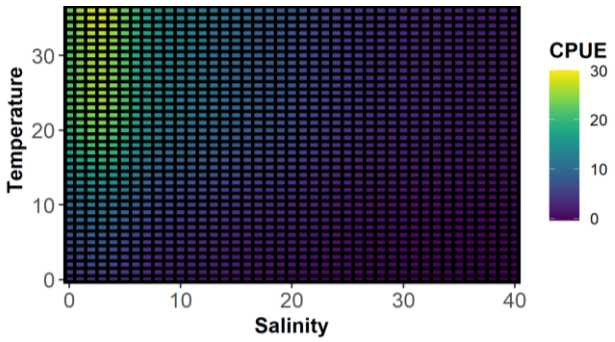

Figure 36. GAMM-Gaussian predicted response of juvenile gulf menhaden CPUE to salinity (ppt) and water temperature (°C).

Adult Gulf Menhaden HSI model

This HSI model is applicable to adult gulf menhaden (median TL = 175 mm) that occur in open waters of estuarine basins primarily between March and November. The model equation is HSI = $(SI_1 \times SI_2)^{1/2}$, where SI_1 is the water quality suitability index and SI_2 is the structural habitat suitability index. The water quality SI is based on the GAMM-Gaussian model, which is depicted in Figure 37, and uses average salinity and water temperature from March through November as model input. The look-up table *gillnet_gulfmenhaden_gamm_table_dec1* provides the suitability scores for salinity and water temperature combinations, and can be found at https://github.com/CPRA-MP/. The structural habitat SI is shown in Figure 28.

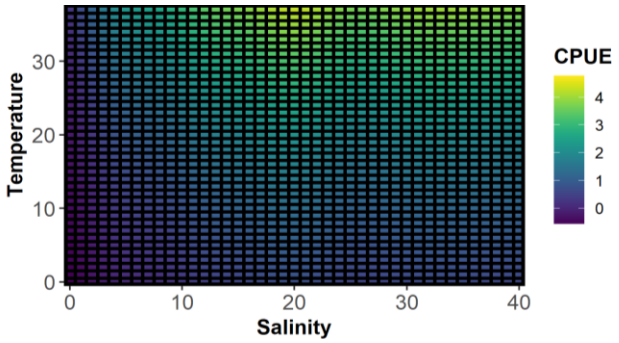

Figure 37. GAMM-Gaussian predicted response of adult gulf menhaden CPUE to salinity (ppt) and water temperature (°C).

Juvenile Spotted Seatrout HSI model

This HSI model is applicable to juvenile spotted seatrout (median TL = 60 mm) that have recently settled to estuaries and are most common between September and November. The model equation is HSI = $(SI_1 \times SI_2)^{1/2}$, where SI_1 is the water quality suitability index and SI_2 is the structural habitat suitability index. The water quality SI is based on the GAMM-Gaussian model, which is depicted in

Figure 38, and uses average salinity and water temperature from September through November as model input. The look-up table *seine_spottedseatrout_gamm_table_dec1* provides the suitability scores for salinity and water temperature combinations, and can be found at https://github.com/CPRA-MP/. The "baseline" structural habitat SI is shown in Figure 27b, but where cells have SAV coverage ≥20% the relationship shown in Figure 27d should be used instead. The meta-analysis showed that juvenile spotted seatrout were uncommon over oyster reef, so an SI relationship for this habitat was not developed.

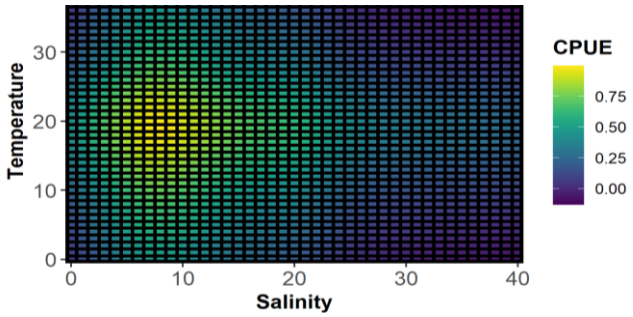

Figure 38. GAMM-Gaussian predicted response of juvenile spotted seatrout CPUE to salinity (ppt) and water temperature (°C).

Adult Spotted Seatrout HSI model

This HSI model is applicable to adult spotted seatrout (median TL >200 mm) that reside in the estuarine basins throughout the year. The model equation is $HSI = (SI_1 \times SI_2)^{1/2}$, where SI_1 is the water quality suitability index and SI_2 is the structural habitat suitability index. The water quality SI is based on the GAMM-Gaussian model, which is depicted in Figure 39, and uses average salinity and water temperature over the entire year as model input. The look-up table *gillnet_spottedseatrout_gamm_table_dec1* provides the suitability scores for salinity and water temperature combinations, and can be found at https://github.com/CPRA-MP/. The structural habitat SI is shown in Figure 29.

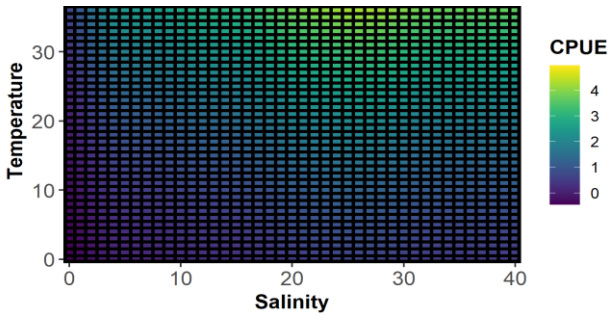

Figure 39. GAMM-Gaussian predicted response of adult spotted seatrout CPUE to salinity (ppt) and water temperature (°C).

Largemouth Bass HSI model

This HSI model is applicable to juvenile and adult largemouth bass (median TL = 200 mm) that occur primarily in the freshwater parts of the estuarine basins throughout the year. The model equation is $HSI = (SI_1 \times SI_2)^{1/2}$, where SI_1 is the water quality suitability index and SI_2 is the structural habitat suitability index. The water quality SI is based on the GLMM-Poisson model, which is represented by the equation below and depicted in Figure 40, and uses average salinity and water temperature over the entire year as model input. The structural habitat SI is shown in Figure 30.

$$SI_1 = \frac{exp(2.50 - 0.25(S_{SI}) + 0.30(T_{SI}) - 0.04(S_{SI}{}^2) - 0.33(T_{SI}{}^2) - 0.05(S_{SI} * T_{SI}))}{14.30}$$

Where,

$$S_{SI} = \frac{Salinity \ - 0.84}{1.84} \qquad S_{SI}{}^2 = \frac{(Salinity * Salinity) - 4.08}{24.91}$$

$$T_{SI} = \frac{Temperature \ - 22.68}{4.64} \qquad T_{SI}{}^2 = \frac{(Temperature * Temperature) - 535.99}{206.16}$$

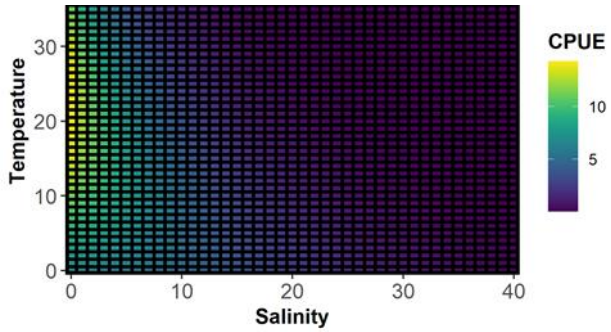

Figure 40. GLMM-Poisson predicted response of largemouth bass CPUE to salinity (ppt) and water temperature (°C).

4.0 INTEGRATION AND TESTING

The 2023 Coastal Master Plan HSI models described herein were integrated with the master plan's Integrated Compartment Model (ICM) so that the effects of environmental scenarios and candidate restoration and protection projects on species habitat could be evaluated. The ICM-HSI code from the 2017 Coastal Master Plan was updated to reflect the modified and new SIs, and the new seaside sparrow and bald eagle HSI models were incorporated. Slight changes to the model set-ups were required so that the ICM could more efficiently and effectively make the required calculations. The GAMM look-up tables were originally generated with the salinity and water temperature input data expressed to two decimals places (i.e., x.xx), which resulted in millions of rows of salinity and temperature combinations. To save computational memory and run time, the salinity and temperature input data was reduced to one decimal place (x.x). This reduction in data precision did not have a significant effect on the CPUE predictions, as the maximum difference in normalized CPUE was only 0.02. In addition, during the 2017 Coastal Master Plan, the ICM utilized ArcGIS to make the geographic calculations required for the brown pelican HSI model, i.e., for the "island area", "distance to mainland", and "distance to human activity" SIs. However, this GIS process was subsequently removed to improve ICM computation speed and efficiency. Therefore, for the 2023 Coastal Master Plan, the GIS calculations for the brown pelican model will be performed outside the ICM framework as an additional post-processing step.

The 2023 HSI models were tested using ICM environmental output from the 2017 Coastal Master Plan future without action scenario, and the results were compared to the 2017 HSI results to evaluate the efficacy of the model improvements. For the most part, the 2023 HSI models produced realistic representations of species' habitat distribution based on professional judgment. Suitability scores for adult spotted seatrout and adult gulf menhaden were relatively low (<0.75) because the average temperatures simulated by the ICM were lower than the optimum temperatures identified by the models; however, the spatial patterns of habitat suitability were reasonable. The large juvenile white shrimp HSI model was the only model to produce unreasonable results, with high suitability scores (>0.9) calculated for nearly the entire ICM domain. A revised large juvenile white shrimp HSI model was created that included Julian date in the water quality SI, because the original model may not adequately capture the effects of intra-annual water temperature variability, which influences when white shrimp emigrate from estuaries. However, this revision did not improve the results, as suitability scores were lower but still relatively uniform across the coast. Consequently, it is recommended that the large juvenile white shrimp HSI model not be used for the 2023 Coastal Master Plan. Future model improvement efforts should focus on improving this model and investigating methods to better account for the effects of intra-annual water temperature variability in the fish, shrimp, and crab HSI models.

5.0 REFERENCES

Bonvillain, C.P. (2012). Red swamp crayfish *Procambarus clarkii* in the Atchafalaya River Basin: biotic and abiotic effects on population dynamics and physiological biomarkers of hypoxic stress. Ph.D. Dissertation. Louisiana State University, Baton Rouge, Louisiana.

Buehler, D.A. (2020). Bald Eagle (*Haliaeetus leucocephalus*). In A. F. Poole & F. B. Gill (Eds.), Birds of the World, version 1.0. Cornell Lab of Ornithology, Ithaca, NY, USA. Retrieved 26 March 2020. From https://doi.org/10.2173/bow.baleag.01

Callaway, J., Hagen, S., Harris, C., Kimmerer, W., & Waldon, W. (2017). 2017 Coastal Master Plan: Attachment C5-1: Predictive Models Technical Advisory Committee Report. Version Final. Coastal Protection and Restoration Authority, Baton Rouge, Louisiana.

Casas, S., La Peyre, J., & La Peyre, M. (2015). Restoration of oyster reefs in an estuarine lake: population dynamics and shell accretion. Marine Ecology Progress Series, 524, 171-184.

Colden, A., & Lipcius, R. (2015). Lethal and sublethal effects of sediment burial on the eastern oyster Crassostrea virginica. Marine Ecology Progress Series, 527, 105-117.

Denapolis, T. (2018). Legacy habitat suitability of eastern oysters (Crassostrea virginica) in Louisiana: a prelude to Mississippi River Delta freshwater diversions. Master's Thesis. University of New Orleans, New Orleans, Louisiana.

Gulf States Marine Fisheries Commission. (2001). The spotted seatrout fishery of the Gulf of Mexico, United States: a regional management plan. Gulf States Marine Fisheries Commission, Ocean Springs, Mississippi.

Gulf States Marine Fisheries Commission. (2015). Gulf menhaden fishery of the Gulf of Mexico: a regional management plan. Gulf States Marine Fisheries Commission, Ocean Springs, Mississippi.

Hucks, K.D. (2017). Evaluation of maximum entropy models for assessing the influence of restoration scenarios on coastal wildlife populations. Master's Thesis. University of Louisiana at Lafayette, Lafayette, Louisiana.

Hupp, C.R., Demas, C.R., Kroes, D.E., Day, R.H., & Doyle, T.W. (2008). Recent sedimentation patterns within the central Atchafalaya Basin, Louisiana. Wetlands, 28, 125-140.

La Peyre, M., Eberline, B., Soniat, T., & La Peyre, J. (2013). Differences in extreme low salinity timing and duration differentially affect eastern oyster (Crassostrea virginica) size class growth and mortality in Breton Sound, LA. Estuarine, Coastal and Shelf Science, 135, 146-157.

Leberg, P. (2017a). 2017 Coastal Master Plan: Attachment C3-6: Gadwall, Anas strepera, Habitat Suitability Index Model. Version Final. Coastal Protection and Restoration Authority, Baton Rouge, Louisiana.

Leberg, P. (2017b). 2017 Coastal Master Plan: Attachment C3-8: Mottled duck, Anas fulvigula, Habitat Suitability Index Model. Version Final. Coastal Protection and Restoration Authority, Baton Rouge, Louisiana.

Leberg, P. (2017c). 2017 Coastal Master Plan: Attachment C3-9: Brown Pelican, Pelecanus occidentalis, Habitat Suitability Index Model. Version Final. Coastal Protection and Restoration Authority, Baton Rouge, Louisiana.

Lowe, M., Sehlinger, T., Soniat, T., & La Peyre, M. (2017). Interactive effects of water temperature and salinity on growth and mortality of eastern oysters, Crassostrea virginica: a meta-analysis using 40 years of monitoring data. Journal of Shellfish Research, 36, 683-698.

Minello, T.J. (1999). Nekton densities in shallow estuarine habitats of Texas and Louisiana and the identification of essential fish habitat. American Fisheries Society Symposium, 22, 43-75.

Minello, T.J. & Rozas, L.P. (2002). Nekton in gulf coast wetlands: fine-scale distributions, landscape patterns, and restoration implications. Ecological Applications, 12, 441-455.

Minello, T.J., Able, K.W., Weinstein, M.P., & Hays, C.G. (2003). Salt marshes as nurseries for nekton: testing hypotheses on density, growth and survival through meta-analysis. Marine Ecology Progress Series, 246, 39-59.

National Audubon Society. (2014). Seaside Sparrow. Retrieved from Audubon Guide to North American Birds: https://www.audubon.org/field-guide/bird/seaside-sparrow

Nifong, J.C. & Silliman, B. (2017). Abiotic factors influence the dynamics of marine habitat use by a highly mobile “freshwater” top predator. Hydrobiologia, 802, 155-174.

Nyman. J.A., Baltz, D.M., Kaller, M.D., Leberg, P.L., Parsons Richards, C., Romaire, R.P., & Soniat, T.M. (2013). Likely changes in habitat quality for fish and wildlife in coastal Louisiana during the next 50 years. Journal of Coastal Research, Special Issue 67, 60-74.

Romaire, R.P. (2017). 2017 Coastal Master Plan: Attachment C3-19: Crayfish, Procambarus clarkii and P. zonangulus, Habitat Suitability Index Model. Version Final. Coastal Protection and Restoration Authority, Baton Rouge, Louisiana.

Rose, K.A. & Sable, S. (2013). 2017 Coastal Master Plan: Strategies for Selecting Fish Modeling Approaches. Report to the Coastal Protection and Restoration Authority, Baton Rouge, Louisiana.

Rybovich, M., La Peyre, M., Hall, S., & La Peyre, J. (2016). Increased temperatures combined with lowered salinities differentially impact oyster size class growth and mortality. Journal of Shellfish Research, 35, 101-114.

Sable, S.E., Lindquist, D.C., D'Acunto, L., Hijuelos, A.C., La Peyre, M.K., O'Connell, A.M., & Robinson, E.M. (2019). 2023 Coastal Master Plan Habitat Suitability Index Model Improvement Recommendations. Coastal Protection and Restoration Authority, Baton Rouge, Louisiana.

Smith, N.R., Afton, A.D., & Hess Jr., T.J. (2017). Winter breeding and summer nonbreeding home ranges of bald eagles from Louisiana. American Midland Naturalist, 178, 203-204.

Soniat, T. (2012). Appendix D3 Eastern Oyster Habitat Suitability Index Technical Report. In: Louisiana's Comprehensive Master Plan for a Sustainable Coast. Baton Rouge, Louisiana

Thomsen, M. & McGlathery, K. (2006). Effects of accumulations of sediments and drift algae on recruitment of sessile organisms associated with oyster reefs. Journal of Experimental Marine Biology and Ecology, 328, 22-34.

United States Fish and Wildlife Service. (1981). Standards for the development of habitat suitability index models. ESM 103. Division of Ecological Services, U.S. Fish and Wildlife Service, Department of Interior, Washington D.C.

Waddle, H. (2017). 2017 Coastal Master Plan: Attachment C3-10: Alligator, Alligator mississippiensis, Habitat Suitability Index Model. Version Final. Coastal Protection and Restoration Authority, Baton Rouge, Louisiana.

Weber, M.M., Stevens, R.D., Diniz-Filho, J.A.F., & Grelle, C.E.V. (2016). Is there a correlation between abundance and environmental suitability derived from ecological niche modelling? A meta-analysis. Ecography, 40, 817-828.

ATTACHMENT 1: SEASIDE SPARROW HSI MODEL DEVELOPMENT

Elizabeth M. Robinson – Louisiana State University AgCenter

1.0 SPECIES PROFILE

The seaside sparrow, *Ammospiza maritima fisheri,* is a year-round resident (non-migratory) and ecosystem specialist commonly found in coastal marshes from Pensacola, Florida to San Antonio Bay, Texas. Seaside sparrows in Louisiana account for 69% of the northern Gulf of Mexico abundance and approximately 55% of the global abundance (Remsen et al., 2019). It has been estimated that the Louisiana breeding population consists of 3.57 million birds (Remsen et al., 2019). The seaside sparrow is listed by the National Audubon Society as a "climate endangered" species due to its sensitivity to marsh deterioration and sea-level rise (National Audubon Society, 2014). The International Union for Conservation of Nature (IUCN) Red List classifies the seaside sparrow as a species of least concern although their populations are decreasing.

Basic life history information is available for the seaside sparrow. Seaside sparrows have an estimated maximum life span of eight to nine years, although most do not live that long. Seaside sparrows spend their entire life cycle in coastal marshes foraging on insects and seeds. Seaside sparrows nest in late spring and early summer months. Male sparrows are territorial and mated pairs can remain socially monogamous from year to year. Females build the nests and incubate the eggs alone. A nest typically includes two to five eggs (Post & Greenlaw, 2018; Post, 1974).

Predation and tidal flooding drive habitat selection for nesting seaside sparrows (Reinert, 2006; Storey et al., 1988; Greenberg, et al., 2006). Intermediate, brackish, and saline marshes, dominated by *Spartina* spp., are preferred habitats by seaside sparrows (Gabrey et al., 2001). Sparrows prefer marshes with vegetation cover between 65.8 to 87.5% of an area (Gabrey & Afton, 2000). This reduces the threat of predation upon nests. Common predators of sparrows include rice rats and mink (Hart, 2017). Sparrow nests within marsh habitats are not constructed directly onto substrate surfaces and are often elevated 5-20 cm aboveground to balance the effects of flooding along with predation (Post & Greenlaw, 2018; Gjerdrum et al., 2005). Marsh elevation reduces flooding risk and nests have been observed at elevations between 0.09 and 0.659 m (Cooper et al., 2016; Lehmicke, 2014).

Table 1. Characteristics associated with seaside sparrow habitat used in the HSI model

Characteristic	Optimum	Suboptimum
Vegetation Type[1]	Intermediate, brackish and saline marsh (*Spartina* spp. dominated)	Open water
Percent Emergent Vegetation[2]	65 -100%	Marsh with less emergent marsh
Elevation[3]	> 0.09 m relative to mean annual water level	Open water Land that floods daily

[1] Based on Cooper et al., 2016; Lehmicke, 2014; Gabrey et al., 2001
[2] Based on Gabrey & Afton, 2000; Gabrey et al., 2001
[3] Based on Cooper et al., 2016; Lehmicke, 2014

2.0 APPROACH

Model variables were selected as a result of a literature review, which attempted to identify important variables associated with habitat used by nesting seaside sparrows. Habitat characteristics were assigned values from 0 to 1, with a value of 1 being assigned to the most preferred habitat state (United States Fish and Wildlife Service [USFWS], 1981). Quantitative measures of habitat use for an environmental variable were divided by the highest value for the variable state. This placed all the values of the variable on a scale from 0 to 1, where 1 is the most suitable or optimal habitat condition. Additional procedures are discussed for the individual variables. The HSI index values were obtained by taking geometric means of the suitability indices of the individual variables (USFWS, 1981).

3.0 HABITAT SUITABILITY INDEX MODEL FOR SEASIDE SPARROW

The HSI model is applicable to nesting seaside sparrows breeding in coastal Louisiana. The HSI model for the seaside sparrow is the geometric mean of three suitability indices (SIs): habitat type, emergent wetland vegetation coverage, and marsh elevation. The model equation is: $HSI = (SI_1 \times SI_2 \times SI_3)^{1/3}$.

SI_1 = Proportion of model cell covered by habitat types (V_1).

$SI_1 = [(1.0 \times V_{1a}) + (0.7 \times V_{1b}) + (0.3 \times V_{1c})]$
Where: V_{1a} = the proportion of a model cell that is saline marsh
V_{1b} = the proportion of a model cell that is brackish marsh
V_{1c} = the proportion of a model cell that is intermediate marsh

Seaside sparrow abundance has been shown to vary among emergent marsh types in Louisiana and elsewhere along the northern Gulf of Mexico. For marsh types, this index is based on surveys conducted in Louisiana, Mississippi, and Alabama by Cooper et al. (2016), Gabrey and Afton (2000), Rush

et al. (2009), and Gabrey et al. (2001). Visual observations in these studies indicate that brackish and saline marshes, dominated by *Spartina alternifloria*, *Spartina patens*, *Juncus roemerianus*, and *Distichlis spicata,* are utilized by sparrows. Since the community composition of these plants reflect a salinity gradient, the relative SI values were gradated such that $SI_1 = 1$ for saline marshes, $SI_2 = 0.7$ for brackish marshes, and $SI_3 = 0.3$ for intermediate marshes. Other emergent habitats and open water habitats have SI values equal to 0.

SI_2 = Percent of model cell covered by wetland vegetation (V_2).

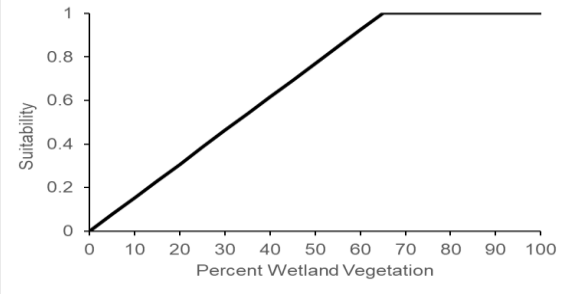

$SI_2 = 0.0154 * V_2$, when $V_2 < 65\%$
1.0, when $V_2 \geq 65$

Figure 1. Suitability relationship for seaside sparrow SI_2, percent wetland.

Seaside sparrows have been shown to nest in dense, herbaceous vegetation to increase nest concealment and reduce nest predation (Lehmicke, 2014; Gjerdrum et al., 2005; Marshall & Reinert, 1990). Sparrows in the Rockefeller Wildlife Refuge in southwest Louisiana were found to build nests in 6.25 hectare coastal marsh sites with 65 to 100% vegetative cover (Gabrey & Afton, 2000; Gabrey et al., 2001). This range of percent vegetation coverage was considered optimal for the HSI model and was assigned a value of 1 for SI_2. The risk of nest depredation increases with decreases in vegetative cover, thus the value of this index decreases to 0 as percent cover decreases to 0.

SI_3 = Mean elevation of marsh relative to mean annual water level (V_3).

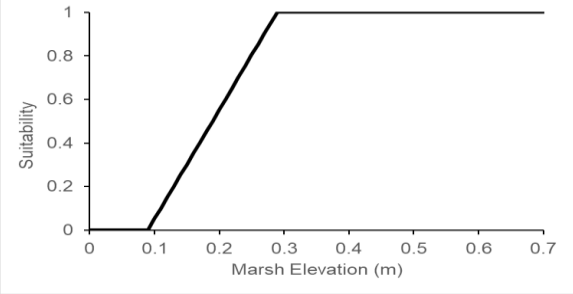

$SI_3 = 0.0$, when $V_3 \leq 0.09$ m
$(5.025 * V_3) - 0.452$, when $0.09 < V_3 < 0.285$
1.0, when $V_3 \geq 0.285$

Figure 2. Suitability relationship for seaside sparrow SI_3, marsh elevation.

Building nests in marshes with higher elevation reduces nest loss due to tidal flooding. This allows sparrows to focus on minimizing predation by building nests closer to the ground, making them better concealed. Though there are no studies in Louisiana describing sparrow nesting relationship to marsh

elevation, studies in Mississippi have shown that nests are built in marshes with elevations between 0.09 and 0.680 m relative to mean water level, with a 95% confidence interval (CI) between 0.285 and 0.659 m (Lehmicke, 2014; Cooper et al., 2016). Thus, SI_3 was assigned a value of 1 based on the 95% CI for marsh elevation seen in Mississippi sparrows. The risk of marsh flooding increases with a decrease in marsh elevation, thus the value of this index decreases to 0 at 0.09 m.

4.0 REFERENCES

Cooper, R., Lehmicke, A., & Woodrey, M. (2016). Testing habitat model assumptions for seaside sparrows (Ammodramus maritimus) in northern Gulf Coast tidal marsh: final report. Retrieved October 16, 2019, from Gulf Coast Joint Venture: http://gcjv.org/documents.php

Gabrey, S. & Afton, A. (2000). Effects of winter marsh burning on abundance and nesting activity of Louisiana seaside sparrows in the Gulf Coast Chenier Plain. The Wilson Journal of Ornithology, 112, 365-372.

Gabrey, S., Afton, A., & Wilson, B. (2001). Effects of structural marsh management and winter burning on plant and bird communities during summer in the Gulf Coast Chenier Plain. Wildlife Society Bulletin, 29, 218-231

Gjerdrum, C., Elphick, C., & Rubega, M. (2005). Nest site selection and nesting success in saltmarsh breeding sparrows: the importance of nest habitat, timing, and study site differences. The Condor, 107, 849-862.

Greenberg, R., Elphick, C., Nordby, J., Gjerdrum, C., Spautz, H., Shriver, W., . . . Winter, M. (2006). Flooding and predation: trade-offs in the nesting ecology of tidal-marsh sparrows. Studies in Avian Biology, 32, 96-109.

Hart, M. (2017). Nest success and nest predators of seaside sparrows (Ammodramus maritimus) following the "Deepwater Horizon" oil spill. M.S. Thesis. Austin Peay State University, Clarksville, Tennessee.

Lehmicke, A. (2014). Breeding ecology of the seaside sparrow (Ammodramus maritimus) in Northern Gulf of Mexico tidal salt marshes. Ph.D. Dissertation. University of Georgia, Athens, Georgia.

Marshall, R. & Reinert, S. (1990). Breeding ecology of seaside sparrows in a Massachusetts salt marsh. The Wilson Bulletin, 102, 501-513.

National Audubon Society. (2014). Seaside Sparrow. Retrieved from Audubon Guide to North American Birds: https://www.audubon.org/field-guide/bird/seaside-sparrow

Post, W. (1974). Functional analysis of space-related behavior in the seaside sparrow. Ecology, 55, 564-575.

Post, W. & Greenlaw, J. (2018). Seaside Sparrow (Ammospiza maritima). The Cornell Lab of Ornithology Birds of North America. Retrieved October 16, 2019 from: https://doi.org/10.2173/bna.seaspa.02.1

Remsen Jr., J., Wallace, B., Seymour, M., O'Malley, D., & Johnson, E. (2019). The regional, national, and international importance of Louisiana's coastal avifauna. The Wilson Journal of Ornithology, 131, 221-242.

Reinert, S. (2006). Avian nesting response to tidal-marsh flooding: literature review and a case for adaptation in the red-winged blackbird. Studies in Avian Biology, 32, 77-95.

Rush, S., Soehren, E., Woodrey, M., Graydon, C., & Cooper, R. (2009). Occupancy of select marsh birds within Northern Gulf of Mexico tidal marsh: current estimates and projected change. Wetlands, 29, 798-808.

Storey, A., Montevecchi, W., Andrews, H., & Sims, N. (1988). Constraints on nest site selection: a comparison of predator and flood avoidance in four species of marsh-nesting birds (Genera: Catoptrophorus, Larus, Rallus, and Sterna). Journal of Comparative Psychology, 102, 14-20.

United States Fish and Wildlife Service. (1981). Standards for the development of habitat suitability index models. ESM 103. Division of Ecological Services, U.S. Fish and Wildlife Service, Department of Interior, Washington D.C.

ATTACHMENT 2: BALD EAGLE HSI MODEL DEVELOPMENT

Katie Percy, Nicole L. Michel, Lindsay Nakashima, and Erik I. Johnson – Audubon Louisiana

1.0 SPECIES PROFILE

The bald eagle (*Haliaeetus leucocephalus*) is the second largest bird of prey in North America, exceeded only by the California condor (*Gymnogyps californianus*; Buehler, 2020). Adult bald eagles are easily recognized by their all-white head and tail, which is not acquired until four to five years of age, and dark brown body and wings. The species is an opportunistic forager that favors fish (Sherrod, 1978; Watson et al., 1991; Brown et al., 1991; Grubb, 1995). Hence, they are seldom far from water and primarily associated with palustrine forested wetlands (Seymour & Coulson, 2019; Buehler, 2020). The bald eagle is endemic to North America, but its range is vast – including northern Mexico, all of the contiguous United States, Alaska and most of Canada (Fink et al., 2020).

Movement and timing of breeding varies greatly with latitude. Northern populations of bald eagles breed during summer months and migrate south in winter. Conversely, the southern subspecies (southern bald eagle; *H. l. leucocephalus*) – including those across the Gulf Coast – are primarily winter breeders that migrate north as far as Canada in spring after nesting (Figure 1; Broley, 1947; Stalmaster, 1987; Mandernack et al., 2012; Smith et al., 2017a; Seymour & Coulson, 2019; Buehler, 2020). However, a small proportion of southern bald eagle appear to be nonmigratory and can be found along the Gulf Coast year-round (Stalmaster, 1987; Fink et al., 2020; Seymour & Coulson, 2019). Juvenile eagles and subadults may wander more than adults, traveling farther and in a rather nomadic fashion (Stalmaster, 1987).

	Jan	Feb	Mar	April	May	June	July	Aug	Sept	Oct	Nov	Dec
Nesting												
Foraging												
Migration												

Figure 1. Seasonal activities of the southern bald eagle along the Northern Gulf of Mexico. White cells indicate the life stage/activity is generally not present. Gray cells indicate life stage activity.

Southern bald eagles are not uncommon in Louisiana, but the population has experienced extreme fluctuations within the state, just as it has across most of its range over the past two centuries (Smith et al., 2016; Buehler, 2020). In 1782, there may have been as many as 100,000 nesting eagles in the continental United States, excluding Alaska. Yet by 1963, only 417 nesting pairs remained (United States Fish and Wildlife Service [USFWS], 2007a; USFWS, 2007b; Buehler, 2020). In Louisiana, bald eagles were described as moderately common into the early to mid-1900s (Beyer, 1900; Beyer et al., 1908; Bailey, 1919; Lowery, 1955). But by the early 1970s, the species had become rare with only approximately five nests known within the state (Lowery, 1974; Seymour & Coulson, 2019). The leading causes of population decline included habitat destruction and degradation, illegal shooting, and contamination of its primary food source (fish) with hydrocarbons, primarily by DDT (dichloro-diphenyl-trichloroethane) and its derivatives (Broley, 1947; Stalmaster, 1987; USFWS, 2007a; Buehler, 2020). By 1967, the bald eagle population south of the 40th parallel was listed in the United States as endangered, and, subsequently, received protection under the Endangered Species Act of 1973 (USFWS, 1967; USFWS, 2007a; USFWS, 2007b). By 1978, the endangered listing status was expanded throughout the conterminous United States, except in Washington, Oregon, Minnesota, Wisconsin, and Michigan, where the species was listed as threatened (USFWS, 1978).

In 1972, the U.S. Environmental Protection Agency (EPA) banned the agricultural use of DDT in the United States (EPA, 2014) and the bald eagle population subsequently rebounded. Smith et al. (2016) quantified the exponential growth in Louisiana of active nests (11.1% per year), number of successful nests (9.8% per year), and number of young produced (11.4% per year) using aerial nest survey data collected annually from 1975 to 2008. Recovery goals of the Southeastern States Bald Eagle Recovery Plan were exceeded by 1990 (Murphy, 1989; Smith et al., 2016). No longer at immediate risk to extinction, the bald eagle was removed from the U.S. endangered species list in August of 2007 (USFWS, 2007a). Continued stability and growth of the population may depend on the ability of bald eagles to cope with increasing levels of human activity, such as land development, habitat fragmentation, and to a lesser extent persecution. Additionally, protection and availability of current and future nesting habitats, as well as the careless and illegal use of pesticides, will influence ongoing bald eagle population stability (Smith et al., 2016; Seymour & Coulson, 2019; Ebersole, 2020).

The recently published Strategic Bird Monitoring Guidelines for the Northern Gulf of Mexico (Wilson et al., 2019) recognized that sea level rise may impact the quality and quantity of eagle nesting and foraging habitat in the northern Gulf of Mexico because of saltwater-induced loss of nesting trees and a change in fish assemblages. In the Chesapeake Bay, for example, bald eagle recoveries were substantially slower in saltwater wetlands than in freshwater wetlands, indicating a habitat preference for freshwater systems, as well as possible sensitivities to the conversion of freshwater to saltwater wetlands (Watts et al., 2006). Watts et al. (2006) suggested that fisheries and the spawning runs of anadromous species along the Atlantic Coast may partially explain the salinity effects. Even so, bald eagles may also do well in intermediate salinities, up to about 10 ppt, with chicks experiencing particularly rapid growth in these wetlands in the Chesapeake Bay (Markham & Watts, 2008). Higher

salinities may reduce the availability or suitability of preferred forage fish and may negatively impact nesting trees (Seymour & Coulson, 2019). Because of the species' preference for freshwater wetlands and potential sensitivities to saltwater intrusion, continued monitoring and predictive modeling of bald eagle populations is essential, as this species is an apex predator that can be an indicator of ecosystem health.

Bald eagles display a high degree of fidelity to breeding home ranges (Harris et al., 1987; Jenkins & Jackman, 1993; Smith et al., 2017a). Nests are typically located near the top of mature, dominant trees capable of supporting large, heavy nests (Stalmaster, 1987; Gerrard & Bortolotti, 1988; Buehler, 2020). Invariably, nests are located in close proximity to water (Stalmaster, 1987; Gerrard & Bortolotti, 1988; Buehler, 2020). Territory size varies greatly and is based on food supply and nesting density (Staltmaster, 1987; Gerrard & Bortolotti, 1988). Frequently, there are alternate nests within a territory, and because nests are susceptible to severe weather, rebuilding is common (Harris et al., 1987).

In Louisiana, southern bald eagles establish breeding territories and begin nesting in the fall (Smith et al., 2016). Of 23 nests surveyed in Louisiana from 1977 to 1980, 93% were in bald cypress trees (*Taxodium distichum*) (Harris et al., 1987), but nests have also been documented in pine and hardwood trees, as well as atop man-made structures like cell towers and electrical pylons (Iles, 2018). Smith et al. (2017b) analyzed bald eagle nest-site selection and success in relation to geographic variables in Louisiana. They categorized 23,897 km^2 as suitable bald eagle nesting habitat (i.e., within 1 km of a large body of water, and in a forested wetland or emergent herbaceous wetland with trees capable of supporting a nest). One third of this suitable habitat was within the south-central and southeastern portion of the state including the Atchafalaya, Terrebonne, Barataria, and Pontchartrain Basins – where land cover is dominated by inland swamps, deltaic coastal marshes, and barrier islands. Despite it covering just 18% of the state, this area contained the highest bald eagle nesting density at that time (81% of active nests in 2007-2008; Smith et al., 2017b). Although nest success was not significantly associated with the landscape-level variables around a site, initial selection of a site did appear to be influenced by some landscape-level factors (Smith et al., 2017b). All active nests during the 2007-2008 season were within 3 km of a large body of water (average distance = 466 m), and wooded wetlands made up the largest proportion of land cover types within 3 km of nests (mean = 44.1%), followed by emergent herbaceous wetland (mean = 26.0%; Smith et al., 2017b). Wooded areas provide essential platforms for nest structures, and emergent herbaceous wetlands – which can support large numbers of both fish and waterfowl in Louisiana – provide foraging opportunities (Dugoni et al., 1986; Remsen et al., 2019; Seymour & Coulson, 2019).

A Habitat Suitability Index (HSI) model was published for the northern bald eagle (Peterson, 1986), but because the model was based on summer-breeding populations early in the post-DDT era recovery, we felt that this may have limited applicability to populations in Louisiana's coastal wetlands. As such, we developed a new HSI for the southern bald eagle based on data collected in Louisiana. Because bald

eagles are representative of upper estuary habitat, we believe the southern bald eagle serves as an appropriate species for HSI modeling. Furthermore, we expect that substantial changes to Louisiana's wetlands over the next 50 years will negatively impact bald eagle populations. This model will provide the opportunity to test two hypotheses: 1) that changes to Louisiana's coastal wetlands will have a discernible impact on bald eagle nesting habitat, and 2) that restoration action will provide benefits to bald eagle habitats compared to a future without restoration action.

2.0 METHODS

Approach

Aerial survey data for known bald eagle nests were collected annually in Louisiana from 1975 to 2008, initially by USFWS and later by the Louisiana Department of Wildlife and Fisheries (LDWF) (Smith et al., 2016; Holcomb et al., 2015). After 2008, the next statewide survey occurred during the 2014-2015 breeding season, and subsequent periodic surveys have only covered the southeastern portion of the state. No other comprehensive survey data exists for the bald eagle population in Louisiana.

To develop an HSI, we used bald eagle nest location data from the last statewide survey (2014-2015), but restricted the dataset to include only nests occurring within the Louisiana Coastal Zone boundary. Land cover data from 2014 (Couvillion, 2017) was also used to develop bird-habitat relationships. The LDWF aerial surveys were conducted between December 2014 and March 2015 by helicopter, focusing on known nest locations from previous surveys and other records from the LDWF Wildlife Diversity Program (formerly the Natural Heritage Program) database. Most nests were visited twice – once to gauge the presence or absence of nesting behaviors, and a return weeks later to gauge nesting productivity. See Holcomb et al. (2015) for more details.

We included only those nests classified as "active" in our analysis, which resulted in a total of 322 bald eagle nests. Because the spatial scale of bald eagle nesting habitat selection in southern Louisiana is unclear, we built models using data summarized at four grid cell sizes based on published home range and core use area estimates (Smith et al., 2017a; Buehler, 2020): 3x3 km (9 km^2), 4x4 km (16 km^2), 5x5 km (25 km^2), and 6x6 km (36 km^2). Within each cell, we calculated the percent cover of nine land cover classes: agriculture, developed and upland, forested wetlands, fresh marsh, brackish marsh, intermediate marsh, salt marsh, flotant marsh, and open water. Because these datasets included many grid cells with complete, or nearly complete, surface water cover, we explored the effects of excluding grid cells with water cover greater than a predefined threshold. For each of the four datasets, we explored two thresholds: 95% water cover and a proportion just greater than the maximum water cover in that dataset, which we determined by rounding up to the nearest integer. Maximum water cover proportions in a grid cell containing a bald eagle nest were 87.4% for 9 km^2,

91.6% for 16 km^2, 97.5% for 25 km^2, and 88.5% for 36 km^2. Therefore, we used water cover thresholds of 88% for 9 km^2, 92% for 16 km^2, 98% for 25 km^2, and 89% for 36 km^2, in addition to the predetermined 95% threshold.

The eight datasets included between 1,214 (36 km^2) and 4,836 (9 km^2) grid cells, of which 135 to 205 cells contained one or more nests. Because of the small proportion of grid cells with nests, the count data were strongly skewed with many zeroes. This skew violated the assumptions of traditional count-based distributions used in modeling (e.g., Gaussian, Poisson), and a log transformation was insufficient to reduce this lack of fit. Therefore, we developed models based on occurrence probability rather than count. These models relate the probability of occurrence of one or more bald eagle nests within a grid cell with the land cover in that grid cell.

Modeling Technique

We modeled the relationship between bald eagle nest occurrence and land cover using boosted regression trees (BRTs). BRTs are a machine learning approach that is ideal for modeling the kind of complex curvilinear relationships with multiple and often correlated environmental variables that are pervasive when modeling wildlife response to land cover (Elith et al., 2008). Models were fit using packages dismo (Hijmans et al., 2015) and gbm (Ridgeway, 2010) in R version 3.5.1 (R Core Team, 2018). The response variable was presence (1) or absence (0) of one or more bald eagle nests.

BRT models use three parameters—learning rate, bag fraction, and model tree complexity—to shrink the number of terms in the final model and thus avoid overfitting. Learning rate shrinks the contribution of each model tree in the boosted model; bag fraction specifies the proportion of data to be selected from the training set at each step; and model tree complexity determines the number of nodes and, consequently, level of interactions between predictors. We iteratively tuned these parameters to optimize model fit while ensuring a minimum of 1,000 model trees using default parameter ranges recommended by Elith et al. (2008): learning rate 0.0001–0.1, bag fraction 0.55–0.75, and model tree complexity 1–3. At each step, we used 10-fold cross-validated area under the receiver operating characteristic curve (AUC), and deviance explained to select the optimal parameter value. AUC is a measure of discriminatory capacity, and deviance explained provides information regarding how much variance in bald eagle nest occurrence was explained by the model. To reduce bias due to spatial autocorrelation, we used spatially-stratified cross-validation. We accomplished this by dividing the dataset into 11 bins by latitude and longitude and withholding one latitudinal bin for testing at each fold (Roberts et al., 2017). Our final model used the following tuning parameters: learning rate of 0.001, a bag fraction of 0.50, and a model tree complexity of 1.

Model Performance

Because BRTs use an iterative machine learning algorithm, each model produces slightly different results. Therefore, we ran the model for 1,000 iterations and calculated multimodel averages for all

parameters. Final model performance of the complete set of eight models (four grid cell sizes, each with two water cover thresholds) was evaluated using three cross-validated model performance measures: deviance explained, correlation, and AUC. Deviance explained and AUC were explained previously. Correlation is a measure of predictive accuracy, evaluating the correlation between predicted and observed nest occurrence. For all model performance measures, higher values indicate better model fit. In the best-fit model, the effects of land cover on probability of nest occurrence were evaluated in three ways. First, the relative importance of each land cover predictor in the model was calculated and scaled so that all importance values sum to 100. Second, the relationship between each land cover type and probability of nest occurrence was plotted as a marginal effect, meaning the probability of bald eagle nest occurrence was estimated across a range of possible coverage values with all other land cover types held to their means. Nest occurrence probability estimates were generated as predictions from the BRT model at each of the 1,000 iterations, and standard errors were derived from these bootstrap samples. Finally, the plotted relationships were examined and classified as "positive," "neutral," or "negative" effects.

Model Prediction

BRT models can also be used to generate predictions given a set of covariate values. For each of the 1,000 model iterations, we generated predicted nest occurrence probability for all grid cells from the observed land cover values. We calculated mean nest occurrence probability across the 1,000 model iterations, and used that to map predicted bald eagle nest occurrence across the study area.

Data Exploration

Prior to building BRT models, we investigated correlations among predictor variables. Though BRTs are relatively robust to correlated predictors, variables with a Pearson's correlation > |~0.8| may produce spurious results (Elith et al., 2008). No variables had correlations stronger than |0.50|, so all land cover variables were included in each model.

3.0 RESULTS

The dataset with 36 km^2 grid cells and a 95% water cover threshold produced the best-fitting model (Table 1). This dataset included 1,214 grid cells, of which 957 cells met the 95% water cover threshold (i.e., included <95% water cover). All further results are drawn from this model.

Forested wetland land cover explained the greatest variation in probability of bald eagle nest occurrence, followed by flotant marsh and open water (Table 2). The remaining six land cover types each explained <5% of the model variation (8.73% combined), with bare ground and agriculture, brackish marsh, and salt marsh each explaining <1% of nest occurrence.

Table 1. Model performance statistics for the set of eight models evaluated for southern bald eagle nest occurrence in the Coastal Zone of Louisiana. The best-fitting model is shown in bold.

Grid Cell Size	% Water Threshold	Deviance Explained	Correlation	AUC
9 km^2	95%	0.32	0.24	0.82
9 km^2	88%	0.31	0.23	0.81
16 km^2	95%	0.38	0.37	0.79
16 km^2	92%	0.37	0.37	0.79
25 km^2	95%	0.43	0.36	0.79
25 km^2	98%	0.42	0.36	0.89
36 km^2	**95%**	**0.43**	**0.40**	**0.80**
36 km^2	89%	0.38	0.38	0.79

Table 2. Variable importance and direction of relationship between land cover classes and probability of southern bald eagle nest occurrence. SE = standard error.

Land cover class	Variable Importance		
	Mean	SE	Direction
Agriculture	0.82	0.01	Negative
Brackish marsh	0.02	0.00	Neutral
Developed and upland	1.04	0.02	Positive
Flotant marsh	37.15	0.07	Positive
Forested wetland	47.43	0.06	Positive
Fresh marsh	3.30	0.03	Positive
Intermediate marsh	3.53	0.03	Positive
Salt marsh	0.02	0.00	Neutral
Open water	6.69	0.03	Positive

Probability of bald eagle nest occurrence was strongly positively related to flotant marsh, forested wetland, and open water, and weakly related to intermediate marsh, fresh marsh, and developed and upland land cover (Figure 2). Meanwhile, bald eagle nest occurrence showed a weak negative response to agriculture, and was neutral to brackish marsh and salt marsh land cover. Probability of bald eagle nest occurrence was highest in southeast Louisiana, between the Atchafalaya and Mississippi Rivers (Figure 3).

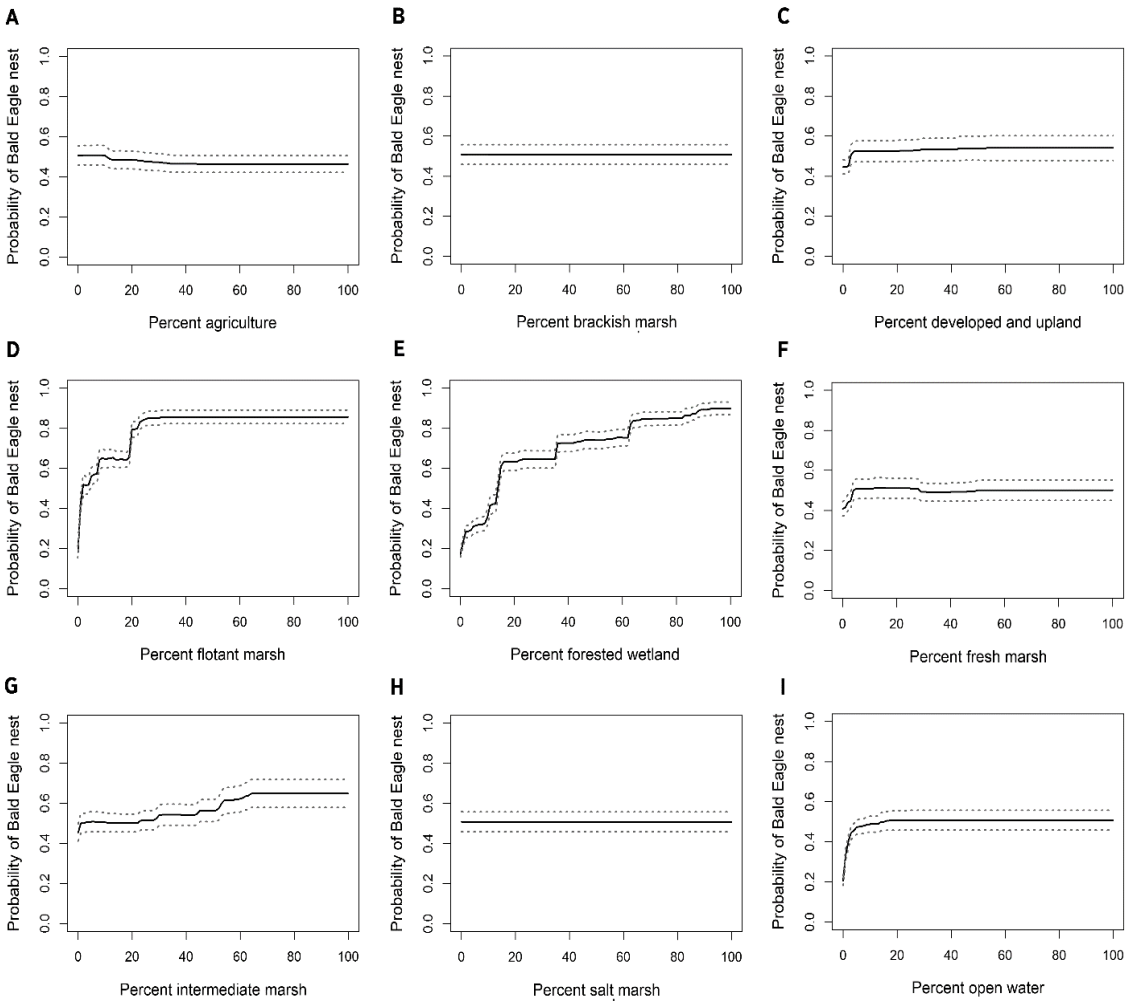

Figure 2. Marginal effects of nine land cover classes on probability of southern bald eagle nest occurrence, with 95% confidence intervals, in the Coastal Zone of Louisiana: agriculture (A), brackish marsh (B), developed and upland (C), flotant marsh (D), forested wetland (E), fresh marsh (F), intermediate marsh (G), salt marsh (H), and open water (I).

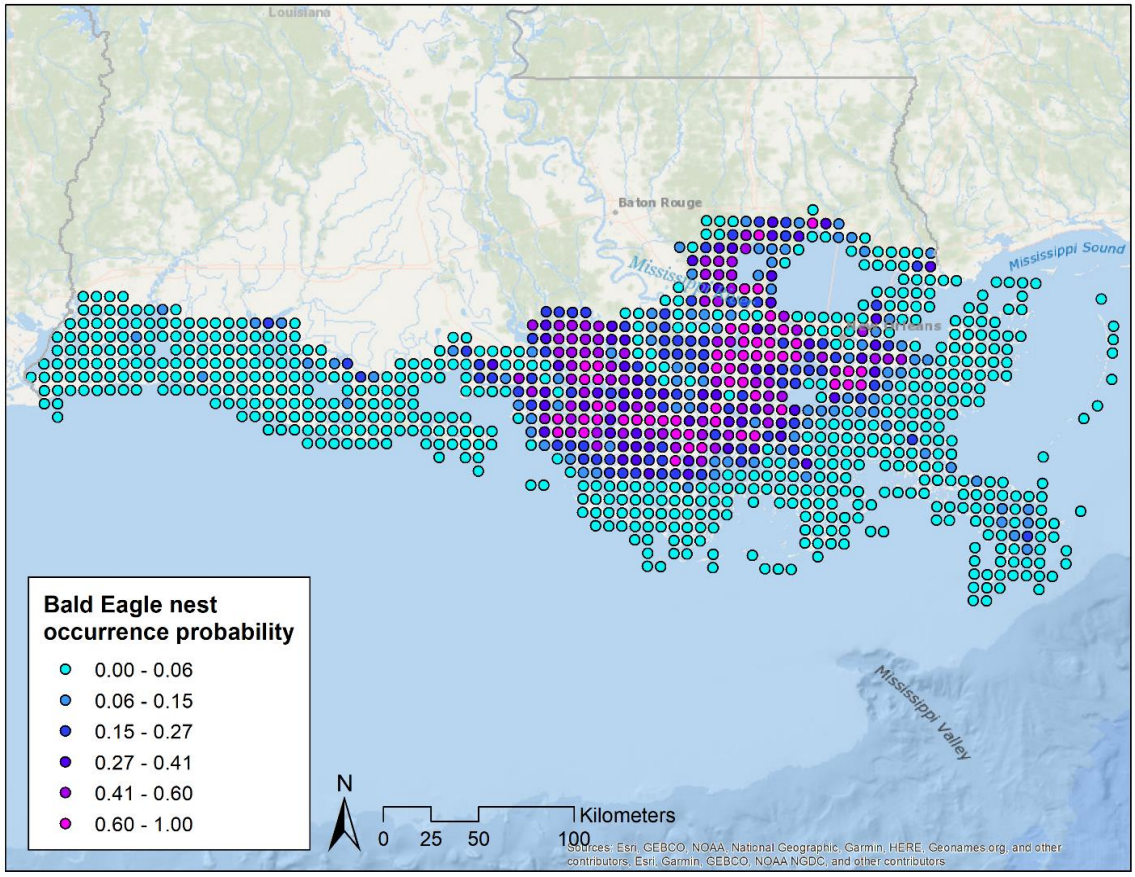

Figure 3. Predicted southern bald eagle nest occurrence across the Coastal Zone of Louisiana, averaged across 1000 model iterations.

4.0 SOUTHERN BALD EAGLE HABITAT SUITABILITY INDEX MODEL

We created a Habitat Suitability Index (HSI) from the six land cover variables that explained >1% of the variation in probability of bald eagle nest occurrence: developed and upland, flotant marsh, forested wetland, fresh marsh, intermediate marsh, and open water. A 1% threshold offered a useful balance for including relevant model parameters and reducing model complexity by removing land cover variables that explained negligible variation in bald eagle habitat suitability. For each land cover variable we created a Suitability Index (SI) based on the relationship between bald eagle nest occurrence probability and the proportion of each land cover type in a 36 km^2 cell (methods per Tirpak et al., 2009). Predicted nest occurrence probability values for the range of possible coverage (0-100%) of the land cover type (Figure 2) were rescaled to span a range of 0 to 1, representing the full range of suitability indices. We then fit a series of curves to the rescaled data, and used Akaike information criterion (AIC) model selection methods to identify the formula that produced the best fit. Specifically,

we fit the following curves: first-order polynomial (linear), second-order polynomial (quadratic), third-order polynomial (cubic), fourth-order polynomial (quartic), inverse, natural log, and exponential. To avoid issues with dividing by or taking the log of 0, a constant of 0.1 was added as needed to rescaled occurrence probability (exponential) or percent cover (inverse, natural log). Model coefficients were derived from the selected model, and were used to populate the equation presented for each land cover variable as its SI. Finally, the overall HSI was calculated as a weighted geometric mean of the individual SIs for each of the six land cover variables that explained >1% of the variation in bald eagle nest occurrence probability. Each SI was weighted by raising the SI to the power of the proportion of variance explained by that land cover type (i.e., relative importance divided by 100; Table 2). The six weighted SIs were multiplied, then raised by the inverse of the sum of the six proportions of variance to calculate a geometric mean of the six SIs, as follows:

$$HSI = ((SI_1)^{0.0104} * (SI_2)^{0.3715} * (SI_3)^{0.4743} * (SI_4)^{0.0330} * (SI_5)^{0.0353} * (SI_6)^{0.0669})^{0.991}$$

Where:

- SI_1 = SI based on percent cover developed and upland (V_1)
- SI_2 = SI based on percent cover flotant march (V_2)
- SI_3 = SI based on percent cover forested wetland (V_3)
- SI_4 = SI based on percent cover fresh marsh (V_4)
- SI_5 = SI based on percent cover intermediate marsh (V_5)
- SI_6 = SI based on percent cover open water (V_6)

Note that we restricted our model to grid cells with ≤95% water, as bald eagles are unable to nest in grid cells without emergent vegetation. Therefore, for grid cells with >95% open water, the HSI should be defined as: HSI = 0. The HSI model is used to calculate the annual habitat suitability index score of a model cell for adult southern bald eagles nesting in coastal Louisiana. Although the model was built using data from the Louisiana Coastal Zone, the relationships developed are also applicable to the slightly larger ICM model domain.

SI_1 = Percent cover of developed and upland habitat (V_1).

V_1 is the proportion of a 36 km^2 cell that is covered by developed or upland habitat. The model that best fit the relationship between probability of bald eagle nest occurrence and developed and upland land cover (Figure 2C), rescaled to range from 0 – 1, was the natural log (Table 3). The SI for developed and upland land cover should be calculated as follows: if $V_1 = 0$, $SI_1 = 0.01$; otherwise

$$SI_1 = 0.408 + 0.142 * \ln V_1$$

Table 3. Model selection table for developed and upland land cover as nesting habitat for the southern bald eagle. AIC and delta AIC are presented for each Suitability Index model fit to the relationship between probability of southern bald eagle nest occurrence and proportion developed and upland land cover.

Model Name	AIC	ΔAIC
Natural log	-213.39	0.00
Quartic	-179.05	34.34
Cubic	-162.32	51.07
Quadratic	-144.92	68.46
Linear	-108.45	104.94
Inverse	-106.93	106.46
Exponential	78.23	291.61

SI_2 = Percent cover of flotant marsh habitat (V_2).

V_2 is the proportion of a 36 km^2 cell that is covered by flotant marsh habitat. The model that best fit the relationship between probability of bald eagle nest occurrence and flotant marsh land cover (Figure 2D), rescaled to range from 0 – 1, was the quartic (Table 4). The SI for flotant marsh land cover should be calculated as follows:

$$SI_2 = 0.282 + 0.047 * V_2 - 1.105e^{-3} * {V_2}^2 + 1.101e^{-5} * {V_2}^3 - 3.967e^{-8} * {V_2}^4$$

Table 4. Model selection table for flotant marsh land cover as nesting habitat for the southern bald eagle. AIC and delta AIC are presented for each Suitability Index model fit to the relationship between probability of southern bald eagle nest occurrence and proportion flotant marsh land cover.

Model Name	AIC	ΔAIC
Quartic	-312.15	0.00
Cubic	-298.91	13.24
Natural log	-262.26	49.89
Quadratic	-216.69	95.47
Linear	-119.15	193.00
Inverse	-98.31	213.84
Exponential	7.13	319.28

SI_3 = Percent cover of forested wetland habitat (V_3).

V_3 is the proportion of a 36 km^2 cell that is covered by forested wetland habitat. The model that best fit the relationship between probability of bald eagle nest occurrence and forested wetland land cover (Figure 2E), rescaled to range from 0 – 1, was the quartic (Table 5). The SI for forested wetland land cover should be calculated as follows:

$$SI_3 = 0.015 + 0.048 * V_3 - 1.178e^{-3} * {V_3}^2 + 1.366e^{-5} * {V_3}^3 - 5.673e^{-8} * {V_3}^4$$

Table 5. Model selection table for forested wetland land cover as nesting habitat for the southern bald eagle. AIC and delta AIC are presented for each Suitability Index model fit to the relationship between probability of southern bald eagle nest occurrence and proportion forested wetland land cover.

Model Name	AIC	ΔAIC
Quartic	-333.25	0.00
Cubic	-300.50	32.75
Quadratic	-246.00	87.26
Natural log	-202.91	130.34
Linear	-162.95	170.30
Inverse	-2.60	330.66
Exponential	30.23	363.49

SI_4 = Percent cover of fresh marsh habitat (V_4).

V_4 is the proportion of a 36 km^2 cell that is covered by fresh marsh habitat. The model that best fit the relationship between probability of bald eagle nest occurrence and fresh marsh land cover (Figure 2F), rescaled to range from 0 – 1, was the quartic (Table 6). The SI for fresh marsh land cover should be calculated as follows:

$$SI_4 = 0.370 + 0.070 * V_4 - 2.655e^{-3} * {V_4}^2 + 3.691e^{-5} * {V_4}^3 - 1.701e^{-7} * {V_4}^4$$

Table 6. Model selection table for fresh marsh land cover as nesting habitat for the southern bald eagle. AIC and delta AIC are presented for each Suitability Index model fit to the relationship between probability of southern bald eagle nest occurrence and proportion fresh marsh land cover.

Model Name	AIC	ΔAIC
Quartic	-158.75	0.00
Inverse	-139.62	19.13
Natural log	-124.60	34.15
Cubic	-109.80	48.95
Quadratic	-95.36	63.39
Linear	-92.54	66.21
Exponential	49.18	207.93

SI_5 = Percent cover of intermediate marsh habitat (V_5).

V_5 is the proportion of a 36 km^2 cell that is covered by intermediate marsh habitat. The model that best fit the relationship between probability of bald eagle nest occurrence and intermediate marsh land cover (Figure 2G), rescaled to range from 0 – 1, was the cubic (Table 7). The SI for intermediate marsh land cover should be calculated as follows:

$$SI_5 = 0.263 - 9.406e^{-3} * V_5 + 5.432e^{-4} * {V_5}^2 - 3.817e^{-6} * {V_5}^3$$

Table 7. Model selection table for intermediate marsh land cover as nesting habitat for the southern bald eagle. AIC and delta AIC are presented for each Suitability Index model fit to the relationship between probability of southern bald eagle nest occurrence and proportion intermediate marsh land cover.

Model Name	AIC	ΔAIC
Cubic	-282.39	0.00
Quartic	-281.17	1.22
Quadratic	-183.94	98.45
Linear	-180.33	102.06
Exponential	-50.92	231.47
Natural log	-39.27	243.12
Inverse	55.69	338.08

SI_6 = Percent cover of open water habitat (V_6).

V_6 is the proportion of a 36 km^2 cell that is covered by open water habitat. The model that best fit the relationship between probability of southern bald eagle nest occurrence and open water cover (Figure 2l), rescaled to range from 0 – 1, was the inverse (Table 8). The SI for open water cover should be calculated as follows: if $V_6 = 0$, $SI_6 = 0.01$; otherwise

$$SI_6 = 0.985 - 0.105 * (1/V_6)$$

TABLE 8. Model selection table for open water land cover as nesting habitat for the southern bald eagle. AIC and delta AIC are presented for each Suitability Index model fit to the relationship between probability of southern bald eagle nest occurrence and proportion open water cover.

Model Name	AIC	ΔAIC
Inverse	-270.82	0.00
Quartic	-247.20	23.62
Natural log	-246.90	23.92
Cubic	-211.63	59.19
Quadratic	-178.64	92.18
Linear	-152.36	118.45
Exponential	3.23	274.05

5.0 MODEL VERIFICATION

We verified the model by estimating four model fit statistics: cross-validated deviance explained, cross-validated correlation, cross-validated AUC, and Moran's I. We calculated the statistics for each of the 1,000 model iterations. We used 10-fold cross-validation, in which 90% of the data are designated training data and used to build the model, while 10% of the data were withheld to use for testing. To reduce bias due to spatial autocorrelation, we used spatially stratified cross-validation by dividing the data set into 11 bins by latitude and longitude and withholding one latitudinal bin for testing at each fold (Roberts et al., 2017). We tested for residual spatial autocorrelation in the final model using Moran's I, calculated in package ape (Paradis et al., 2004). The model fit statistics all indicated good fit between the model and the observed data. The BRT model explained 43% of the deviance (SE: 0.13) in southern bald eagle nest occurrence across the study area, the cross-validated correlation was 0.38 (SE: 0.06), and the cross-validated AUC was 0.80 (SE: 0.04; AUC scores >0.80 indicate good model fit). Moran's I values were 0.02 (SE: 0.001) indicating that there was no residual spatial autocorrelation in the model.

We further verified the HSI model created using the SIs derived from the BRT model. We calculated the HSI score for each of the 957 grid cells in the 36 km^2 dataset using the formula presented in section 4.0, and calculated the Pearson's correlation for the relationship between the grid-level HSI scores and predicted nest occurrence probabilities. HSI scores were significantly ($P < 0.0001$) and strongly correlated with predicted nest occurrence probabilities ($r = 0.87$; Figure 4).

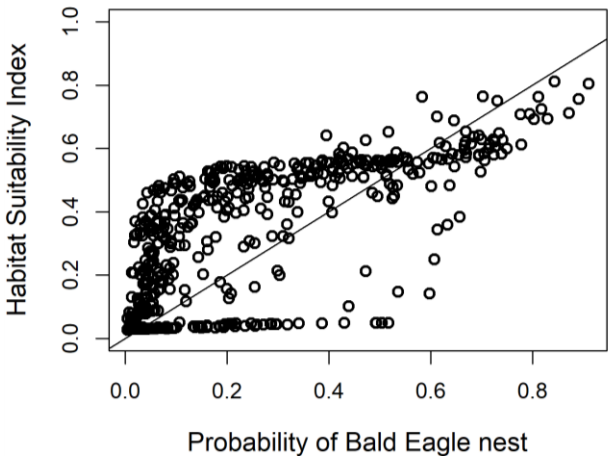

Figure 4. Relationship between HSI score and BRT model-estimated probability of southern bald eagle nest occurrence for the Coastal Zone of Louisiana, with 1:1 line shown ($r = 0.87$, $P < 0.0001$).

6.0 REFERENCES

Bailey, A. M. (1919). The bald eagle in Louisiana. The Wilson Bulletin, 31, 52–55.

Beyer, G. E. (1900). The avifauna of Louisiana: With an annotated list of the birds of the state. Proceedings of the Louisiana Society of Naturalists—1897-1899, 75–120.

Beyer, G. E., Allison, A., & Kopman, H. H. (1908). List of the birds of Louisiana. Part V. (Continued). The Auk, 25, 439–448.

Broley, C. L. (1947). Migration and nesting of Florida bald eagles. Wilson Bulletin, 59, 1-68.

Brown, B. T., Leibfried, W. C., Huels, T. R., & Olivera, J. A. (1991). Prey remains from bald eagle nests in Sonora, Mexico. The Southwest Naturalist, 36, 259-262.

Buehler, D. A. (2020). Bald Eagle (Haliaeetus leucocephalus). In A. F. Poole & F. B. Gill (Eds.), Birds of the World, version 1.0. Cornell Lab of Ornithology, Ithaca, NY, USA. Retrieved 26 March 2020. From https://doi.org/10.2173/bow.baleag.01

Couvillion, B. (2017). 2017 Coastal Master Plan: Attachment C3-27: Landscape Data. Version Final. Coastal Protection and Restoration Authority, Baton Rouge, Louisiana.

Dugoni, J. A., Zwank, P. J., & Furman, G. C. (1986). Foods of nesting bald eagles in Louisiana. Journal of Raptor Research, 20, 124–127.

Ebersole, R. (2020). Death Spiral. Audubon, 122, 22-27.

Elith, J., Leathwick, J. R., & Hastie, T. (2008). A working guide to boosted regression trees. Journal of Animal Ecology, 77, 802–813.

Fink, D., Auer, T., Johnston, A., Strimas-Mackey, M., Robinson, O., Ligocki, S., Petersen, B., . . .Kelling, S. (2020). eBird Status and Trends, Data Version: 2018; released: 2020. Cornell Lab of Ornithology, Ithaca, New York. Retrieved 02 April 2020. From https://doi.org/10.2173/ebirdst.2018.

Gerrard, J. M. & Bortolotti, G. R. (1988). The bald eagle: haunts and habits of a wilderness monarch. Washington, D.C: Smithsonian Institution Press.

Grubb, T. G. (1995). Food habits of bald eagles breeding in the Arizona desert. Wilson Bulletin, 107, 258-274.

Harris, J. O., Zwank, P.J., & Dugoni, J. A. (1987). Habitat selection and behavior of nesting bald eagles in Louisiana. Journal of Raptor Research, 2, 27-31.

Hijmans, R. J., Phillips, S., Leathwick, J., & Elith, J. (2015). dismo: Species distribution modeling. R package version 1.0-12. R Foundation for Statistical Computing.

Holcomb, S. R., Bass, A. A., Reid, C. S., Seymour, M. A., Lorenz, N. F., Gregory, B. B., Javed, S. M., & Balkum, K. F. (2015). Louisiana Wildlife Action Plan. Louisiana Department of Wildlife and Fisheries. Baton Rouge, Louisiana.

Iles, T. (2018). Soaring return. Louisiana Conservationist, 69, 14-16.

Jenkins, J. M. & Jackman, R. E. (1993). Mate and nest site fidelity in a resident population of bald eagles. The Condor, 95, 1053–1056.

Lowery, G. H. Jr. (1955). Louisiana Birds. Louisiana State University Press, Baton Rouge, LA.

Lowery, G. H. Jr. (1974). Louisiana Birds. Louisiana State University Press, Baton Rouge, LA.

Mandernack, B. A., Solensky, M., Martell, M., & Schmitz, R. T. (2012). Satellite tracking of bald eagles in the Upper Midwest. Journal of Raptor Research, 46, 258–73.

Markham, A.C. & Watts, B.D. (2008). The influence of salinity on the diet of nesting Bald Eagles. Journal of Raptor Research, 42, 99-109.

Murphy, T. M. (1989). Southeastern states bald eagle recovery plan. US Fish and Wildlife Service, Atlanta, Georgia.

Paradis, E., Claude, J., & Strimmer, K. (2004). APE: analyses of phylogenetics and evolution in R language. Bioinformatics, 20, 289–290.

Peterson, A. (1986). Habitat Suitability Index Models: Bald eagle (breeding season). U.S. Fish and Wildlife Service, Biological Report, 82 (10.126), 25 pp.

R Core Team. (2018). R: A language and environment for statistical computing. R Foundation for Statistical Computing, Vienna, Austria.

Remsen, J. V., Wallace, B. P., Seymour, M. A., O'Malley, D. A. & Johnson, E. I. (2019). The regional, national, and international importance of Louisiana's coastal avifauna. The Wilson Journal of Ornithology, 131, 221–434.

Ridgeway, G. (2010). gbm: generalized boosted regression models. R package version 1.6-3.1.

Roberts, D. R., Bahn, V., Ciuti, S., Boyce, M. S., Elith, J., Guillera-Arroita, G., Hauenstein, S., . . .Thuiller, W. (2017). Cross-validation strategies for data with temporal, spatial, hierarchical, or phylogenetic structure. Ecography, 40, 913-929.

Seymour, M. A. & Coulson, J. O. (2019). GoMAMN strategic bird monitoring guidelines: Raptors. In R. R. Wilson, A. M. V. Fournier, J. S. Gleason, J. E. Lyons, & M. S. Woodrey (Eds.), pp. 97-128. Strategic Bird Monitoring Guidelines for the Northern Gulf of Mexico. Mississippi Agricultural and Forestry Experiment Station Research Bulletin 1228, Mississippi State University, Mississippi State, MS.

Sherrod, S. K. (1978). Diets of North American Falconiformes. Raptor Research, 12, 49-121.

Smith, N. R., Hess T. J. Jr., & Afton, A. D. (2016). History and nesting population of bald eagles in Louisiana. Southeastern Naturalist, 15, 12-25.

Smith, N. R., Afton, A. D., & Hess Jr., T. J. (2017a). Winter breeding and summer nonbreeding home ranges of bald eagles from Louisiana. American Midland Naturalist, 178, 203-204.

Smith, N. R., Hess T. J. Jr., & Afton, A. D. (2017b). Nest-site selection and success of Louisiana bald eagles. Southeastern Naturalist, 16, 343-361.

Stalmaster, M. V. (1987). The Bald Eagle. New York: Universe Books.

Tirpak, J. M., Jones-Farrand, D. T., Thompson, F. R. III, Twedt, D. J., & Uihlein, W. B. III. (2009). Multiscale Habitat Suitability Index Models for priority landbirds in the Central Hardwoods and West Gulf Coastal Plain/Ouachitas Bird Conservation Regions. General Technical Report NRS-49, U.S. Department of Agriculture, U.S. Forest Service, Northern Research Station, Newtown Square, PA, USA.

U.S. Environmental Protection Agency (USEPA). (2014). DDT - A brief history and status. Overviews and Factsheets. Retrieved 26 March 2020. From https://www.epa.gov/ingredients-used-pesticide-products/ddt-brief-history-and-status

U.S. Fish and Wildlife Service (USFWS). (1967). Endangered Species. Federal Register, 32, 4001. Retrieved 26 March 2020. From https://www.fws.gov/endangered/species/pdf/32FedReg_pg%204001.pdf

U.S. Fish and Wildlife Service (USFWS). (1978). Endangered and threatened wildlife and plants: Determination of certain bald eagle populations as endangered or threatened, final rule. Federal Register, 43, 6230–6233.

U.S. Fish and Wildlife Service (USFWS). (2007a). Endangered and threatened wildlife and plants; Removing the bald eagle in the lower 48 states from the list of endangered and threatened wildlife. Federal Register, 72, 37345-37372.

U.S. Fish and Wildlife Service (USFWS). (2007b). Bald eagle (Haliaeetus leucocephalus). Endangered Species Program. Retrieved 26 March 2020. From https://www.fws.gov/birds/management/managed-species/bald-and-golden-eagle-information.php

Wilson, R. R., Fournier, A. M. V., Gleason, J. S., Lyons, J. E., & Woodrey, M. S. (Editors). (2019). Strategic bird monitoring guidelines for the Northern Gulf of Mexico. Mississippi Agricultural and Forestry Experiment Station Research Bulletin 1228, Mississippi State University, Mississippi State, MS. USA. 324 pp.

Watson, J., Garrett, M., & Anthony, R. (1991). Foraging ecology of bald eagles in the Columbia River Estuary. The Journal of Wildlife Management, 55, 492-499.

Watts, B. D., Markham, A. C., & Byrd, M. A. (2006). Salinity and population parameters of bald eagles (Haliaeetus leucocephalus) in the Lower Chesapeake Bay. Auk, 123, 393-404.

ATTACHMENT 3: FISH, SHRIMP, AND CRAB WATER QUALITY SUITABILITY INDEX

Ann C. Hijuelos and Laura D'Acunto– U.S. Geological Survey, Wetland and Aquatic Research Center

1.0 INTRODUCTION

Habitat suitability index (HSI) models have been used in previous master plan modeling efforts to evaluate the effects of coastal restoration and protection projects on habitat for key coastal fish, shellfish, and wildlife species. In the 2017 Coastal Master Plan, HSI models for blue crab, brown shrimp, white shrimp, gulf menhaden, spotted seatrout, and largemouth bass included a statistical-based water quality suitability index (SI). A subsequent review of the models (Callaway et al., 2017) indicated that the approach used to develop the water quality SI should be revisited and alternate modeling approaches should be explored. To address this comment, we reviewed the habitat suitability model development literature and considered each of the general steps of model development, from data preparation and model fitting to model evaluation, while considering the ecological justification and rationalization through every step. In keeping with widely accepted principles of model development (e.g., Guisan & Thuiller, 2005) and working within the framework of available data, the 2023 Coastal Master Plan HSI team identified and executed three components for model improvements, 1) detect and resolve data and statistical issues, 2) identify and implement alternative models, and 3) evaluate model fit and performance. Our goal for this model improvement exercise was to select a single water quality model for the HSIs; one that performs well statistically and is ecologically reasonable. In the following sections, we describe the implementation of the model improvement components. For each species, we provide a brief summary of the results and also indicate which water quality model was selected for incorporation into the final HSI model.

2.0 METHODS

Preparation of Environmental Data

Salinity and temperature measurements associated with seine, trawl, and gill net samples were investigated for potential outliers by examining the frequency distribution of the raw data and using expert judgement of what was considered reasonable for the areas being sampled. All years of available data were examined: 1967 to 2019 for trawl, 1986 to 2019 for gillnet and seine, and 1998 to 2019 for

electrofishing. Outliers were defined as those larger than the 75th percentile by at least 1.5 times the interquartile range (IQR) (IQR = 75th percentile – 25th percentile), or smaller than the 25th percentile by at least 1.5 times the IQR, for each month. Water temperature outliers were verified against air temperature data collected by the National Oceanic and Atmospheric Administration at the New Orleans[1] and Lake Charles[2] airports. If the outlier fell outside of the range of the data at either airport on that day, the outlier was considered a confirmed outlier and was removed from the dataset. If the outlier did fall within the range, the outlier was kept in the dataset to be included in subsequent analyses. For salinity data, no additional data over the full time period of the dataset were available to confirm outliers and as such, a conservative approach was taken to remove outliers identified in the boxplots from the dataset, for the seine, trawl, and gillnet gear types. Salinity measurements removed were generally values greater than 37 ppt and less than 0 ppt. In some cases, two measurements were taken at each site: one at the bottom of the water column and one at the top. Once outliers were removed, these measurements were averaged. Salinity and temperature boxplots, with and without outliers removed, are provided for seines (Figure 1, Figure 2), 16-foot trawls (Figure 3, Figure 4), and gillnets (Figure 5, Figure 6).

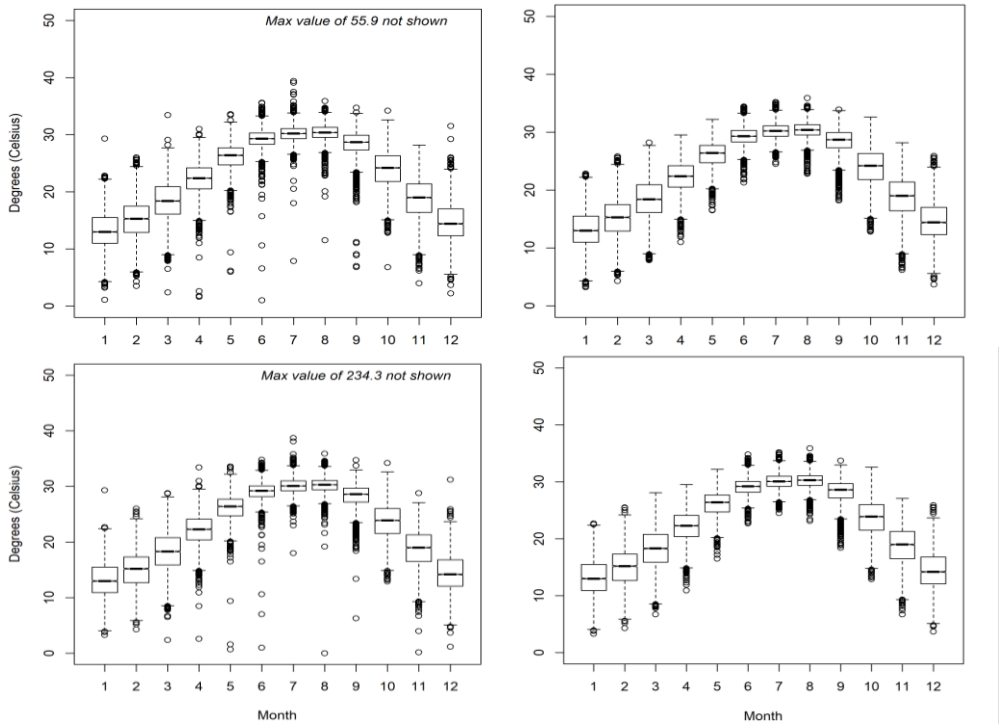

Figure 1. Water temperature from the seine dataset collected at the top and bottom of the water column (top and bottom panels, respectively); raw data (left panels) and with outliers removed (right panels).

[1] https://www.ncdc.noaa.gov/cdo-web/datasets/GHCND/stations/GHCND:USW00012916/detail
[2] https://www.ncdc.noaa.gov/cdo-web/datasets/GHCND/stations/GHCND:USW00003937/detail

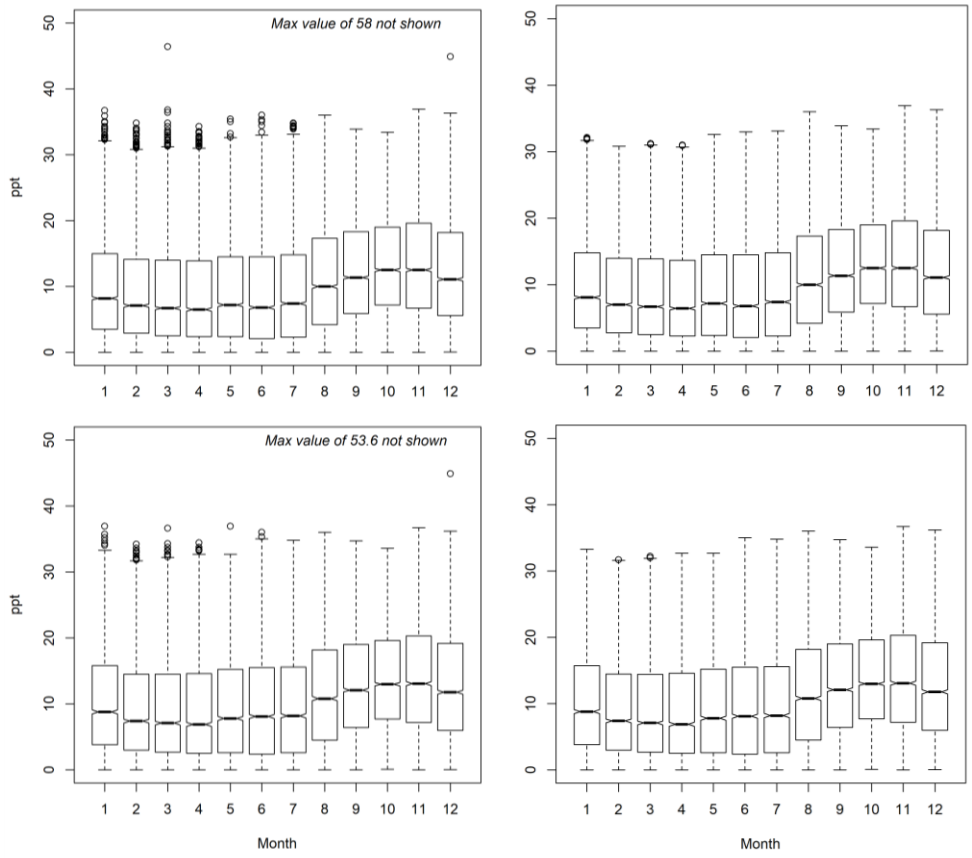

Figure 2. Salinity from the seine dataset collected at the top and bottom of the water column (top and bottom panels, respectively); raw data (left panels) and with outliers removed (right panels).

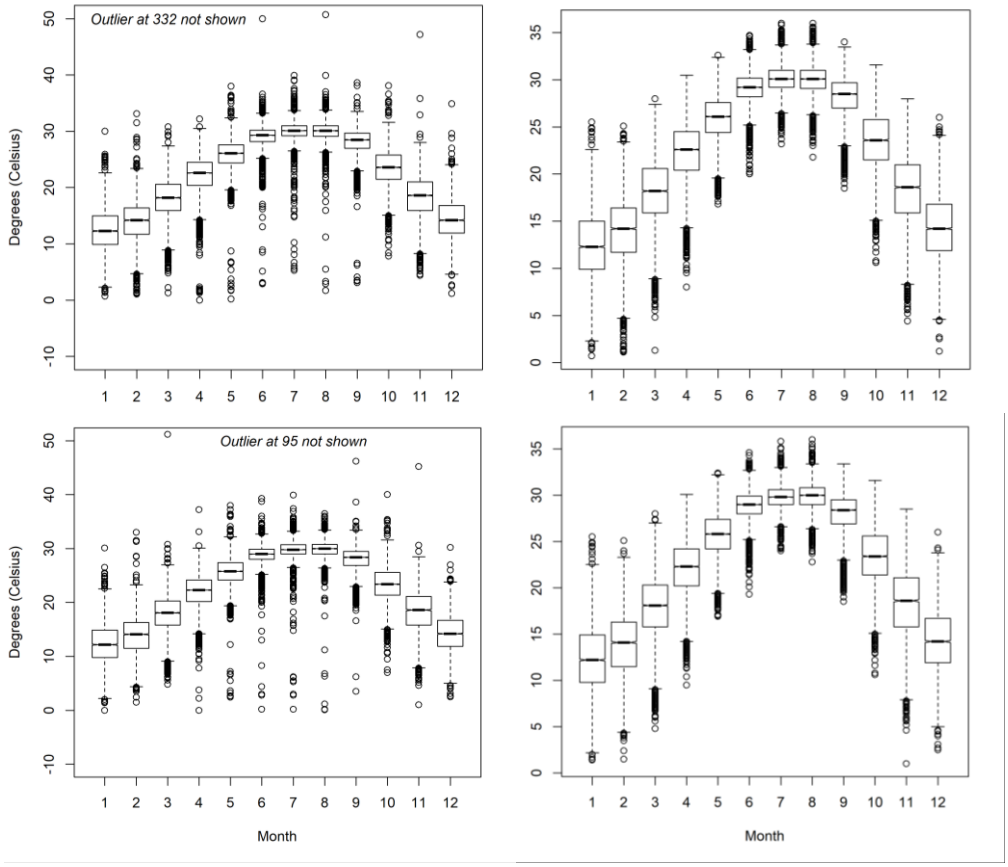

Figure 3. Water temperature from the 16-foot trawl dataset collected at the top and bottom of the water column (top and bottom panels, respectively); raw data (left panels) and with outliers removed (right panels). Note change in y-axes on left and right panels.

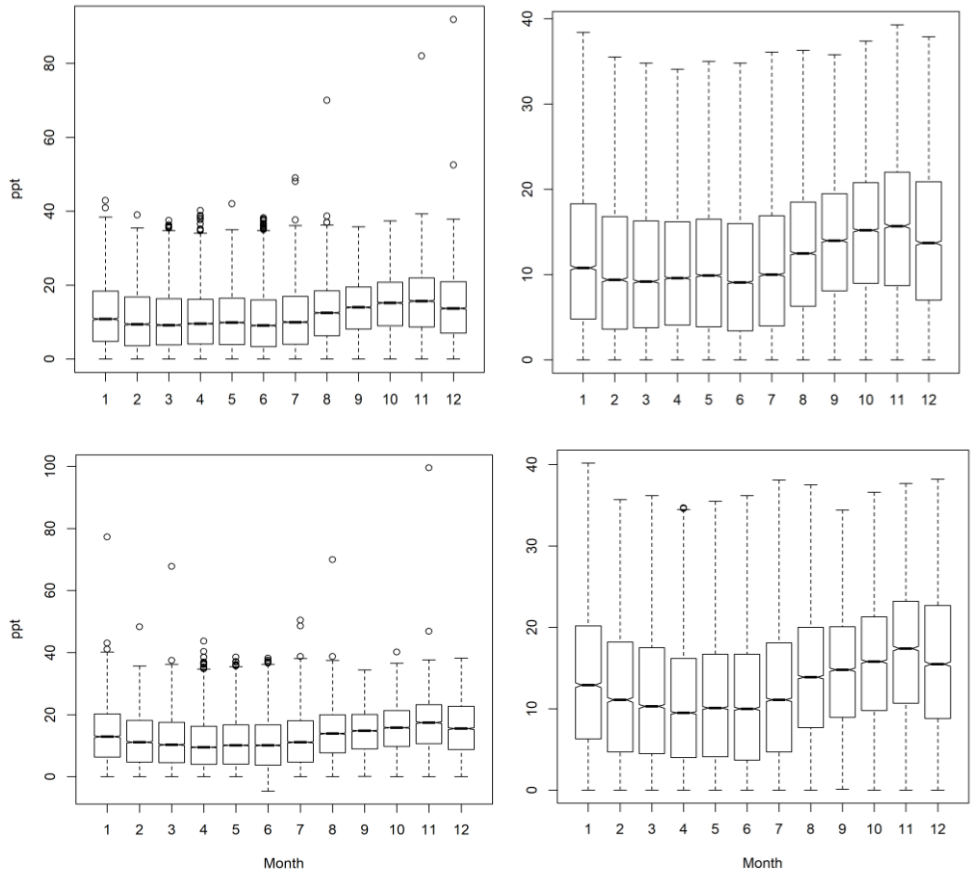

Figure 4. Salinity from the 16-foot trawl dataset collected at the top and bottom of the water column (top and bottom panels, respectively); raw data (left panels) and with outliers removed (right panels). Note change in y-axes on left and right panels.

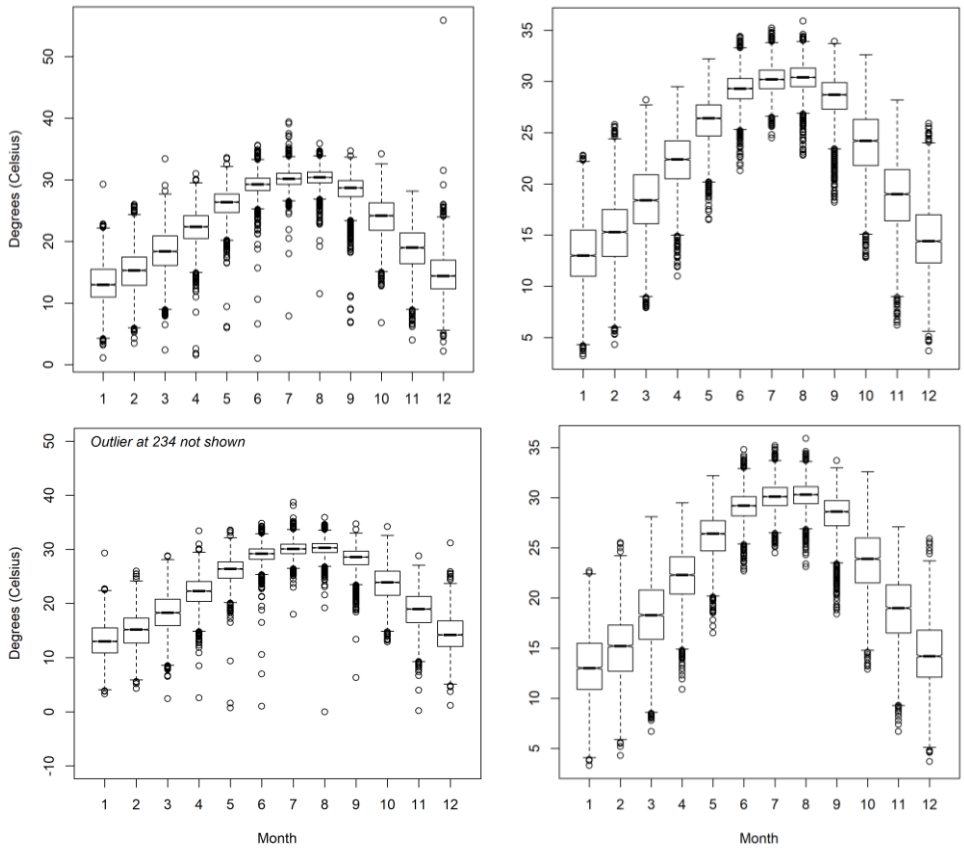

Figure 5. Water temperature from the gillnet dataset collected at the top and bottom of the water column (top and bottom panels, respectively); raw data (left panels) and with outliers removed (right panels). Note change in y-axes on left and right panels.

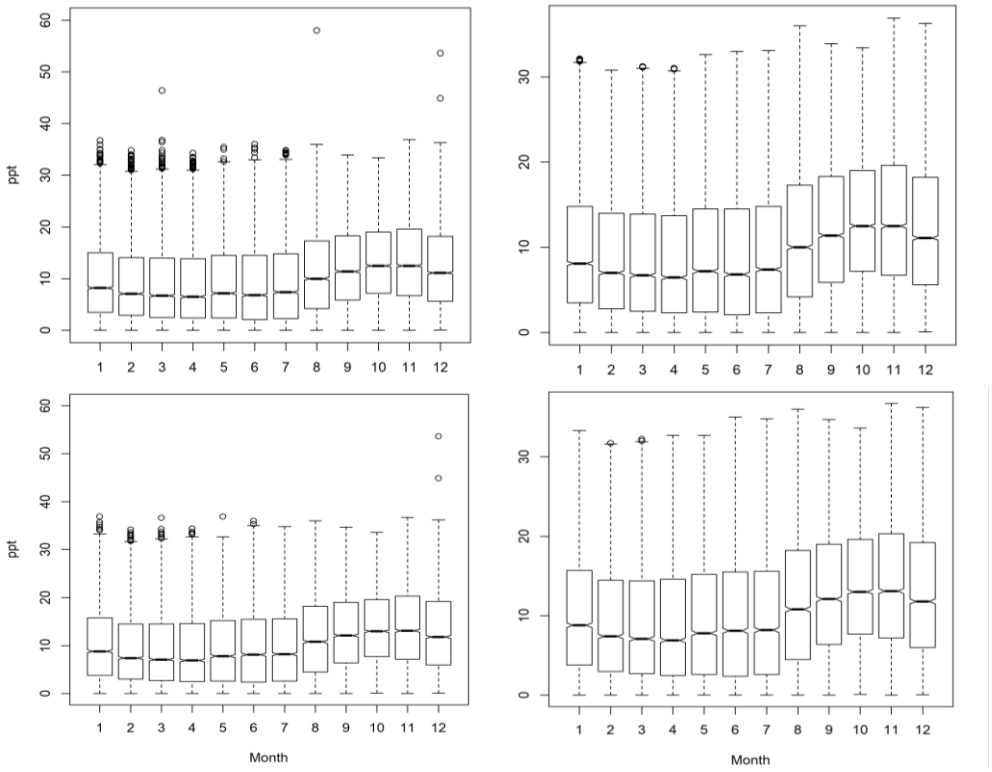

Figure 6. Salinity from the gillnet dataset collected at the top and bottom of the water column (top and bottom panels, respectively); raw data (left panels) and with outliers removed (right panels). Note change in y-axes.

Water temperature outliers in the electrofishing dataset were identified and removed using the same approach described for the seines, trawls, and gill nets. Outliers from the historical dataset (1990-2013) were analyzed separately from the present-day dataset (2014-2019) because of differences in the structure and organization of the datasets (Figure 7, Figure 8). The datasets were then merged once all outliers were removed. The salinity outlier approach differed from the seine, trawl, and gillnet gear types. The electrofishing sampling program mainly samples freshwater habitats, but brackish conditions are not uncommon. As a result, outliers detected in the boxplots were often brackish conditions that were considered ecologically reasonable for this sampling regime (Figure 9). As a result, these data points were not removed. Turbidity data in the electrofishing gear type were also examined for outliers, however numerous turbidity equipment types were reported in the dataset with different units used among them. It was not clear whether the correct unit of measure was assigned to the values, and as such, conversion from one unit to another became questionable. As a result, we determined that the turbidity data were not suitable for the purposes of model development, and this parameter was not used in the largemouth bass model.

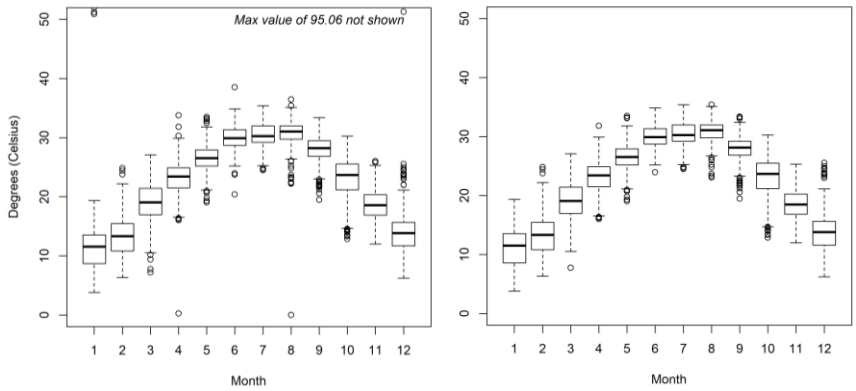

Figure 7. Water temperature from the electrofishing dataset collected at a single depth in the water column from 1990-2013; raw data (left panel) and with outliers removed (right panel).

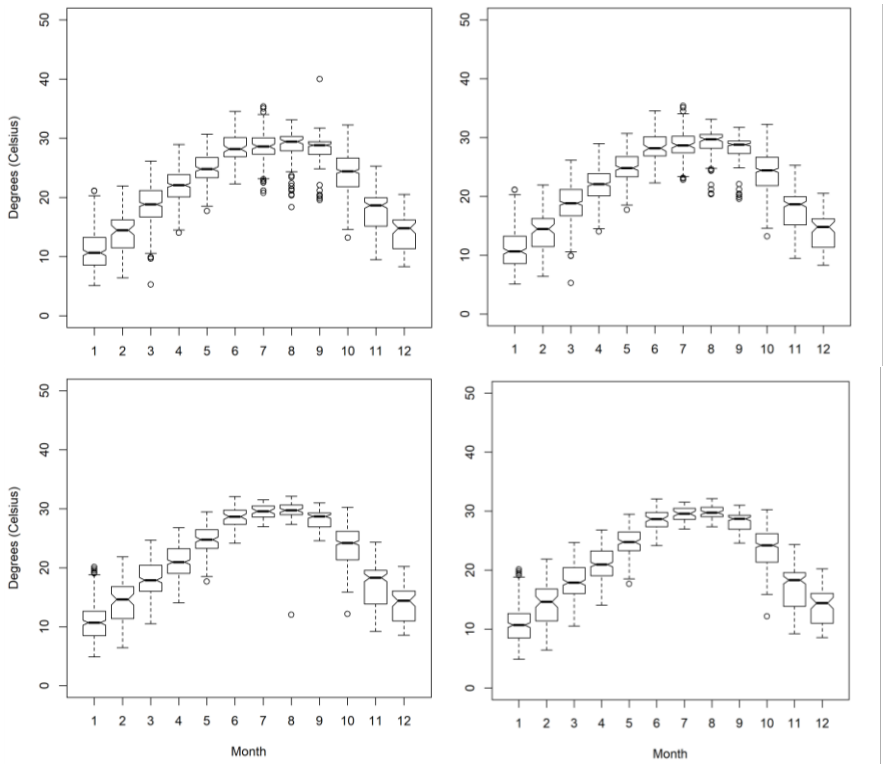

Figure 8. Water temperature from the electrofishing dataset collected at the top and bottom of the water column (top and bottom panels, respectively) from 2014-2019; raw data (left panels) and with outliers removed (right panels).

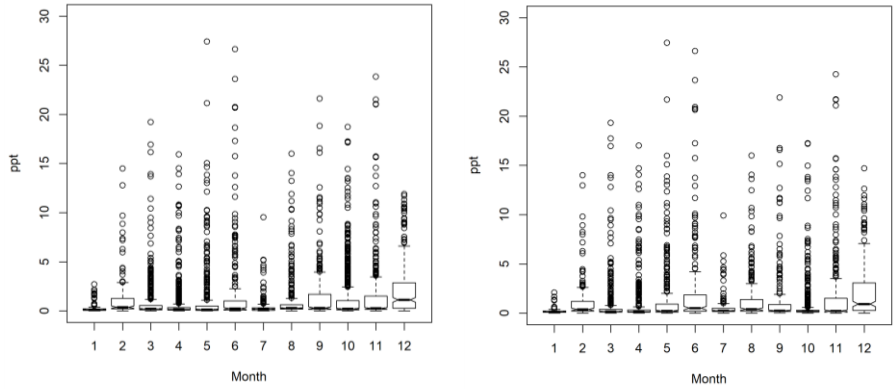

Figure 9. Salinity from the electrofishing dataset collected at the top and bottom of the water column (left and right panels, respectively) from 1990-2019.

Preparation of Biological Data

Catch per unit effort (CPUE) data were examined monthly using boxplots for all gear types. These plots allowed for identifying which months, over all years, had consistent catch relative to months that had variable or no catch. Patterns were then verified with the life history of the species to ensure the analysis was focused on those times of the year that the species was in the estuary (for migratory species). These plots can be found in Section 3 for each species.

Modeling Approach

For each species and gear type, we ran a series of generalized linear mixed models (GLMM) and a second series of generalized additive mixed models (GAMM) to estimate the effect that water temperature and salinity had on CPUE. For all models, we first cleaned the associated datasets to ensure no outliers or spurious data points occurred. We then standardized each predictor variable to a mean of 0 and a standard deviation of 1 (i.e., converted to z-scores) to ensure proper convergence across all models. In the following, we describe each model that was fit, how we assessed whether the data met model assumptions, and how we assessed model performance and accuracy. Before each model was fit, we split the species and gear-specific datasets into 'training' and 'testing' sets. We randomly selected 70% of the data to be our training set, while the remaining 30% was set aside as the testing set for model validation purposes.

Generalized linear mixed models were fit using Program R (R Core Team, 2019) and the packages 'lme4' (Bates et al., 2015) and 'glmmTMB' (Brooks et al., 2017). We fit four models that varied in error structure: a Gaussian, Poisson, negative binomial, and zero-inflated Poisson model. All models used CPUE as the response variable, but CPUE was transformed to a natural log + 1 in the Gaussian model to meet that model's assumption of normally distributed errors. Salinity, temperature, Julian date, and the interaction between temperature and salinity were predictor variables within the models. Because

we recognized that the relationships may be nonlinear, we also included a quadratic effect of temperature, salinity, and Julian date in the models. Finally, we included a random effect on the model's intercept of month nested within year to account for the occurrence of repeated samples within the same month and year within the dataset. The model call into R was thus: glmmTMB(CPUE ~ Salinity + Temperature + Salinity^2 + Temperature^2 + Salinity*Temperature + Julian date + Julian date^2 + (1|Year/Month)).

Generalized additive models were fit using Program R (R Core Team, 2019) and the package 'mgcv' (Wood et al., 2016). We fit four models that varied in error structure: a Gaussian, Poisson, negative binomial, and zero-inflated Poisson model. All models used CPUE as the response variable, but CPUE was transformed to a natural log + 1 in the Gaussian model to meet that model's assumption of normally distributed errors. Salinity, temperature, and Julian date were predictor variables within the models and modeled using a spline-based smoothing function. We also included a random effect modeled as a spline-based smoothing function of month nested within year to account for the occurrence of repeated samples within the same month and year within the dataset. The model call into R was thus: gam(CPUE ~ s(Salinity) + s(Temperature) + s(Julian date) + s(Year, Month, bs='re')).

Spatial autocorrelation, or the tendency for data closer together in space to be more similar, is a well-known phenomenon in ecology (Legendre, 1993) and its presence within the data can influence the fitted model. The presence of spatial autocorrelation can both impact the coefficient estimates and the strength of the relationships within a model (Lichstein et al., 2002). In models of habitat suitability or species distribution, accounting for spatial autocorrelation within the observation data can change predictor variable importance and improve the fit (or reduce levels of uncertainty; Dormann, 2007). We conducted a preliminary analysis to examine whether spatial autocorrelation is present within models by generating correlograms of the Moran's I statistic on model residuals plotted at varying distances (Bjornstad & Falk, 2001; Dormann, 2007) using the 'ncf' package in R (Bjornstad, 2020) for the seine data. Our preliminary results revealed very little evidence of spatial autocorrelation present within the residuals of the model for the seine data. During this exercise, it also became apparent there was considerable uncertainty in the accuracy of sample site coordinates, which meant we would not be fully confident in our autocorrelation analysis. Because of this uncertainty, we did not attempt to assess spatial autocorrelation in the models for this iteration of model improvements.

Model Selection

We examined several metrics with which to compare the performance of each model to one another. First, we plotted the response of CPUE to changes in salinity and temperature as predicted by each model while holding all other predictor variables at their mean. By examining the response and associated 95% confidence intervals, we could determine the amount of uncertainty associated with the model's predictions and whether the model predicted relationships that made biological sense. Additionally, we constructed heat maps to examine the relationship between salinity and temperature on

CPUE for each model. Similarly, we used these plots to determine whether the relationships derived from the fitted models made biological sense and could reasonably be used to construct a habitat suitability model. Second, we calculated model R^2 values using the 'MuMIn' package (Barton, 2009) in R to determine how much of the variance in CPUE was explained by the model's predictor variables and random effects. In mixed models, we can calculate a marginal and conditional R^2 value. The marginal R^2 provides an indication of the variance explained by only the fixed effects in the model, while the conditional R^2 provides an indication of the variance explained by the entire model—fixed and random effects (Nakagawa & Schielzeth, 2013). R^2 values range from 0 to 1, with values closer to 1 indicating a model with more explanatory power (a value of 1 indicates a perfect model). It is important to note that for zero-inflated Poisson models, there is not a straightforward way to calculate R^2 that is comparable to the other models we ran, thus we did not report R^2 values for models run with a zero-inflated Poisson error structure. Third, we calculated the root mean squared error (RMSE) for each model to compare how close, on average, the fitted values from the model were to the data used to train the model. Relative to other models run with the same data, a smaller RMSE value indicates more accurate fitted values (Gotelli & Ellison, 2004). For GAMMs, we also report the deviance explained by the model, which is sometimes preferred to R^2 values for models that do not use a Gaussian error structure. The deviance explained can be interpreted in the same way as R^2: a value closer to 100% represents a model that explains more of the variance within CPUE (Gotelli & Ellison, 2004).

Sometimes, models fail to converge to reasonable estimates due to problems with model specification or the nature of the data used to fit the model. In these situations, a model that fails to converge could produce nonsensical estimates or no estimates at all. In these cases, the R packages used to fit the models will throw a non-convergence warning or error indicating that the model could not converge and that output from these models should not be used for inference.

We validated each model using several metrics and diagnostic plots. First, for each model, we regressed the observed CPUE in the testing dataset against predicted CPUE using the fitted model of interest. Then, we calculated R^2 and RMSE values against this new regression under the assumption that the predicted and observed CPUE using the testing dataset should have a strong relationship if the model predicts well (Gotelli & Ellison, 2004). Thus, a high R^2 value and low RMSE value during validation indicate a model that more accurately predicts CPUE on pseudo-independent data. Additionally, we calculated the correlation coefficient between observed and predicted CPUE as an additional metric of how closely the two values are related. The closer the correlation coefficient was to 1, the better the model was at predicting CPUE of the testing dataset. Finally, we plotted predicted CPUE against actual CPUE using the testing dataset as an additional visual diagnostic.

We collectively used the performance metrics, response curves, and validation results to eliminate models for consideration that did not perform statistically well (e.g., low R^2, high RMSE) or did not result in response curves that were ecologically reasonable. When the model performance metrics were

similar among models, we selected the model whose response curves were most ecologically reasonable (i.e., consistent with information of the species' life history, spatial distribution, and salinity and temperature tolerances). These decisions were based on expert opinion by collaborators familiar with the species and underlying datasets. Future efforts may consider a model ensemble approach where multiple competing models are averaged to produce a robust model that incorporates the strengths of all modeling approaches.

For the final selected model, we reviewed a series of diagnostic plots to determine whether the model's main assumptions were met. First, we plotted the Pearson (in Gaussian models) or deviance (in non-Gaussian models) residuals against the fitted values to look for unexplainable patterns. An ideal residual plot should show a random spread of residuals around the zero line (Gotelli & Ellison, 2004). Second, we examined whether the choice of error structure was appropriate for the model by examining normal quantile-quantile (Q-Q) plots and the distributions of the response variables via histograms. In a Gaussian model, the data quantiles should remain close to the Q-Q line within the plot. For other error structures, the data should not follow the line within the Q-Q plot, but histograms of the CPUE variable should reveal a shape akin to the distribution used within the model (e.g. Poisson, zero-inflated Poisson, or negative binomial). For models run as GAMMs, we also checked the basis dimension values for each smooth term to ensure the correct number of knots were present. This is done by comparing the estimated degrees of freedom (edf) to the number of knots used in modeling and generating a p-value from this comparison. If the p-value is non-significant, this is an indication that the number of knots selected for the smooth term is adequate (Wood, 2017).

3.0 RESULTS

Model results for each species are presented below. Gear type is referenced to facilitate crosswalk between sections of this report and to differentiate species where two models were developed. A brief overview of the models' performance and validation is provided, followed by a series of graphs and tables that provide opportunities for additional interpretation and inspection of results, where desired by the reader. Lastly, we identify which water quality model was ultimately selected for inclusion in the final HSI model for the species. Although all response curves use the same ranges of salinity and temperature on their axes, the models should only be applied to the data range used in each of the analyses, as shown in the figures provided in the *Preparation of Environmental Data* subsection and indicated below for each species.

Small Juvenile Brown Shrimp (Seines)

Examination of mean CPUE by month, averaged over all years of available seine data, indicated that small juvenile brown shrimp were collected in highest numbers from April through July (Figure 10). These months are consistent with the time period when recently-settled juvenile brown shrimp are

utilizing shallow estuarine habitats as a nursery. The environmental and biological data were subset to include the months of April through July, resulting in 5108 unique data points; 70% of the data points were used for model development and 30% were used for model validation. Water temperature during this time period ranged from 12.9 to 35.2°C; whereas salinity ranged from 0 to 33 ppt.

The Poisson and Zero-Inflated Poisson GLMM resulted in higher R^2 than any other model, followed by Gaussian GAMM (Table 1). Zero-Inflated Poisson GAMM had the highest deviance explained relative to other error structures. RMSE were generally similar among the GAMM and GLMM error structures. Examination of the response curves indicate the Gaussian GLMM and Poisson GLMM captured the expected response to salinity and temperature in a biologically defensible way, more so than the other models (Figure 11 through Figure 16). Model validation results reveal high R^2 and correlation values for Gaussian GAMM and Gaussian GLMM, while RMSE were generally similar among models (Table 2, Figure 17, Figure 18). Given these results, the Gaussian GLMM was selected for inclusion in the overall HSI model for small juvenile brown shrimp because the response curves were biologically feasible and validation results performed generally well, relative to other models. Diagnostic plots for the selected model are provided in Figure 19 for reference purposes.

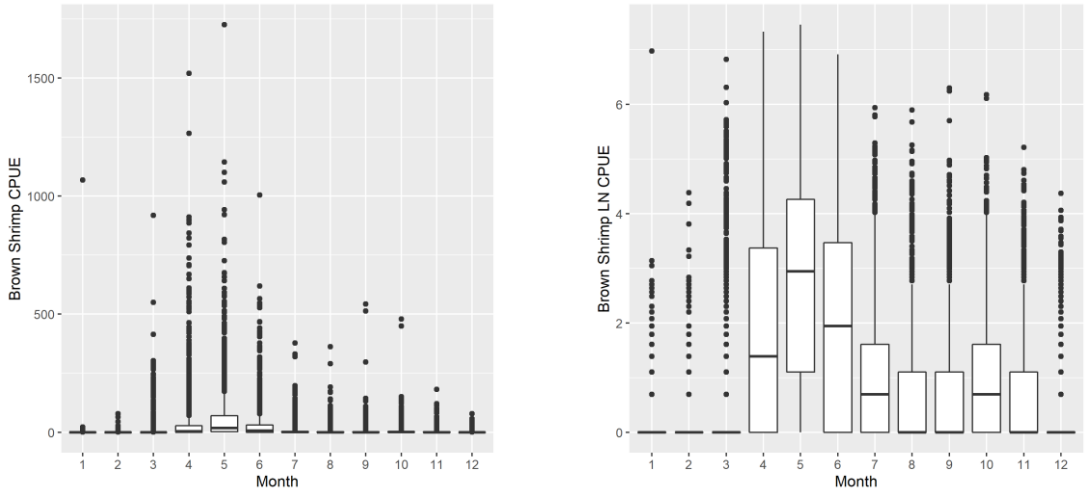

Figure 10. Small juvenile brown shrimp CPUE in seines; raw scale (left panel), natural log scale (right panel)

Table 1. Summary of model fit metrics for small juvenile brown shrimp. *Denotes selected model.

Model Approach	Error Structure	Adjusted R^2	Deviance explained (GAMM only)	RMSE
GAMM	Gaussian	0.30	31.7%	91.06
	Poisson	0.15	32%	81.91
	Zero-Inflated Poisson	.	96.1%	82.32
	Negative Binomial	0.09	28.5%	85.05
GLMM	*Gaussian	0.25	.	91.62
	Poisson	0.98	.	82.77
	Zero-Inflated Poisson	0.58	.	83.79
	Negative Binomial	0.06	.	84.03

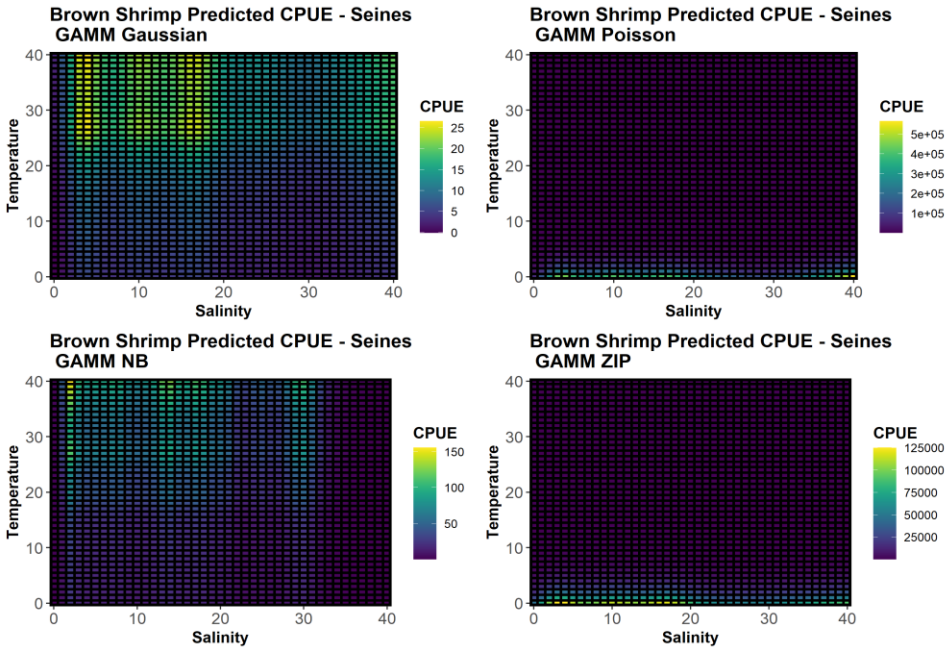

Figure 11. GAMM predicted response of small juvenile brown shrimp CPUE to salinity and temperature.

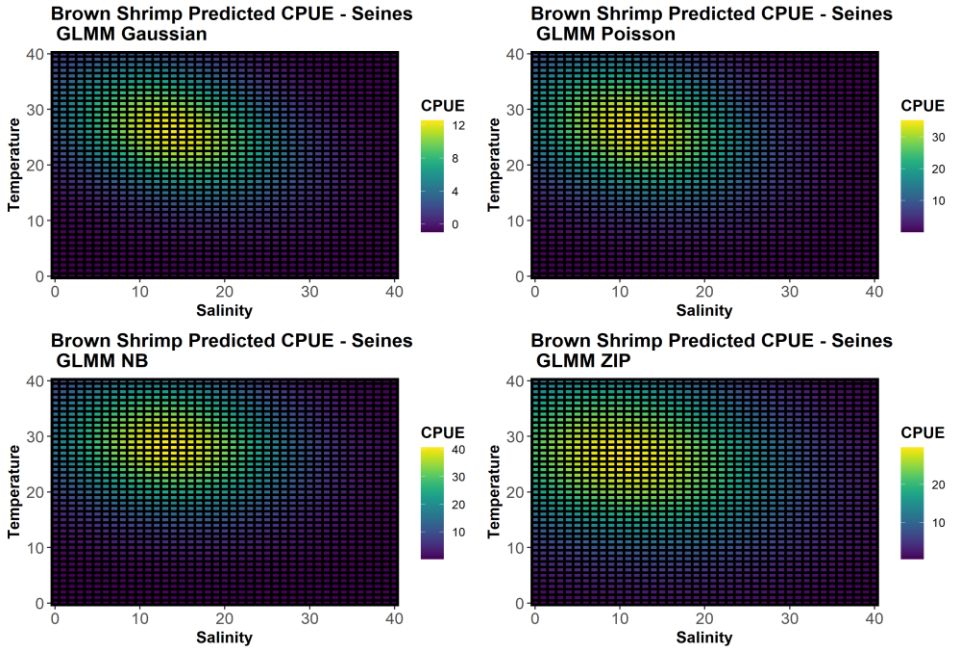

Figure 12. GLMM predicted response of small juvenile brown shrimp CPUE to salinity and temperature.

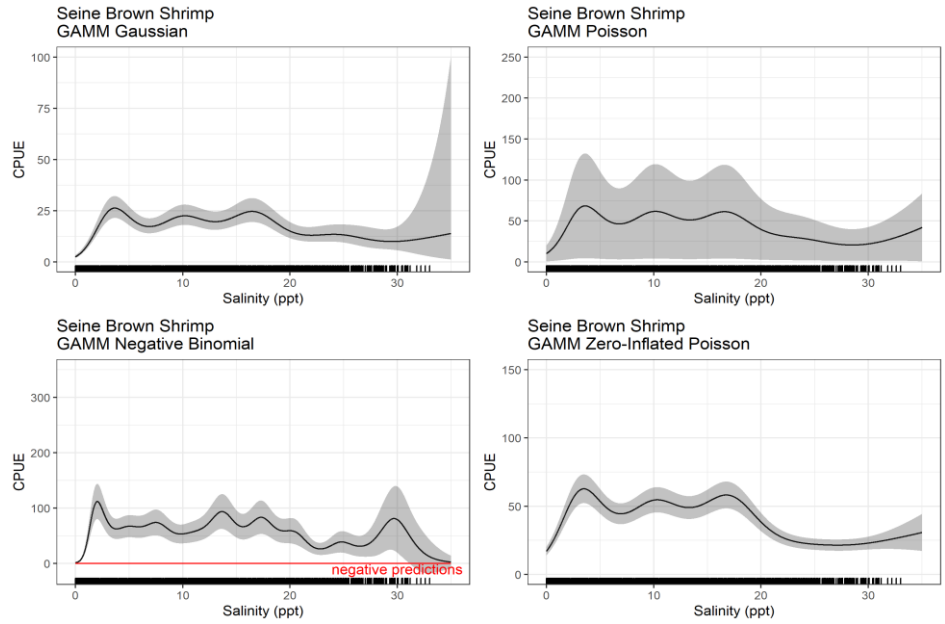

Figure 13. GAMM predicted response of small juvenile brown shrimp CPUE to salinity, with other variables held constant. Shaded gray area represents 95% confidence interval.

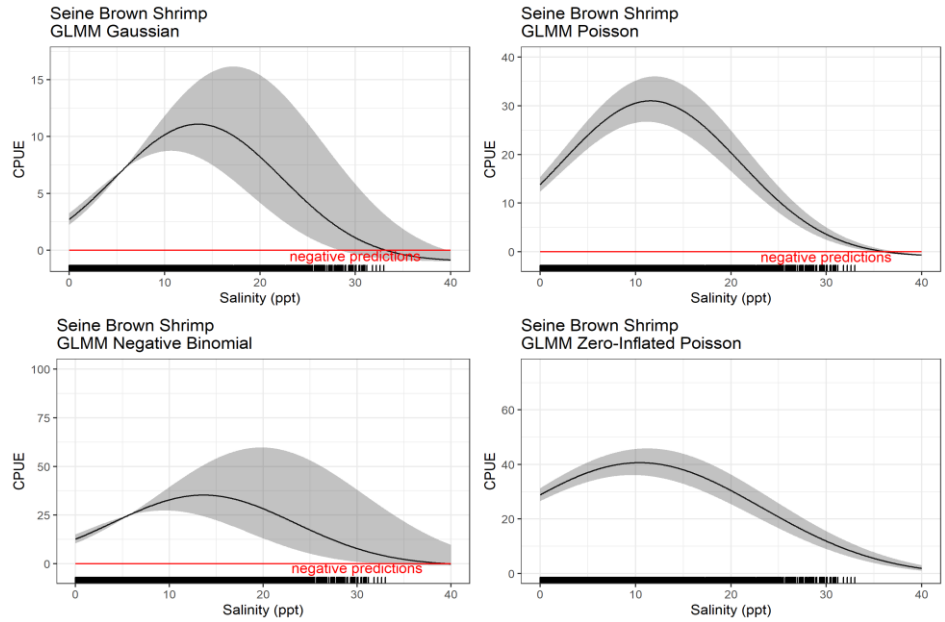

Figure 14. GLMM predicted response of small juvenile brown shrimp CPUE to salinity, with other variables held constant. Shaded gray area represents 95% confidence interval.

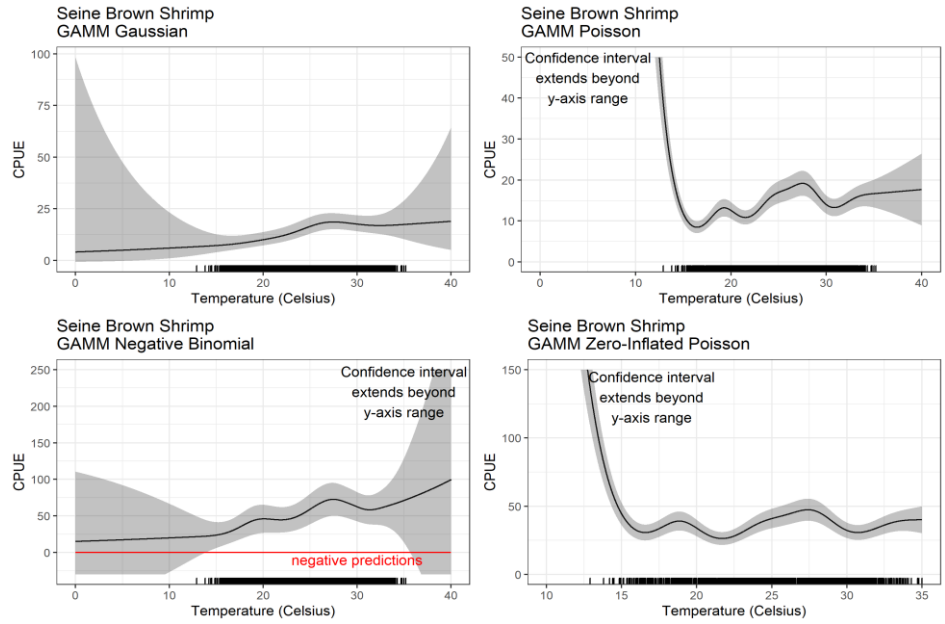

Figure 15. GAMM predicted response of small juvenile brown shrimp CPUE to temperature, with other variables held constant. Shaded gray area represents 95% confidence interval.

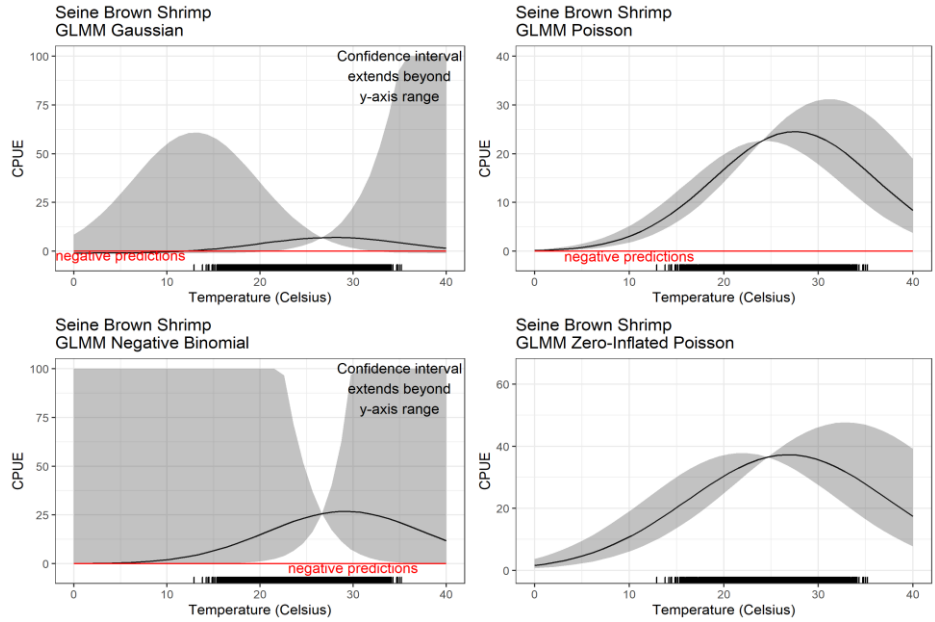

Figure 16. GLMM predicted response of small juvenile brown shrimp CPUE to temperature, with other variables held constant. Shaded gray area represents 95% confidence interval.

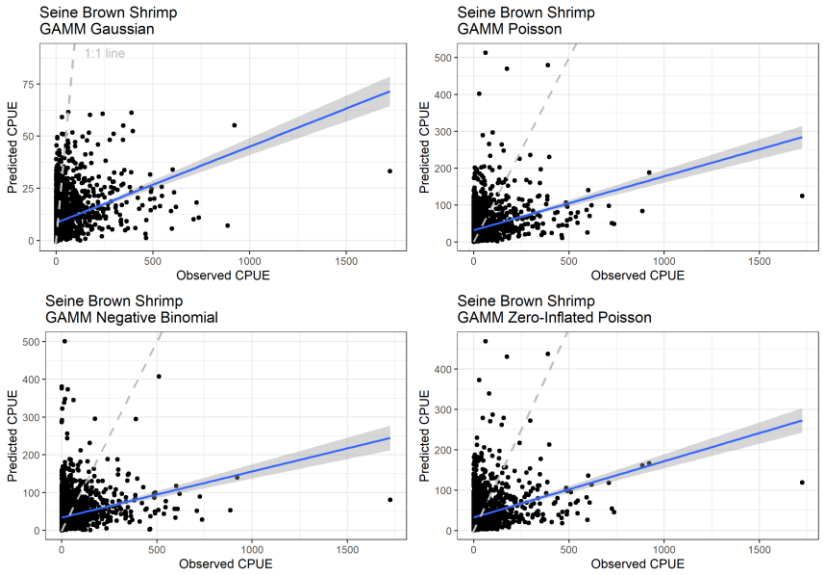

Figure 17. GAMM predicted small juvenile brown shrimp CPUE plotted against observed CPUE using the 30% randomly selected testing dataset. Dashed line provided for reference purposes of 1:1 relationship. Blue line indicates linear relationship between predicted and observed.

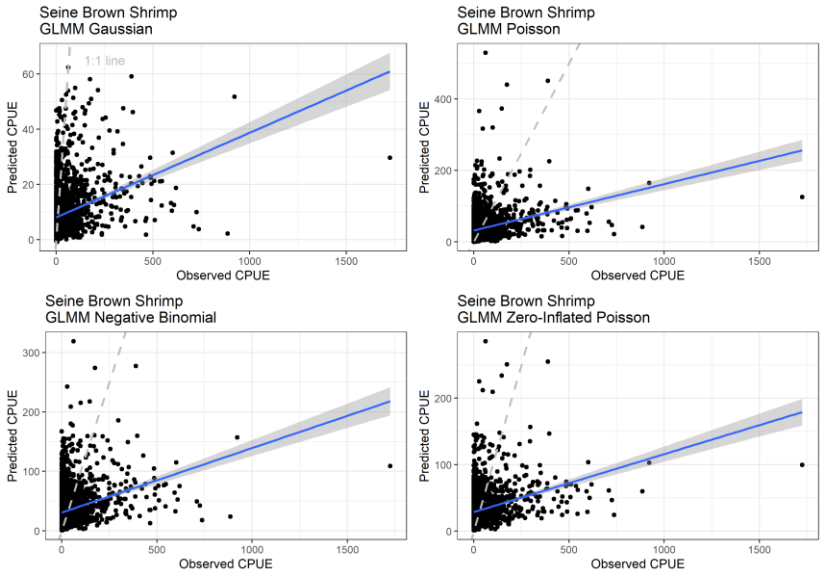

Figure 18. GLMM predicted small juvenile brown shrimp CPUE plotted against observed CPUE using the 30% randomly selected testing dataset. Dashed line provided for reference purposes of 1:1 relationship. Blue line indicates linear relationship between predicted and observed.

Table 2. Summary of model validation metrics for small juvenile brown shrimp. *Denotes selected model.

Model Approach	Error Structure	Adjusted R^2	Correlation	RMSE
GAMM	Gaussian	0.30	0.55	94.15
	Poisson	0.10	0.32	88.70
	Zero-Inflated Poisson	0.10	0.31	89.25
	Negative Binomial	0.07	0.26	92.08
GLMM	*Gaussian	0.25	0.50	94.80
	Poisson	0.09	0.30	89.66
	Zero-Inflated Poisson	0.09	0.30	88.86
	Negative Binomial	0.10	0.31	88.39

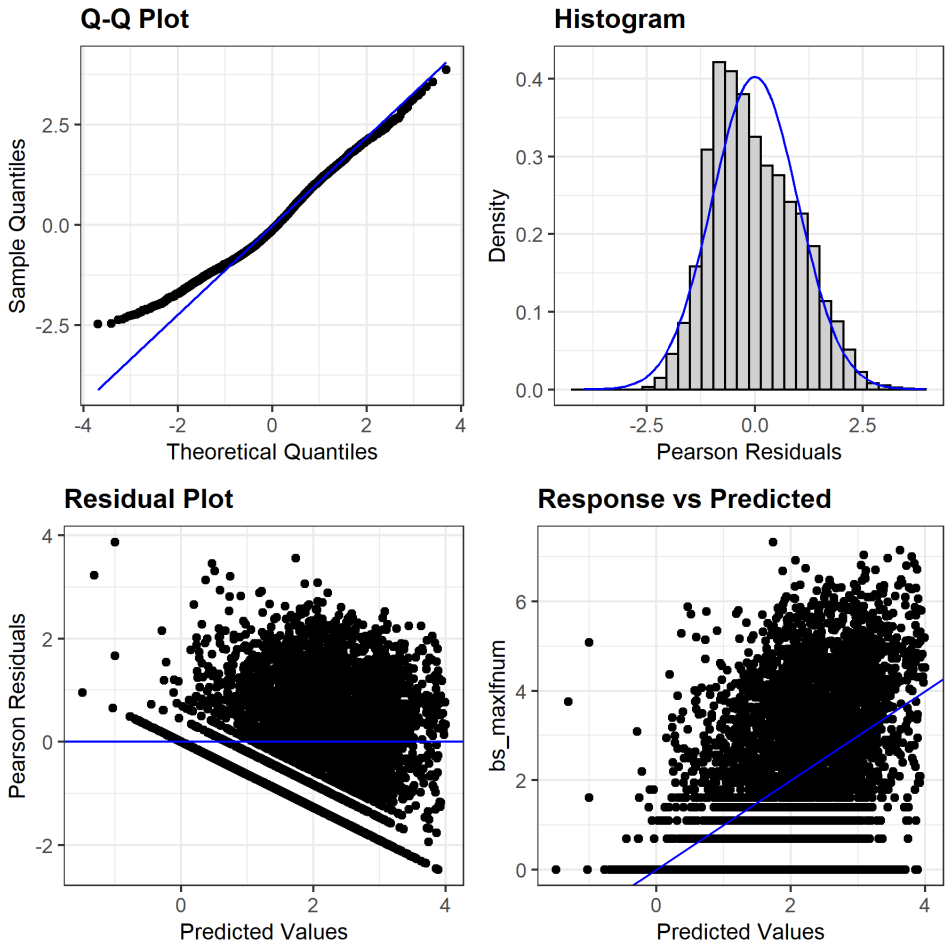

Figure 19. Gaussian GLMM diagnostic plots for small juvenile brown shrimp.

Large Juvenile Brown Shrimp (16-foot Trawls)

Examination of mean CPUE by month, averaged over all years of available 16-foot trawl data, indicated that brown shrimp were collected in highest numbers from April through July (Figure 20). These collections represent larger juveniles that moved from shallow habitats into deeper estuarine habitats prior to emigration offshore. The 16-foot trawl environmental and biological data were subset to include the months of April through July, resulting in 22,241 unique data points; 70% of the data points were used for model development and 30% were used for model validation. Water temperature during this time period ranged from 11.7 to 35.2°C; whereas salinity ranged from 0 to 37 ppt.

The Poisson GLMM resulted in higher R^2, followed by Zero-Inflated Poisson GLMM and Gaussian GAMM (Table 3). Zero-Inflated Poisson GAMM had highest deviance explained, while RMSE was similar among all of the models. Examination of the response curves indicate the Gaussian GLMM captured the expected response to salinity and temperature in a biologically defensible way, more so than any other model (Figure 21 through Figure 26). Although the shape of the response curves within the GLMMs were similar (Figure 24 and Figure 26), the interacting effect of salinity and temperature in the Gaussian GLMM was considered biological defensible (Figure 22). Model validation results indicated highest R^2 and correlation values for Gaussian GAMM and Gaussian GLMM relative to other models (Table 4, Figure 27, Figure 28). Given these results, the Gaussian GLMM was selected for inclusion in the overall HSI model for large juvenile brown shrimp. Diagnostic plots for the selected model are provided in Figure 29 for reference purposes.

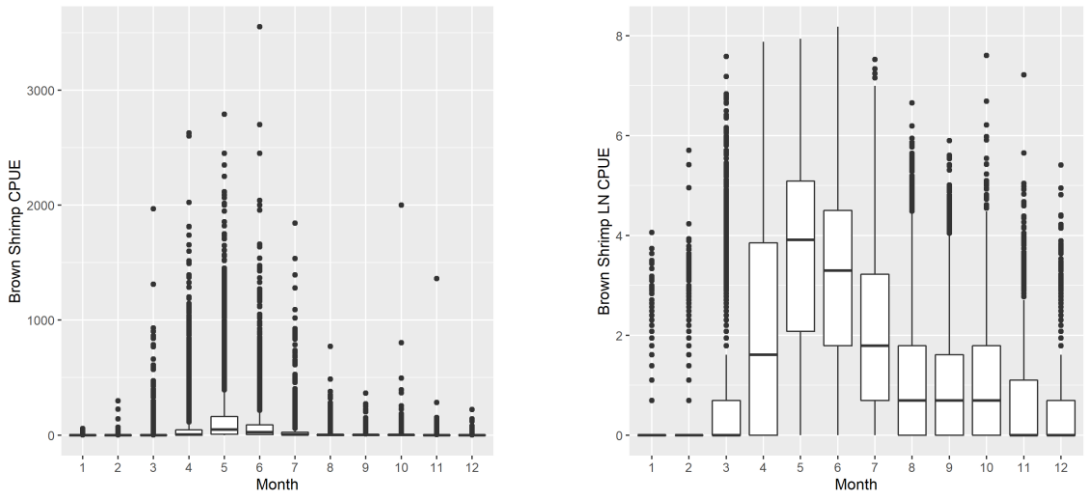

Figure 20. Large juvenile brown shrimp CPUE in 16-foot trawl; raw scale (left panel), natural log scale (right panel).

Table 3. Summary of model fit metrics for large juvenile brown shrimp. *Denotes selected model.

Model Approach	Error Structure	Adjusted R^2	Deviance explained (GAMM only)	RMSE
GAMM	Gaussian	0.33	34%	159.04
	Poisson	0.14	29.1%	145.61
	Zero-Inflated Poisson	.	100%	145.72
	Negative Binomial	0.11	23.8%	148.45
GLMM	*Gaussian	0.28	.	159.62
	Poisson	0.98	.	145.25
	Zero-Inflated Poisson	0.36	.	146.33
	Negative Binomial	0.09	.	146.40

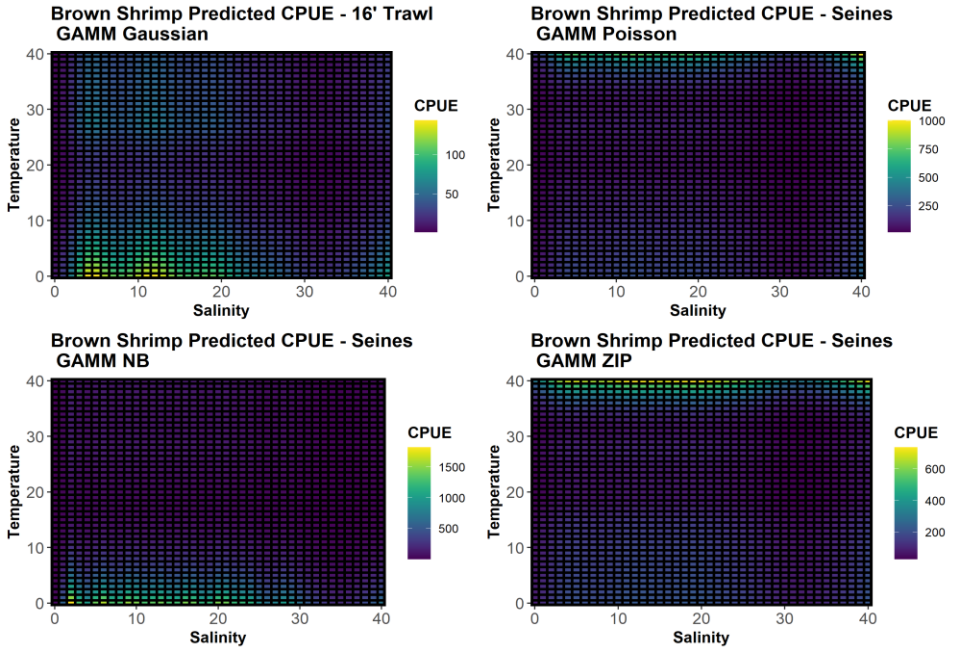

Figure 21. GAMM predicted response of large juvenile brown shrimp CPUE to salinity and temperature.

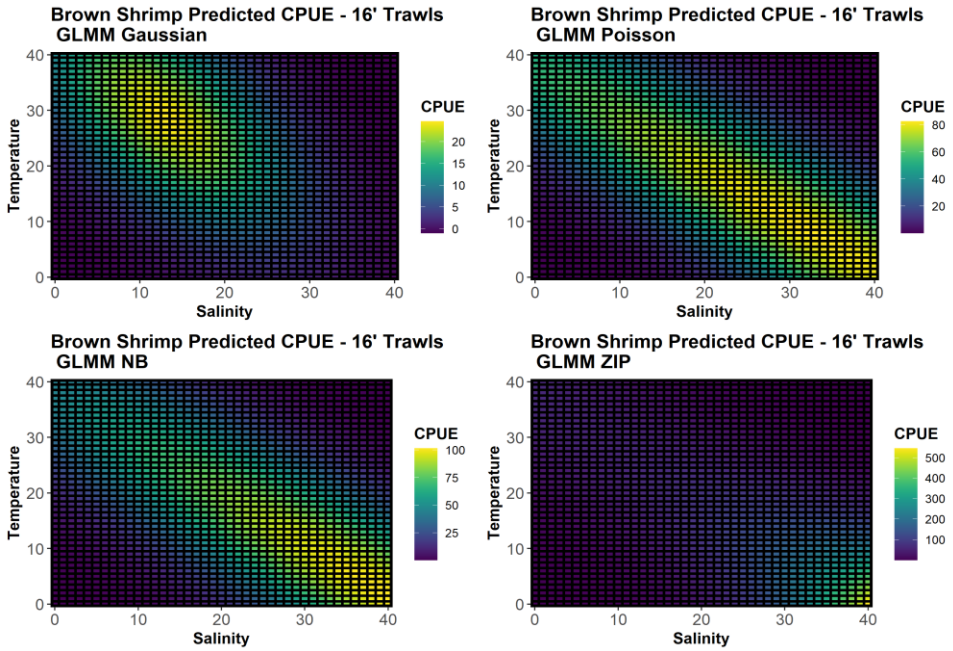

Figure 22. GLMM predicted response of large juvenile brown shrimp CPUE to salinity and temperature.

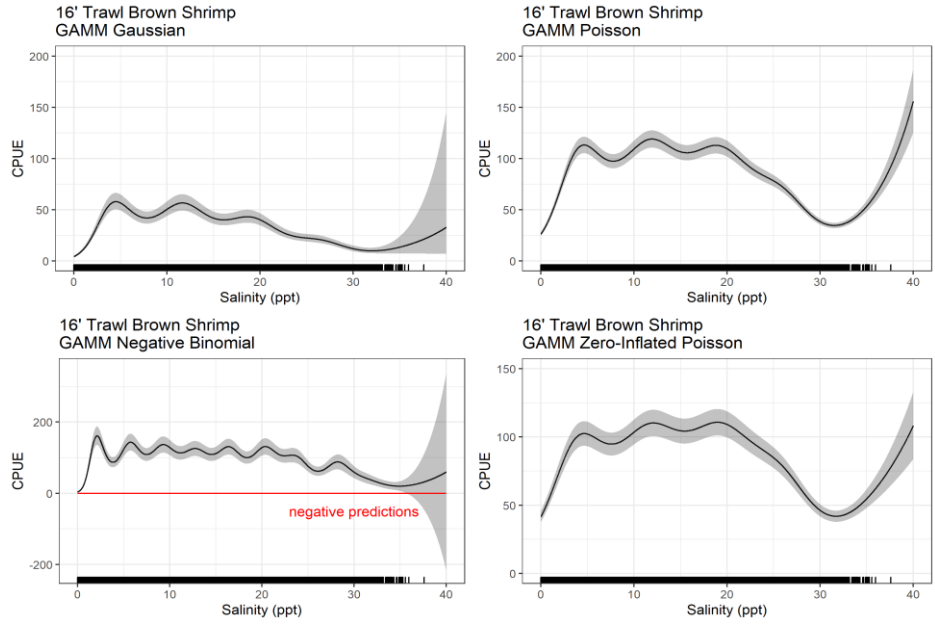

Figure 23. GAMM predicted response of large juvenile brown shrimp CPUE to salinity, with other variables held constant. Shaded gray area represents 95% confidence interval.

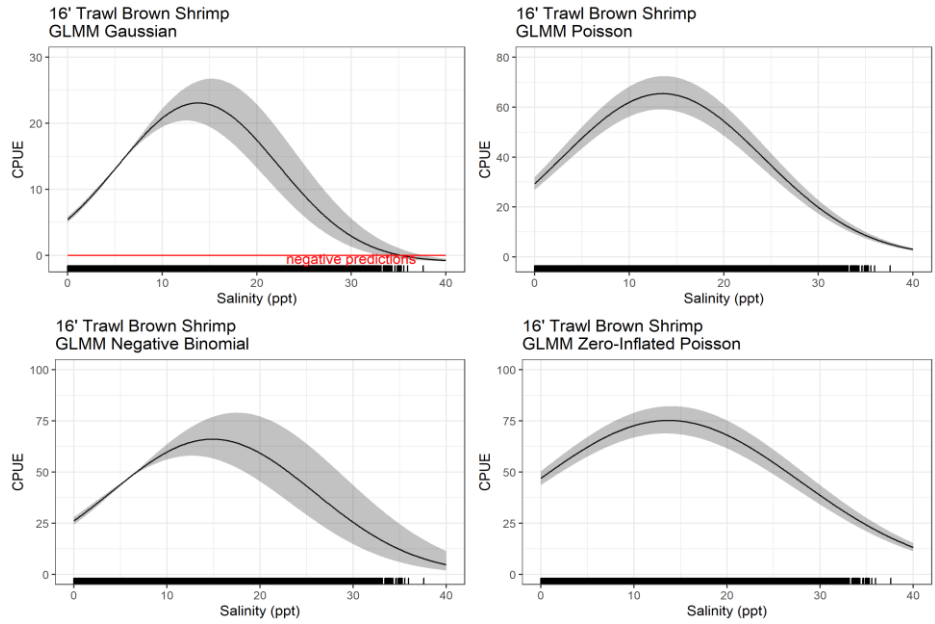

Figure 24. GLMM predicted response of large juvenile brown shrimp CPUE to salinity, with other variables held constant. Shaded gray area represents 95% confidence interval.

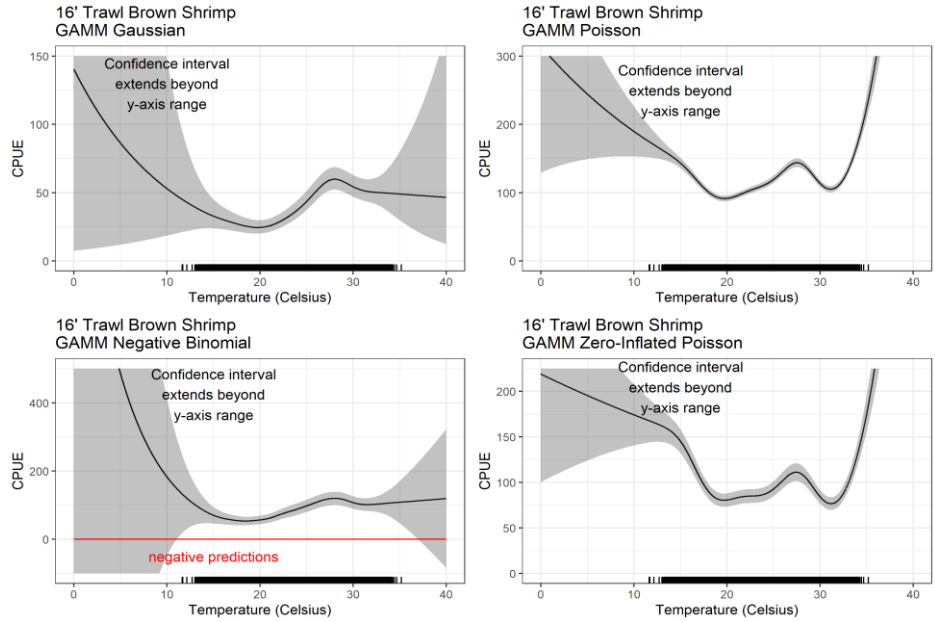

Figure 25. GAMM predicted response of large juvenile brown shrimp CPUE to temperature, with other variables held constant. Shaded gray area represents 95% confidence interval.

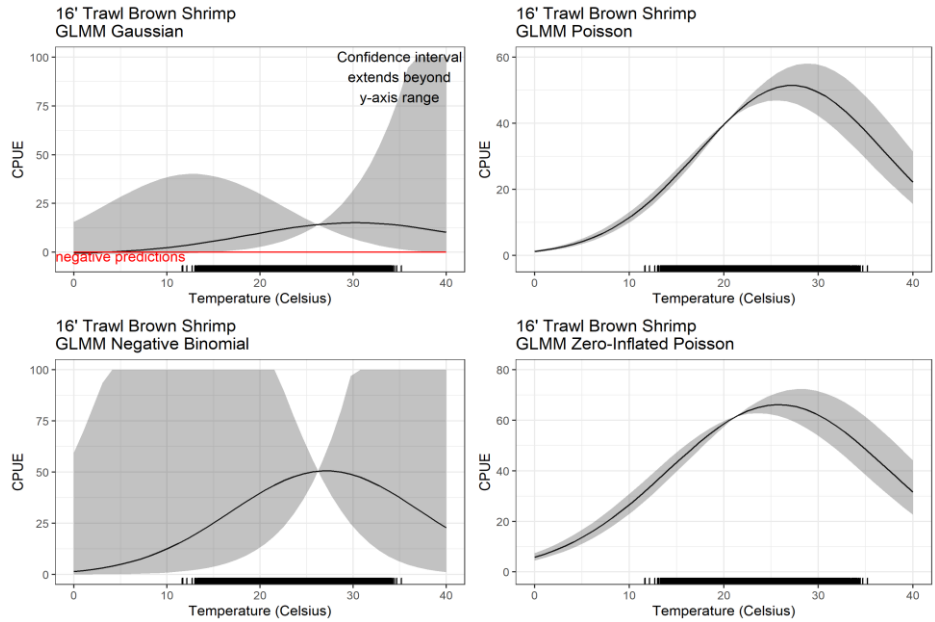

Figure 26. GLMM predicted response of large juvenile brown shrimp CPUE to temperature, with other variables held constant. Shaded gray area represents 95% confidence interval.

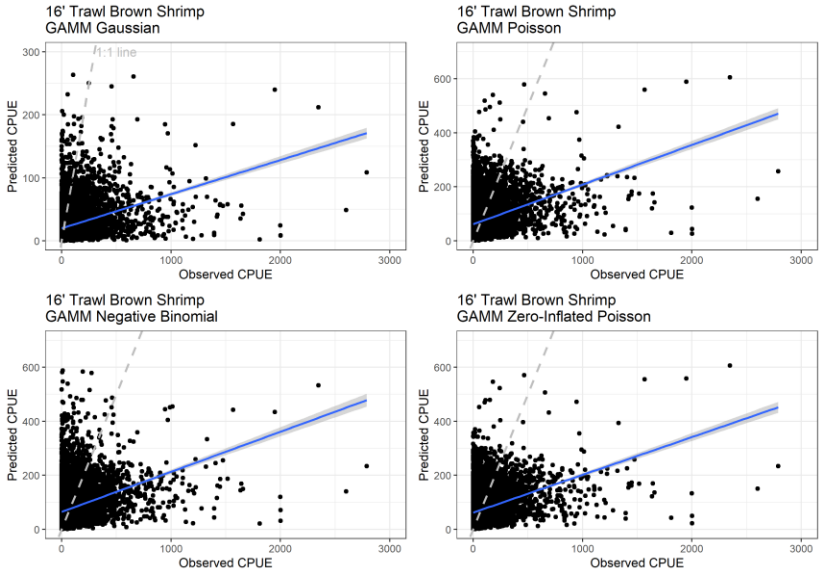

Figure 27. GAMM predicted large juvenile brown shrimp CPUE plotted against observed CPUE using the 30% randomly selected testing dataset. Dashed line provided for reference purposes of 1:1 relationship. Blue line indicates linear relationship between predicted and observed.

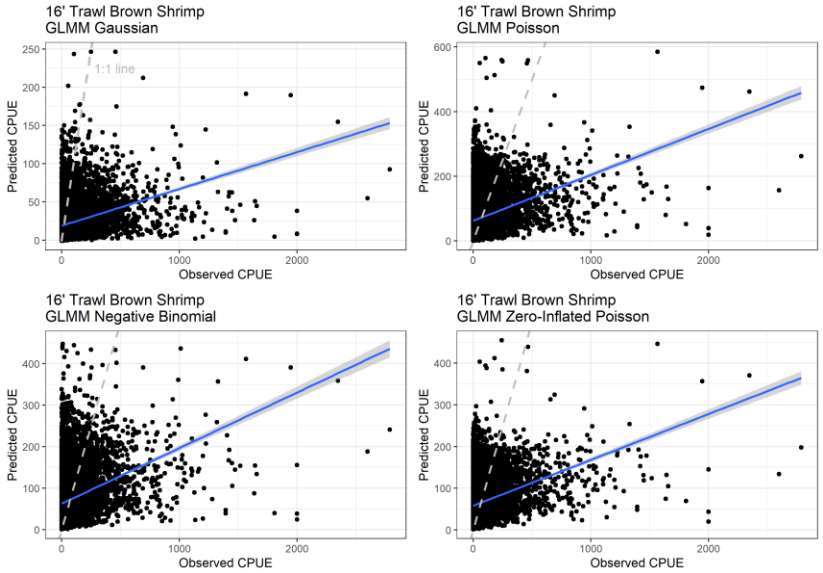

Figure 28. GLMM predicted large juvenile brown shrimp CPUE plotted against observed CPUE using the 30% randomly selected testing dataset. Dashed line provided for reference purposes of 1:1 relationship. Blue line indicates linear relationship between predicted and observed.

Table 4. Summary of model validation metrics for large juvenile brown shrimp. *Denotes selected model.

Model Approach	Error Structure	Adjusted R^2	Correlation	RMSE
GAMM	Gaussian	0.32	0.56	160.28
	Poisson	0.13	0.36	148.88
	Zero-Inflated Poisson	0.13	0.35	149.10
	Negative Binomial	0.11	0.32	152.20
GLMM	*Gaussian	0.28	0.53	161.32
	Poisson	0.12	0.35	149.21
	Zero-Inflated Poisson	0.12	0.35	149.51
	Negative Binomial	0.11	0.34	150.20

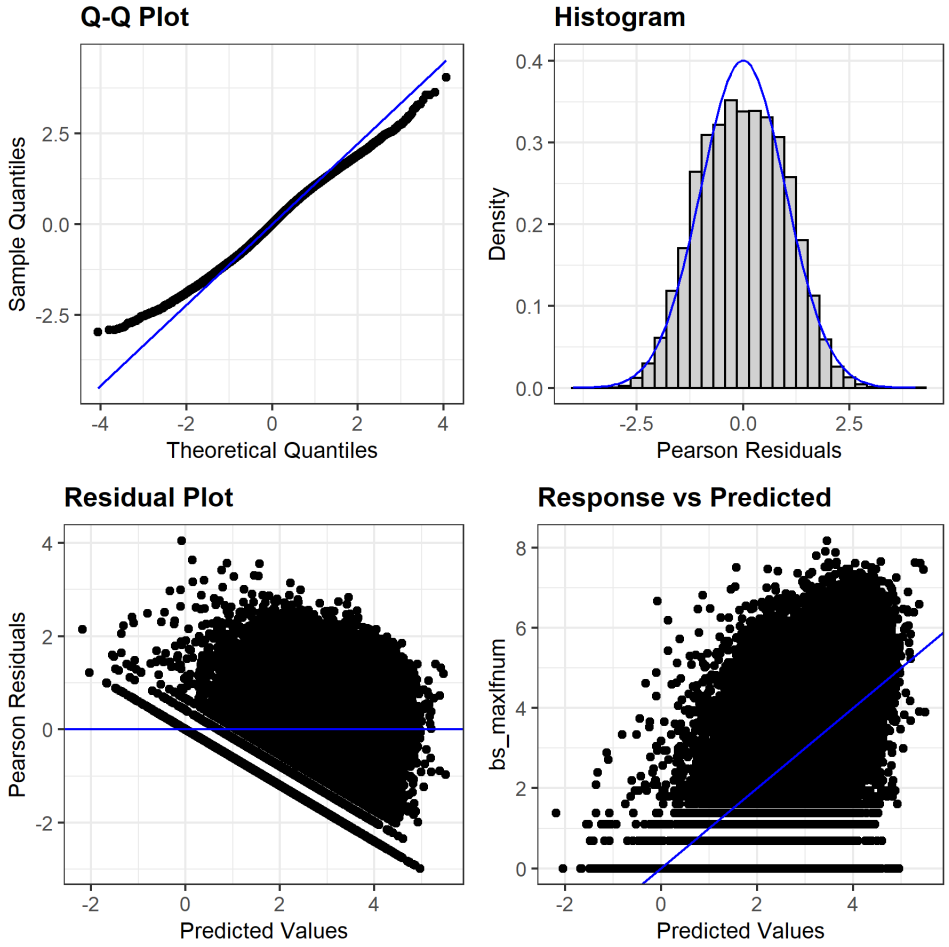

Figure 29. Gaussian GLMM diagnostic plots for large juvenile brown shrimp.

Small Juvenile White Shrimp (Seines)

Examination of mean CPUE by month, averaged over all years of available seine data, revealed that small juvenile white shrimp were collected in highest numbers from June through December (Figure 30). These months are consistent with the time period when recently-settled juvenile white shrimp are utilizing shallow estuarine habitats as a nursery. The seine environmental and biological data were subset to include the months of June through December, resulting in 11,197 unique data points; 70% of the data points were used for model development and 30% were used for model validation. Water temperature during this time period ranged from 4.7 to 35.2°C; whereas salinity ranged from 0 to 37 ppt.

The Poisson and Zero-Inflated Poisson GLMM resulted in higher R^2 than any other model and RMSE were similar among all models (Table 5). Zero-Inflated Poisson GAMM had highest deviance explained. Examination of the response curves indicated the Gaussian GLMM, Negative Binomial GLMM, and Gaussian GAMM captured the expected response to salinity and temperature in a biologically defensible way, more so than other model (Figure 31 through Figure 36). Model validation results indicated relatively low R^2 values for all models, similar RMSE values among models, and higher correlation values for Gaussian GAMM and Gaussian GLMM, relative to other models (Table 6, Figure 37, Figure 38). Given these results, the Gaussian GLMM was selected for inclusion in the overall HSI model for small juvenile white shrimp because the response curves were biologically defensible. Diagnostic plots (Figure 39) for the selected model are provided for reference purposes.

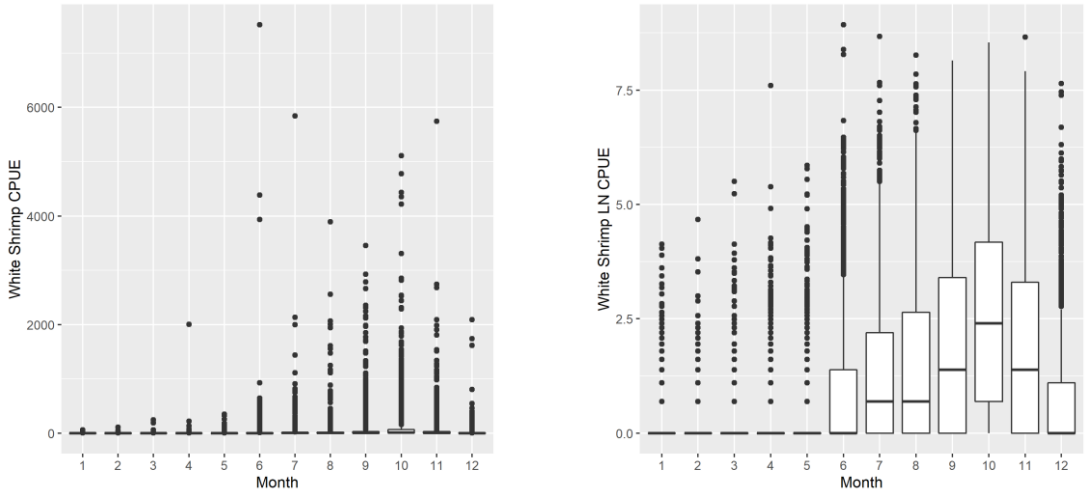

Figure 30. Small juvenile white shrimp CPUE in seines; raw scale (left panel), natural log scale (right panel).

Table 5. Summary of model fit metrics for small juvenile white shrimp. *Denotes selected model.

Model Approach	Error Structure	Adjusted R^2	Deviance explained (GAMM only)	RMSE
GAMM	Gaussian	0.18	19.1%	218.54
	Poisson	0.09	28.1%	203.63
	Zero-Inflated Poisson	.	99.4%	204.20
	Negative Binomial	0.06	22.1%	207.29
GLMM	*Gaussian	0.16		218.73
	Poisson	0.99		206.41
	Zero-Inflated Poisson	0.62		207.90
	Negative Binomial	0.05		208.56

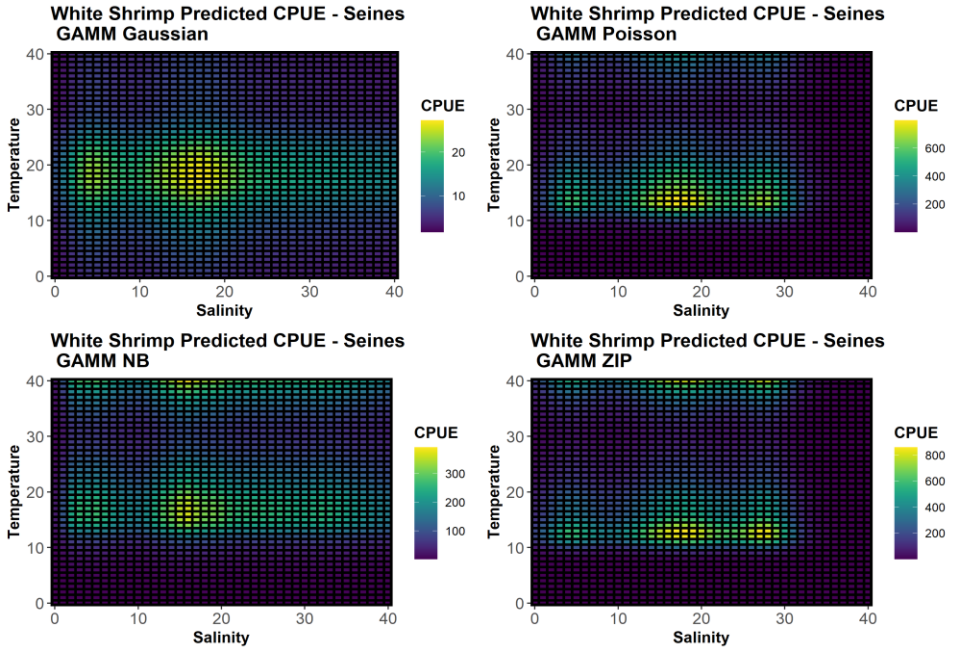

Figure 31. GAMM predicted response of small juvenile white shrimp CPUE to salinity and temperature.

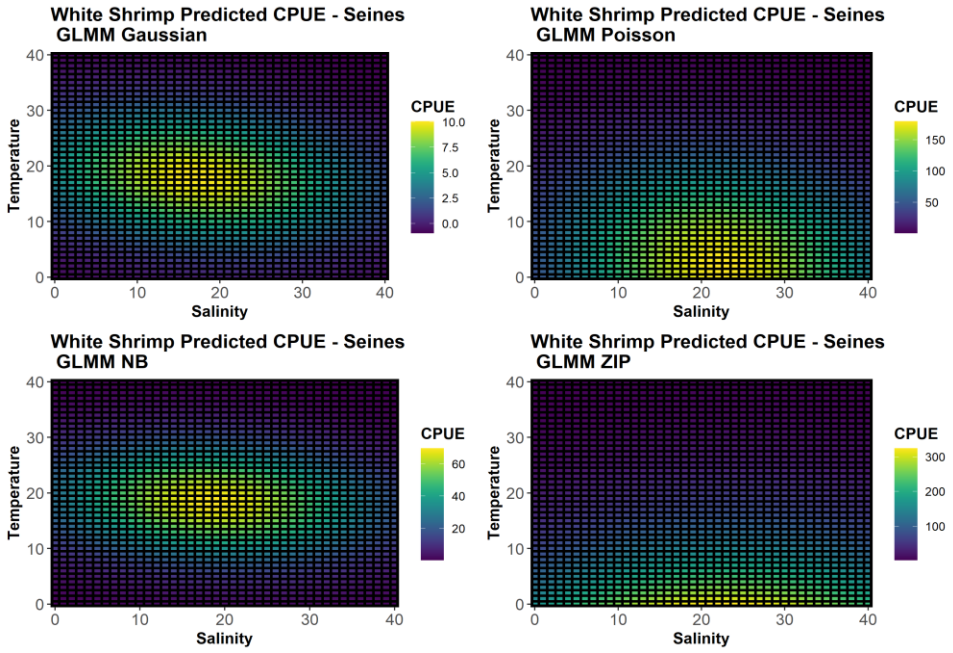

Figure 32. GLMM predicted response of small juvenile white shrimp CPUE to salinity and temperature.

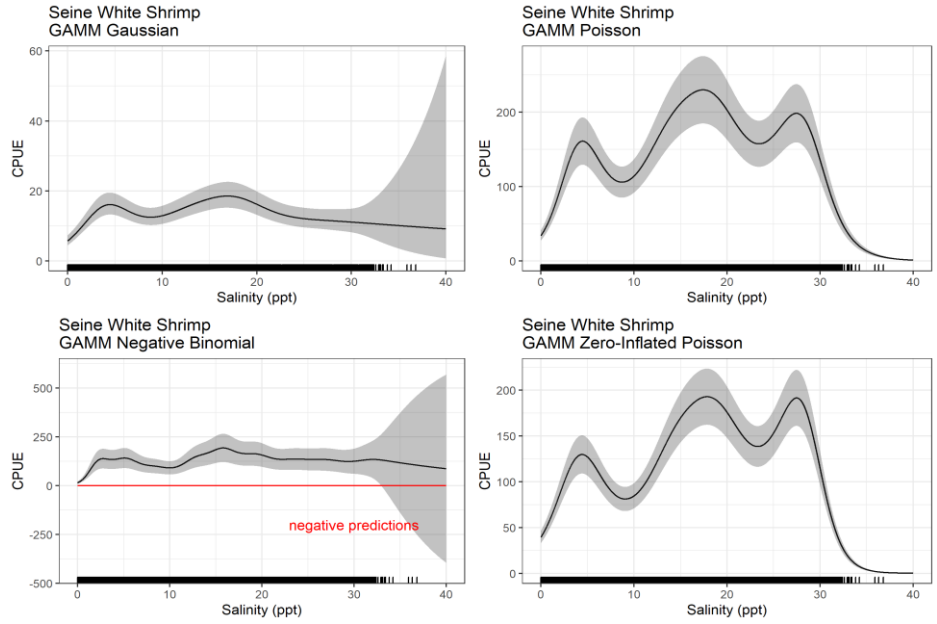

Figure 33. GAMM predicted response of small juvenile white shrimp CPUE to salinity, with other variables held constant. Shaded gray area represents 95% confidence interval.

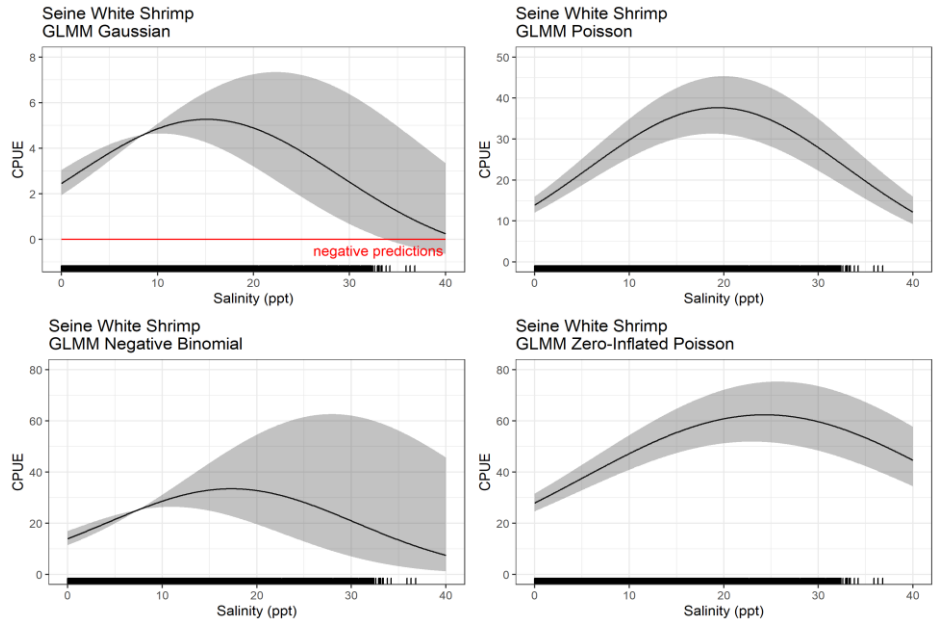

Figure 34. GLMM predicted response of small juvenile white shrimp CPUE to salinity, with other variables held constant. Shaded gray area represents 95% confidence interval.

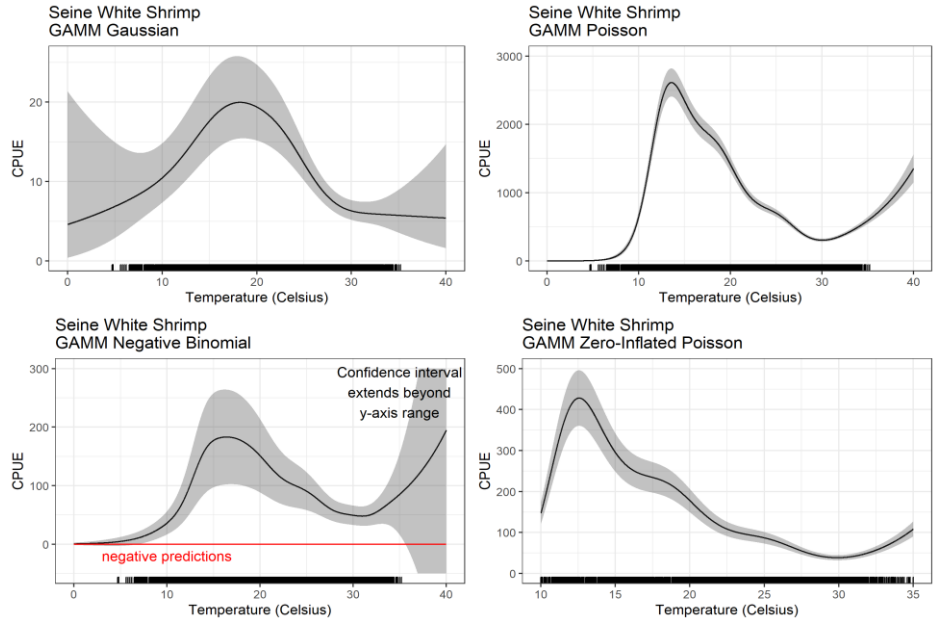

Figure 35. GAMM predicted response of small juvenile white shrimp CPUE to temperature, with other variables held constant. Shaded gray area represents 95% confidence interval.

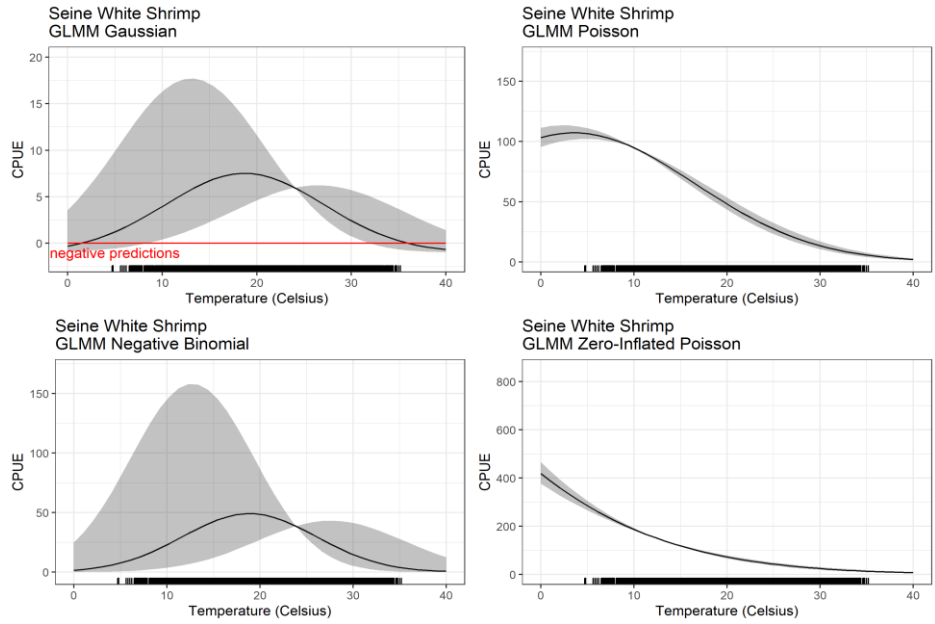

Figure 36. GLMM predicted response of small juvenile white shrimp CPUE to temperature, with other variables held constant. Shaded gray area represents 95% confidence interval.

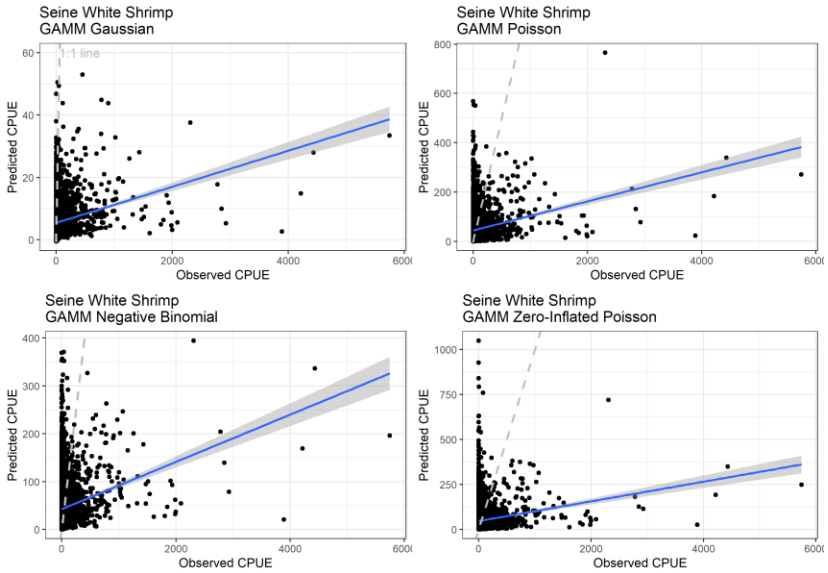

Figure 37. GAMM predicted response of small juvenile white shrimp plotted against observed CPUE using the 30% randomly selected testing dataset. Dashed line provided for reference purposes of 1:1 relationship. Blue line indicates linear relationship between predicted and observed.

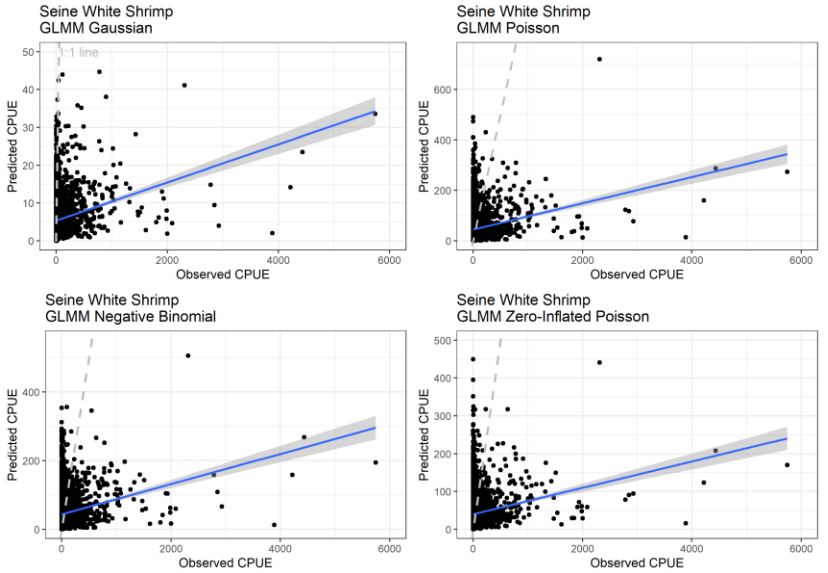

Figure 38. GLMM predicted response of small juvenile white shrimp plotted against observed CPUE using the 30% randomly selected testing dataset. Dashed line provided for reference purposes of 1:1 relationship. Blue line indicates linear relationship between predicted and observed.

Table 6. Summary of model validation metrics for small juvenile white shrimp. *Denotes selected model.

Model Approach	Error Structure	Adjusted R^2	Correlation	RMSE
GAMM	Gaussian	0.16	0.39	220.06
	Poisson	0.05	0.22	211.58
	Zero-Inflated Poisson	0.03	0.17	215.39
	Negative Binomial	0.05	0.23	211.11
GLMM	*Gaussian	0.15	0.38	220.23
	Poisson	0.04	0.21	211.85
	Zero-Inflated Poisson	0.03	0.18	213.16
	Negative Binomial	0.04	0.20	212.25

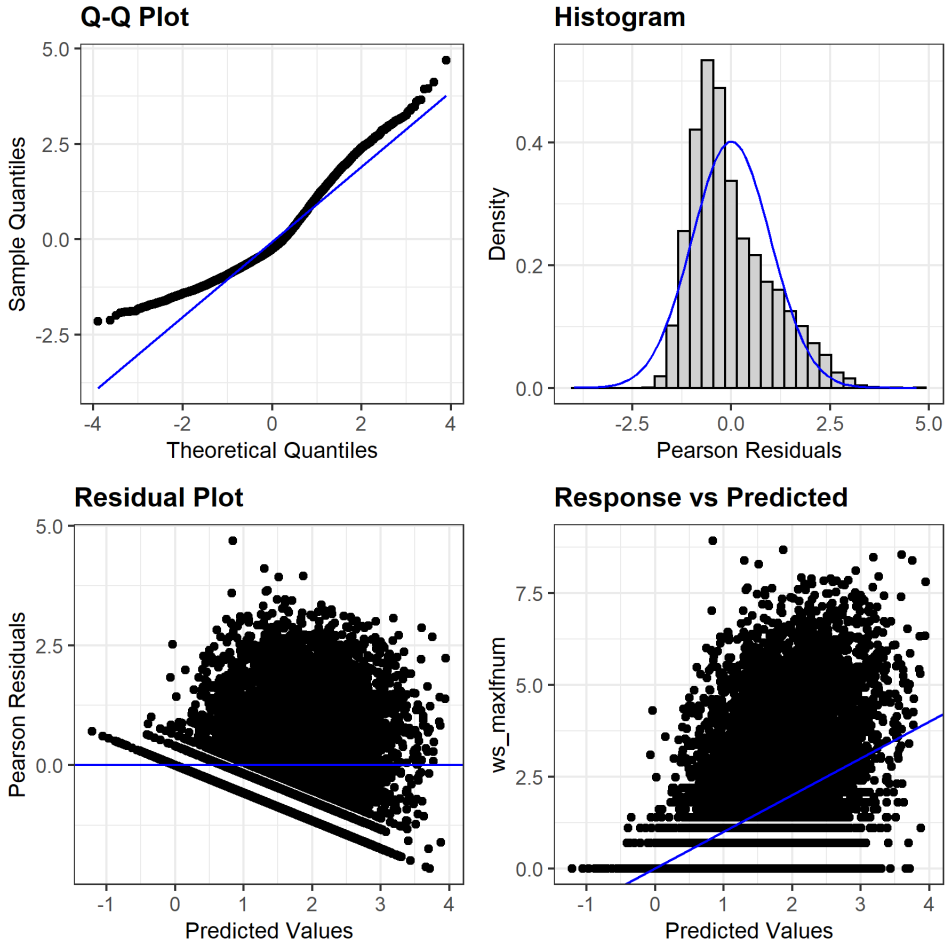

Figure 39. Gaussian GLMM diagnostic plots for small juvenile white shrimp.

Large Juvenile White Shrimp (16-foot Trawls)

Examination of mean CPUE by month, averaged over all years of available 16-foot trawl data, indicated that white shrimp were collected in relatively high numbers year-round (Figure 40). For the most part, these collections represent larger juveniles that moved from shallow habitats into deeper estuarine habitats prior to emigration during July through November. However, juvenile and sub-adult white shrimp may also over-winter in estuaries or return during the spring, and therefore can be present in estuaries year-round. Use of the entire 16-foot trawl environmental and biological data resulted in 52,432 unique data points; 70% of the data points were used for model development and 30% were used for model validation. Water temperature during this time period ranged from 2.5 to 35.4°C; whereas salinity ranged from 0 to 37 ppt.

The Poisson GLMM resulted in higher R^2, followed by Zero-Inflated Poisson GLMM (Table 7). Zero-Inflated Poisson GAMM had highest deviance explained, while RMSE was similar among all of the models. Examination of the response curves indicated the Poisson GAMM and Zero-Inflated GAMM captured the expected response to salinity, while Gaussian GLMM and Negative Binomial GLMM seemed more reasonable for the temperature response (Figure 41 through Figure 46). In considering the interacting effect of salinity and temperature, the Gaussian GLMM was considered the most biological defensible among the models. Model validation results indicated highest R^2 and correlation values for Gaussian GAMM and Gaussian GLMM relative to other models (Table 8, Figure 47, Figure 48). Given these results, the Gaussian GLMM was selected for inclusion in the overall HSI model for large juvenile white shrimp. Diagnostic plots for the selected model are provided in Figure 49 for reference purposes.

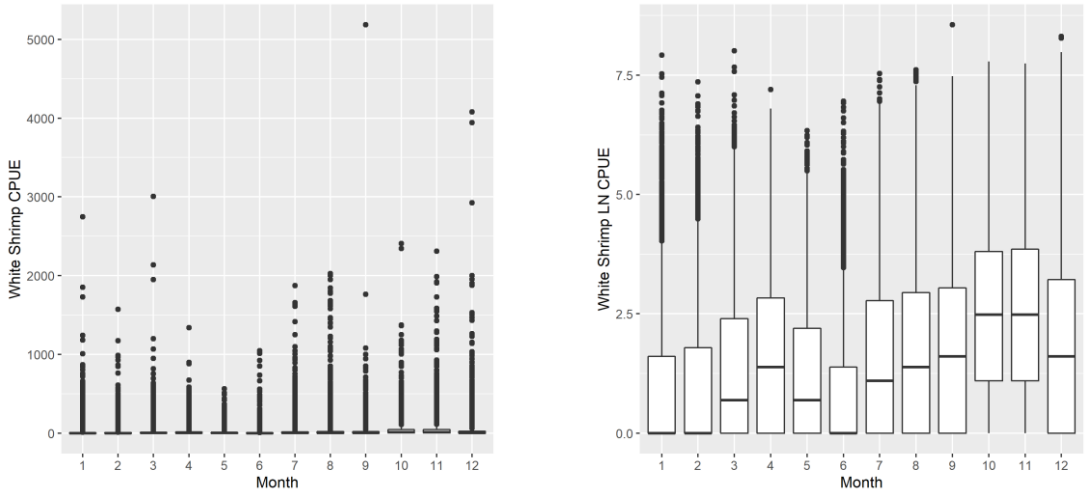

Figure 40. Large juvenile white shrimp CPUE in 16-foot trawl; raw scale (left panel), natural log scale (right panel).

Table 7. Summary of model fit metrics for large juvenile white shrimp. *Denotes selected model.

Model Approach	Error Structure	Adjusted R^2	Deviance explained (GAMM only)	RMSE
GAMM	Gaussian	0.21	22.1%	91.24
	Poisson	0.07	25.5%	86.59
	Zero-Inflated Poisson	.	58%	87.01
	Negative Binomial	0.02	21.2%	88.96
GLMM	*Gaussian	0.23	.	91.31
	Poisson	0.98	.	86.63
	Zero-Inflated Poisson	0.70	.	87.21
	Negative Binomial	0.08	.	87.69

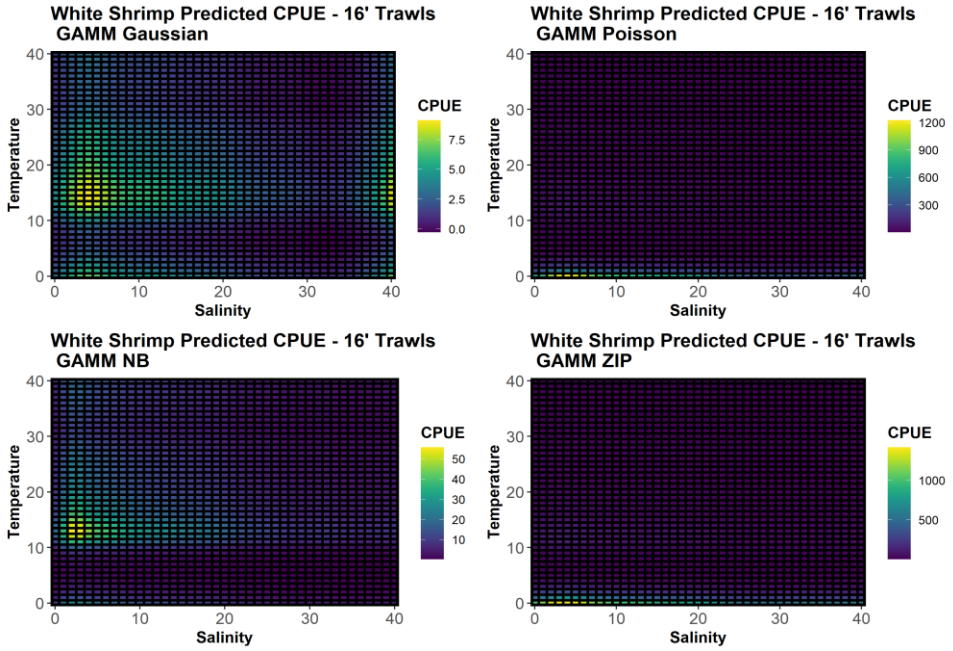

Figure 41. GAMM predicted response of large juvenile white shrimp CPUE to salinity and temperature.

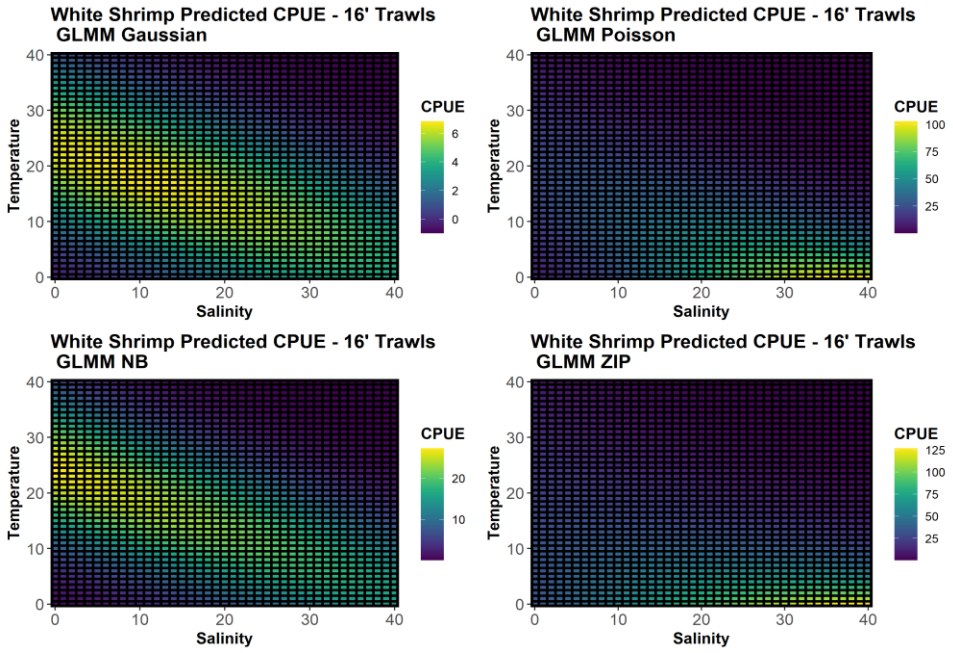

Figure 42. GLMM predicted response of large juvenile white shrimp CPUE to salinity and temperature.

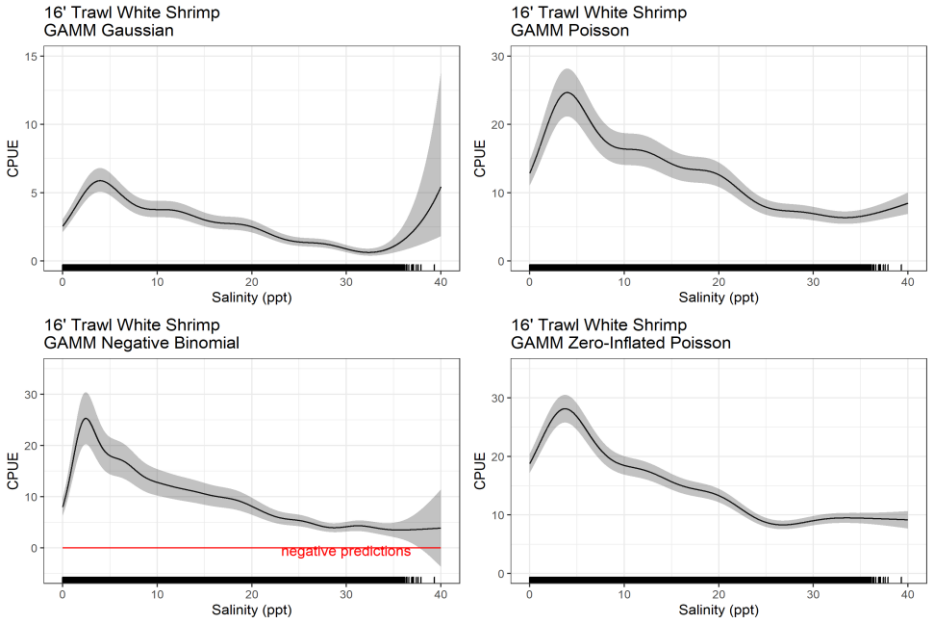

Figure 43. GAMM predicted response of large juvenile white shrimp CPUE to salinity, with other variables held constant. Shaded gray area represents 95% confidence interval.

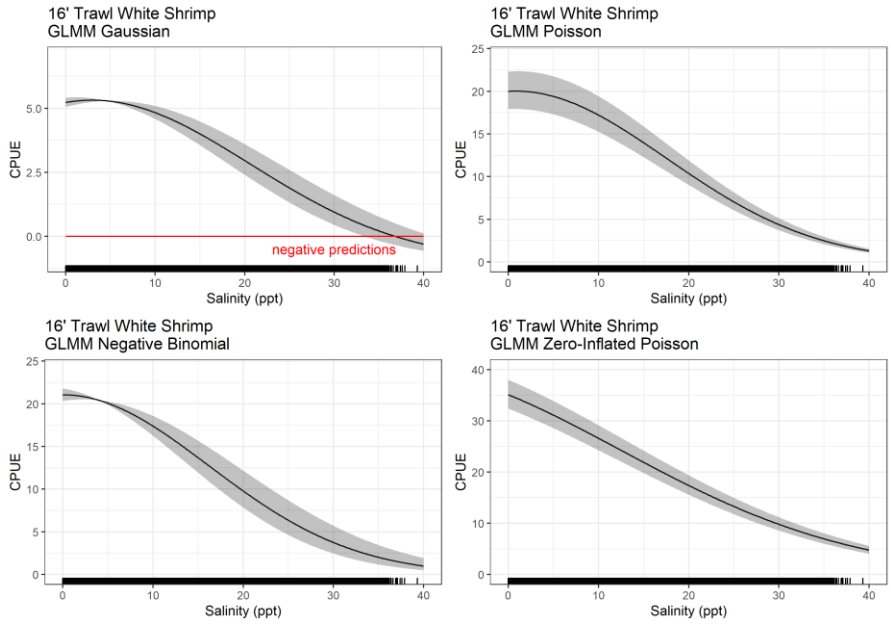

Figure 44. GLMM predicted response of large juvenile white shrimp CPUE to salinity, with other variables held constant. Shaded gray area represents 95% confidence interval.

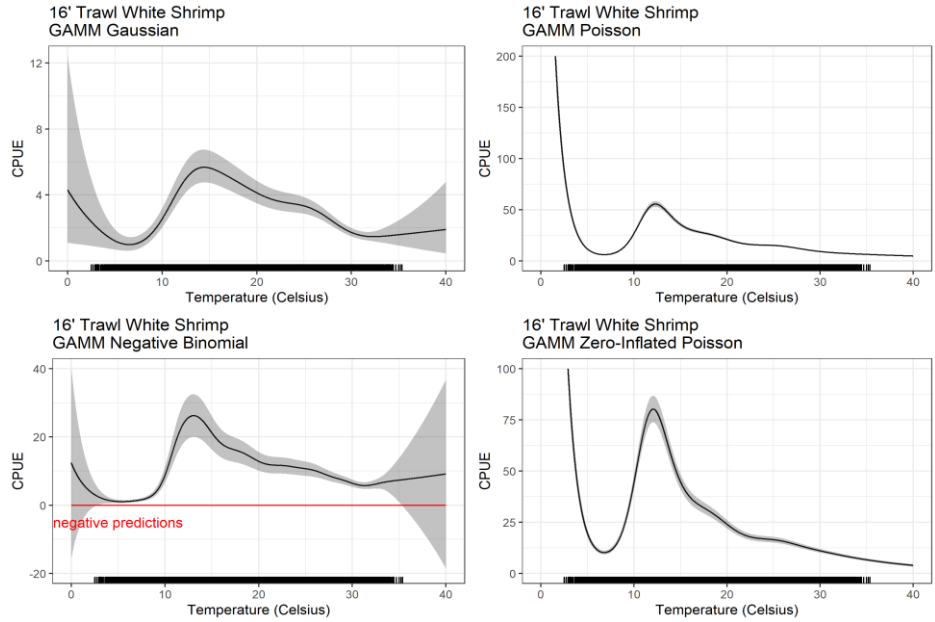

Figure 45. GAMM predicted response of large juvenile white shrimp CPUE to temperature, with other variables held constant. Shaded gray area represents 95% confidence interval.

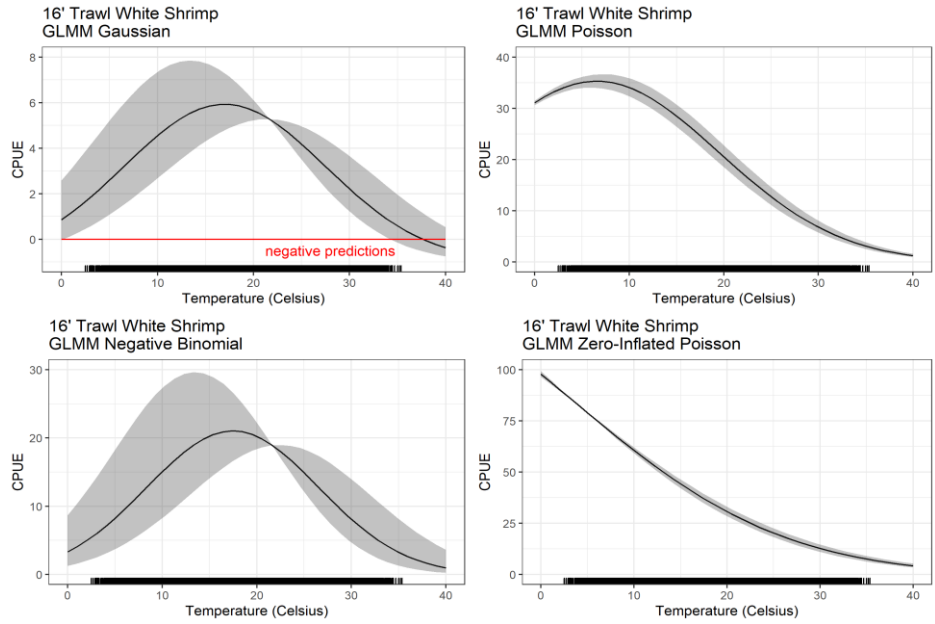

Figure 46. GLMM predicted response of large juvenile white shrimp CPUE to temperature, with other variables held constant. Shaded gray area represents 95% confidence interval.

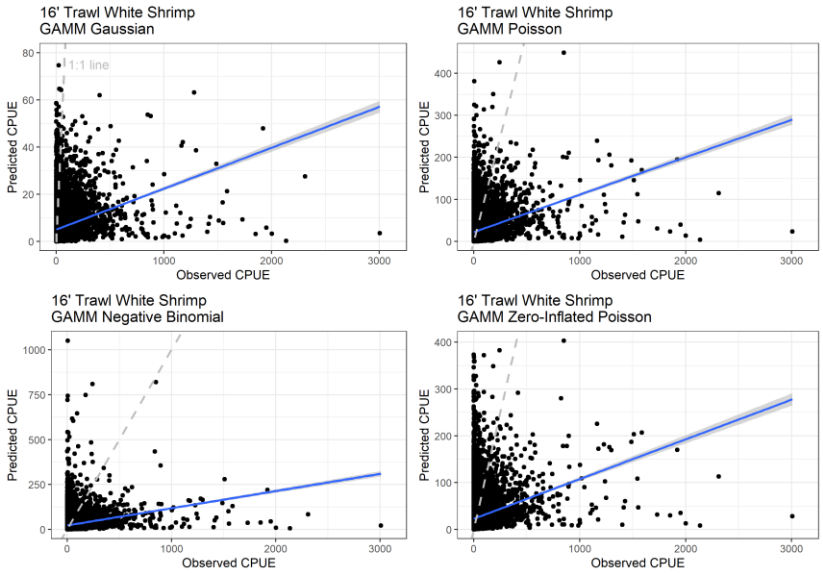

Figure 47. GAMM predicted response of large juvenile white shrimp CPUE plotted against observed CPUE using the 30% randomly selected testing dataset. Dashed line provided for reference purposes of 1:1 relationship. Blue line indicates linear relationship between predicted and observed.

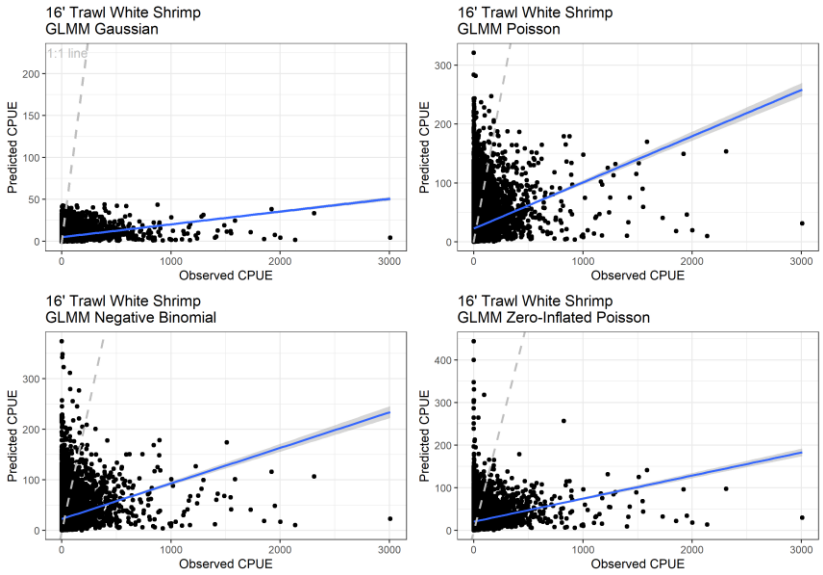

Figure 48. GLMM predicted response of large juvenile white shrimp CPUE plotted against observed CPUE using the 30% randomly selected testing dataset. Dashed line provided for reference purposes of 1:1 relationship. Blue line indicates linear relationship between predicted and observed.

Table 8. Summary of model validation metrics for large juvenile white shrimp. *Denotes selected model.

Model Approach	Error Structure	Adjusted R^2	Correlation	RMSE
GAMM	Gaussian	0.20	0.45	87.13
	Poisson	0.08	0.28	82.92
	Zero-Inflated Poisson	0.06	0.25	84.10
	Negative Binomial	0.06	0.24	84.89
GLMM	*Gaussian	0.20	0.45	87.31
	Poisson	0.07	0.26	83.49
	Zero-Inflated Poisson	0.05	0.22	84.15
	Negative Binomial	0.05	0.23	84.28

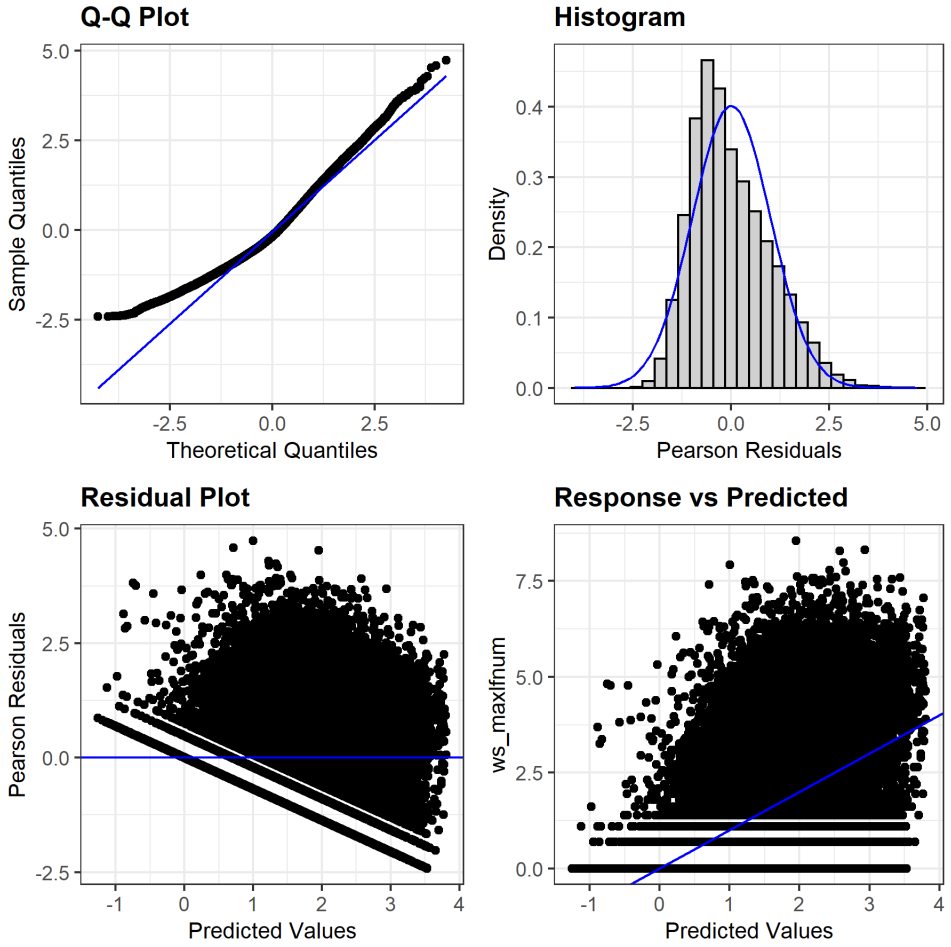

Figure 49. Gaussian GLMM diagnostic plots for large juvenile white shrimp.

Juvenile Blue Crab (Seines)

Examination of mean CPUE by month, averaged over all years of available seine data, indicated that juvenile blue crab were collected in high numbers year-round (Figure 50). Blue crab spawn from spring to fall in Louisiana, and therefore juvenile blue crab may be found in shallow estuarine habitats throughout the year. Use of the year-round data set resulted in 17,747 unique data points; 70% of the data points were used for model development and 30% were used for model validation. Water temperature during this time period ranged from 3.2 to 35.2°C; whereas salinity ranged from 0 to 37 ppt.

The Poisson and Zero-Inflated Poisson GLMM resulted in higher R^2 than any other model, while RMSE were similar among the models (Table 9). Among the GAMMs, Poisson and Zero-Inflated Poisson had slightly higher deviance explained than the other GAMM error structures. Examination of the response curves indicate the GAMMs captured the expected response to salinity in a biologically defensible way, with highest predicted catches at 2-5 ppt rather than at 0 ppt for the GLMMs. The temperature relationships in the GAMMs indicate blue crabs may tolerate a wide range of temperatures throughout the year (Figure 51 through Figure 56). Model validation results indicated low R^2 values for all models, similar RMSE values among models, and higher correlation values for Gaussian GAMM and Gaussian GLMM, relative to other models (Table 10, Figure 57, Figure 58). The Gaussian GAMM was ultimately selected for inclusion in the overall HSI model for blue crab because the response curves were biologically defensible. Basis dimensions (Table 11) and diagnostic plots (Figure 59) for the selected model are provided for reference purposes.

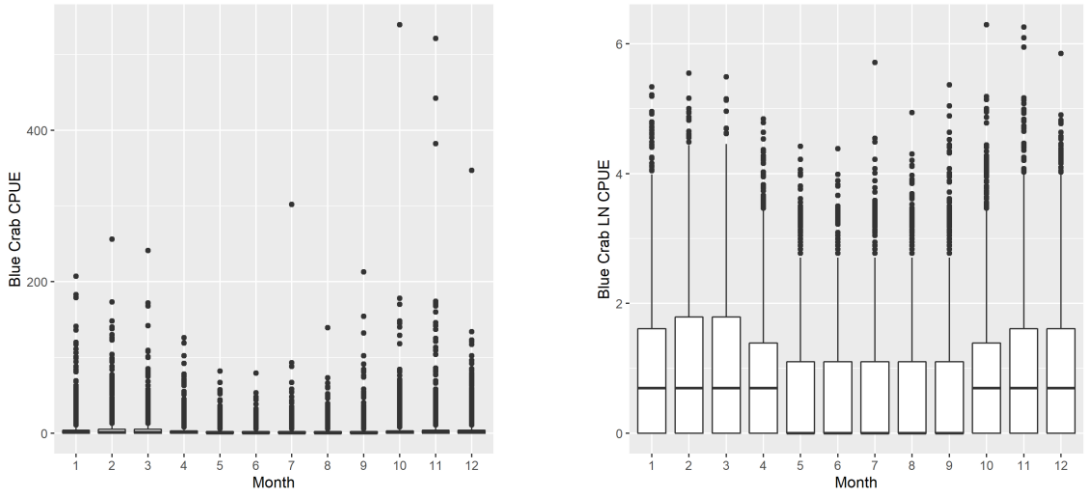

Figure 50. Juvenile blue crab CPUE in seines; raw scale (left panel), natural log scale (right panel).

Table 9. Summary of model fit metrics for juvenile blue crab. *Denotes selected model.

Model Approach	Error Structure	Adjusted R^2	Deviance explained (GAMM only)	RMSE
GAMM	*Gaussian	0.10	11%	12.36
	Poisson	0.06	18.7%	11.76
	Zero-Inflated Poisson	.	17.8%	11.82
	Negative Binomial	0.04	14.2%	11.88
GLMM	Gaussian	0.10	.	12.37
	Poisson	0.71	.	11.82
	Zero-Inflated Poisson	0.45	.	11.90
	Negative Binomial	0.03	.	11.91

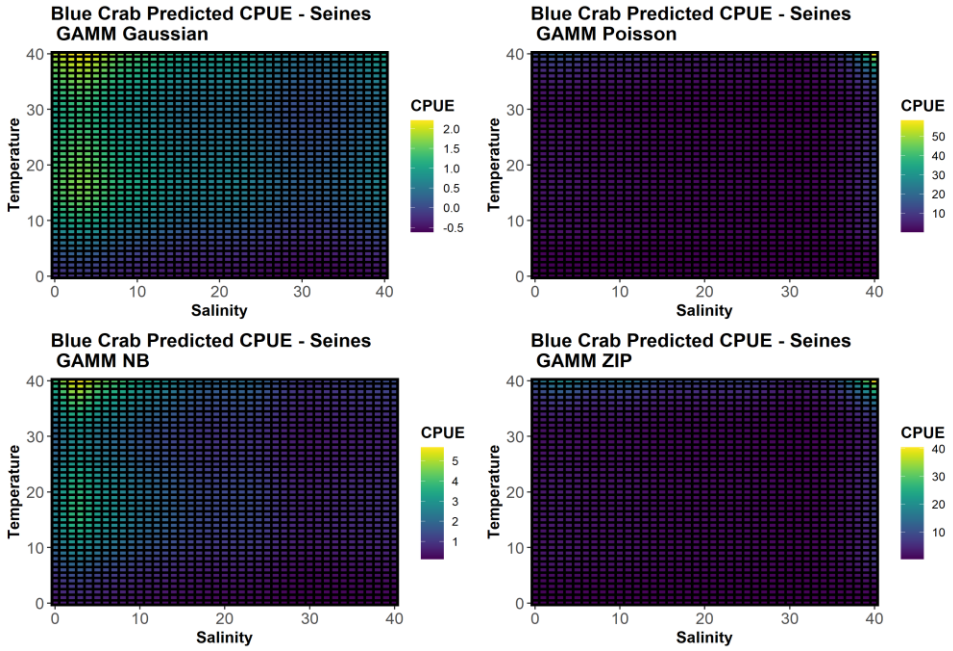

Figure 51. GAMM predicted response of juvenile blue crab CPUE to salinity and temperature.

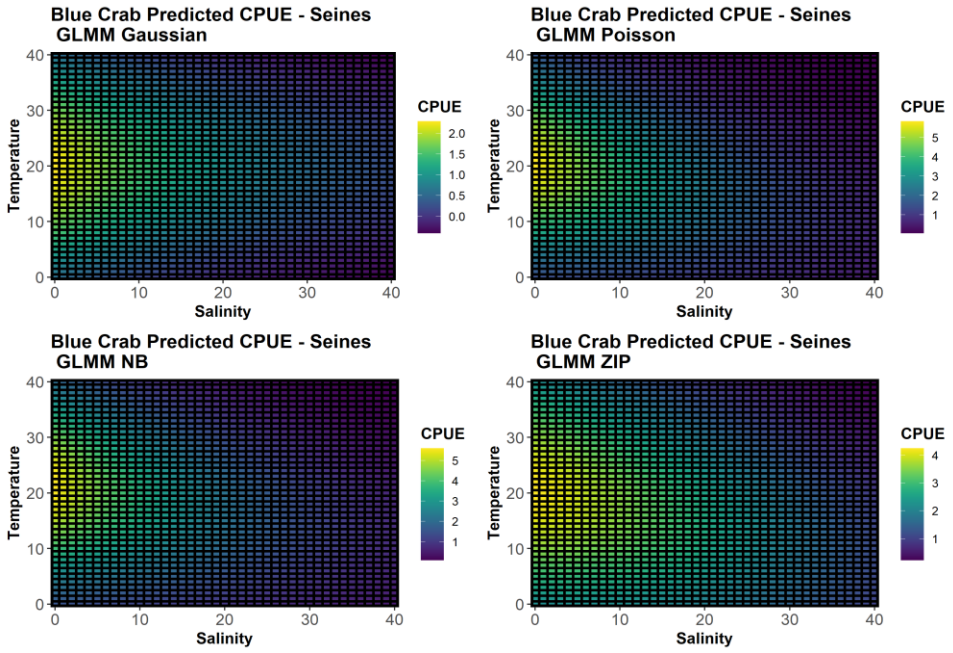

Figure 52. GLMM predicted response of juvenile blue crab CPUE to salinity and temperature.

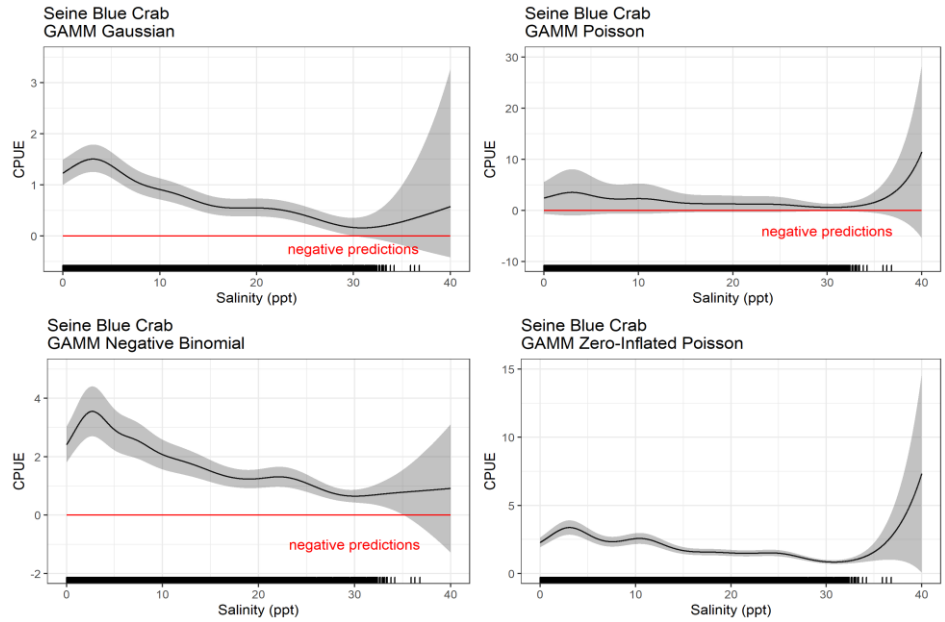

Figure 53. GAMM predicted response of juvenile blue crab CPUE to salinity, with other variables held constant. Shaded gray area represents 95% confidence interval.

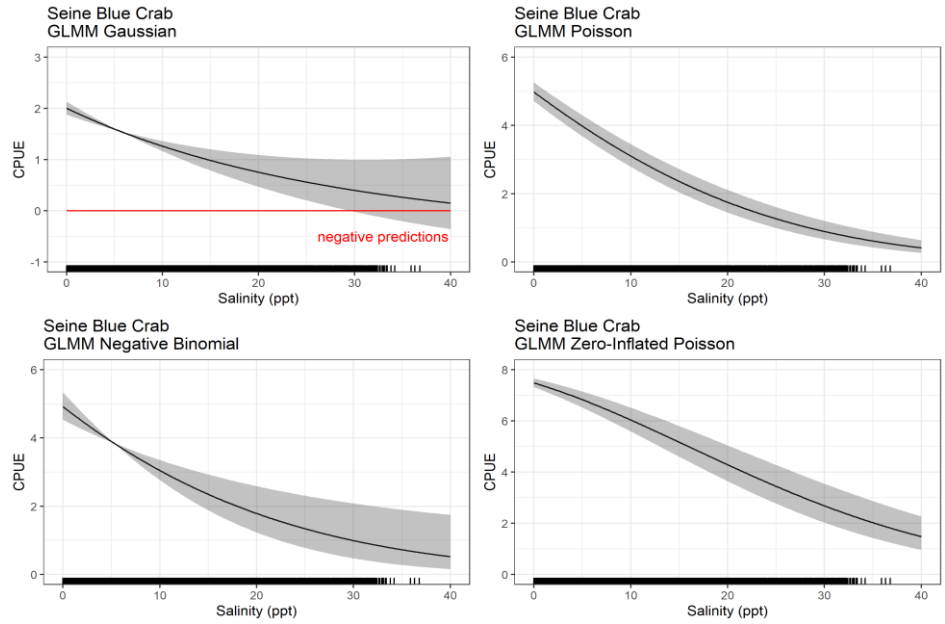

Figure 54. GLMM predicted response of juvenile blue crab CPUE to salinity, with other variables held constant. Shaded gray area represents 95% confidence interval.

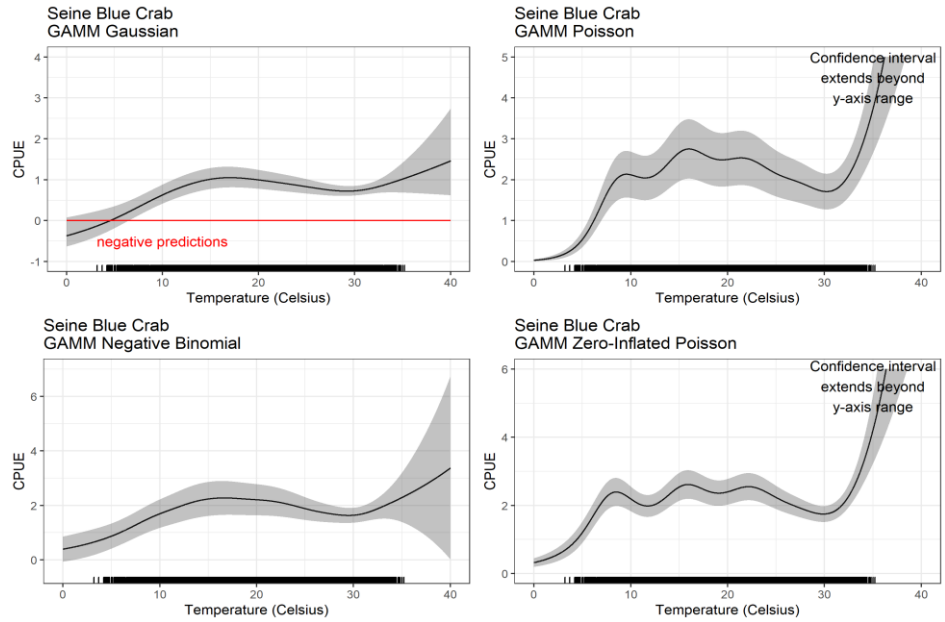

Figure 55. GAMM predicted response of juvenile blue crab CPUE to temperature, with other variables held constant. Shaded gray area represents 95% confidence interval.

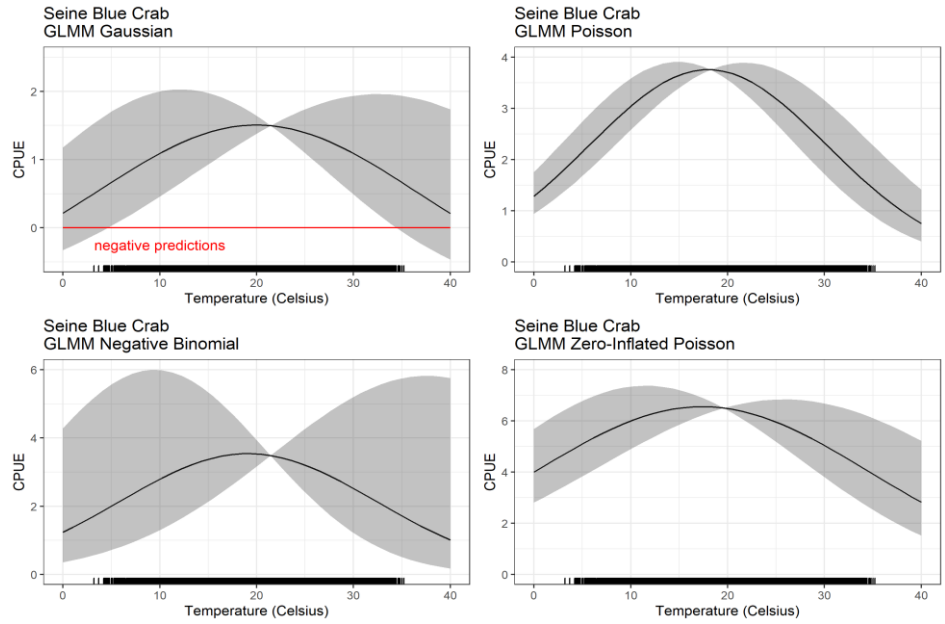

Figure 56. GLMM predicted response of juvenile blue crab CPUE to temperature, with other variables held constant. Shaded gray area represents 95% confidence interval.

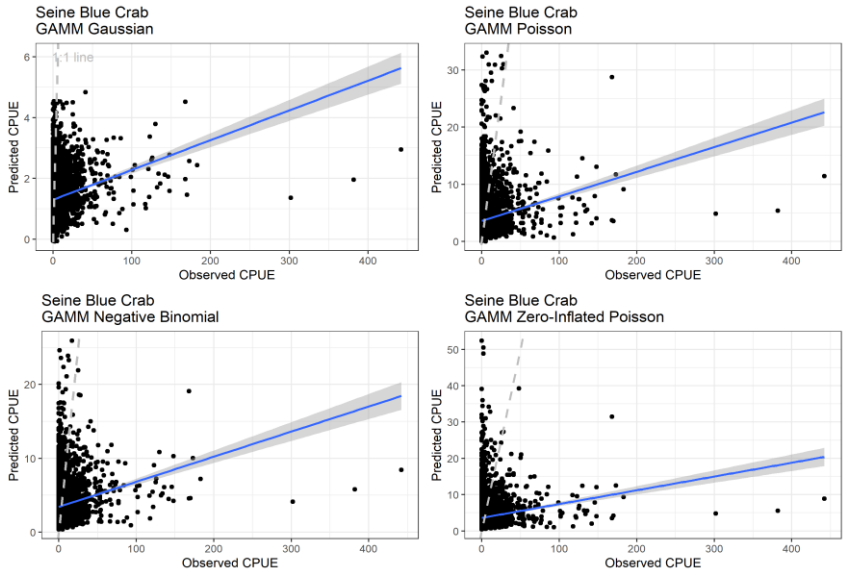

Figure 57. GAMM predicted juvenile blue crab CPUE plotted against observed CPUE using the 30% randomly selected testing dataset. Dashed line provided for reference purposes of 1:1 relationship. Blue line indicates linear relationship between predicted and observed.

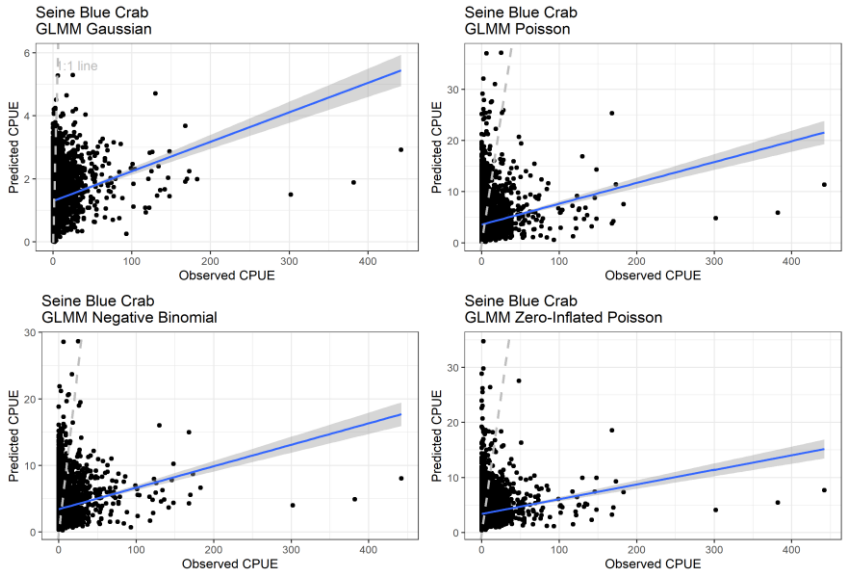

Figure 58. GLMM predicted juvenile blue crab CPUE plotted against observed blue crab CPUE using the 30% randomly selected testing dataset. Dashed line provided for reference purposes of 1:1 relationship. Blue line indicates linear relationship between predicted and observed.

Table 10. Summary of model validation metrics for juvenile blue crab. *Denotes selected model.

Model Approach	Error Structure	Adjusted R^2	Correlation	RMSE
GAMM	*Gaussian	0.09	0.30	13.43
	Poisson	0.03	0.18	13.11
	Zero-Inflated Poisson	0.15	0.15	13.22
	Negative Binomial	0.03	0.18	13.08
GLMM	Gaussian	0.08	0.29	13.43
	Poisson	0.03	0.17	13.10
	Zero-Inflated Poisson	0.02	0.15	13.14
	Negative Binomial	0.03	0.18	13.08

Table 11. Basis dimension (k') for each smooth term within the juvenile blue crab Gaussian GAMM.

	Parameter	k'	edf	k-index	p-value
Gaussian	Salinity	9.00	7.56	1.00	0.64
	Temperature	9.00	5.61	1.01	0.88
	Julian date	9.00	5.57	0.98	0.05

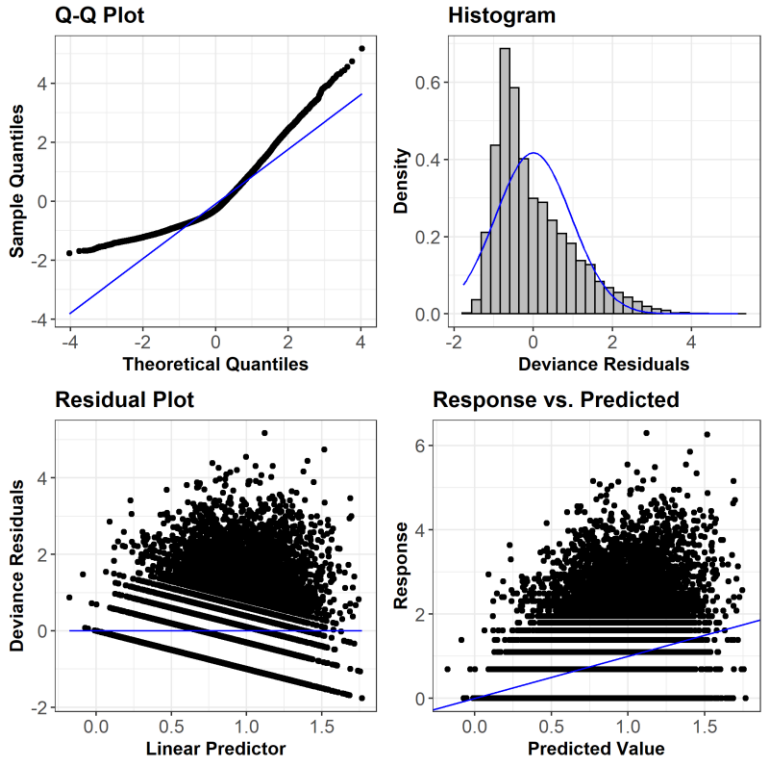

Figure 59. Gaussian GAMM diagnostic plots for juvenile blue crab.

Juvenile Gulf Menhaden (Seines)

Examination of mean CPUE by month, averaged over all years of available seine data, revealed that juvenile gulf menhaden were collected in highest numbers from January through August (Figure 60). These months are consistent with the time period when recently-recruited juvenile gulf menhaden are utilizing shallow estuarine habitats as a nursery. The seine environmental and biological data were subset to include the months of January through August, resulting in 10,386 unique data points; 70% of the data points were used for model development and 30% were used for model validation. Water temperature during this time period ranged from 3.2 to 35.2°C; whereas salinity ranged from 0 to 36 ppt.

The Poisson and Zero-Inflated Poisson GLMM resulted in higher R^2 than any other model and RMSE were lowest for Poisson GAMM and Zero-Inflated Poisson (Table 12). Among the GAMMs, Zero-Inflated Poisson had highest deviance explained. Examination of the response curves indicate the GAMMs captured the expected response to salinity in a biologically defensible way, with highest predicted catches at 1-4 ppt rather than at 0 ppt for the GLMMs (Figure 61 through Figure 66). The response to temperature appeared most reasonable in the Gaussian GAMM. Model validation results indicated relatively low R^2 values for all models, similar RMSE values among models, and higher correlation values for Gaussian GAMM and Gaussian GLMM, relative to other models (Table 13, Figure 67, Fi gure 68). Given these results, the Gaussian GAMM was selected for inclusion in the overall HSI model for juvenile gulf menhaden because the response curves were biologically defensible. Basis dimensions (Table 14) and diagnostic plots (Figure 69) for the selected model are provided for reference purposes.

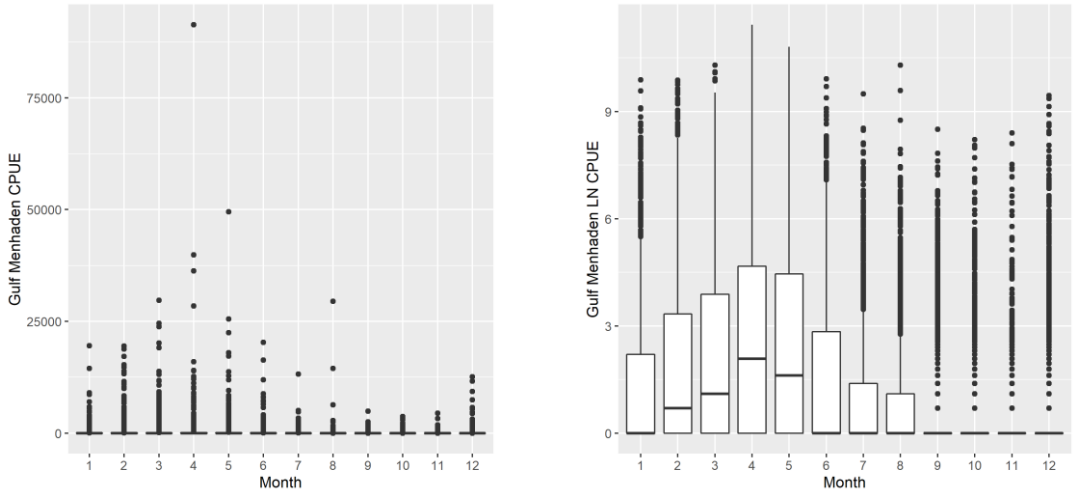

Figure 60. Juvenile gulf menhaden CPUE in seines; raw scale (left panel), natural log scale (right panel).

Table 12. Summary of model fit metrics for juvenile gulf menhaden. *Denotes selected model.

Model Approach	Error Structure	Adjusted R^2	Deviance explained (GAMM only)	RMSE
GAMM	*Gaussian	0.15	16.7%	1598.88
	Poisson	0.08	35.3%	1496.03
	Zero-Inflated Poisson	.	100%	1494.18
	Negative Binomial	0.03	23%	1542.54
GLMM	Gaussian	0.16		1598.95
	Poisson	0.99		1516.13
	Zero-Inflated Poisson	0.72		1527.97
	Negative Binomial	0.04		1543.54

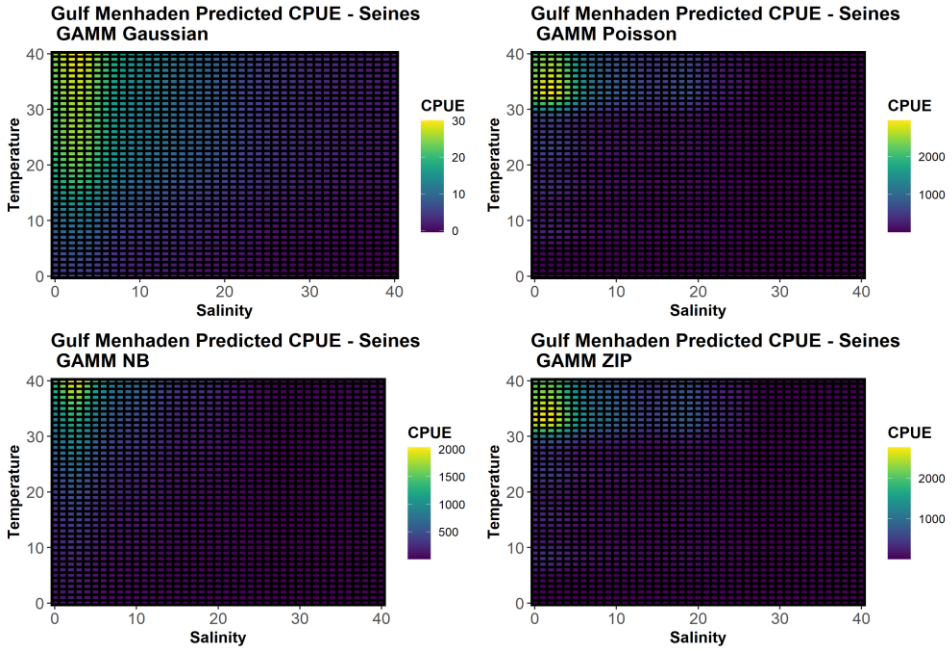

Figure 61. GAMM predicted response of juvenile gulf menhaden CPUE to salinity and temperature.

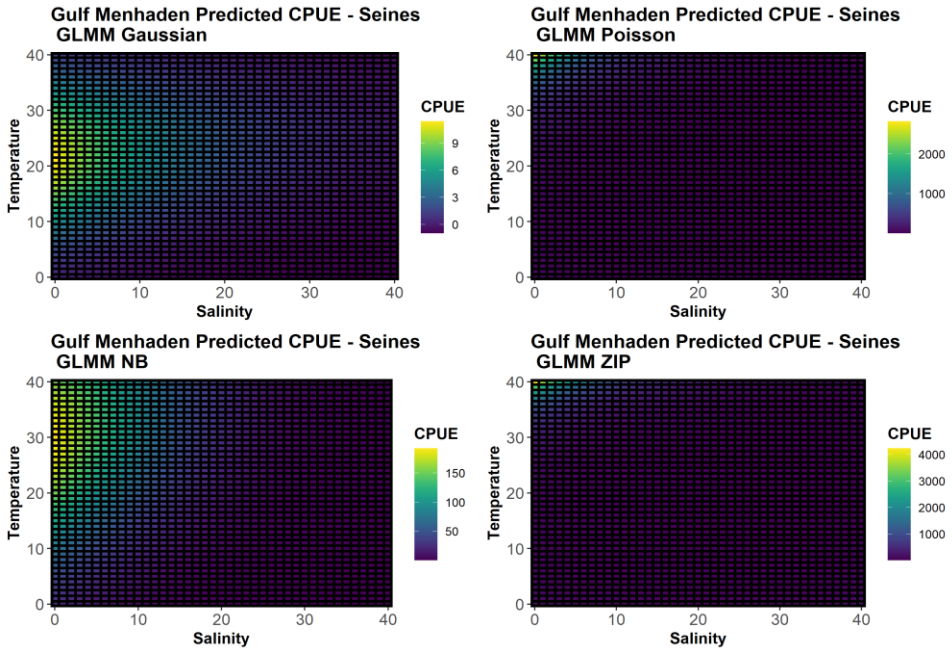

Figure 62. GLMM predicted response of juvenile gulf menhaden CPUE to salinity and temperature.

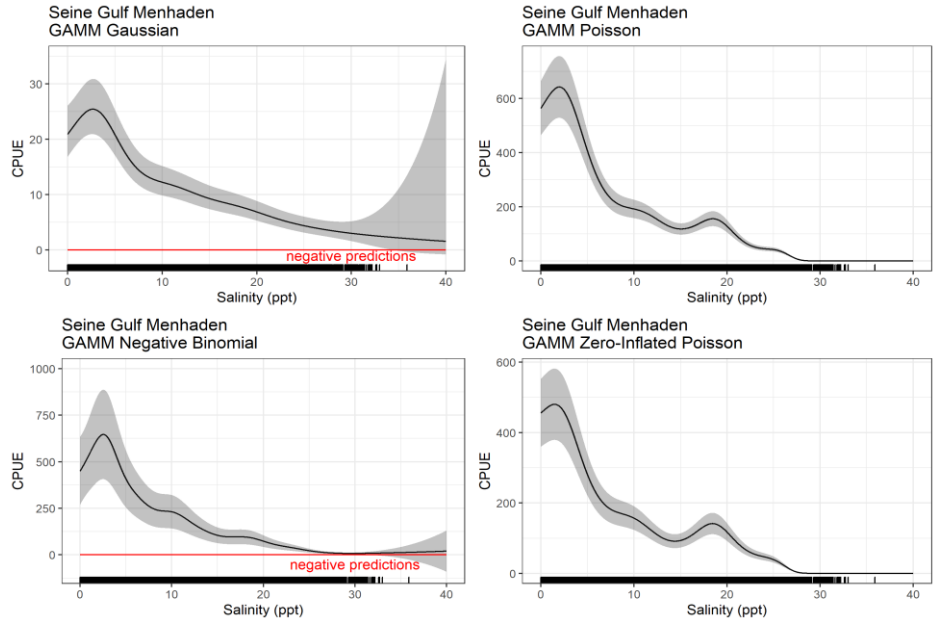

Figure 63. GAMM predicted response of juvenile gulf menhaden CPUE to salinity, with other variables held constant. Shaded gray area represents 95% confidence interval.

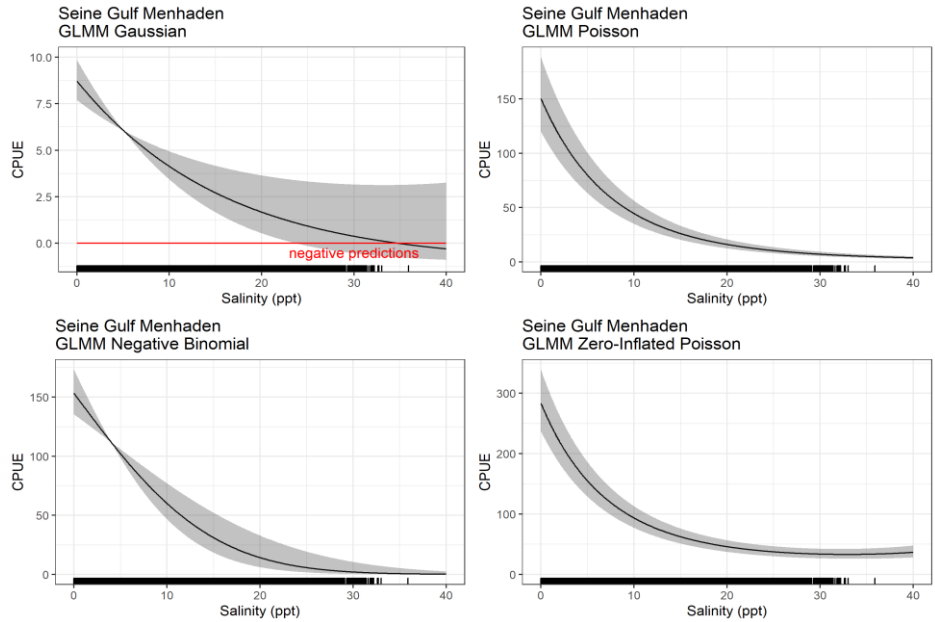

Figure 64. GLMM predicted response of juvenile gulf menhaden CPUE to salinity, with other variables held constant. Shaded gray area represents 95% confidence interval.

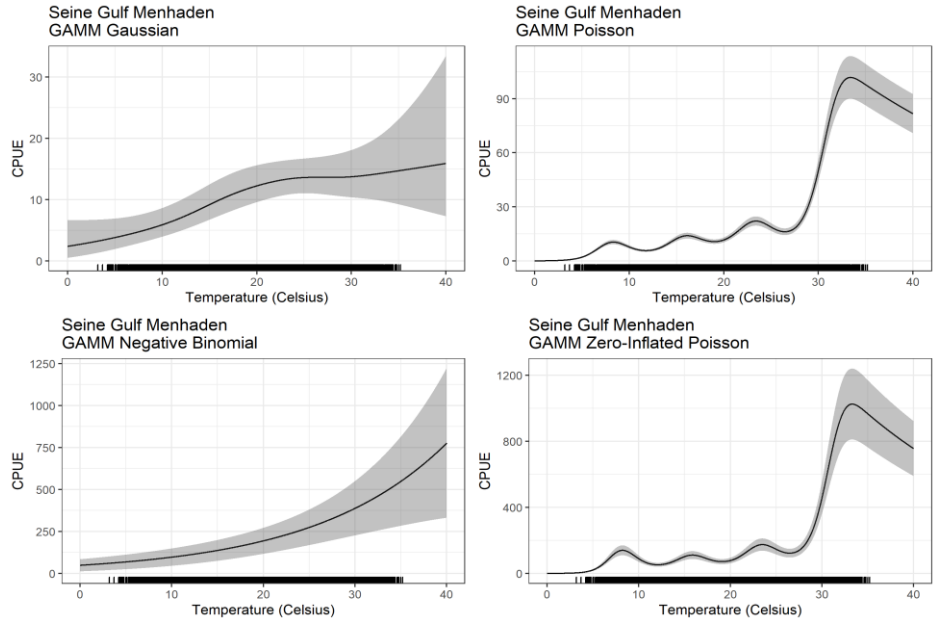

Figure 65. GAMM predicted response of juvenile gulf menhaden CPUE to temperature, with other variables held constant. Shaded gray area represents 95% confidence interval.

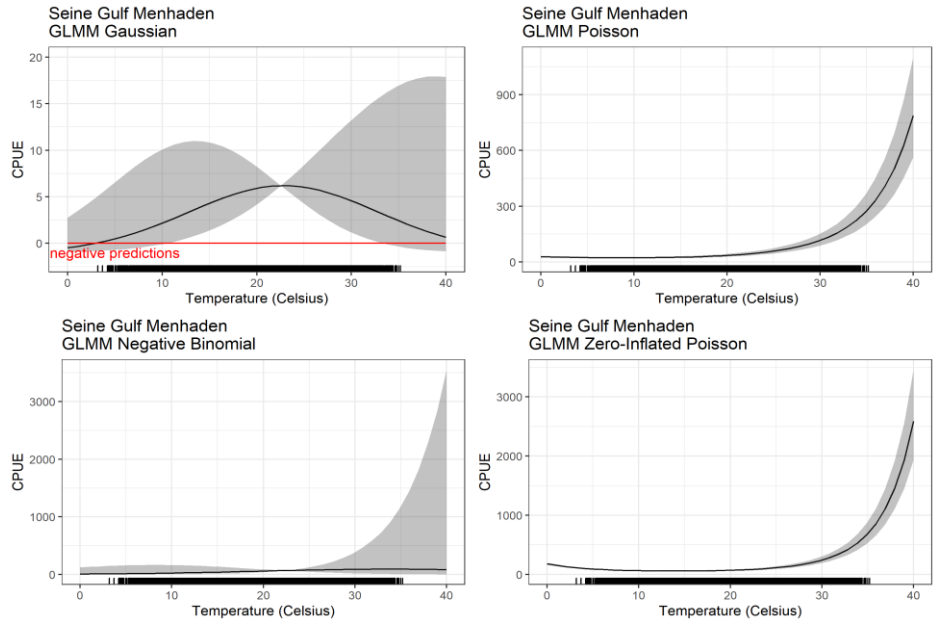

Figure 66. GLMM predicted response of juvenile gulf menhaden CPUE to temperature, with other variables held constant. Shaded gray area represents 95% confidence interval.

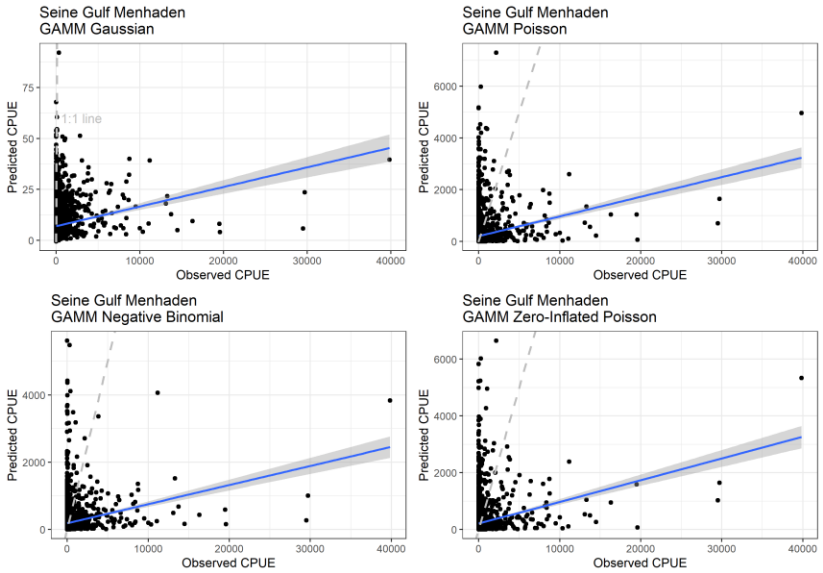

Figure 67. GAMM predicted juvenile gulf menhaden CPUE plotted against observed CPUE using the 30% randomly selected testing dataset. Dashed line provided for reference purposes of 1:1 relationship. Blue line indicates linear relationship between predicted and observed.

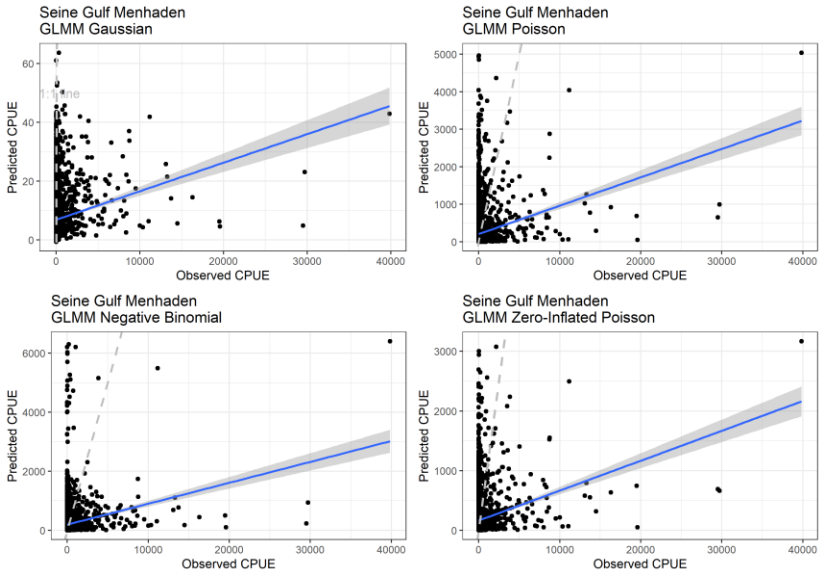

Figure 68. GLMM predicted juvenile gulf menhaden CPUE plotted against observed CPUE using the 30% randomly selected testing dataset. Dashed line provided for reference purposes of 1:1 relationship. Blue line indicates linear relationship between predicted and observed.

Table 13. Summary of model validation metrics juvenile gulf menhaden. *Denotes selected model.

Model Approach	Error Structure	Adjusted R^2	Correlation	RMSE
GAMM	*Gaussian	0.13	0.36	1345.03
	Poisson	0.22	0.22	1309.55
	Zero-Inflated Poisson	0.05	0.22	1306.53
	Negative Binomial	0.04	0.20	1305.35
GLMM	Gaussian	0.12	0.35	1345.04
	Poisson	0.05	0.23	1301.76
	Zero-Inflated Poisson	0.05	0.23	1294.79
	Negative Binomial	0.04	0.21	1312.03

Table 14. Basis dimension (k') for each smooth term within the juvenile gulf menhaden Gaussian GAMM.

	Parameter	k'	edf	k-index	p-value
Gaussian	Salinity	9.00	6.67	0.99	0.29
	Temperature	9.00	3.14	0.98	0.14
	Julian date	9.00	7.50	0.99	0.26

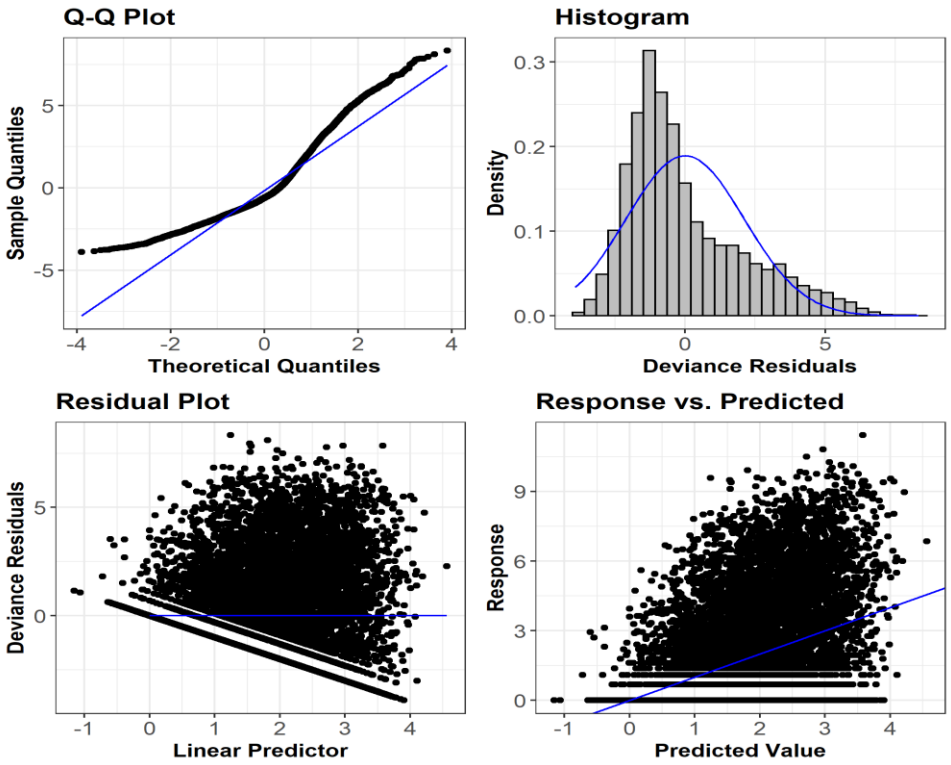

Figure 69. Gaussian GAMM diagnostic plots for juvenile gulf menhaden.

Adult Gulf Menhaden (Gill Nets)

Examination of mean CPUE by month, averaged over all years of available gillnet data, revealed that adult gulf menhaden were collected in highest numbers from March through November (Figure 70). These collections represent gulf menhaden utilizing deeper estuarine habitats prior to moving offshore in the winter months to spawn. The gillnet environmental and biological data were subset to include the months of March through November, resulting in 18,879 unique data points; 70% of the data points were for model development and 30% were used for model validation. Water temperature during this time period ranged from 6.7 to 35.9°C; whereas salinity ranged from 0 to 37 ppt.

The Poisson GAMM and Poisson GLMM had highest deviance explained and highest R^2, respectively (Table 15). Examination of response curves, however, indicated that gulf menhaden CPUE did not respond to salinity and temperature in a biological defensible way for either Poisson model (Figure 71 through Figure 76), so these models were removed from consideration. Instead, the Gaussian GLMM, Zero-Inflated Poisson GLMM, and Gaussian GAMM were more aligned with the hypothesized response for this species. Model validation results indicated relatively low R^2 and similar RMSE across all models, while Gaussian GAMM and Gaussian GLMM had highest correlation score (Table 16, Figure 77, and Figure 78). The Gaussian GAMM model was selected for inclusion in the overall HSI model for adult gulf menhaden because the response curves were biologically feasible and validation results performed generally well, relative to other models. Basis dimensions (Table 17) and diagnostic plots (Figure 79) for Gaussian GAMM are provided for reference purposes.

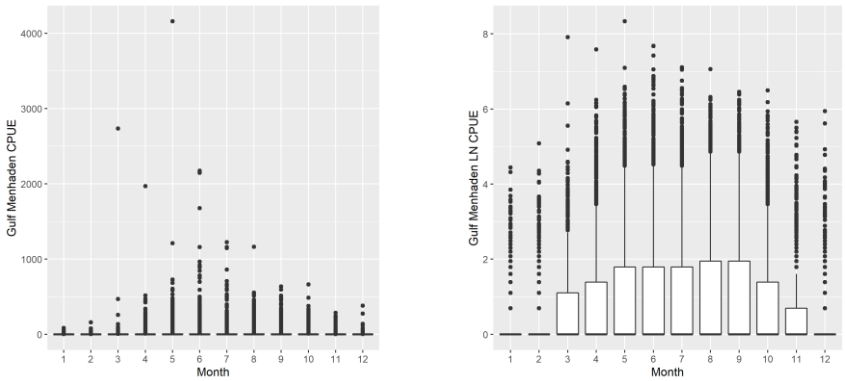

Figure 70. Adult gulf menhaden CPUE in gillnet; raw scale (left panel), natural log scale (right panel).

Table 15. Summary of model fit metrics for adult gulf menhaden. *Denotes selected model.

Model Approach	Error Structure	Adjusted R^2	Deviance explained (GAMM only)	RMSE
GAMM	*Gaussian	0.13	14.3%	63.23
	Poisson	0.05	25.4%	60.65
	Zero-Inflated Poisson	Model did not converge		
	Negative Binomial	0.03	20.2%	61.48
GLMM	Gaussian	0.15	NA	63.21
	Poisson	0.95	NA	60.90
	Zero-Inflated Poisson	0.68	NA	61.35
	Negative Binomial	0.04	NA	61.67

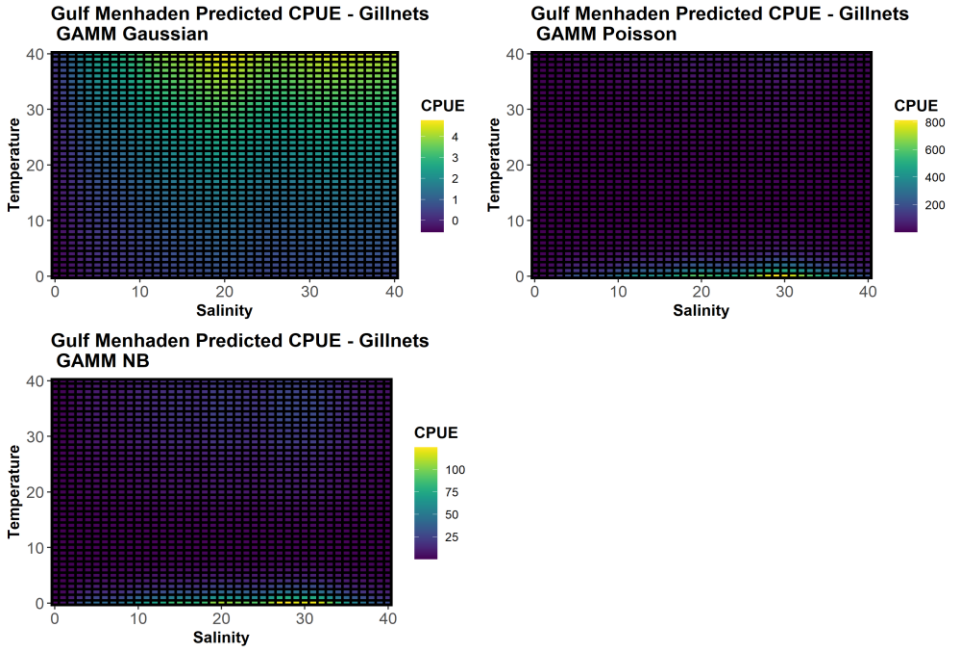

Figure 71. GAMM predicted response of adult gulf menhaden CPUE to salinity and temperature.

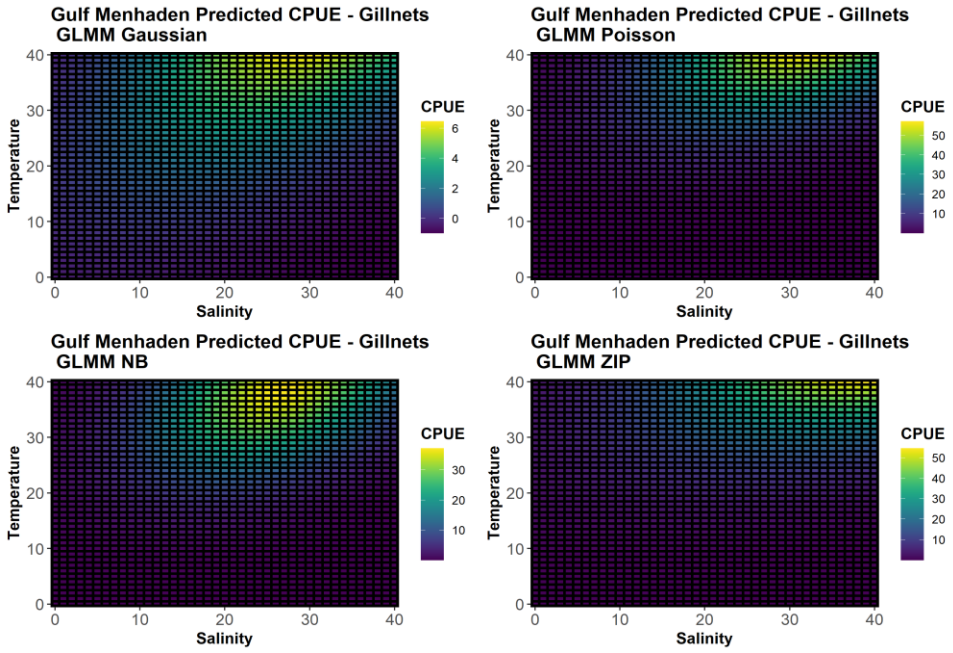

Figure 72. GLMM predicted response of adult gulf menhaden CPUE to salinity and temperature.

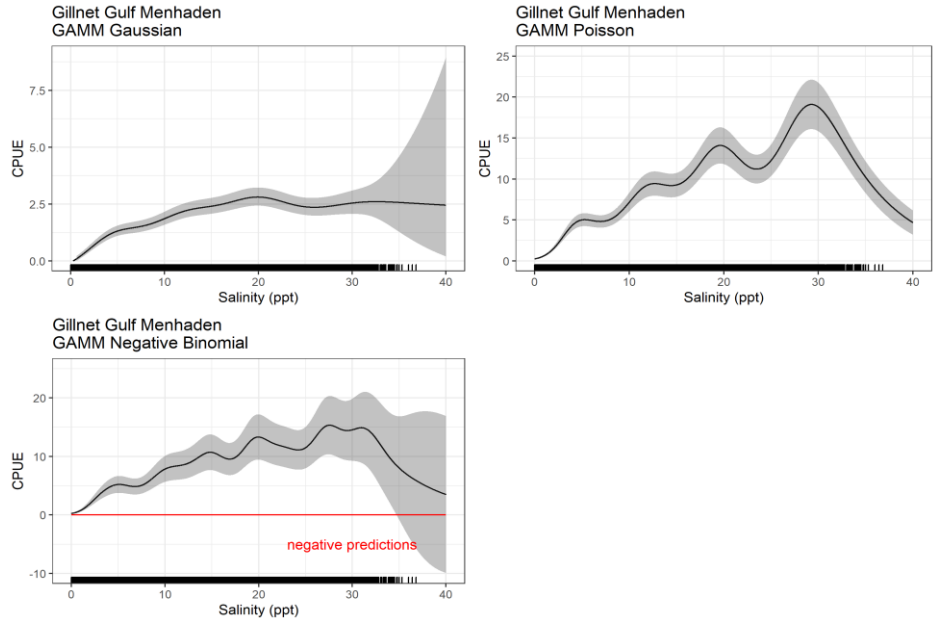

Figure 73. GAMM predicted response of adult gulf menhaden CPUE to salinity, with other variables held constant. Shaded gray area represents 95% confidence interval.

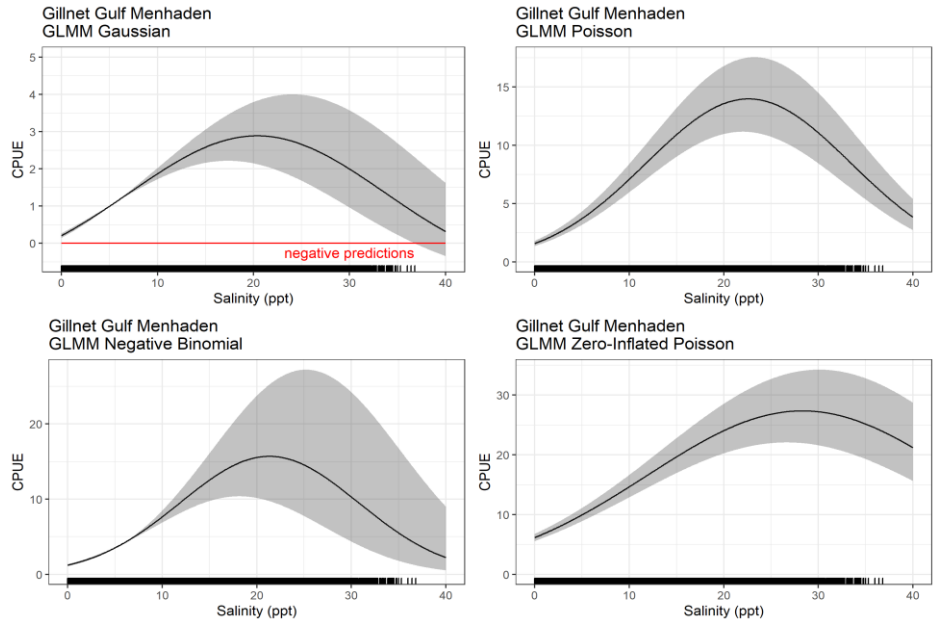

Figure 74. GLMM predicted response of adult gulf menhaden CPUE to salinity, with other variables held constant. Shaded gray area represents 95% confidence interval.

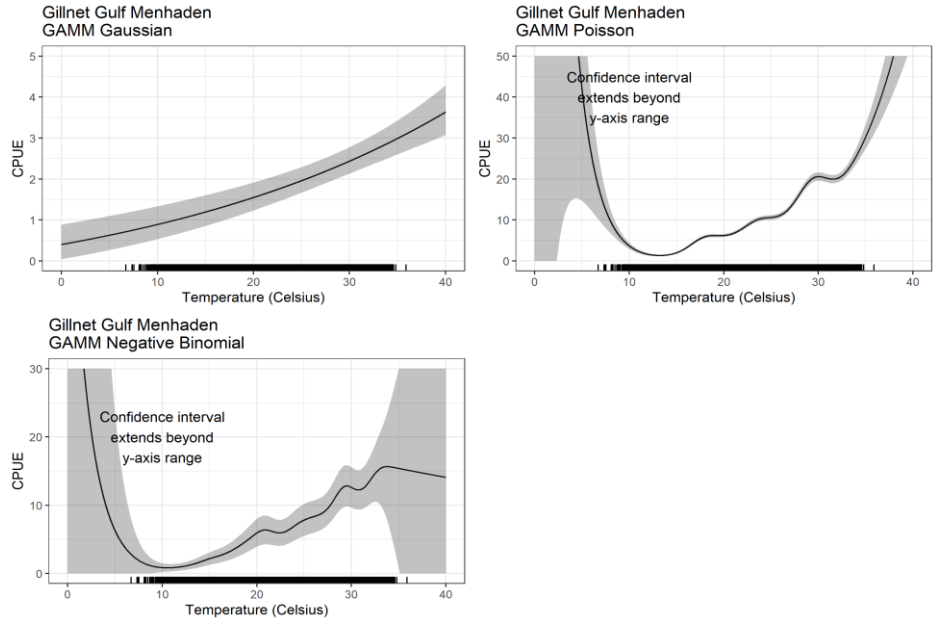

Figure 75. GAMM predicted response from of adult gulf menhaden CPUE to temperature, with other variables held constant. Shaded gray area represents 95% confidence interval.

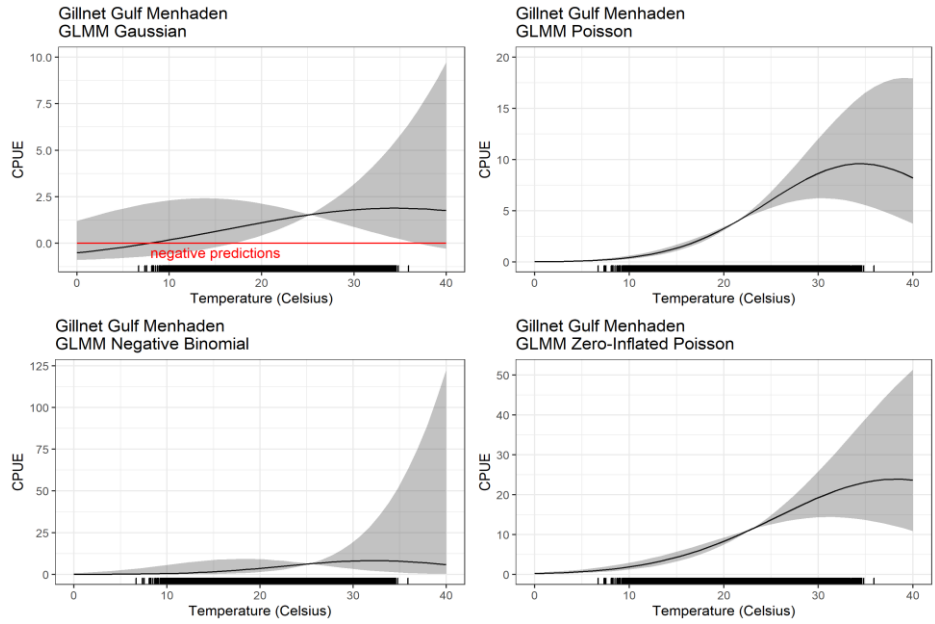

Figure 76. GLMM predicted response of adult gulf menhaden CPUE to temperature, with other variables held constant. Shaded gray area represents 95% confidence interval.

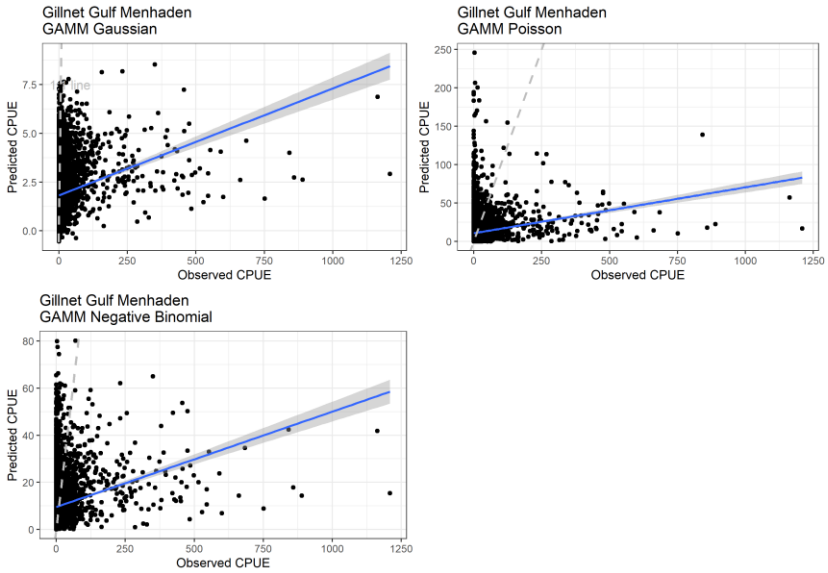

Figure 77. GAMM predicted adult gulf menhaden CPUE plotted against observed CPUE using the 30% randomly selected testing dataset. Dashed line provided for reference purposes of 1:1 relationship, while blue line indicates linear relationship between predicted and observed.

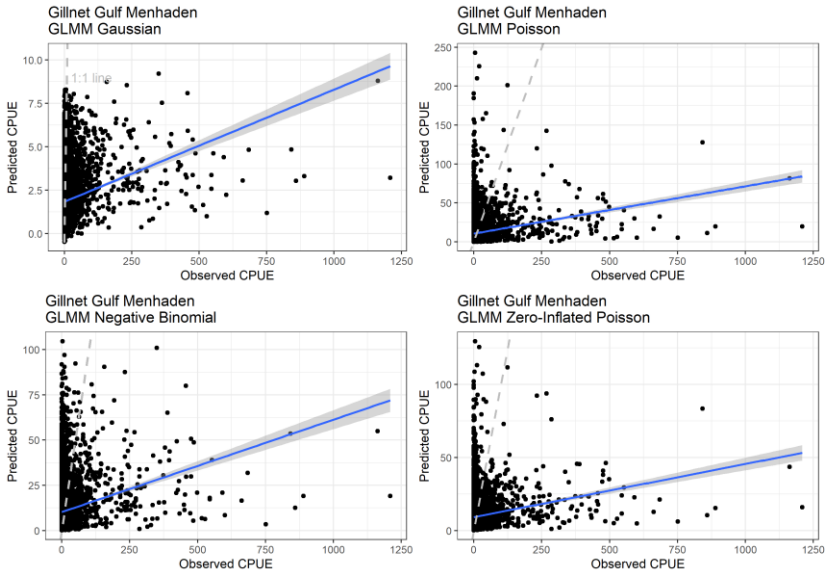

Figure 78. GLMM predicted adult gulf menhaden CPUE plotted against observed CPUE using the 30% randomly selected testing dataset. Dashed line provided for reference purposes of 1:1 relationship. Blue line indicates linear relationship between predicted and observed.

Table 16. Summary of model validation metrics for adult gulf menhaden. *Denotes selected model.

Model Approach	Error Structure	Adjusted R^2	Correlation	RMSE
GAMM	*Gaussian	0.13	0.36	49.69
	Poisson	0.04	0.19	48.59
	Zero-Inflated Poisson	NA	NA	NA
	Negative Binomial	0.04	0.20	48.05
GLMM	Gaussian	0.14	0.37	49.64
	Poisson	0.04	0.20	48.46
	Zero-Inflated Poisson	0.03	0.18	48.31
	Negative Binomial	0.04	0.21	48.06

Table 17. Basis dimension (k') for each smooth term within the adult gulf menhaden Gaussian GAMM.

	Parameter	k'	edf	k-index	p-value
Gaussian GAMM	Salinity	9	8	0.98	0.13
	Temperature	9	1	1.01	0.68
	Julian date	9	6.38	1.01	0.78

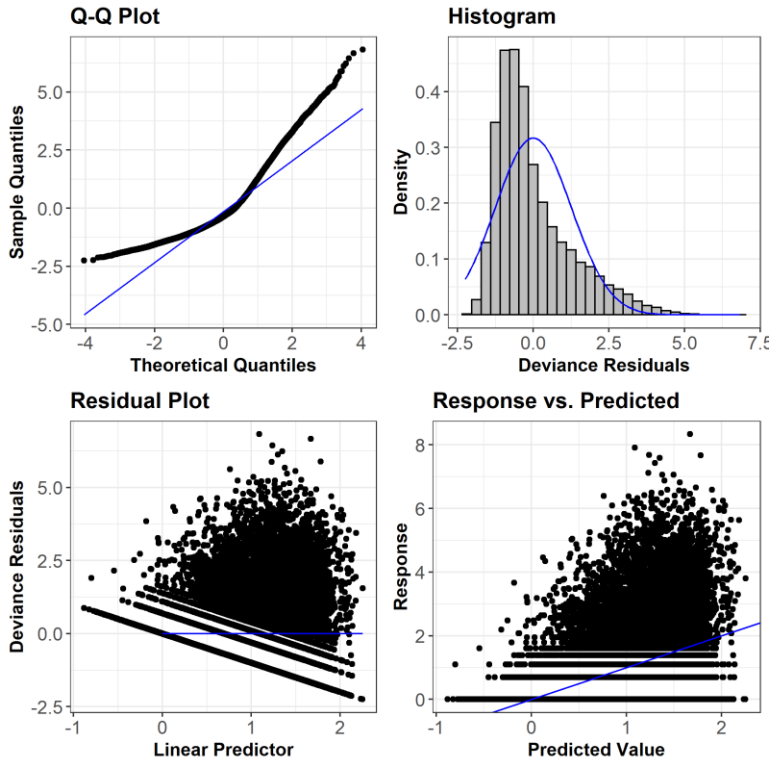

Figure 79. Gaussian GAMM diagnostic plots for adult gulf menhaden.

Juvenile Spotted Seatrout (Seines)

Examination of mean CPUE by month, averaged over all years of available seine data, revealed that juvenile spotted seatrout were collected in highest numbers from September through November (Figure 80). These months are consistent with the time period when recently-settled juvenile spotted seatrout are utilizing shallow estuarine habitats as a nursery. The seine environmental and biological data were subset to include the months of September through November, resulting in 7,977 unique data points; 70% of the data points were used for model development and 30% were used for model validation. Water temperature during this time period ranged from 6.2 to 33.9°C; whereas salinity ranged from 0 to 37 ppt.

The Poisson and Zero-Inflated Poisson GLMM resulted in higher R^2 than any other model and RMSE were similar among all models (Table 18). Among the GAMMs, Poisson and Zero-Inflated Poisson had highest deviance explained. Examination of the response curves indicated the Gaussian GAMM, Negative Binomial GAMM, and Negative Binomial GLMM captured the expected response to salinity and temperature in a biologically defensible way, more so than other model (Figure 81 through Figure 86). Model validation results indicated relatively low R^2 values for all models, similar RMSE values among models, and higher correlation values for Gaussian GAMM and Gaussian GLMM, relative to other models (Table 19, Figure 87, Figure 88). Given these results, the Gaussian GAMM was selected for inclusion in the overall HSI model for juvenile spotted seatrout because the response curves were biologically defensible. Basis dimensions (Table 20) and diagnostic plots (Figure 89) for the selected model are provided for reference purposes.

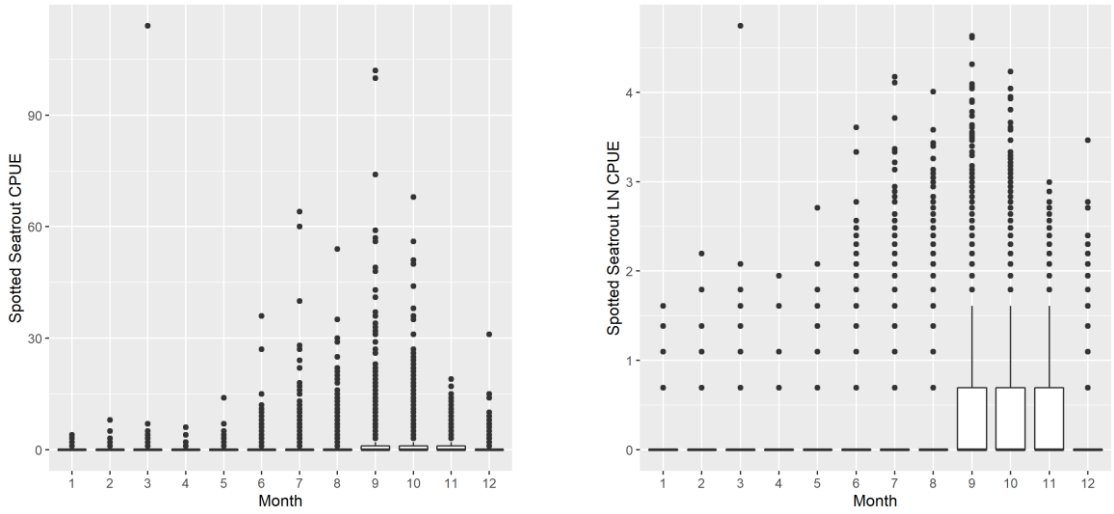

Figure 80. Juvenile spotted seatrout CPUE in seines; raw scale (left panel), natural log scale (right panel).

Table 18. Summary of model fit metrics for juvenile spotted seatrout. *Denotes selected model.

Model Approach	Error Structure	Adjusted R^2	Deviance explained (GAMM only)	RMSE
GAMM	*Gaussian	0.13	14.6%	3.88
	Poisson	0.09	24%	3.69
	Zero-Inflated Poisson	.	24.3%	3.73
	Negative Binomial	0.07	21.9%	3.74
GLMM	Gaussian	0.14	.	3.90
	Poisson	0.48	.	3.72
	Zero-Inflated Poisson	0.56	.	3.77
	Negative Binomial	0.04	.	3.75

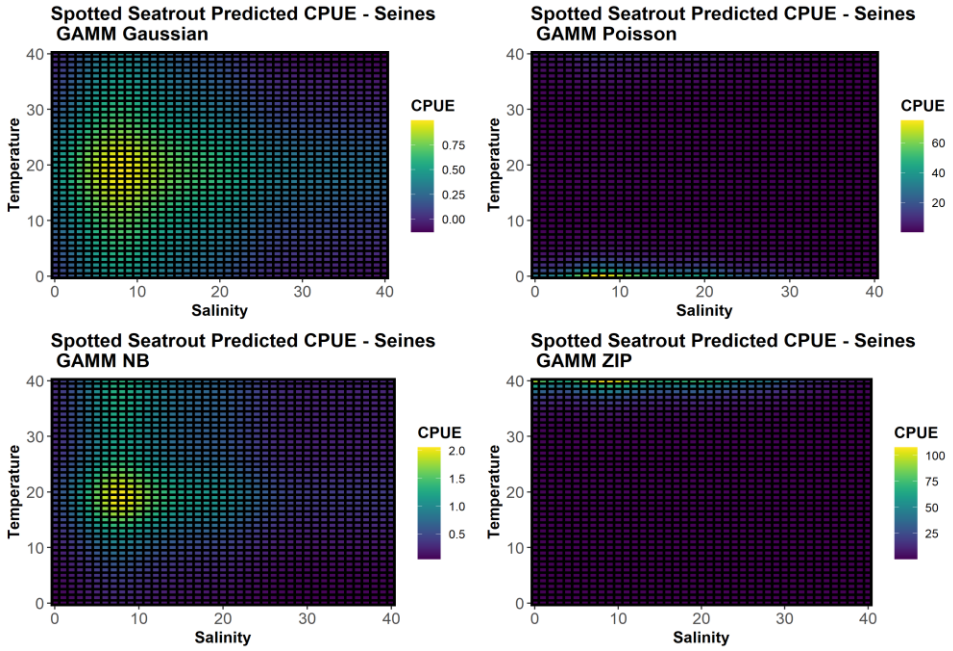

Figure 81. GAMM predicted response of juvenile spotted seatrout CPUE to salinity and temperature.

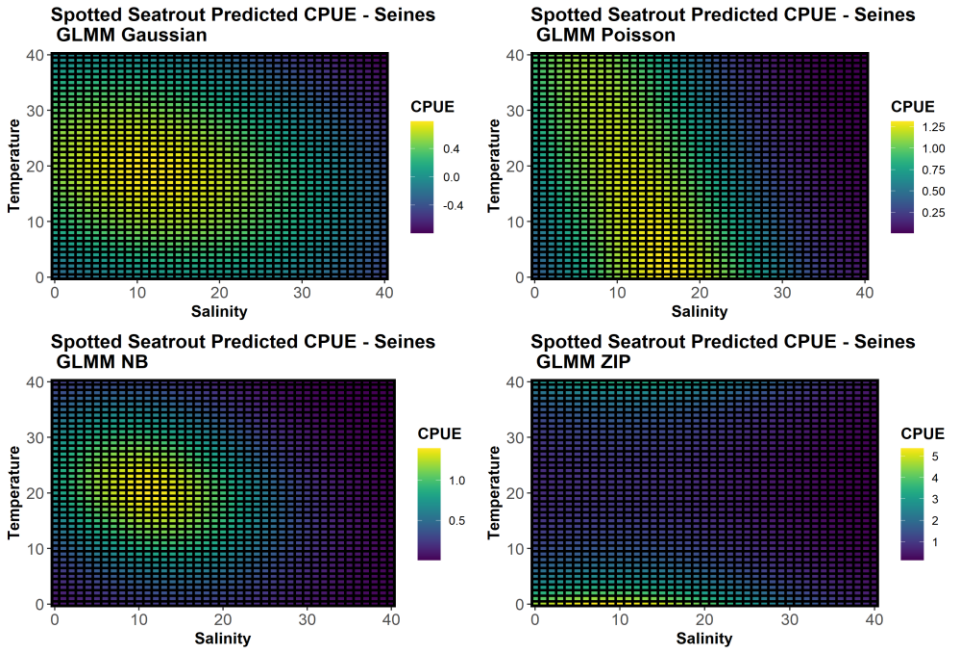

Figure 82. GLMM predicted response of juvenile spotted seatrout CPUE to salinity and temperature.

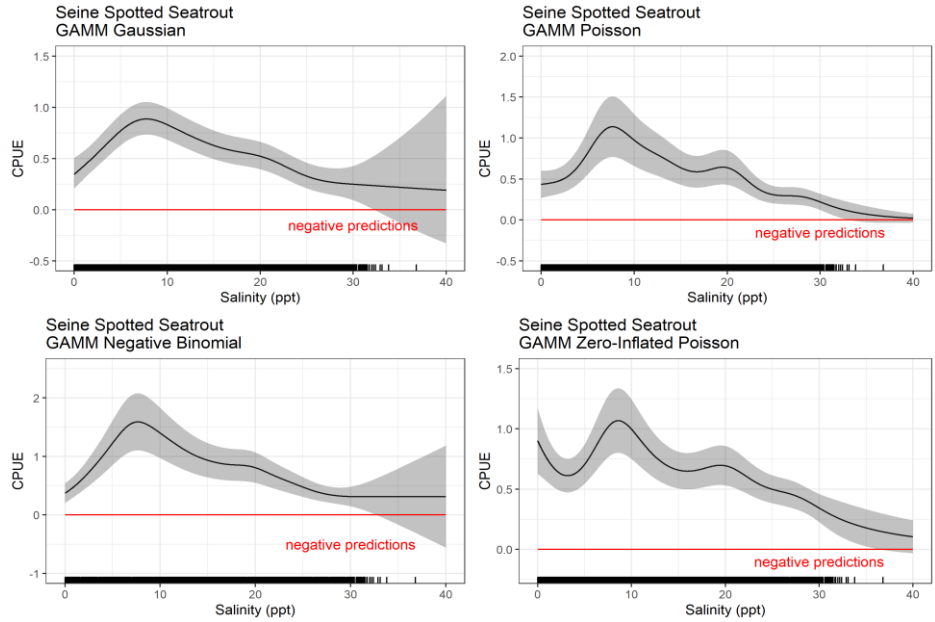

Figure 83. GAMM predicted response of juvenile spotted seatrout CPUE to salinity, with other variables held constant. Shaded gray area represents 95% confidence interval.

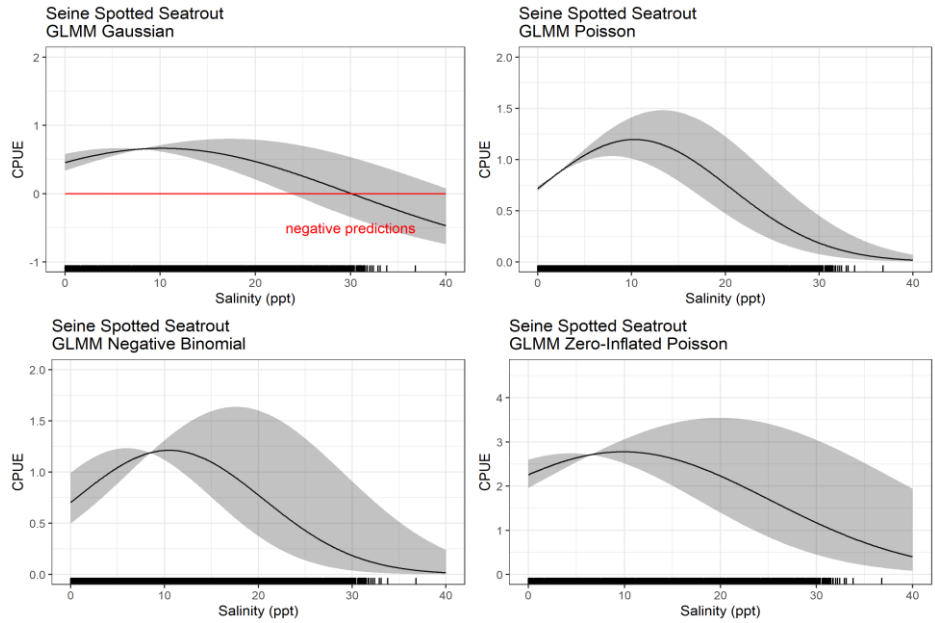

Figure 84. GLMM predicted response of juvenile spotted seatrout CPUE to salinity, with other variables held constant. Shaded gray area represents 95% confidence interval.

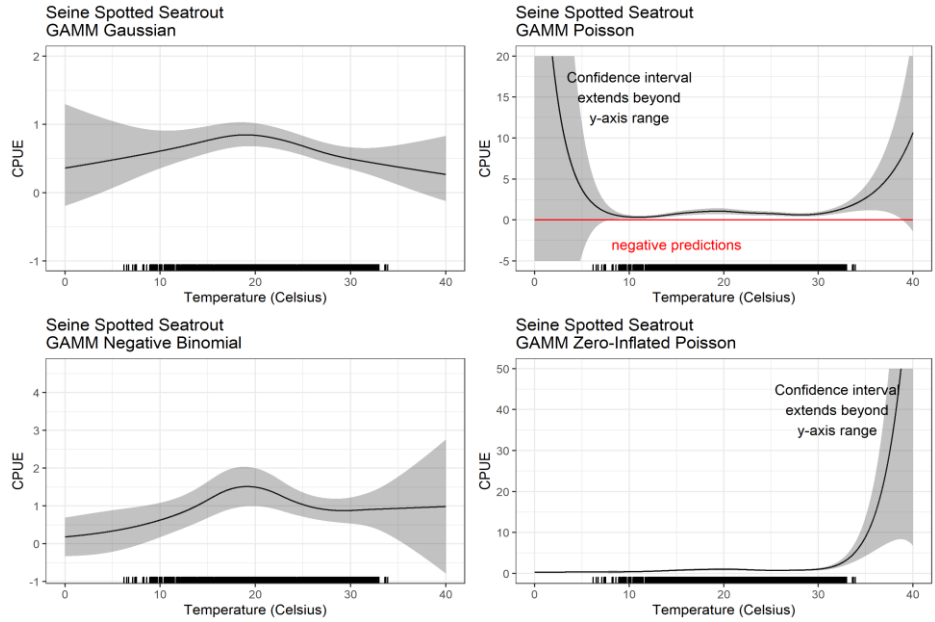

Figure 85. GAMM predicted response of juvenile spotted seatrout CPUE to temperature, with other variables held constant. Shaded gray area represents 95% confidence interval.

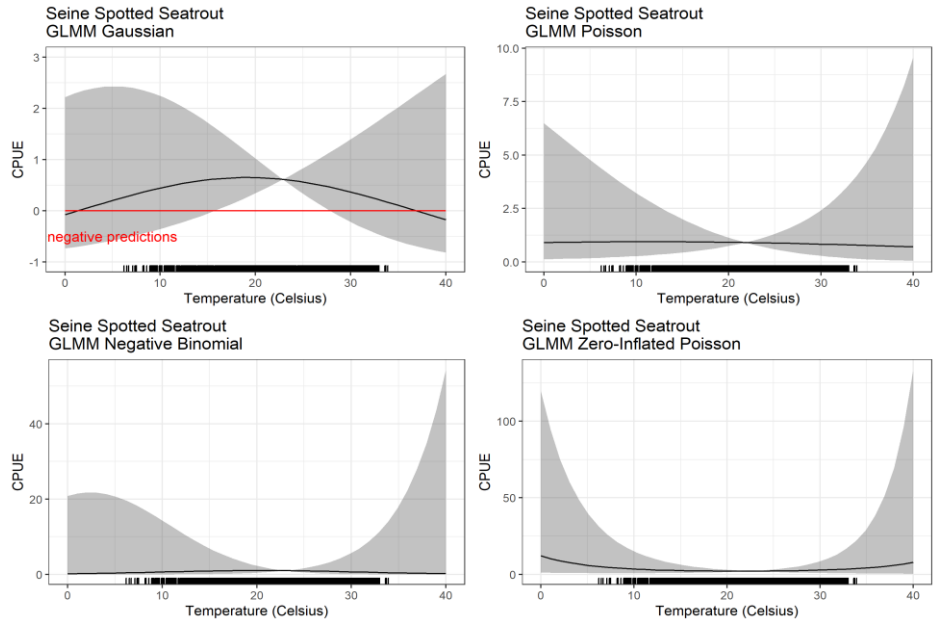

Figure 86. GLMM predicted response of juvenile spotted seatrout CPUE to temperature, with other variables held constant. Shaded gray area represents 95% confidence interval.

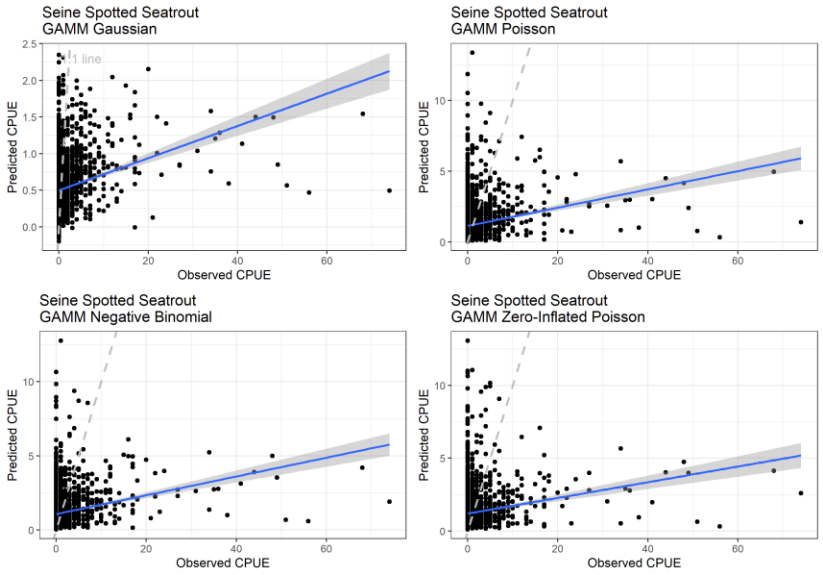

Figure 87. GAMM predicted juvenile spotted seatrout CPUE plotted against observed CPUE using the 30% randomly selected testing dataset. Dashed line provided for reference purposes of 1:1 relationship. Blue line indicates linear relationship between predicted and observed.

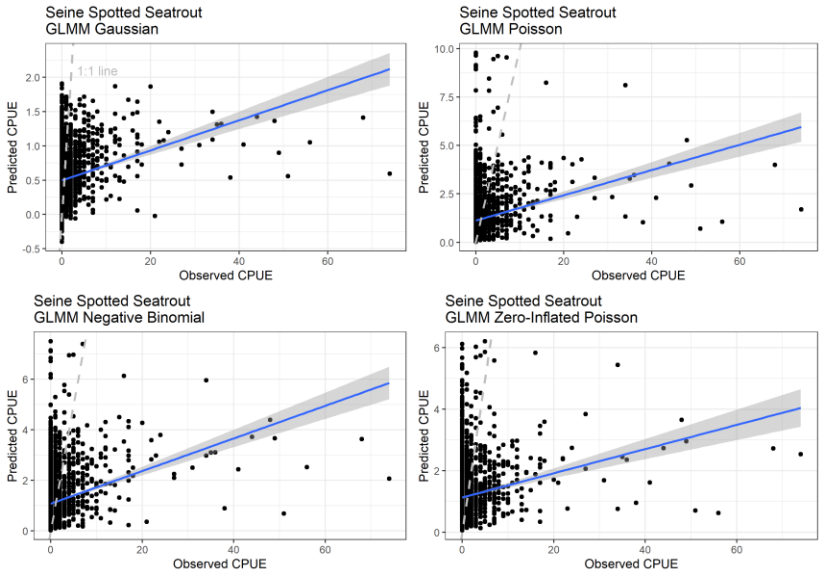

Figure 88. GLMM predicted juvenile spotted seatrout CPUE plotted against observed CPUE using the 30% randomly selected testing dataset. Dashed line provided for reference purposes of 1:1 relationship. Blue line indicates linear relationship between predicted and observed.

Table 19. Summary of model validation metrics for juvenile spotted seatrout. *Denotes selected model.

Model Approach	Error Structure	Adjusted R^2	Correlation	RMSE
GAMM	*Gaussian	0.11	0.33	4.43
	Poisson	0.05	0.22	4.34
	Zero-Inflated Poisson	0.03	0.18	4.40
	Negative Binomial	0.06	0.24	4.31
GLMM	Gaussian	0.11	0.33	4.43
	Poisson	0.06	0.24	4.31
	Zero-Inflated Poisson	0.03	0.18	4.37
	Negative Binomial	0.08	0.28	4.27

Table 20. Basis dimension (k') for each smooth term within the juvenile spotted seatrout Gaussian GAMM.

	Parameter	k'	edf	k-index	p-value
Gaussian	Salinity	9.00	5.67	0.97	0.02
	Temperature	9.00	3.25	1.00	0.49
	Julian date	9.00	4.38	1.00	0.52

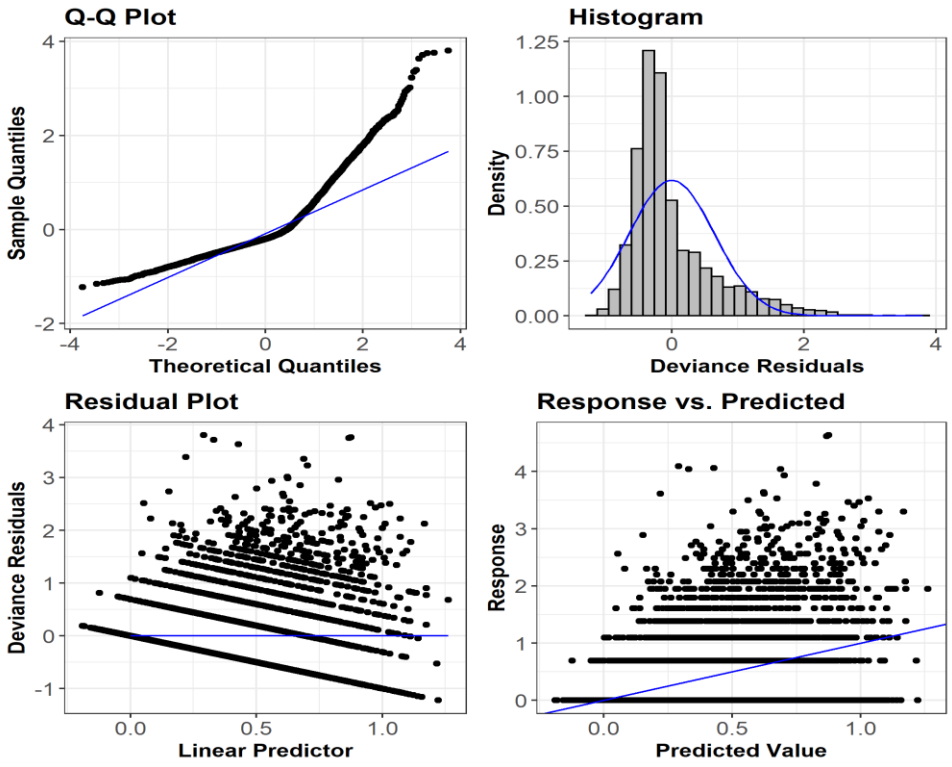

Figure 89. GAMM Gaussian diagnostic plots for juvenile spotted seatrout.

Adult Spotted Seatrout (Gill Nets)

Examination of mean CPUE by month, averaged over all years of available gillnet data, indicated that adult spotted seatrout were collected in relatively high numbers year round (Figure 90). This is consistent with the life history of spotted seatrout, which are estuarine residents but may move just outside the basins to spawn during the summer. Use of the entire dataset (all months) resulted in 23,135 unique data points; 70% of the data points were used for model development and 30% were used for model validation. Water temperature during this time period ranged from 3.4 to 35.9°C; whereas salinity ranged from 0 to 37 ppt.

The Poisson and Zero-Inflated Poisson GLMM resulted in higher R^2 than any other model, while RMSE were similar among the models (Table 21). Among the GAMMs, Poisson and Zero-Inflated Poisson had higher deviance explained than the other GAMM error structures. Examination of response curves indicated Gaussian GAMM and Gaussian GLMM were more aligned with the expected ecological response for this species to salinity and temperature (Figure 91 through Figure 96). Model validation results indicated all models performed similarly, with low R^2 values and similar RMSE values among models. There were some slightly larger differences among correlation values. (Table 22, Figure 97, Figure 98). Given these results, the Gaussian GAMM was selected for inclusion in the overall HSI model for adult spotted seatrout because the response curves were biologically feasible and model performance was similar to other models. Basis dimensions (Table 23) and diagnostic plots (Figure 99) for the GAMM Gaussian model are provided for reference purposes.

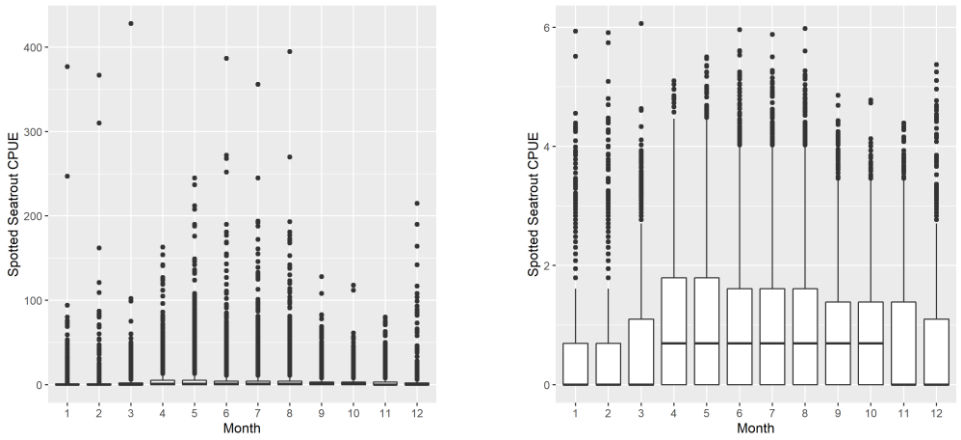

Figure 90. Adult spotted seatrout CPUE in gillnet; raw scale (left panel), natural log scale (right panel)

Table 21. Summary of model fit metrics for adult spotted seatrout. *Denotes selected model.

Model Approach	Error Structure	Adjusted R^2	Deviance explained (GAMM only)	RMSE
GAMM	*Gaussian	0.13	14%	13.74
	Poisson	0.11	23%	12.79
	Zero-Inflated Poisson	.	20.6%	13.01
	Negative Binomial	0.07	17.2%	13.10
GLMM	Gaussian	0.18		13.64
	Poisson	0.82		12.71
	Zero-Inflated Poisson	0.61		12.96
	Negative Binomial	0.06		12.96

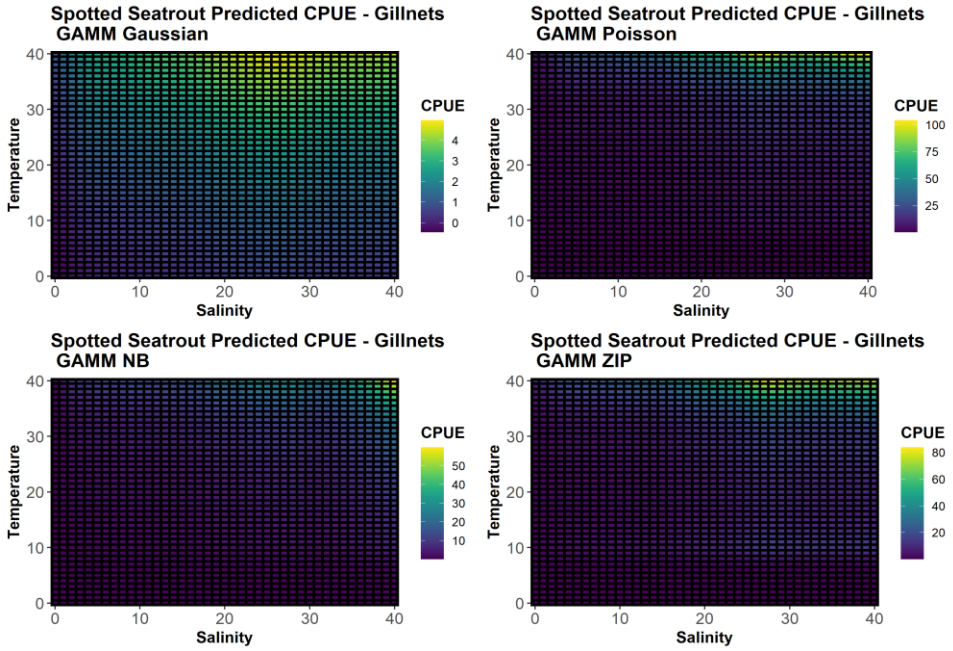

Figure 91. GAMM predicted response of adult spotted seatrout CPUE to salinity and temperature.

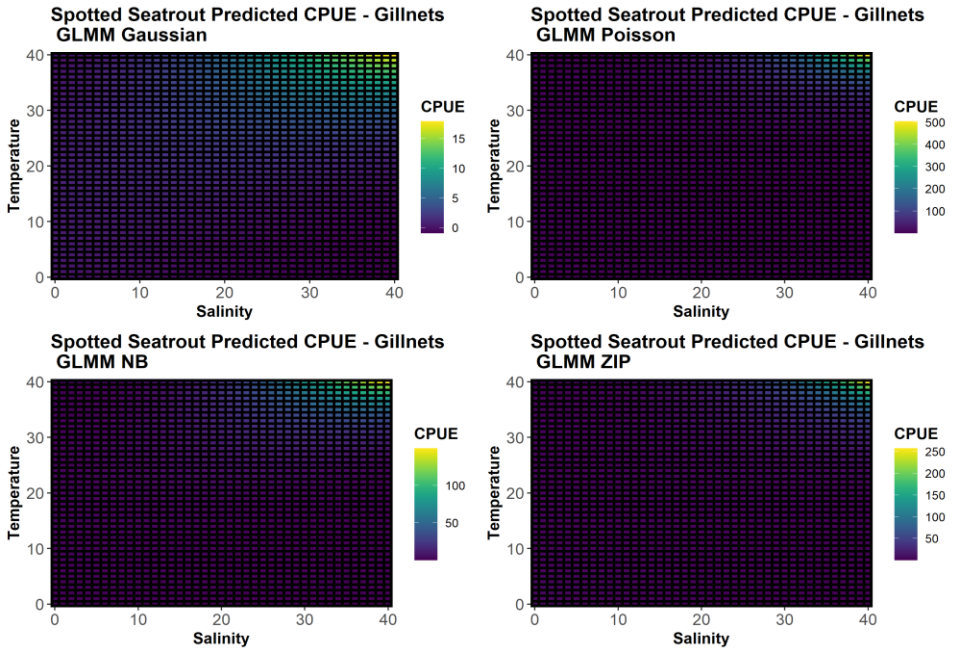

Figure 92. GLMM predicted response of adult spotted seatrout CPUE to salinity and temperature.

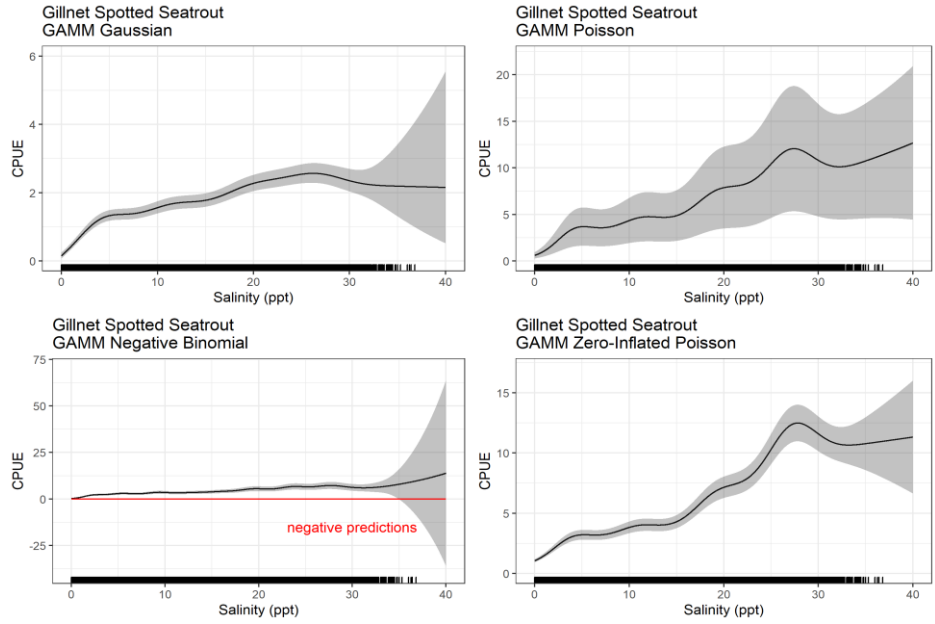

Figure 93. GAMM predicted response of adult spotted seatrout CPUE to salinity, with other variables held constant. Shaded gray area represents 95% confidence interval.

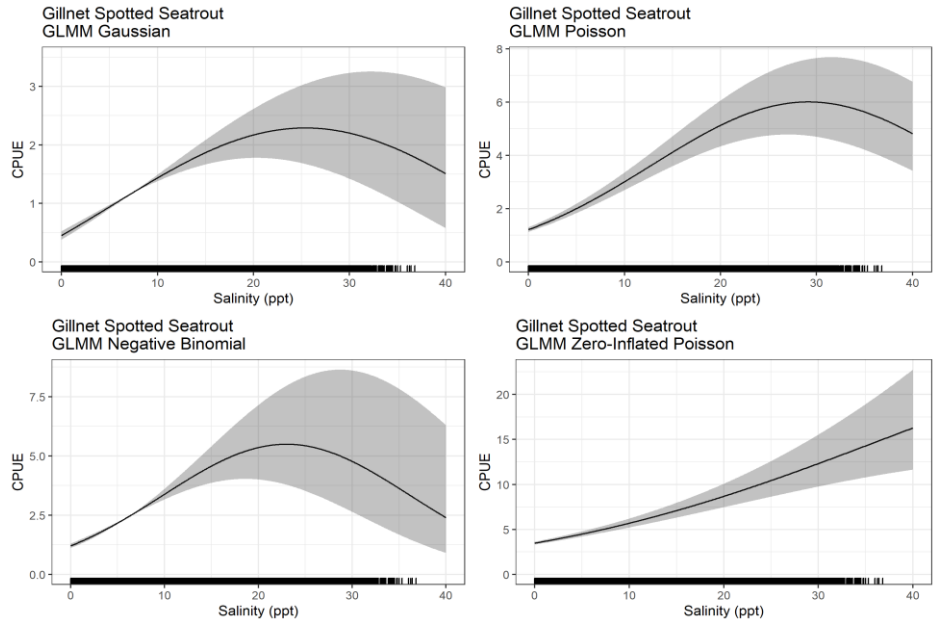

Figure 94. GLMM predicted response of adult spotted seatrout CPUE to salinity, with other variables held constant. Shaded gray area represents 95% confidence interval.

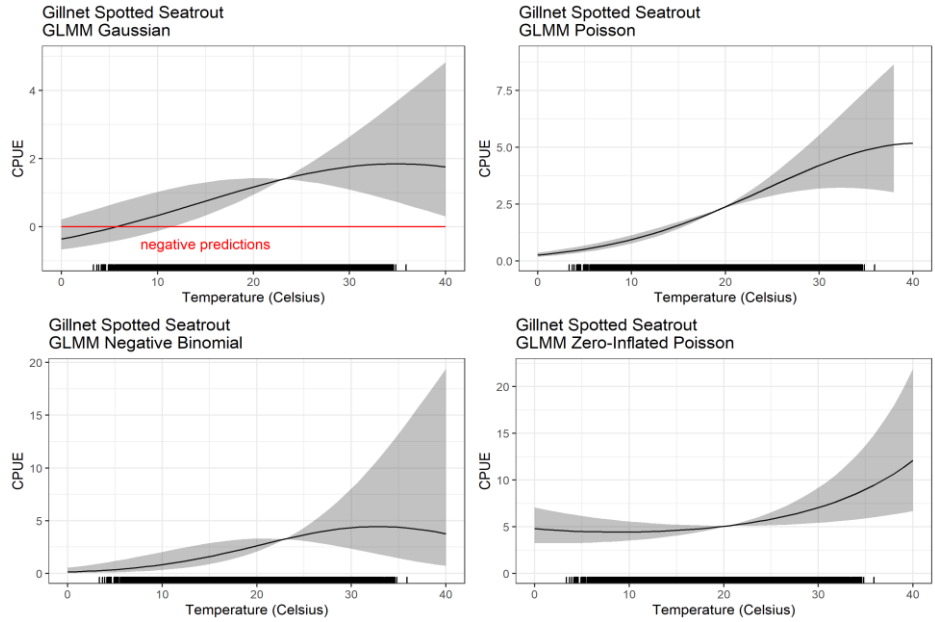

Figure 95. GLMM predicted response of adult spotted seatrout CPUE to temperature, with other variables held constant. Shaded gray area represents 95% confidence interval.

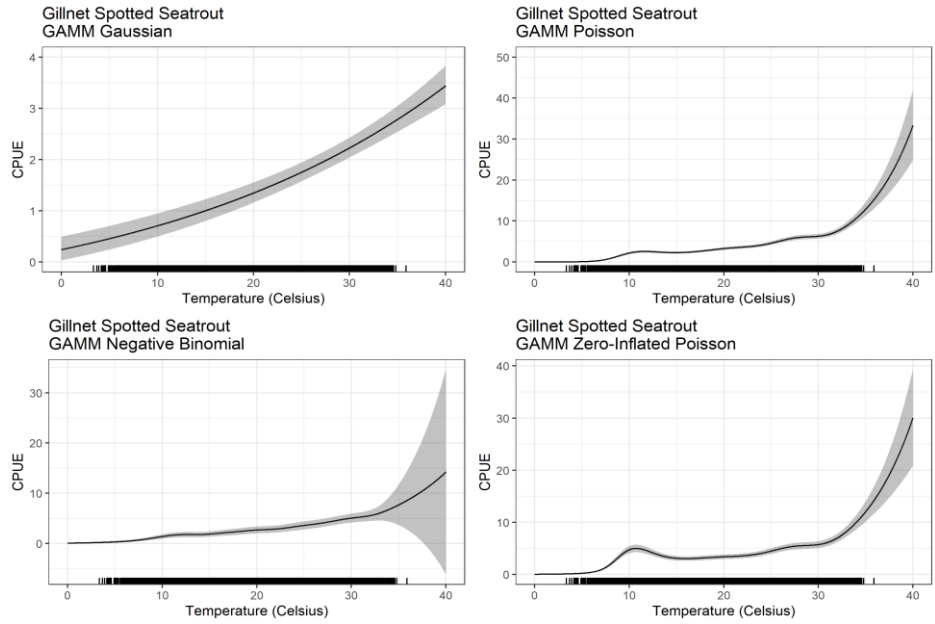

Figure 96. GAMM predicted response of adult spotted seatrout CPUE to temperature, with other variables held constant. Shaded gray area represents 95% confidence interval.

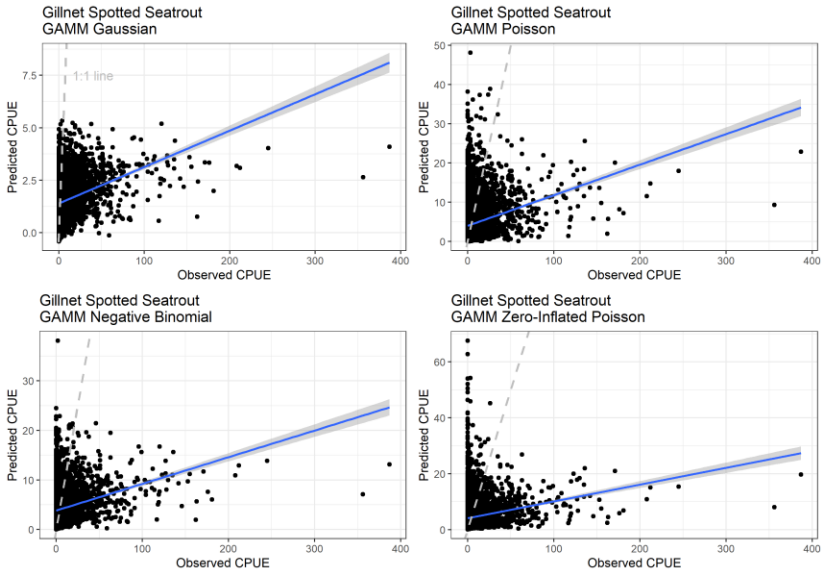

Figure 97. GAMM predicted adult spotted seatrout CPUE plotted against observed CPUE using the 30% randomly selected testing dataset. Dashed line provided for reference purposes of 1:1 relationship. Blue line indicates linear relationship between predicted and observed.

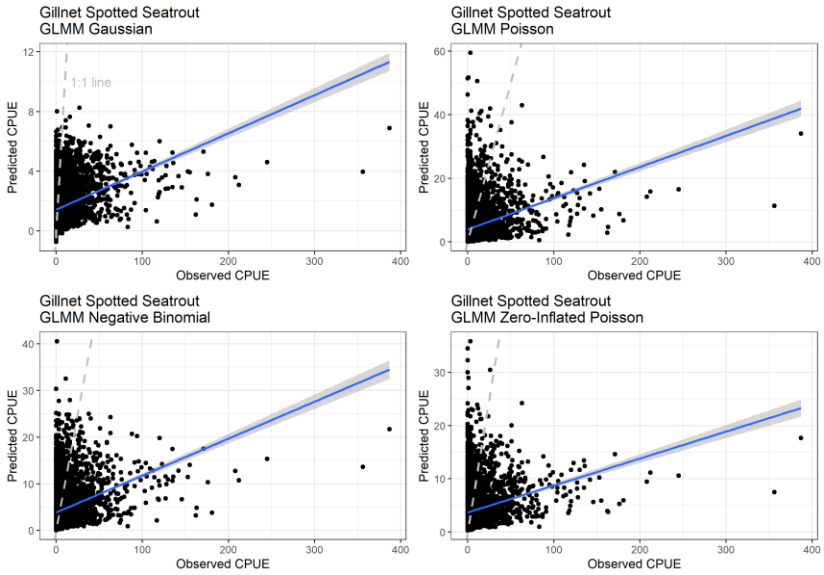

Figure 98. GLMM predicted adult spotted seatrout CPUE plotted against observed CPUE using the 30% randomly selected testing dataset. Dashed line provided for reference purposes of 1:1 relationship. Blue line indicates linear relationship between predicted and observed.

Table 22. Summary of model validation metrics for adult spotted seatrout. *Denotes selected model.

Model Approach	Error Structure	Adjusted R^2	Correlation	RMSE
GAMM	*Gaussian	0.12	0.35	13.65
	Poisson	0.07	0.26	13.08
	Zero-Inflated Poisson	0.03	0.19	13.41
	Negative Binomial	0.06	0.24	13.12
GLMM	Gaussian	0.15	0.39	13.54
	Poisson	0.08	0.28	13.00
	Zero-Inflated Poisson	0.05	0.23	13.16
	Negative Binomial	0.08	0.29	12.95

Table 23. Basis dimension (k') for each smooth term within the adult spotted seatrout Gaussian GAMM.

	Parameter	k'	edf	k-index	p-value
Gaussian GAMM	Salinity	9.00	8.01	0.99	0.34
	Temperature	9.00	1.00	1.01	0.86
	Julian date	9.00	6.80	1.00	0.61

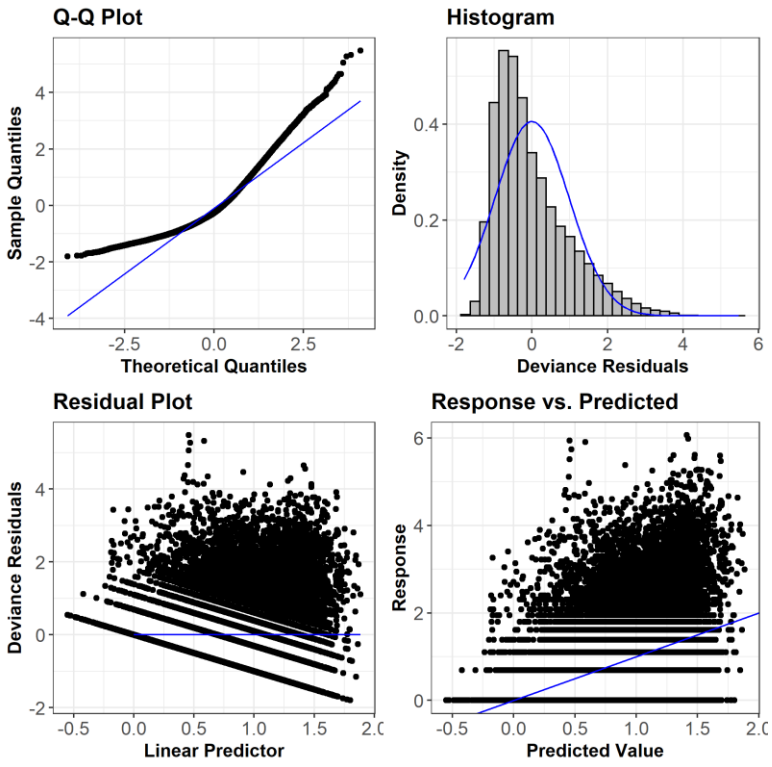

Figure 99. Gaussian GAMM diagnostic plots for adult spotted seatrout.

Largemouth Bass (Electrofishing)

Examination of mean CPUE by month, averaged over all years of available electrofishing data, indicated that that largemouth bass were collected in relatively high numbers year-round (Figure 100). Largemouth bass are year-round residents of the upper estuarine basins. Use of the year-round dataset resulted in 2974 unique data points; 70% of the data points were used for model development and 30% were used for model validation. Water temperature during this time period ranged from 7.1 to 34.8°C; whereas salinity ranged from 0 to 27.4 ppt.

The Poisson GLMM and Zero-Inflated Poisson GLMM resulted in higher R^2 than any other model, although the Gaussian GLMM and Gaussian GAMM had statistically acceptable R^2 scores as well (Table 24). Among the GAMMs, Zero-Inflated Poisson had highest deviance explained. RMSE was low for Poisson Gamm, Zero-Inflated Poisson GAMM, and Poisson GLMM. Examination of the response curves indicate the Poisson GLMM, Negative Binomial GLMM, Gaussian GAMM, and Negative Binomial GAMM captured the expected response to salinity in a biologically defensible way, while the temperature response was more reasonable across the GLMMs rather than the GAMMs (Figure 101 through Figure 106). Model validation results indicated low R^2 values for all models, similar RMSE values among models, and higher correlation values for Gaussian GAMM and Gaussian GLMM, relative to other models (Table 25, Figure 107, Figure 108). Given these results, the Poisson GLMM was selected for inclusion in the overall HSI model for largemouth bass because the response curves were biologically feasible and validation results performed similarly to other models. Diagnostic plots for the selected model are provided in Figure 109 for reference purposes.

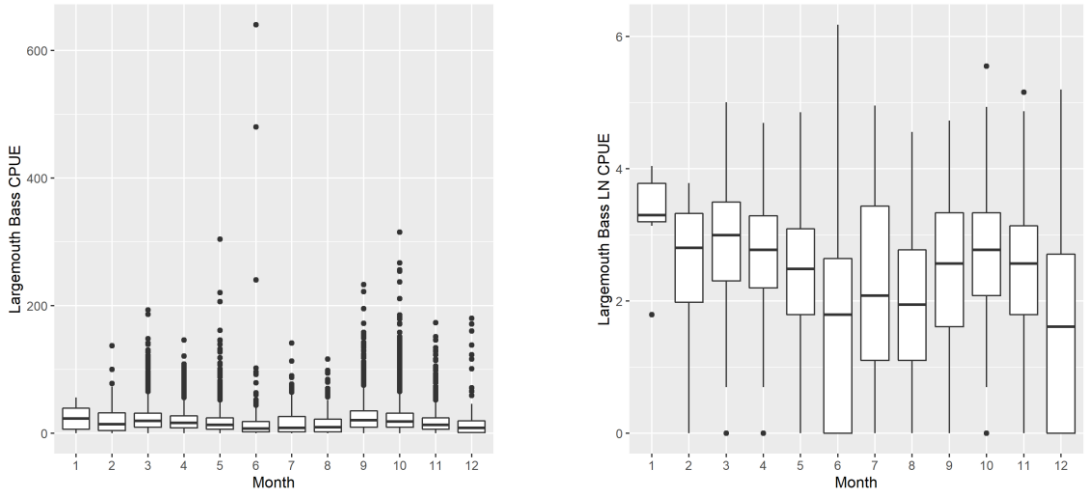

Figure 100. Largemouth bass CPUE in electrofishing; raw scale (left panel), natural log scale (right panel).

Table 24. Summary of model fit metrics for largemouth bass. *Denotes selected model.

Model Approach	Error Structure	Adjusted R^2	Deviance explained (GAMM only)	RMSE
GAMM	Gaussian	0.30	35.4%	19.48
	Poisson	0.17	31.4%	17.59
	Zero-Inflated Poisson	.	63.4%	17.70
	Negative Binomial	0.15	24%	18.16
GLMM	Gaussian	0.34	.	19.74
	*Poisson	0.97	.	17.75
	Zero-Inflated Poisson	0.81	.	19.46
	Negative Binomial	0.26	.	18.22

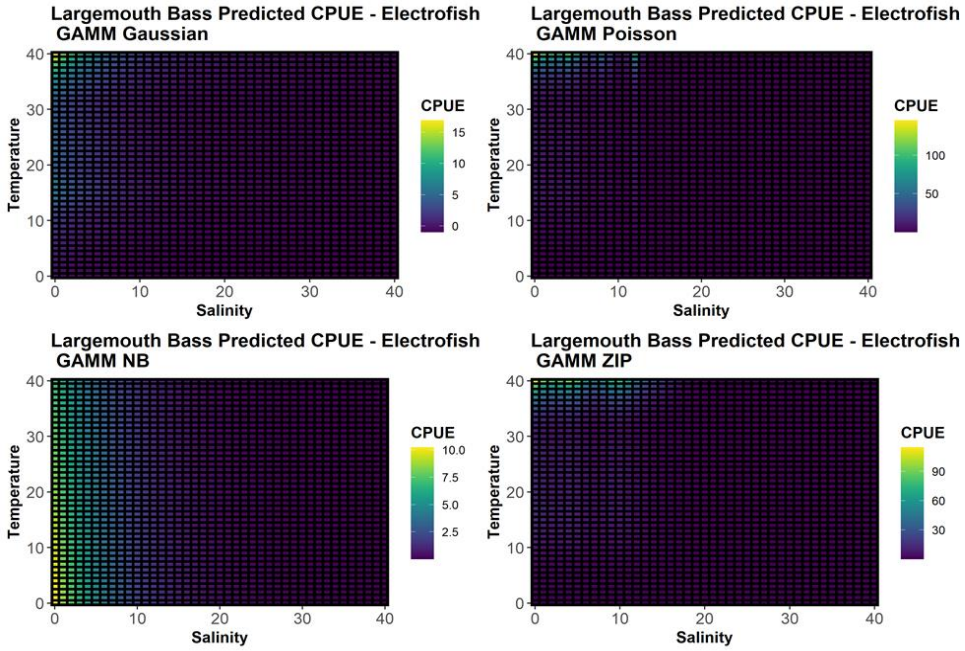

Figure 101. GAMM predicted response of largemouth bass CPUE to salinity and temperature.

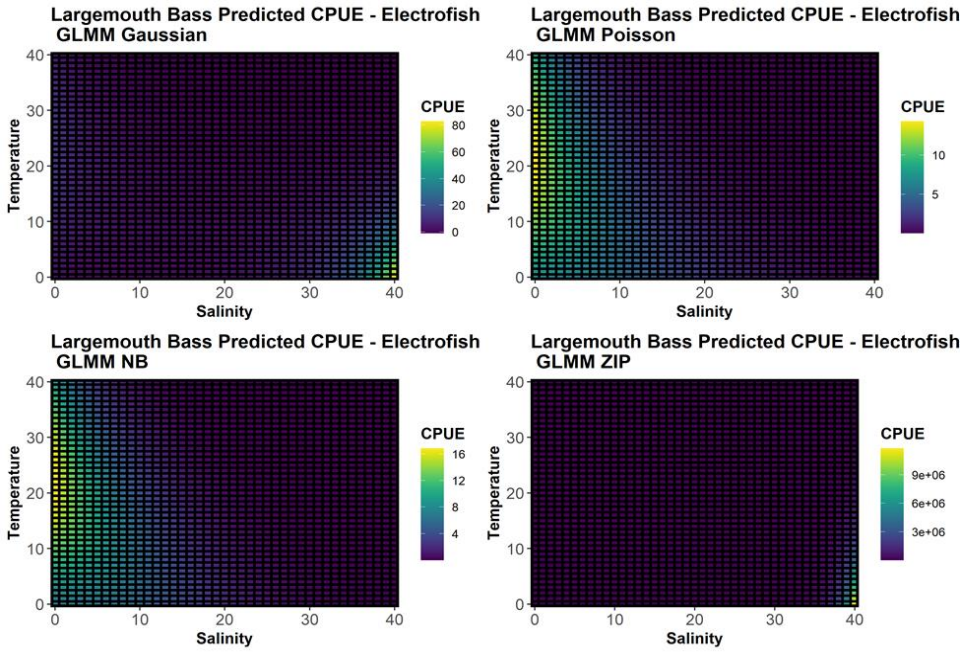

Figure 102. GLMM predicted response of largemouth bass CPUE to salinity and temperature.

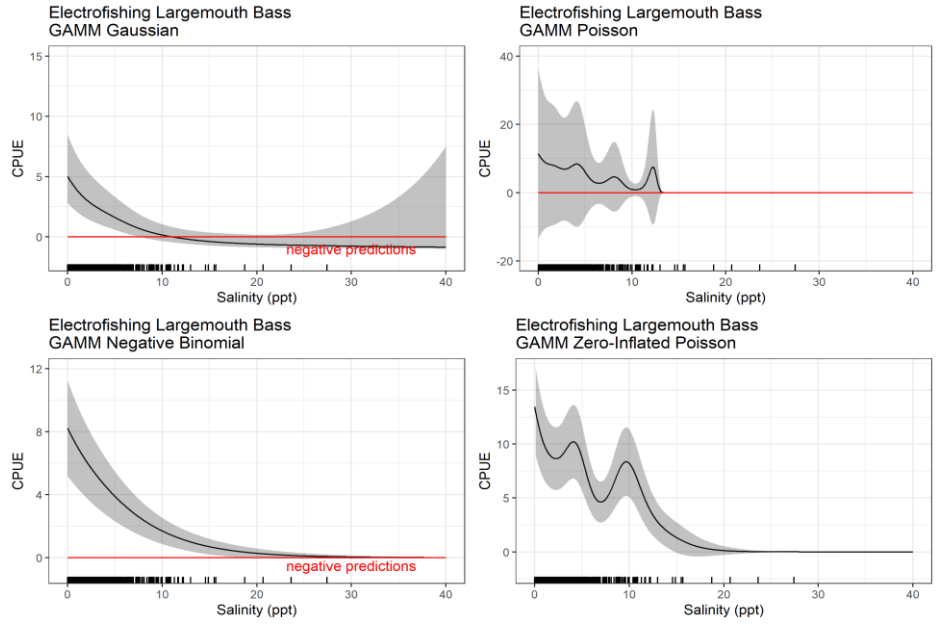

Figure 103. GAMM predicted response of largemouth bass CPUE to salinity, with other variables held constant. Shaded gray area represents 95% confidence interval.

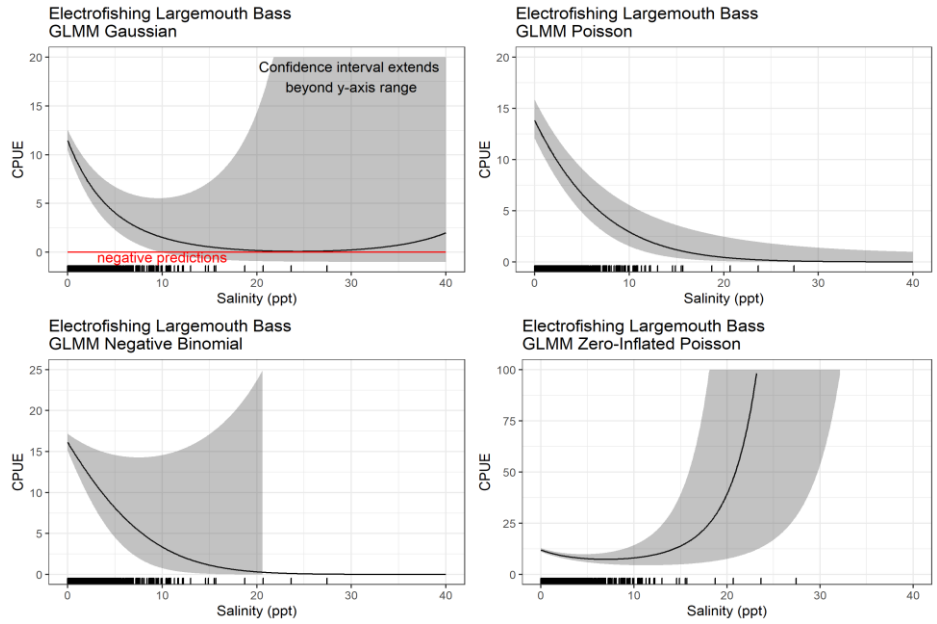

Figure 104. GLMM predicted response of largemouth bass CPUE to salinity, with other variables held constant. Shaded gray area represents 95% confidence interval.

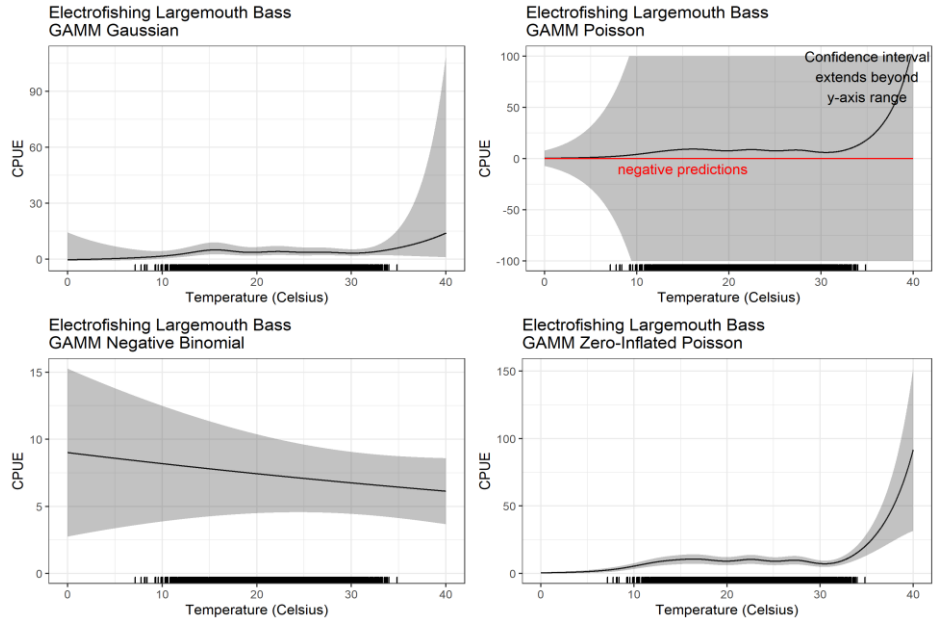

Figure 105. GAMM predicted response of largemouth bass CPUE to temperature, with other variables held constant. Shaded gray area represents 95% confidence interval.

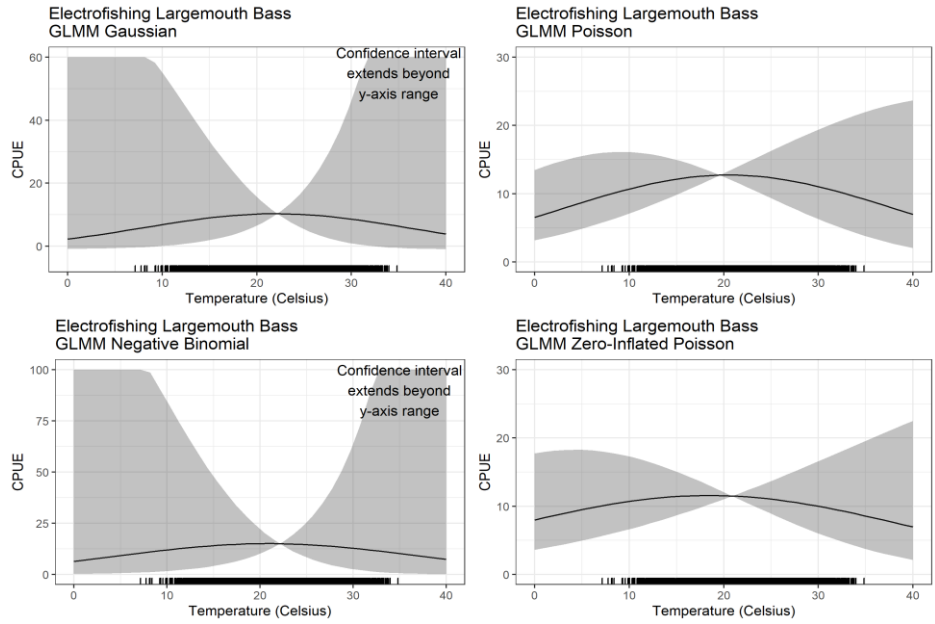

Figure 106. GLMM predicted response of largemouth bass CPUE to temperature, with other variables held constant. Shaded gray area represents 95% confidence interval.

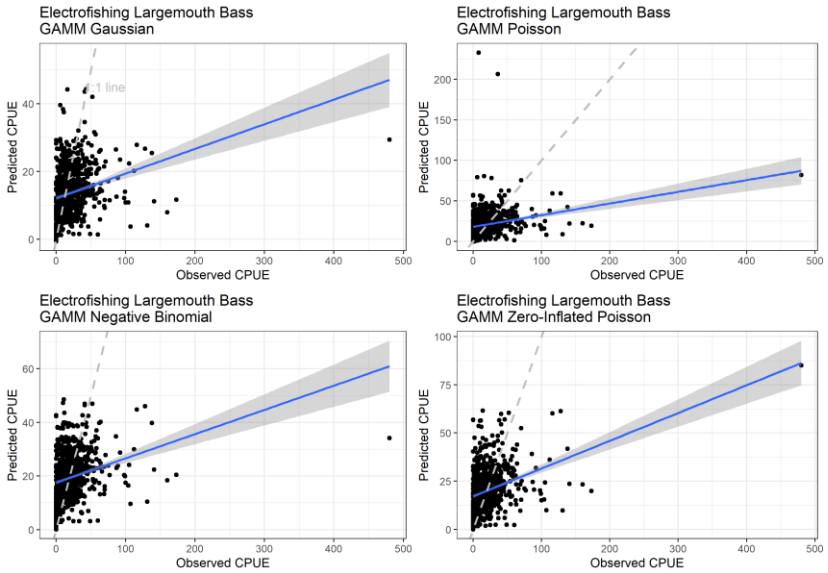

Figure 107. GAMM predicted largemouth bass CPUE plotted against observed CPUE using the 30% randomly selected testing dataset. Dashed line provided for reference purposes of 1:1 relationship. Blue line indicates linear relationship between predicted and observed.

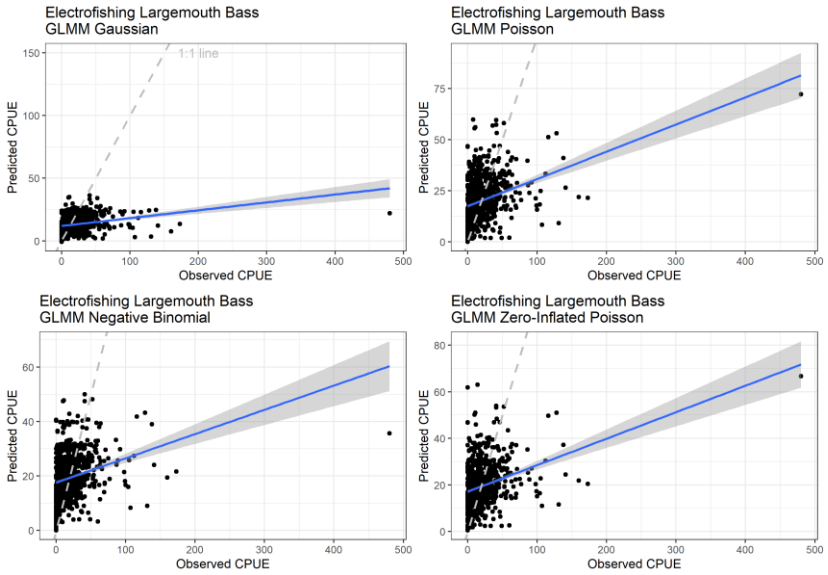

Figure 108. GLMM predicted largemouth bass CPUE plotted against observed CPUE using the 30% randomly selected testing dataset. Dashed line provided for reference purposes of 1:1 relationship. Blue line indicates linear relationship between predicted and observed.

Table 25. Summary of model validation metrics for largemouth bass. *Denotes selected model.

Model Approach	Error Structure	Adjusted R^2	Correlation	RMSE
GAMM	Gaussian	0.22	0.46	25.62
	Poisson	0.06	0.25	26.24
	Zero-Inflated Poisson	0.12	0.35	24.11
	Negative Binomial	0.08	0.28	24.76
GLMM	Gaussian	0.20	0.45	25.78
	*Poisson	0.12	0.34	24.20
	Zero-Inflated Poisson	0.11	0.33	24.32
	Negative Binomial	0.08	0.28	24.69

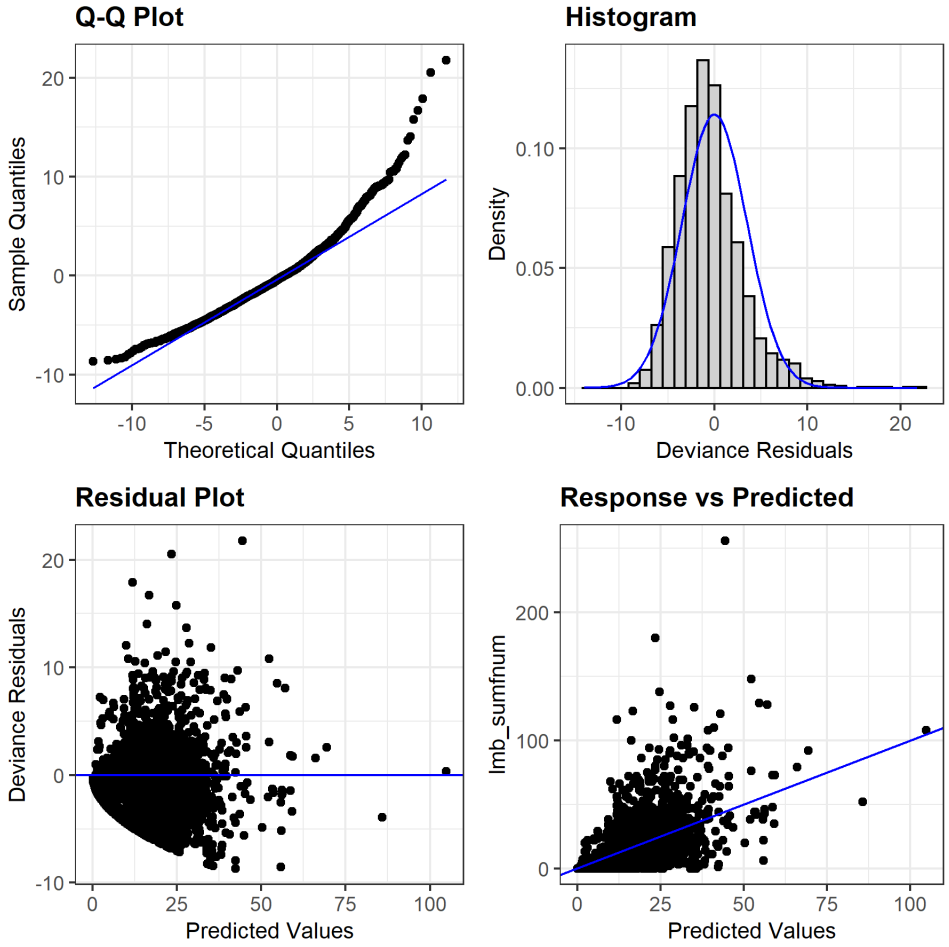

Figure 109. Poisson GLMM Diagnostic plots for largemouth bass.

4.0 REFERENCES

Barton, K. (2009). Mu-MIn: Multi-model inference. R Package v. 0.12.2/r18. From: http://R-Forge.R-project.org/projects/mumin/

Bates, D., Machler, M., Bolker, B., & Walker, S. (2015). Fitting linear mixed-effects models using lme4. Journal of Statistical Software, 67, 1-48.

Bjornstad, O.N. (2020). ncf: Spatial covariance functions. R package v. 1.2-9. From: https://CRAN.R-project.org/package=ncf.

Bjornstad, O.N. & Falk, W. (2001). Nonparametric spatial covariance functions: estimation and testing. Environmental and Ecological Statistics, 8, 53-70.

Brooks, M.E., Kristensen, K., van Benthem, K.J., Magnusson, A., Berg, C.W., Nielsen, A., ... Bolker, B.M. (2017). glmmTMB balances speed and flexibility among packages for zero-inflated generalized linear mixed modeling. The R Journal, 9, 378-400.

Callaway, J., Hagen, S., Harris, C., Kimmerer, W., & Waldon, M. (2017). 2017 Coastal Master Plan: Attachment C5-1: Predictive Models Technical Advisory Committee Report. Version Final. Coastal Protection and Restoration Authority, Baton Rouge, Louisiana.

Dormann, C.F. (2007). Effects of incorporating spatial autocorrelation into the analysis of species distribution data. Global Ecology and Biogeography, 16, 129-138.

Gotelli, N.J. & Ellison, A.M. (2004). A Primer of Ecological Statistics, 2nd edition. Sunderland, MA: Sinauer Associates.

Guisan, A., & Thuiller, W. (2005). Predicting species distribution: offering more than simple habitat models. Ecology Letters, 8, 993–1009.

Legendre, P. (1993). Spatial autocorrelation: trouble or new paradigm? Ecology, 74, 1659-1673.

Lichstein, J.W., Simons, T.R., Shriner, S.A., & Franzreb, K.E. (2002). Spatial autocorrelation and autoregressive models in ecology. Ecological Monographs, 72, 445-463.

Nakagawa, S. & Schielzeth, H. (2013). A general and simple method for obtaining R^2 from generalized linear mixed-effects models. Methods in Ecology and Evolution, 4, 133-142.

R Core Team (2019). R: A language and environment for statistical computing. R Foundation for Statistical Computing, Vienna, Austria. From: https://www.R-project.org

Wood, S.N. (2017). Generalized additive models: an introduction with R, 2nd ed., Boca Raton, FL: CRC/Taylor & Francis.

Wood, S.N., Pya, N., & Safken, B. (2016). Smoothing parameter and model selection for general smooth models (with discussion). Journal of the American Statistical Association, 99, 673-686.

ATTACHMENT 4: FISH, SHRIMP, AND CRAB STRUCTURAL HABITAT SUITABILITY INDEX

Ann M. O'Connell – University of New Orleans

1.0 INTRODUCTION

The 2017 Habitat Suitability Index (HSI) models for blue crab, brown shrimp, white shrimp, gulf menhaden, spotted seatrout, and largemouth bass each included component structural habitat suitability indices (SIs, where SI is a component model within the overall HSI) based on the areal proportion of marsh vegetation to open water simulated for each grid cell of the Integrated Compartment Model (ICM). The relationship used for the species' juvenile stage SI models was adapted from Minello and Rozas (2002) and represents the observed increase in juvenile fish, shrimp, and crab densities in fragmented marsh habitats (Figure 1). However, the relationship does not take into account the effects of other estuarine habitats, such as submerged aquatic vegetation or oyster reefs, that are differentially important to juvenile, subadult, and adult life stages of fish and shellfish as foraging grounds or predation refugia (Humphries & La Peyre, 2015; Humphries et al., 2011a; Stunz et al., 2010; Grabowski et al., 2008; Castellanos & Rozas, 2001). Considering these habitats can also be simulated by the ICM, their inclusion into the structural habitat SI functions was warranted. The following describes the process used to determine the relative value of aquatic estuarine habitats to the species or life stage and refine the structural habitat SIs for the 2023 Coastal Master Plan.

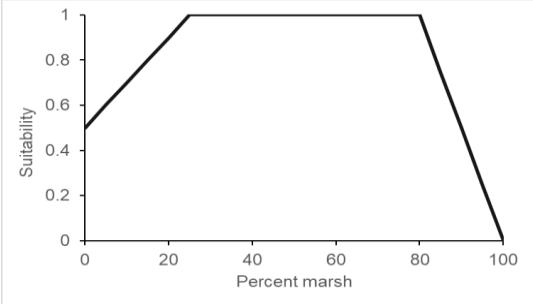

$SI_2 = (0.02*V_2) + 0.5$, when $V_2 < 25$
1.0, when $25 \leq V_2 \leq 80$
$5.0 - (0.05*V_2)$, when $V_2 > 80$

Figure 1. Graphic and numerical representation of the SI used to describe juvenile species habitat suitability based on the Percent Marsh within a cell.

2.0 METHODS

Structural habitat SIs for juvenile life stages

The methodology used for refining the structural habitat SIs for small juvenile brown shrimp, small juvenile white shrimp, juvenile blue crab, juvenile gulf menhaden, and juvenile spotted seatrout had two components. The first component was to add habitat types beyond the marsh and open water classification. Based on an updated review of recent literature (e.g., La Peyre et al., 2019; Hollweg et al., 2019; Minello, 2017), six estuarine habitat types were identified that have been repeatedly sampled and compared relative to each other through independent field studies measuring (usually juvenile) fish, shrimp, and crab densities in the northern Gulf of Mexico. The six habitat types identified from the literature were marsh interior (MI), marsh edge (ME), shallow non-vegetated bottom (SNVB), deep non-vegetated bottom (DNVB), submerged aquatic vegetation (SAV) and oyster reef (Oyster). The suitability scores of each habitat type were estimated relative to each other from a meta-analysis of field data available from 36 studies primarily in the western part of the northern Gulf of Mexico (13 from Louisiana; 16 from Texas) with the rest from the Atlantic Coast and the eastern Gulf of Mexico. The meta-analysis of the 36 field studies followed the methodology from previous meta-analyses by Minello (1999) and Minello et al. (2003) by using the data for each species from each study to compare across the estuarine habitat types.

Not all field studies included within the meta-analysis measured the same habitat types or species abundance metrics. Table 1 lists the field studies considered for the meta-analysis including the species abundance, gear types, and months or seasons sampled. Note that, because of the gear types used, these field studies mostly sampled the juvenile life stages of the species that are using the estuarine habitats as nursery grounds. The drop sampler and throw trap gears used across most fine-scale habitat studies typically sample small fishes (<100 mm total length) and juvenile shrimp and crabs (Minello, 1999). The juvenile densities of species reported from these field studies were sampled at various distances into the marsh and offshore. Minello et al. (2008; Figure 2) previously depicted brown shrimp density distribution in relation to marsh edge, and this pattern was used to approximate species distributions by distance from marsh edge for the other field studies (Table 1). The habitats sampled in the field studies were classified as ME (vegetated marsh ≤1 m from the marsh-water interface), MI (vegetated marsh >1 m from the marsh-water interface), SNVB (0 m < distance offshore <5 m, or undefined SNVB), and DNVB (>5 m distance offshore), and as SAV and Oyster, for those classified in the literature as such. Distance offshore was used as a proxy for bathymetry (which was not usually available from the study) when defining SNVB and DNVB.

Catch metrics within a study were averaged if many areas or time periods were sampled or if there was more than one category for a habitat, taking care to average them correctly based on sample sizes. The catch (density or abundance) data by habitat type was then standardized to the maximum habitat value recorded for each sample period within a study. For example, if nekton density was

highest in SAV, then the SAV suitability score was equal to 1.0 and the lower-density habitats were scaled relative to the maximum density. Some studies had more than one sample period (e.g., month, season, area) for a species. These lines of data were kept separate within a study to account for differences in effort among studies. Scaled habitat scores were then averaged across the data lines regardless of study. This way, no one study was more important than any other (i.e., greater weight was given to those studies with more effort). This is a similar approach to Minello (1999) who calculated mean species density for a habitat as the mean of means from various studies (keeping sampling periods separate) in order to compare the overall mean densities among the various habitats.

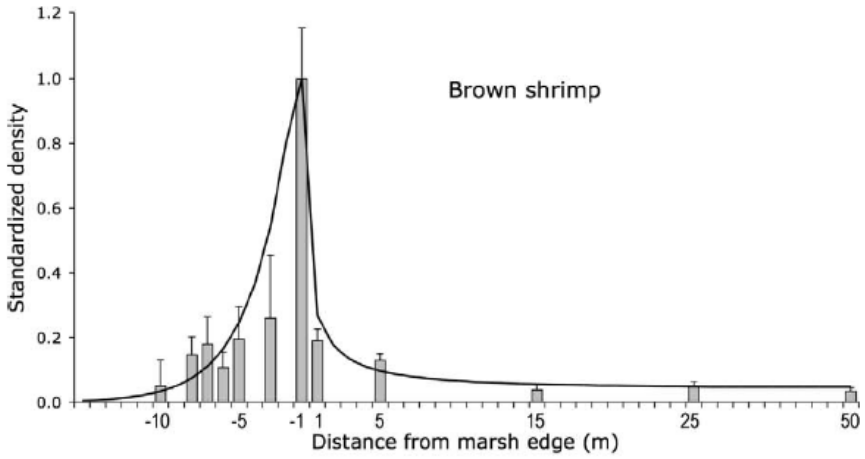

Figure 2. Fine-scale distribution of juvenile brown shrimp density in relation to the marsh edge. Negative values represent distance onto the marsh surface and positive values represent distance into open water. Bars represent standardized measured densities, and the black line is the modeled regression curve (from Minello et al., 2008).

The species' plots of the standardized catch data (between 0.0 and 1.0) by habitat type for each data line (see Table 1) are shown in Figures 3 to 7. The relative suitability score of each habitat type for each of the five key species was determined by simply estimating the mean score. The overall mean habitat scores were then increased by a constant multiplier to bring the maximum habitat suitability score to 1.0 for each species (see bold values in Figures 3-7).

The second component to refining the structural habitat SIs required applying the suitability scores to the habitats simulated for each ICM model cell. It was initially proposed in Sable et al. (2019) to weight the areal proportion of each habitat type by its respective suitability score and then sum across habitat types to produce the structural habitat SI for each species. However, this process had issues with scaling because the marsh edge habitats would never reach 100% cell coverage, and thus the suitability of cells with this important nursery habitat would be underestimated in the calculations.

Therefore, the results of the meta-analysis were used to modify the 2017 structural habitat SI relationship (Figure 1). Specifically, the y-intercept of the relationship, which represents cells of 100% open water, was adjusted in accordance with the suitability score of open water for the species (DNVB scores were used because this category best reflects open water habitats). The remainder of the relationship was unchanged because the 25-80% marsh landscape configuration was still considered optimal for these species as it contains the maximum amount of valuable marsh edge nursery habitat (Minello & Rozas, 2002). The resulting relationship was termed the "baseline relationship" for the species and was used for most model cells. Additional relationships were developed to account for the added habitat value of SAV and oyster reef occurring in open water cells. Thus, the y-intercepts of the baseline relationship were increased in accordance with the higher suitability scores of these habitats. These relationships were applied to model cells with high levels of SAV or oyster reef habitat, the threshold values for which were subjectively chosen because there is a lack of research describing how fish and shellfish abundance responds to changes in SAV or oyster reef coverage. The SAV relationship was used when SAV coverage comprised ≥20% of a model cell, with this threshold value subjectively chosen based on the ICM SAV output data distribution. The oyster reef relationship was used when the average decadal oyster HSI score for a model cell was ≥0.50. Oyster HSI score was used as a proxy for oyster reef habitat because the ICM does not simulate changes in reef (i.e., cultch) coverage. Model tests showed that areas of existing oyster reefs and oyster production had HSI scores ≥0.50; therefore it was assumed that cells with such high suitability scores would continue to support oyster reef habitat throughout the ICM simulations. An average decadal value was used to prevent interannual variability in oyster HSI scores from causing large swings in reef habitat.

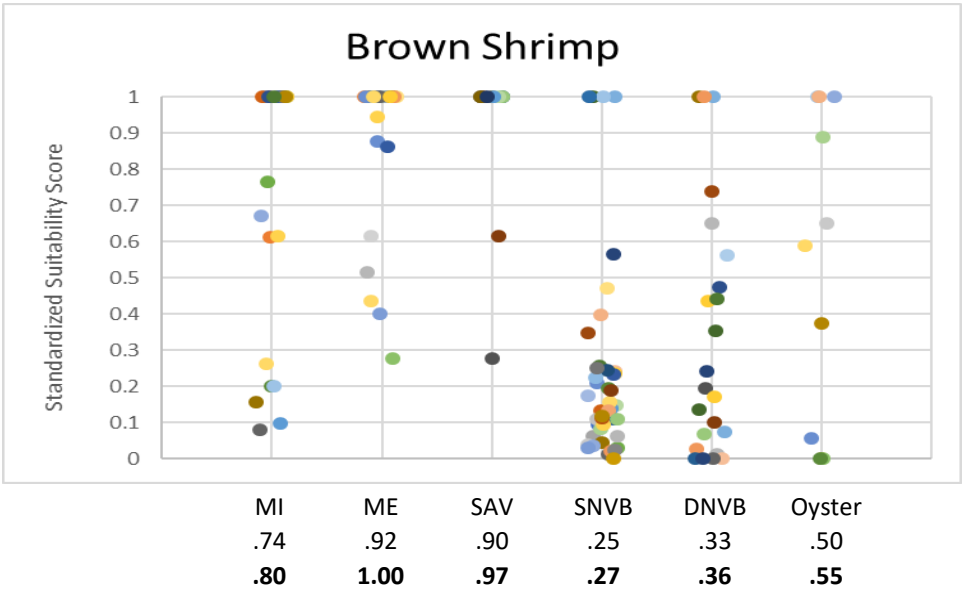

Figure 3. Plots of the average standardized suitability scores for small juvenile brown shrimp by habitat type for each of the data lines listed in Table 1. Bolded values indicate the adjusted suitability scores for each habitat.

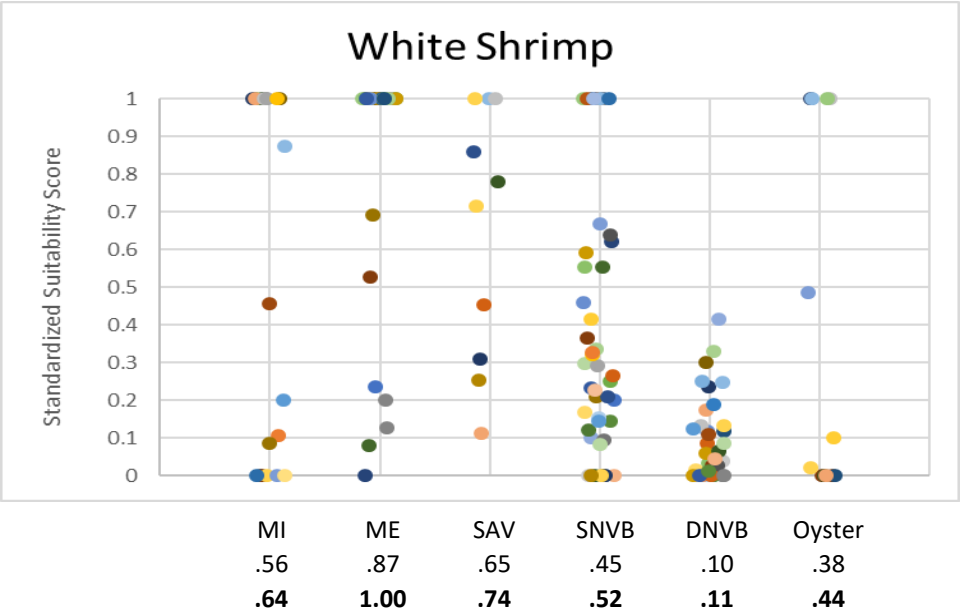

Figure 4. Plots of the average standardized suitability scores for small juvenile white shrimp by habitat type for each of the data lines listed in Table 1. Bolded values indicate the adjusted suitability scores for each habitat.

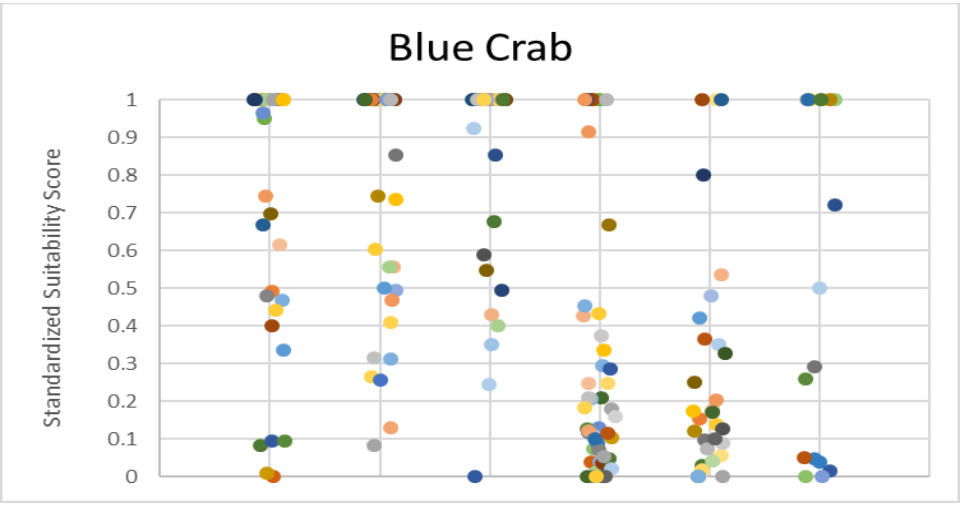

Figure 5. Plots of the average standardized suitability scores for juvenile blue crab by habitat type for each of the data lines listed in Table 1. Bolded values indicate the adjusted suitability scores for each habitat.

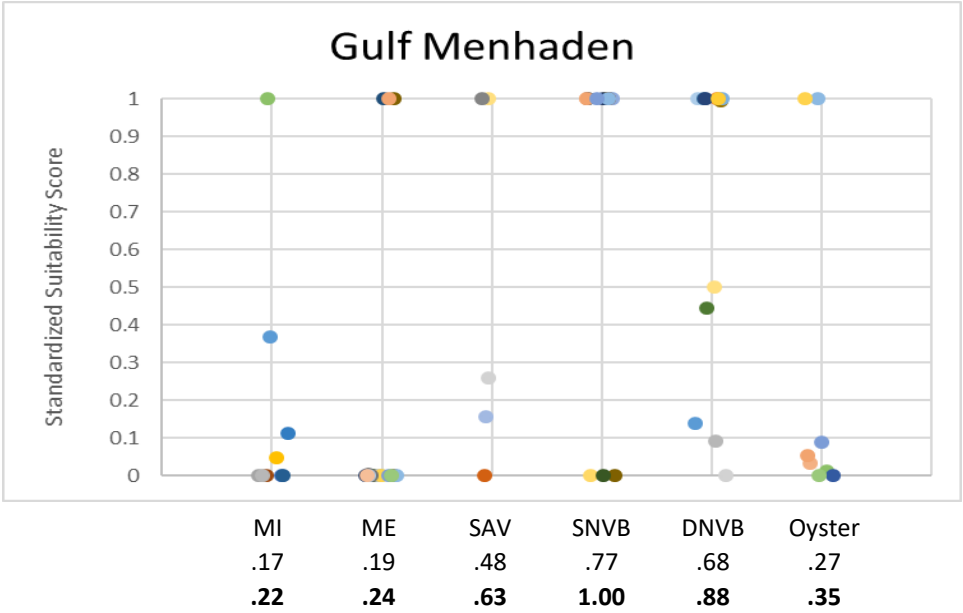

Figure 6. Plots of the average standardized suitability scores for juvenile gulf menhaden by habitat type for each of the data lines listed in Table 1. Bolded values indicate the adjusted suitability scores for each habitat.

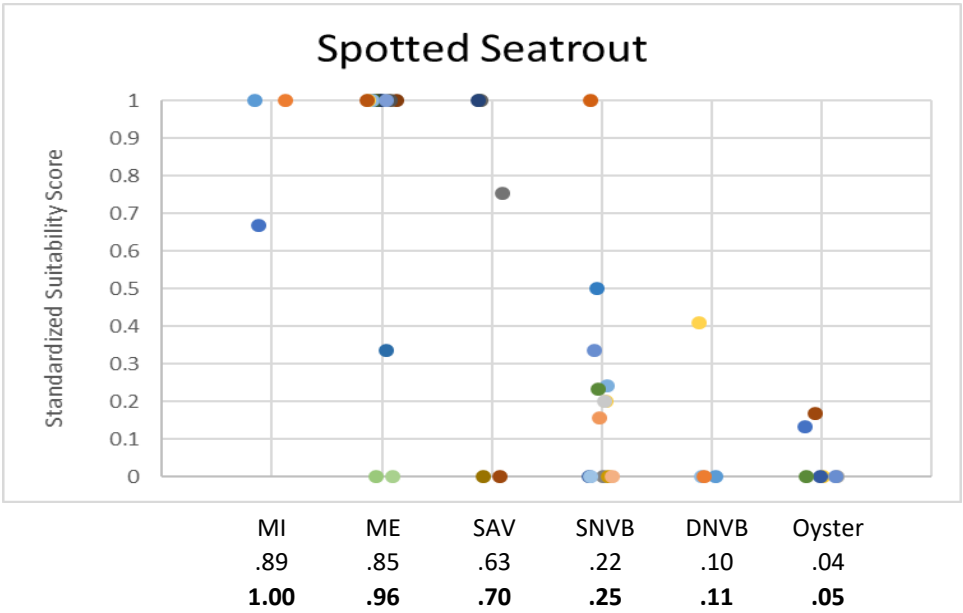

Figure 7. Plots of the average standardized suitability scores for juvenile spotted seatrout by habitat type for each of the data lines listed in Table 1. Bolded values indicate the adjusted suitability scores for each habitat.

Structural habitat SIs for older life stages and largemouth bass

Variations of the marsh-to-open water relationship adapted from Minello and Rozas (2002) were developed for the 2017 structural habitat SIs for large juvenile brown shrimp, large juvenile white shrimp, adult gulf menhaden, and adult spotted seatrout, and were differentially skewed toward open water having greater suitability scores. This reflected their occurrence over non-vegetated bottoms as they move throughout the estuary in search of food (seatrout, gulf menhaden) and towards spawning grounds in the bay, tidal passes, or continental shelf (seatrout, shrimps).

For example, spotted seatrout adults show no consistent pattern of habitat selection among oyster, sandy bottom, and marsh edge habitats in Louisiana, and their distribution seems tied to prey availability and areas with suitable salinity and temperature (MacRae, 2006; Harding & Mann, 1999; Perret et al., 1980; Gulf States Marine Fisheries Commission, 2001). While they associate with seagrass, adult spotted seatrout limit spatial overlap with other species and their diel movements result in the usage of more than one habitat (Moulton et al., 2017). A telemetry study in Lake Calcasieu, Louisiana did show an affinity for reef structures by larger adult spotted seatrout (Callihan, 2011). Because of similarities in prey across adult sizes, this preference was not likely related to prey availability, but rather the tendency for larger adults to school less than smaller individuals and to use these structures for rest. It is not clear however, that this conveys any more value to reefs than other habitats.

There are fewer studies available comparing estuarine habitat use for larger juvenile/sub-adult shrimp and gulf menhaden. The distribution of adult gulf menhaden, which consume phytoplankton and zooplankton, is based on the availability of larger-sized prey in the ecosystem, and this results in post-juvenile menhaden moving further out of the estuary to where more appropriate sized prey are found (Gulf States Marine Fisheries Commission, 2015). Otherwise, older life stages of menhaden, and shrimp, are not selecting certain habitats, but occur in lower open-water bays and tidal passes prior to emigration to the shelf.

For largemouth bass, the 2017 structural habitat SI relationship reflected the value of emergent and submerged aquatic vegetation for: 1) providing foraging opportunities for juveniles and adults that feed on insects, fish, and other invertebrates, 2) providing protection to juveniles from larger predators, and 3) serving as potential spawning habitat for adults. These relationships showed higher values at moderate levels of coverage because these levels do not interfere with foraging success.

Because of the relative lack of research into habitat selection, a meta-analysis was not conducted for the larger juvenile shrimps, adult gulf menhaden, adult spotted seatrout, and largemouth bass. However, a structural habitat relationship was needed to place the HSI results in the proper geographic context. Therefore, the 2017 structural habitat Sis were re-used for the 2023 Coastal Master Plan.

3.0 STRUCTURAL HABITAT SUITABILITY INDICES

The structural habitat SIs for the 2023 Coastal Master Plan small juvenile brown shrimp, small juvenile white shrimp, juvenile blue crab, juvenile gulf menhaden, and juvenile spotted seatrout HSI models are shown in Figure 8. The standardized suitability scores derived from the meta-analysis were similar between brown shrimp, white shrimp, and blue crab, so a single suitability relationship was developed for these three crustacean species. For the baseline relationship, the y-intercept was adjusted to 0.25, which is the average of the DNVB scores for the species (Figure 8a). Open water areas do have value as habitat for juvenile shrimp and crab, but these are predominantly SNVB that occur in association with fragmented marsh habitats and are thus included in the 25-80% marsh optimum part of the curve. Oyster reef and particularly SAV provide more habitat value to open waters and therefore, the y-intercepts were increased to 0.5 and 0.8, respectively, in accordance with the average standardized suitability score of these habitats for the species (Figures 8b and 8c).

Juvenile gulf menhaden are most prevalent in shallow, open water habitats (as shown by the high standardized score for SNVB; Figure 6). However, these habitats primarily occur in association with marsh habitats, which have been recognized as the primary nursery habitat for juvenile menhaden (Deegan et al., 1990). Furthermore, even if they are not using the vegetation itself for habitat, marsh detritus is an important food source for juvenile menhaden during their residence in marsh shallow waters (Deegan et al., 1990). As the 2017 relationship captures the value of both SNVB and marsh habitat for this species, it was re-used for the 2023 gulf menhaden structural habitat SI (Figure 8b).

The standardized suitability scores for juvenile spotted seatrout reflect this species' association with vegetated habitats and the unsuitability of open water habitats where juvenile seatrout cannot easily avoid predation (Figure 7). Therefore, for the juvenile seatrout's baseline suitability relationship, the y-intercept was lowered to 0.1 based on its DNVB score (Figure 8d). For cells with high SAV coverage, the same relationship developed for juvenile shrimp and crab was used for juvenile seatrout (Figure 8c). Although juvenile seatrout's standardized suitability score for SAV was somewhat lower (0.63) than that indicated in the relationship, the literature shows the importance of this habitat for this species.

The structural habitat SIs for the 2023 large juvenile brown shrimp, large juvenile white shrimp, adult gulf menhaden, adult spotted seatrout, and largemouth bass HSI models are shown in Figures 9 to 11. As discussed in Section 2.0, the structural habitat SIs are the same as those used for the 2017 HSIs for these life stages/species.

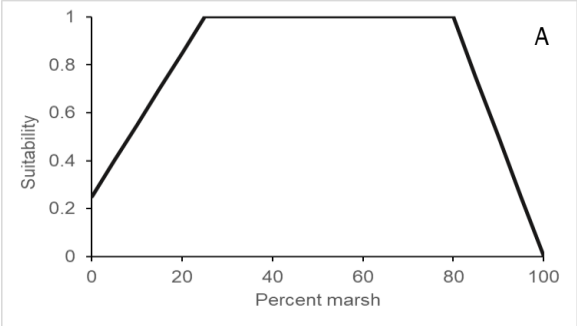

$SI_2 = (0.03*V_2) + 0.25$, when $V_2 < 25$
1.0, when $25 \leq V_2 \leq 80$
$5.0 - (0.05*V_2)$, when $V_2 > 80$

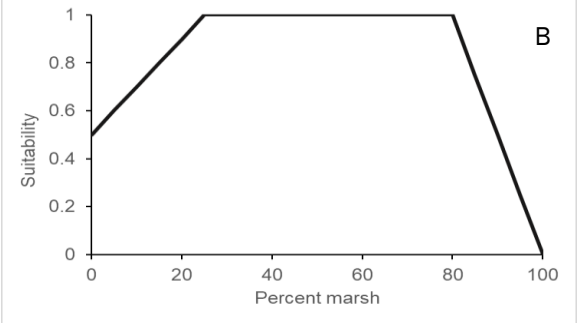

$SI_2 = (0.02*V_2) + 0.5$, when $V_2 < 25$
1.0, when $25 \leq V_2 \leq 80$
$5.0 - (0.05*V_2)$, when $V_2 > 80$

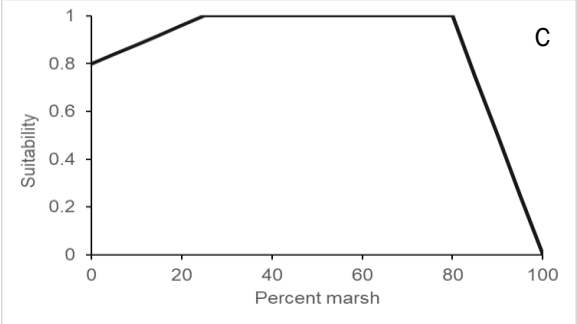

$SI_2 = (0.008*V_2) + 0.8$, when $V_2 < 25$
1.0, when $25 \leq V_2 \leq 80$
$5.0 - (0.05*V_2)$, when $V_2 > 80$

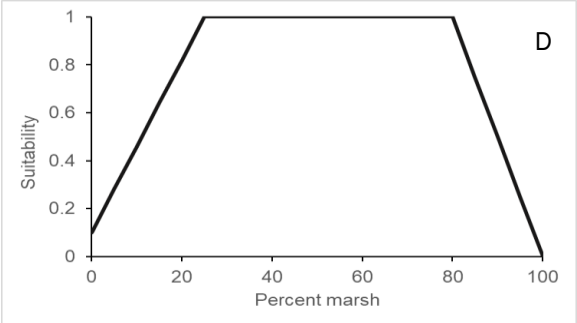

$SI_2 = (0.036*V_2) + 0.1$, when $V_2 < 25$
1.0, when $25 \leq V_2 \leq 80$
$5.0 - (0.05*V_2)$, when $V_2 > 80$

Figure 8. Graphic and numerical representations of the structural habitat SI relationships for A) small juvenile shrimp and juvenile blue crab baseline relationship, B) juvenile gulf menhaden baseline relationship, and shrimp and crab relationship for cells with high oyster HSI scores (≥0.5), C) shrimp, crab, and juvenile spotted seatrout relationship for cells with high SAV coverage (≥20%), and D) juvenile spotted seatrout baseline relationship.

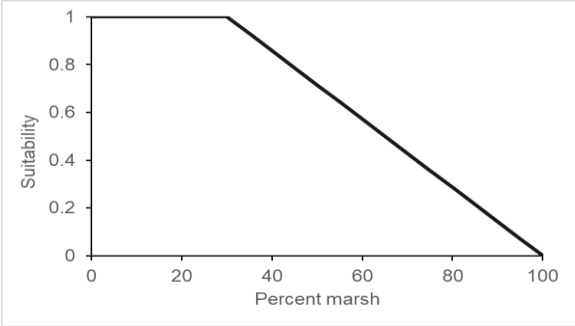

SI_2 = 1.0, when $V_2 \leq 30$
1.43 - (0.0143*V_2), when $V_2 > 30$

Figure 9. Graphic and numerical representation of the structural habitat SI relationship for larger juvenile brown shrimp, larger juvenile white shrimp, and adult gulf menhaden.

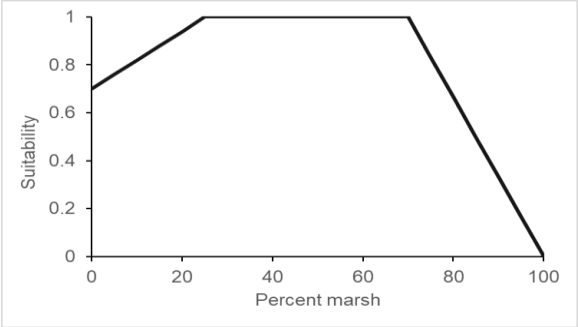

SI_2 = (0.012*V_2) + 0.7, when $V_2 < 25$
1.0, when $25 \leq V_2 \leq 70$
3.33 - (0.0333*V_2), when $V_2 > 70$

Figure 10. Graphic and numerical representation of the structural habitat SI relationship for adult spotted seatrout.

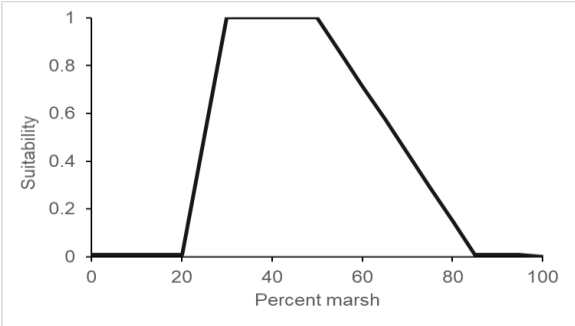

SI_2 = 0.01, when $V_2 < 20$
(0.099*V_2) - 1.997, when $20 \leq V_2 < 30$
1.0, when $30 \leq V_2 < 50$
(-0.0283*V_2) + 2.414, when $50 \leq V_2 < 85$
0.01, when $85 \leq V_2 < 100$
0.0, when V_2 = 100

Figure 11. Graphic and numerical representation of the structural habitat SI relationship for largemouth bass.

Table 1. Data table showing nekton catch (density or abundance) by habitat types from 36 studies (mostly from Louisiana and Texas), where MI = interior marsh (vegetated marsh >1-m from the marsh-water interface), ME = marsh edge (vegetated marsh ≤1-m from the marsh-water interface), SAV = submerged aquatic vegetation, SNVB = shallow non-vegetated bottom (0-m < distance offshore ≤5-m or undefined SNVB), DNVB = deep non-vegetated bottom (>5-m distance offshore), and Oyster = Oyster reef.

Citation	Location	Gear Type	Season/Month	Metric	Species	MI	ME	SAV	SNVB	DNVB	Oyster
Castellanos & Rozas, 2001	Atchafalaya Delta, LA,	Drop sampler	Spring 1995	Density (#/m2)	C. sapidus	0.4		0.6	0.2		
	Atchafalaya Delta, LA,	Drop sampler	Summer 1994	Density (#/m2)	C. sapidus	0.4		1			
	Atchafalaya Delta, LA,	Drop sampler	Fall 1994	Density (#/m2)	C. sapidus						
Cicchetti, 1998	Chesapeake Bay	Drop sampler	June 1995	Density (#/m2)	C. sapidus	0	0.4			0.8	
	Chesapeake Bay	Drop sampler	July 1995	Density (#/m2)	C. sapidus	0.1	0.2			0.1	
	Chesapeake Bay	Drop sampler	August 1995	Density (#/m2)	C. sapidus	0.1	0.7	8.6		0.3	
	Chesapeake Bay	Drop sampler	September 1995	Density (#/m2)	C. sapidus	1.4	11.4	15.5		6.5	
	Chesapeake Bay	Drop sampler	October 1995	Density (#/m2)	C. sapidus	2.0	5.4	21.4		3.2	
	Chesapeake Bay	Drop sampler	June 1995	Density (#/m2)	C. nebulosus		0				
	Chesapeake Bay	Drop sampler	July 1995	Density (#/m2)	C. nebulosus		0				
	Chesapeake Bay	Drop sampler	August 1995	Density (#/m2)	C. nebulosus		0.1	0			
	Chesapeake Bay	Drop sampler	September 1995	Density (#/m2)	C. nebulosus		0.1	0.1			
	Chesapeake Bay	Drop sampler	October 1995	Density (#/m2)	C. nebulosus		0	0			
	Chesapeake Bay	Drop sampler	August 1995	Density (#/m2)	F. aztecus			0.9		0	

Citation	Location	Gear Type	Season/Month	Metric	Species	MI	ME	SAV	SNVB	DNVB	Oyster
	Chesapeake Bay	Drop sampler	September 1995	Density (#/m2)	F. aztecus			0.5		0.3	
	Chesapeake Bay	Drop sampler	October 1995	Density (#/m2)	F. aztecus			1.3		0	
Gain, 2009	Corpus Christi Bay, TX	Throw trap	Spring 2008	Density (#/m2)	C. sapidus		2.2	7.1			2.1
	Corpus Christi Bay, TX	Throw trap	Fall 2008	Density (#/m2)	B. patronus		0	0.1			0
	Corpus Christi Bay, TX	Throw trap	Fall 2008	Density (#/m2)	C. sapidus		7.3	14.3			15.5
	Corpus Christi Bay, TX	Throw trap	Fall 2008	Density (#/m2)	L. setiferus		0.4	0.3			0.17
Glancy et al., 2003	Crystal River, FL	Drop sampler	July-August 1999	Abundance over 40 samples	C. sapidus		63	74			1
	Crystal River, FL	Drop sampler	March-April 2000	Abundance over 36 samples	C. sapidus		26	35			9
Howe & Wallace, 2000	Mobile Bay, AL	Drop sampler	July 1994-November 1995	Density (#/1.5 m2)	F. aztecus		33	120	14		
	Mobile Bay, AL	Drop sampler	July 1994-November 1995	Density (#/1.5 m2)	L. setiferus		49	35	16		
Howe et al., 1999	Mobile Bay, AL	Drop sampler	October 1989-December 1990	Density (#/m2)	F. aztecus		2.4		0.6		
	Mobile Bay, AL	Drop sampler	October 1989-December 1990	Density (#/m2)	L. setiferus		1.4		0.2		
Humphries et al., 2011b	Caillou Lake, LA	Drop sampler	2009	Density (#/m2)	C. sapidus					0.3	1.8
	Caillou Lake, LA	Drop sampler	2010	Density (#/m2)	C. sapidus					0	1.1
	Caillou Lake, LA	Drop sampler	2009	Density (#/m2)	F. aztecus					0	0.4
	Caillou Lake, LA	Drop sampler	2010	Density (#/m2)	F. aztecus					0.3	0.9

Citation	Location	Gear Type	Season/Month	Metric	Species	MI	ME	SAV	SNVB	DNVB	Oyster
	Caillou Lake, LA	Drop sampler	2009	Density (#/m2)	L. setiferus					0.8	4.3
	Caillou Lake, LA	Drop sampler	2010	Density (#/m2)	L. setiferus					0	0
Jerabek et al., 2017	Terrebonne, LA	Throw trap	May 2016	Density (#/m2)	F. aztecus		2.8	6.5		2.8	
Kanouse et al., 2006	Marsh Island, LA	Drop sampler	All Seasons 2001-2002	Abundance over 96 samples	B. patronus			22.5		10	
	Marsh Island, LA	Drop sampler	All Seasons 2001-2002	Abundance over 96 samples	L. setiferus			113		13	
	Marsh Island, LA	Drop sampler	All Seasons 2001-2002	Abundance over 96 samples	C. sapidus			16.5		6	
La Peyre & Gordon, 2012	Western LA	Throw trap	Summer 2007	Density (#/m2)	C. sapidus		0.8	6.2			
	Western LA	Throw trap	Summer 2007	Density (#/m2)	L. setiferus		2.6	0.8			
	Western LA	Throw trap	Summer 2007	Density (#/m2)	F. aztecus		0.7	0.8			
	Western LA	Throw trap	Fall 2007	Density (#/m2)	C. sapidus		3.2	10.2			
	Western LA	Throw trap	Fall 2007	Density (#/m2)	L. setiferus		10.9	8.5			
	Western LA	Throw trap	Fall 2007	Density (#/m2)	F. aztecus		1.3	0.8			
	Western LA	Throw trap	Summer 2008	Density (#/m2)	C. sapidus		0.9	2.2			
	Western LA	Throw trap	Summer 2008	Density (#/m2)	L. setiferus		0.1	0.8			
	Western LA	Throw trap	Summer 2008	Density (#/m2)	F. aztecus		4.7	1.3			

Citation	Location	Gear Type	Season/Month	Metric	Species	MI	ME	SAV	SNVB	DNVB	Oyster
La Peyre et al., 2013	Lake Eloi, LA	Seine	Winter, Spring, Summer 2012	CPUE	B. patronus					38	2
	Lake Fortuna, LA	Seine	Winter, Spring, Summer 2012	CPUE	B. patronus					0	0
	Grande Isle, LA	Seine	Spring, Summer 2011-2012	CPUE	B. patronus					7.9	88
	Lake Eloi, LA	Seine	Winter, Spring, Summer 2012	CPUE	F. aztecus					2	1.3
	Lake Fortuna, LA	Seine	Winter, Spring, Summer 2012	CPUE	F. aztecus					1.7	1
	Grande Isle, LA	Seine	Spring, Summer 2011-2012	CPUE	F. aztecus					5	7.7
	Lake Eloi, LA	Seine	Winter, Spring, Summer 2012	CPUE	L. setiferus					0	1
	Lake Fortuna, LA	Seine	Winter, Spring, Summer 2012	CPUE	L. setiferus					0	0
	Grande Isle, LA	Seine	Spring, Summer 2011-2012	CPUE	L. setiferus					0	13.3
	Lake Eloi, LA	Seine	Winter, Spring, Summer 2012	CPUE	C. sapidus					0	0
	Lake Fortuna, LA	Seine	Winter, Spring, Summer 2012	CPUE	C. sapidus					1	1
	Grande Isle, LA	Seine	Spring, Summer 2011-2012	CPUE	C. sapidus					1	1
Mace & Rozas, 2017	Sabine Lake, LA (intermediate salinity)	Throw trap	July 12, 2011	Density (#/m2)	L. setiferus				0.6	0	
	Sabine Lake, LA (intermediate salinity)	Throw trap	July 26, 2011	Density (#/m2)	L. setiferus				4.1	0	
	Sabine Lake, LA (intermediate salinity)	Throw trap	August 9, 2011	Density (#/m2)	L. setiferus				8.5	0	

Citation	Location	Gear Type	Season/Month	Metric	Species	MI	ME	SAV	SNVB	DNVB	Oyster
	Sabine Lake, LA (intermediate salinity)	Throw trap	September 7, 2011	Density (#/m2)	L. setiferus		61.8		12.8	0.2	
	Sabine Lake, LA (intermediate salinity)	Throw trap	September 20, 2011	Density (#/m2)	L. setiferus		16		9.9	0.6	
	Sabine Lake, LA (intermediate salinity)	Throw trap	October 4, 2011	Density (#/m2)	L. setiferus		46.8		25.9	0.6	
	Sabine Lake, LA (brackish)	Throw trap	July 12, 2011	Density (#/m2)	L. setiferus				5.8	2.4	
	Sabine Lake, LA (brackish)	Throw trap	July 26, 2011	Density (#/m2)	L. setiferus				9.1	3	
	Sabine Lake, LA (brackish)	Throw trap	August 9, 2011	Density (#/m2)	L. setiferus				18.8	2.2	
	Sabine Lake, LA (brackish)	Throw trap	September 7, 2011	Density (#/m2)	L. setiferus		74		30.7	1.8	
	Sabine Lake, LA (brackish)	Throw trap	September 20, 2011	Density (#/m2)	L. setiferus		64.8		29.7	1.6	
	Sabine Lake, LA (brackish)	Throw trap	October 4, 2011	Density (#/m2)	L. setiferus		31.4		17.3	9.4	
	Sabine Lake, LA (saline)	Throw trap	July 12, 2011	Density (#/m2)	L. setiferus				6.8	1.6	
	Sabine Lake, LA (saline)	Throw trap	July 26, 2011	Density (#/m2)	L. setiferus		63		16.6	4	
	Sabine Lake, LA (saline)	Throw trap	August 9, 2011	Density (#/m2)	L. setiferus				40.7	10	
	Sabine Lake, LA (saline)	Throw trap	September 7, 2011	Density (#/m2)	L. setiferus		60.4		35.6	10.4	
	Sabine Lake, LA (saline)	Throw trap	September 20, 2011	Density (#/m2)	L. setiferus		43		9.9	5.6	
	Sabine Lake, LA (saline)	Throw trap	October 4, 2011	Density (#/m2)	L. setiferus		174		25	22.8	

Citation	Location	Gear Type	Season/Month	Metric	Species	MI	ME	SAV	SNVB	DNVB	Oyster
Minello & Rozas, 2002	Galveston Bay, TX	Drop sampler	Spring 1995	Density (#/m2)	C. sapidus	0.9	2.6				
	Galveston Bay, TX	Drop sampler	Fall 1995	Density (#/m2)	C. sapidus	4.0	8.1				
	Galveston Bay, TX	Drop sampler	Spring 1995	Density (#/m2)	F. aztecus	0.3	3.5				
	Galveston Bay, TX	Drop sampler	Fall 1995	Density (#/m2)	F. aztecus	0.4	0.6				
	Galveston Bay, TX	Drop sampler	Spring 1995	Density (#/m2)	L. setiferus	0.1	0.5				
	Galveston Bay, TX	Drop sampler	Fall 1995	Density (#/m2)	L. setiferus	4.1	39.5				
Minello & Webb, 1997	Galveston Bay, TX	Drop sampler	Fall 1990	Density (#/2.6 m2)	C. nebulosus	0.2	0.3		0.1		
	Galveston Bay, TX	Drop sampler	Fall 1990	Density (#/2.6 m2)	B. patronus	0	0		0		
	Galveston Bay, TX	Drop sampler	Fall 1990	Density (#/2.6 m2)	C. sapidus	19.7	28.3		3.3		
	Galveston Bay, TX	Drop sampler	Fall 1990	Density (#/2.6 m2)	F. aztecus	4.6	17.6		4.1		
	Galveston Bay, TX	Drop sampler	Spring 1991	Density (#/2.6 m2)	B. patronus	0	0.3		359		
	Galveston Bay, TX	Drop sampler	Spring 1991	Density (#/2.6 m2)	F. aztecus	41	61.2		12.8		
	Galveston Bay, TX	Drop sampler	Spring 1991	Density (#/2.6 m2)	C. sapidus	11.3	6.8		0.4		
	Galveston Bay, TX	Drop sampler	Spring 1991	Density (#/2.6 m2)	L. setiferus	0	0.4		1.7		
Minello et al., 1991	West Galveston Bay, TX	Drop sampler	May 1990	Density (#/2.6 m2)	B. patronus	0	0		0	0.7	
	West Galveston Bay, TX	Drop sampler	May 1990	Density (#/2.6 m2)	C. sapidus	5.3	8.7		0	0.2	
	West Galveston Bay, TX	Drop sampler	May 1990	Density (#/2.6 m2)	F. aztecus	6	9.8		1.5	0.7	

Citation	Location	Gear Type	Season/Month	Metric	Species	MI	ME	SAV	SNVB	DNVB	Oyster
	West Galveston Bay, TX	Drop sampler	May 1990	Density (#/2.6 m2)	L. setiferus	0	1.4		0	0.2	
Minello et al., 2008	Galveston Bay, TX	Drop sampler	May 2000	Density (#/m2)	F. aztecus		14.3		2.5	1.0	
	Galveston Bay, TX	Drop sampler	May 2000	Density (#/m2)	C. sapidus		1.3		0.05	0.2	
	Galveston Bay, TX	Drop sampler	August 2000	Density (#/m2)	F. aztecus		3.8		0.6	0.1	
	Galveston Bay, TX	Drop sampler	August 2000	Density (#/m2)	L. setiferus		5.4		1.1	0	
	Galveston Bay, TX	Drop sampler	August 2000	Density (#/m2)	C. sapidus		1.9		0.8	0.1	
	Galveston Bay, TX	Drop sampler	November 2000	Density (#/m2)	F. aztecus		4.9		0.7	0.1	
	Galveston Bay, TX	Drop sampler	November 2000	Density (#/m2)	L. setiferus		1.7		0.4	0.1	
	Galveston Bay, TX	Drop sampler	November 2000	Density (#/m2)	C. sapidus		19.3		2.5	1.1	
Nevins et al., 2014	Sabine Lake, LA	Epibenthic sled	Fall 2011-Spring 2013	Density (#/m2)	C. nebulosus		0.2			0	0.03
	Sabine Lake, LA	Epibenthic sled	Fall 2011-Spring 2013	Density (#/m2)	B. patronus		0.1			0.1	0
Plunket & La Peyre, 2005	Barataria Bay, LA	Tray sampler	October2001-October 2002	Density (#/tray)	C. sapidus					1.4	2.1
	Barataria Bay, LA	Tray sampler	October2001-October 2002	Density (#/tray)	F. aztecus					0.1	0
Robillard et al., 2010	Lavaca Bay, TX	Epibenthic sled	Summer, Fall 2006 and Winter, Spring 2007	Density (#/m2)	B. patronus		0	0		0.5	0.04
	Lavaca Bay, TX	Epibenthic sled	Summer, Fall 2006 and Winter, Spring 2007	Density (#/m2)	C. nebulosus		0.01	0.03		0	0

Citation	Location	Gear Type	Season/Month	Metric	Species	MI	ME	SAV	SNVB	DNVB	Oyster
	Lavaca Bay, TX	Epibenthic sled	Summer, Fall 2006 and Winter, Spring 2007	Density (#/m2)	L. setiferus		1.0	0.3		0.01	0.02
	Lavaca Bay, TX	Epibenthic sled	Summer, Fall 2006 and Winter, Spring 2007	Density (#/m2)	C. sapidus		0.4	0.4		0.04	0.02
Rozas & Minello, 1998	Aransas Wildlife Refuge, TX	Drop sampler	September 1993	Density (#/m2)	C. nebulosus		0.5	0.5	0.1		
	Aransas Wildlife Refuge, TX	Drop sampler	September 1993	Density (#/m2)	F. aztecus		5	5.3	0.1		
	Aransas Wildlife Refuge, TX	Drop sampler	September 1993	Density (#/m2)	L. setiferus		4.2		0		
	Aransas Wildlife Refuge, TX	Drop sampler	September 1993	Density (#/m2)	C. sapidus		11.1	7.5	0.4		
	Aransas Wildlife Refuge, TX	Drop sampler	May 1994	Density (#/m2)	F. aztecus		4.5	11.3	0.7		
	Aransas Wildlife Refuge, TX	Drop sampler	May 1994	Density (#/m2)	C. sapidus		10.3	2.5	0.1		
Rozas & Minello, 2001	Calcasieu Lake, LA	Drop sampler	May 1999	Density (#/m2)	C. sapidus		7			0.5	
	Calcasieu Lake, LA	Drop sampler	May 1999	Density (#/m2)	B. patronus		0			4.4	
	Calcasieu Lake, LA	Drop sampler	May 1999	Density (#/m2)	L. setiferus		64.2			7.8	
	Calcasieu Lake, LA	Drop sampler	May 1999	Density (#/m2)	C. sapidus		14.6			2	
	Calcasieu Lake, LA	Drop sampler	May 1999	Density (#/m2)	F. aztecus		3.1			0.6	
Rozas & Minello, 2006	Barataria Bay, LA, oligohaline	Drop sampler	Fall 2003	Density (#/m2)	C. sapidus	3.6		7.7		0.8	
	Barataria Bay, LA, oligohaline	Drop sampler	Fall 2003	Density (#/m2)	L. setiferus	0.7		1.5		0.1	

Citation	Location	Gear Type	Season/Month	Metric	Species	MI	ME	SAV	SNVB	DNVB	Oyster
	Barataria Bay, LA, oligohaline	Drop sampler	Spring 2004	Density (#/m2)	C. sapidus	2.8		3.8		0.5	
	Barataria Bay, LA, oligohaline	Drop sampler	Spring 2004	Density (#/m2)	B. patronus	0		0.3		2.2	
Rozas & Minello, 2015	Barataria Bay, LA	Drop sampler	Spring 2002-2006	Density (#/m2)	F. aztecus	0.6	6.6		7.7	1.8	
	Barataria Bay, LA	Drop sampler	Spring 2002-2006	Density (#/m2)	C. sapidus	1.5	3.4		1	0.1	
	Barataria Bay, LA	Drop sampler	Spring 2002-2006	Density (#/m2)	B. patronus	0	0		1.6	0	
	Barataria Bay, LA	Drop sampler	Fall 2002-2006	Density (#/m2)	C. sapidus	10.8	11.2		10.3	3.9	
	Barataria Bay, LA	Drop sampler	Fall 2002-2006	Density (#/m2)	L. setiferus	0.9	10.8		3.5	0.9	
	Barataria Bay, LA	Drop sampler	Fall 2002-2006	Density (#/m2)	F. aztecus	0.5	3.2		1.5	0.4	
Rozas & Zimmerman, 2000	Galveston Bay, TX	Drop sampler	May 1993	Density (#/m2)	B. patronus	8.7				8.6	
	Galveston Bay, TX	Drop sampler	May 1993	Density (#/m2)	F. aztecus	3.2				1.5	
	Galveston Bay, TX	Drop sampler	May 1993	Density (#/m2)	C. sapidus	0.8				0.1	
	Galveston Bay, TX	Drop sampler	October 1993	Density (#/m2)	L. setiferus	5.3				1.3	
	Galveston Bay, TX	Drop sampler	October 1993	Density (#/m2)	C. sapidus	2.4				0.6	
	Galveston Bay, TX	Drop sampler	October 1993	Density (#/m2)	F. aztecus	0.7				0.3	
	Galveston Bay, TX	Drop sampler	April 1984	Density (#/m2)	B. patronus	3.0				26.9	
	Galveston Bay, TX	Drop sampler	April 1984	Density (#/m2)	F. aztecus	8.8				4.9	

Citation	Location	Gear Type	Season/Month	Metric	Species	MI	ME	SAV	SNVB	DNVB	Oyster
	Galveston Bay, TX	Drop sampler	April 1984	Density (#/m2)	C. sapidus	1.3				1	
	Galveston Bay, TX	Drop sampler	September 1994	Density (#/m2)	L. setiferus	13.1				0	
	Galveston Bay, TX	Drop sampler	September 1994	Density (#/m2)	C. sapidus	3.1				1	
	Galveston Bay, TX	Drop sampler	September 1994	Density (#/m2)	F. aztecus	1.4				0	
Rozas et al., 2007	Galveston Bay, TX	Drop sampler	1982-1992	Density (#/m2)	B. patronus	0.03			0.6		
	Galveston Bay, TX	Drop sampler	1982-1992	Density (#/m2)	C. nebulosus	0.3			0.04		
	Galveston Bay, TX	Drop sampler	1982-1992	Density (#/m2)	F. aztecus	10.7			2.6		
	Galveston Bay, TX	Drop sampler	1982-1992	Density (#/m2)	L. setiferus	5.8			1.7		
	Galveston Bay, TX	Drop sampler	1982-1992	Density (#/m2)	C. sapidus	6.1			1.3		
Rozas et al., 2012	St. Andrews Sound, FL	Drop sampler	May-June 2006	Density (#/m2)	C. sapidus	0.2	1.2	2.4		1.3	
	St. Andrews Sound, FL	Drop sampler	September 2006	Density (#/m2)	C. sapidus	4.6	2.6	2.3		0.4	
Shervette & Gelwick, 2008	Grand Bay, NERR, MS	Drop sampler	Fall 2003 and Spring and Summer 2004	Number	C. nebulosus		1			0	0
	Grand Bay, NERR, MS	Drop sampler	Fall 2003 and Spring and Summer 2004	Number	F. aztecus		53			9	47
	Grand Bay, NERR, MS	Drop sampler	Fall 2003 and Spring and Summer 2004	Number	L. setiferus		193			16	368
	Grand Bay, NERR, MS	Drop sampler	Fall 2003 and Spring and Summer 2004	Number	C. sapidus		82			14	59

Citation	Location	Gear Type	Season/Month	Metric	Species	MI	ME	SAV	SNVB	DNVB	Oyster
Stunz et al., 2010	Galveston Bay, TX	Drop sampler	All seasons 2001-2002	Density (#/m2)	B. patronus		0.3			0.04	0.01
	Galveston Bay, TX	Drop sampler	All seasons 2001-2002	Density (#/m2)	C. nebulosus		0.06			0.02	0.01
	Galveston Bay, TX	Drop sampler	All seasons 2001-2002	Density (#/m2)	C. sapidus		6.3			1.3	3.1
	Galveston Bay, TX	Drop sampler	All seasons 2001-2002	Density (#/m2)	F. aztecus		6.2			0.6	2.3
	Galveston Bay, TX	Drop sampler	All seasons 2001-2002	Density (#/m2)	L. setiferus		2.0			0.2	0.2
Tolley & Volety, 2005	Caloosahatchee Estuary, FL	Lift Net	July-September 2001 and March-May 2002		C. sapidus					0	0.1
Wilson et al., 1990	Great Bay, NJ	Suction sampler	July 1986	Density (#/m2)	C. sapidus			0	0.2		
	Great Bay, NJ	Suction sampler	August 1986	Density (#/m2)	C. sapidus			0.4	0		
	Great Bay, NJ	Suction sampler	September 1986	Density (#/m2)	C. sapidus			0.4	1.2		
	Great Bay, NJ	Suction sampler	October 1986	Density (#/m2)	C. sapidus			0.3	0.7		
	Great Bay, NJ	Suction sampler	November 1986	Density (#/m2)	C. sapidus			1.5	1.5		
	Great Bay, NJ	Suction sampler	March 1987	Density (#/m2)	C. sapidus			0.9	0		
	Great Bay, NJ	Suction sampler	May 1987	Density (#/m2)	C. sapidus			0.9	0.6		
	Great Bay, NJ	Suction sampler	June 1987	Density (#/m2)	C. sapidus			0.6	1.5		
	Great Bay, NJ	Suction sampler	August 1987	Density (#/m2)	C. sapidus			0.3	0		
	Great Bay, NJ	Suction sampler	September 1987	Density (#/m2)	C. sapidus			2.1	1.0		

Citation	Location	Gear Type	Season/Month	Metric	Species	MI	ME	SAV	SNVB	DNVB	Oyster
	Great Bay, NJ	Suction sampler	October 1987	Density (#/m2)	C. sapidus			0.5	0.9		
	Great Bay, NJ	Suction sampler	November 1987	Density (#/m2)	C. sapidus			0.3	0.6		
	Great Bay, NJ	Suction sampler	March 1988	Density (#/m2)	C. sapidus			0.3	0		
Zimmerman & Minello, 1984	Galveston Island, TX	Drop sampler	March 1982	Density (#/m2)	F. aztecus	13.3			0.8		
	Galveston Island, TX	Drop sampler	April 1982	Density (#/m2)	F. aztecus	21.1			2.8		
	Galveston Island, TX	Drop sampler	May 1982	Density (#/m2)	F. aztecus	10.6			1		
	Galveston Island, TX	Drop sampler	June 1982	Density (#/m2)	F. aztecus	6.8			0.2		
	Galveston Island, TX	Drop sampler	July 1982	Density (#/m2)	F. aztecus	15			1.6		
	Galveston Island, TX	Drop sampler	August 1982	Density (#/m2)	F. aztecus	14.4			5		
	Galveston Island, TX	Drop sampler	October 1982	Density (#/m2)	F. aztecus	9.9			0.1		
	Galveston Island, TX	Drop sampler	November 1982	Density (#/m2)	F. aztecus	9.6			0.4		
	Galveston Island, TX	Drop sampler	December 1982	Density (#/m2)	F. aztecus	2.3			1.3		
	Galveston Island, TX	Drop sampler	February 1983	Density (#/m2)	F. aztecus	0.1			0.5		
	Galveston Island, TX	Drop sampler	March 1983	Density (#/m2)	F. aztecus	0.1			0.5		
	Galveston Island, TX	Drop sampler	March 1982	Density (#/m2)	L. setiferus	0			0		
	Galveston Island, TX	Drop sampler	April 1982	Density (#/m2)	L. setiferus	0			0		
	Galveston Island, TX	Drop sampler	May 1982	Density (#/m2)	L. setiferus	0.2			0		

Citation	Location	Gear Type	Season/Month	Metric	Species	MI	ME	SAV	SNVB	DNVB	Oyster
	Galveston Island, TX	Drop sampler	June 1982	Density (#/m2)	L. setiferus	0.6			0.1		
	Galveston Island, TX	Drop sampler	July 1982	Density (#/m2)	L. setiferus	2			0.2		
	Galveston Island, TX	Drop sampler	August 1982	Density (#/m2)	L. setiferus	36.3			12.1		
	Galveston Island, TX	Drop sampler	October 1982	Density (#/m2)	L. setiferus	6.8			7.8		
	Galveston Island, TX	Drop sampler	November 1982	Density (#/m2)	L. setiferus	14.3			5.2		
	Galveston Island, TX	Drop sampler	December 1982	Density (#/m2)	L. setiferus	3.3			2.1		
	Galveston Island, TX	Drop sampler	February 1983	Density (#/m2)	L. setiferus	0			0		
	Galveston Island, TX	Drop sampler	March 1983	Density (#/m2)	L. setiferus	0			0		
	Galveston Island, TX	Drop sampler	March 1982	Density (#/m2)	C. sapidus	4.1			0.3		
	Galveston Island, TX	Drop sampler	April 1982	Density (#/m2)	C. sapidus	3.5			0.3		
	Galveston Island, TX	Drop sampler	May 1982	Density (#/m2)	C. sapidus	2.6			0.1		
	Galveston Island, TX	Drop sampler	June 1982	Density (#/m2)	C. sapidus	2.9			0.2		
	Galveston Island, TX	Drop sampler	July 1982	Density (#/m2)	C. sapidus	3.9			0.4		
	Galveston Island, TX	Drop sampler	August 1982	Density (#/m2)	C. sapidus	2.8			0.8		
	Galveston Island, TX	Drop sampler	October 1982	Density (#/m2)	C. sapidus	15			1.9		
	Galveston Island, TX	Drop sampler	November 1982	Density (#/m2)	C. sapidus	22.3			2.4		
	Galveston Island, TX	Drop sampler	December 1982	Density (#/m2)	C. sapidus	8.2			3.5		

Citation	Location	Gear Type	Season/Month	Metric	Species	MI	ME	SAV	SNVB	DNVB	Oyster
	Galveston Island, TX	Drop sampler	February 1983	Density (#/m2)	C. sapidus	5.1			1.9		
	Galveston Island, TX	Drop sampler	March 1983	Density (#/m2)	C. sapidus	7.3			1.8		
Zimmerman et al., 1984	Galveston Bay, TX	Drop sampler	March 1982, Overall	Density (#/m2)	F. aztecus		12.6		2.8		
	Galveston Bay, TX	Drop sampler	April 1982, Overall	Density (#/m2)	F. aztecus		21.1		2.8		
	Galveston Bay, TX	Drop sampler	May 1982, Overall	Density (#/m2)	F. aztecus		8.3		0.9		
	Galveston Bay, TX	Drop sampler	May 1982, Overall	Density (#/m2)	F. aztecus		10.8		1		
	Galveston Bay, TX	Drop sampler	June 1982, Overall	Density (#/m2)	F. aztecus		6.8		0.2		
	Galveston Bay, TX	Drop sampler	July 1982, Overall	Density (#/m2)	F. aztecus		15		1.6		
Zimmerman et al., 1989	West Bay, TX	Drop sampler	December 1988	Density (#/2.6 m2)	C. nebulosus		0.1		0		0
	West Bay, TX	Drop sampler	December 1988	Density (#/2.6 m2)	F. aztecus		3.8		7.4		0.4
	West Bay, TX	Drop sampler	December 1988	Density (#/2.6 m2)	C. sapidus		1.4		5.3		0
	West Bay, TX	Drop sampler	December 1988	Density (#/2.6 m2)	L. setiferus		0.1		0.5		0
	West Bay, TX	Drop sampler	July 1989	Density (#/2.6 m2)	C. nebulosus		2		0.4		0
	West Bay, TX	Drop sampler	July 1989	Density (#/2.6 m2)	B. patronus		0		0.3		0.3
	West Bay, TX	Drop sampler	July 1989	Density (#/2.6 m2)	F. aztecus		25		2.8		0
	West Bay, TX	Drop sampler	July 1989	Density (#/2.6 m2)	C. sapidus		21.5		1.1		0.8
	West Bay, TX	Drop sampler	July 1989	Density (#/2.6 m2)	L. setiferus		11		0.9		0

Citation	Location	Gear Type	Season/Month	Metric	Species	MI	ME	SAV	SNVB	DNVB	Oyster
Zimmerman et al., 1990a	Lavaca Bay, TX	Drop sampler	Fall 1985, Spartina	Density (#/2.6 m2)	C. nebulosus		0.8		0		
	Lavaca Bay, TX	Drop sampler	Fall 1985, Spartina	Density (#/2.6 m2)	C. sapidus		28.5		1.3		
	Lavaca Bay, TX	Drop sampler	Fall 1985, Spartina	Density (#/2.6 m2)	L. setiferus		12.7		2.6		
	Lavaca Bay, TX	Drop sampler	Fall 1985, Spartina	Density (#/2.6 m2)	F. aztecus		10.5		0.4		
	Lavaca Bay, TX	Drop sampler	Fall 1985, Juncus	Density (#/2.6 m2)	C. nebulosus		0.4		0.1		
	Lavaca Bay, TX	Drop sampler	Fall 1985, Juncus	Density (#/2.6 m2)	C. sapidus		41.9		0.9		
	Lavaca Bay, TX	Drop sampler	Fall 1985, Juncus	Density (#/2.6 m2)	F. aztecus		17.4		1.4		
	Lavaca Bay, TX	Drop sampler	Fall 1985, Juncus	Density (#/2.6 m2)	L. setiferus		9.5		1.1		
	Lavaca Bay, TX	Drop sampler	Spring 1986, Spartina	Density (#/2.6 m2)	B. patronus		0		15.3		
	Lavaca Bay, TX	Drop sampler	Spring 1986, Spartina	Density (#/2.6 m2)	C. nebulosus		0.1		0		
	Lavaca Bay, TX	Drop sampler	Spring 1986, Spartina	Density (#/2.6 m2)	F. aztecus		60.9		14.9		
	Lavaca Bay, TX	Drop sampler	Spring 1986, Spartina	Density (#/2.6 m2)	L. setiferus		13.4		2.0		
	Lavaca Bay, TX	Drop sampler	Spring 1986, Spartina	Density (#/2.6 m2)	C. sapidus		5.8		1.4		
	Lavaca Bay, TX	Drop sampler	Spring 1986, Juncus	Density (#/2.6 m2)	B. patronus		0		15.6		
	Lavaca Bay, TX	Drop sampler	Spring 1986, Juncus	Density (#/2.6 m2)	F. aztecus		36.1		6.8		
	Lavaca Bay, TX	Drop sampler	Spring 1986, Juncus	Density (#/2.6 m2)	L. setiferus		17.0		3.8		
	Lavaca Bay, TX	Drop sampler	Spring 1986, Juncus	Density (#/2.6 m2)	C. sapidus		4.4		0.7		

Citation	Location	Gear Type	Season/Month	Metric	Species	MI	ME	SAV	SNVB	DNVB	Oyster
Zimmerman et al., 1990b	Galveston Bay, TX	Drop sampler	Spring 1987, Upper bay average	Density (#/2.6 m2)	B. patronus		0		0.2		
	Galveston Bay, TX	Drop sampler	Spring 1987, Upper bay average	Density (#/2.6 m2)	C. sapidus		1.3		1.3		
	Galveston Bay, TX	Drop sampler	Spring, Middle bay average	Density (#/2.6 m2)	F. aztecus		5.8		0.8		
	Galveston Bay, TX	Drop sampler	Spring, Middle bay average	Density (#/2.6 m2)	C. sapidus		8.1		1.7		
	Galveston Bay, TX	Drop sampler	Spring 1987, Lower bay average	Density (#/2.6 m2)	B. patronus		0		2.9		
	Galveston Bay, TX	Drop sampler	Spring 1987, Lower bay average	Density (#/2.6 m2)	F. aztecus		40.4		0.9		
	Galveston Bay, TX	Drop sampler	Spring 1987, Lower bay average	Density (#/2.6 m2)	C. sapidus		7.5		0.9		
	Galveston Bay, TX	Drop sampler	Summer 1987, Upper bay average	Density (#/2.6 m2)	B. patronus		0.3		0		
	Galveston Bay, TX	Drop sampler	Summer 1987, Upper bay average	Density (#/2.6 m2)	C. sapidus		3.2		0.7		
	Galveston Bay, TX	Drop sampler	Summer 1987, Upper bay average	Density (#/2.6 m2)	L. setiferus		0.7		0		
	Galveston Bay, TX	Drop sampler	Summer 1987, Upper bay average	Density (#/2.6 m2)	F. aztecus		2.5		0		
	Galveston Bay, TX	Drop sampler	Summer 1987, Upper bay average	Density (#/2.6 m2)	B. patronus		0		1.2		

Citation	Location	Gear Type	Season/Month	Metric	Species	MI	ME	SAV	SNVB	DNVB	Oyster
	Galveston Bay, TX	Drop sampler	Summer 1987, Upper bay average	Density (#/2.6 m2)	L. setiferus		4.2		2.8		
	Galveston Bay, TX	Drop sampler	Summer 1987, Upper bay average	Density (#/2.6 m2)	F. aztecus		18.1		4.2		
	Galveston Bay, TX	Drop sampler	Summer 1987, Upper bay average	Density (#/2.6 m2)	C. sapidus		8.6		1.6		
	Galveston Bay, TX	Drop sampler	Summer 1987, Upper bay average	Density (#/2.6 m2)	C. nebulosus		0.5		0.3		
	Galveston Bay, TX	Drop sampler	Summer 1987, Upper bay average	Density (#/2.6 m2)	F. aztecus		23.4		4.6		
	Galveston Bay, TX	Drop sampler	Summer 1987, Upper bay average	Density (#/2.6 m2)	C. sapidus		1.1		15.3		
	Galveston Bay, TX	Drop sampler	Summer 1987, Upper bay average	Density (#/2.6 m2)	L. setiferus		2		2.9		
	Galveston Bay, TX	Drop sampler	Fall 1987, Upper bay average	Density (#/2.6 m2)	C. nebulosus		0		0.3		
	Galveston Bay, TX	Drop sampler	Fall 1987, Upper bay average	Density (#/2.6 m2)	C. sapidus		4.1		7.3		
	Galveston Bay, TX	Drop sampler	Fall 1987, Upper bay average	Density (#/2.6 m2)	F. aztecus		0.4		0.7		
	Galveston Bay, TX	Drop sampler	Fall 1987, Upper bay average	Density (#/2.6 m2)	L. setiferus		0		0.4		
	Galveston Bay,	Drop sampler	Fall 1987,	Density	C.		0.9		0		

Citation	Location	Gear Type	Season/Month	Metric	Species	MI	ME	SAV	SNVB	DNVB	Oyster
	TX		Middle bay average	(#/2.6 m2)	nebulosus						
	Galveston Bay, TX	Drop sampler	Fall 1987, Middle bay average	Density (#/2.6 m2)	C. sapidus		163		16.2		
	Galveston Bay, TX	Drop sampler	Fall 1987, Middle bay average	Density (#/2.6 m2)	F. aztecus		7.1		2.8		
	Galveston Bay, TX	Drop sampler	Fall 1987, Middle bay average	Density (#/2.6 m2)	L. setiferus		0.4		4.4		
	Galveston Bay, TX	Drop sampler	Fall 1987, Lower bay average	Density (#/2.6 m2)	C. nebulosus		0.7		0		
	Galveston Bay, TX	Drop sampler	Fall 1987, Lower bay average	Density (#/2.6 m2)	C. sapidus		22.4		2.6		
	Galveston Bay, TX	Drop sampler	Fall 1987, Lower bay average	Density (#/2.6 m2)	L. setiferus		5.5		0.5		
	Galveston Bay, TX	Drop sampler	Fall 1987, Lower bay average	Density (#/2.6 m2)	F. aztecus		14.1		0.5		

4.0 REFERENCES

Callihan, J. L. (2011). Spatial ecology of adult spotted seatrout, Cynoscion nebulosus, in Louisiana coastal waters. PhD Dissertation. Louisiana State University, Baton Rouge, Louisiana.

Castellanos, D. L. & Rozas, L. P. (2001). Nekton use of submerged aquatic vegetation, marsh, and shallow unvegetated bottom in the Atchafalaya River Delta, a Louisiana tidal freshwater ecosystem. Estuaries, 24, 184-197.

Cicchetti, G. (1998). Habitat use, secondary production, and trophic export by salt marsh nekton in shallow waters. PhD Dissertation. College of William and Mary, Williamsburg, Virginia.

Deegan, L. A., Peterson, B. J., & Portier, R. (1990). Stable isotopes and cellulase activity as evidence for detritus as a food source for juvenile Gulf menhaden. Estuaries, 13, 14-19.

Gain, I. (2009). Oyster reefs as nekton habitat in estuarine ecosystems. PhD Dissertation. Texas A & M University, Corpus Christi, Texas.

Glancy, T. P., Frazer, T. K., Cichra, C. E., & Lindberg, W. J. (2003). Comparative patterns of occupancy by decapod crustaceans in seagrass, oyster, and marsh-edge habitats in a northeast Gulf of Mexico estuary. Estuaries, 26, 1291-1301.

Grabowski, J. H., Hughes, A. R., & Kimbro, D. L. (2008). Habitat complexity influences cascading effects of multiple predators. Ecology, 89, 3413-3422.

Gulf States Marine Fisheries Commission. (2001). The spotted seatrout fishery of the Gulf of Mexico, United States: a regional management plan. Gulf States Marine Fisheries Commission, Ocean Springs, Mississippi.

Gulf States Marine Fisheries Commission. (2015). Gulf menhaden fishery of the Gulf of Mexico: a regional management plan. Gulf States Marine Fisheries Commission, Ocean Springs, Mississippi.

Harding, J. M. & Mann, R. (1999). Fish species richness in relation to restored oyster reefs, Piankatank River, Virginia. Bulletin of Marine Science, 65, 289-300.

Hollweg, T. A., Christman, M. C., Cebrian, J., Wallace, B. P., Friedman, S. L., Ballestero, H. R., Huisenga, M. T., & Benson, K. G. (2019). Meta-analysis of nekton utilization of coastal habitats in the Northern Gulf of Mexico. Estuaries and Coasts. Special Section: Restoration Benefits in the

Gulf of Mexico.

Howe, J. C. & Wallace, R. K. (2000). Relative abundance of postlarval and juvenile penaeid shrimps in submerged aquatic vegetation and emergent marsh habitats. Gulf of Mexico Science, 18, 130-137

Howe, J. C., Wallace, R. K., & Rikard, F. S. (1999). Habitat utilization by postlarval and juvenile penaeid shrimps in Mobile Bay, Alabama. Estuaries, 22, 971-979.

Humphries, A. T. & La Peyre, M. K. (2015). Oyster reef restoration supports increased nekton biomass and potential commercial fishery value. PeerJ, 3, e1111, DOI 10.7717/peerj.1111

Humphries, A. T., La Peyre, M. K., & Decossas, G. A. (2011a). The effect of structural complexity, prey density, and "predator-free space" on prey survivorship at created oyster reef mesocosms. PLoS ONE 6(12), e28339, DOI 10.1371/journal.pone.0028339.

Humphries, A.T., La Peyre, M. K., Kimball, M. E., & Rozas, L. P. (2011b). Testing the effect of habitat structure and complexity on nekton assemblages using experimental oyster reefs. Journal of Experimental Marine Biology and Ecology, 409, 172-179.

Jerabek, A., Darnell, K. M., Pellerin, C., & Carruthers, T. J. (2017). Use of marsh edge and submerged aquatic vegetation as habitat by fish and crustaceans in degrading southern Louisiana coastal marshes. Southeastern Geographer, 57, 212-230.

Kanouse, S., La Peyre, M. K., & Nyman, J. A. (2006). Nekton use of *Ruppia maritima* and non-vegetated bottom habitat types within brackish marsh ponds. Marine Ecology Progress Series, 327, 61-69.

La Peyre, M. K., Aguilar Marshall, D., Miller, L. S., & Humphries, A. T. (2019). Oyster reefs in Northern Gulf of Mexico estuaries harbor diverse fish and decapod crustacean assemblages: a meta-synthesis. Frontiers in Marine Science, 6, 666, doi: 10.3389/fmars.2019.00666.

La Peyre, M.K. & Gordon, J. (2012). Nekton density patterns and hurricane recovery in submerged aquatic vegetation, and along non-vegetated natural and created edge habitats. Estuarine, Coastal and Shelf Science, 98, 108-118.

La Peyre, M. K., Schwarting, L., & Miller, S. (2013). Preliminary assessment of bioengineered fringing shoreline reefs in Grand Isle and Breton Sound, Louisiana. US Department of the Interior, US Geological Survey.

Mace III, M. M. & Rozas, L. P. (2017). Population dynamics and secondary production of juvenile white shrimp (*Litopenaeus setiferus*) along an estuarine salinity gradient. Fishery Bulletin, 115, 74-88.

MacRae, P. S. D. (2006). A community approach to identifying essential fish habitat of spotted seatrout, *Cynoscion nebulosus*, in Barataria Bay, LA. PhD Dissertation. Louisiana State University, Baton Rouge, Louisiana.

Minello, T. J. (1999). Nekton densities in shallow estuarine habitats of Texas and Louisiana and the identification of essential fish habitat. American Fisheries Society Symposium, 22, 43-75.

Minello, T. J. (2017). Fishery habitat in estuaries of the Gulf of Mexico: reflections on geographical variability in salt marsh value and function. Gulf and Caribbean Research, 28, ii-xi.

Minello, T. J., Able, K. W., Weinstein, M. P., & Hays, C. G. (2003). Salt marshes as nurseries for nekton: testing hypotheses on density, growth and survival through meta-analysis. Marine Ecology Progress Series, 246, 39-59.

Minello, T. J., Matthews, G. A., Caldwell, P. A., & Rozas, L. P. (2008). Population and production estimates for decapod crustaceans in wetlands of Galveston Bay, Texas. Transactions of the American Fisheries Society, 137, 129-146.

Minello, T. J. & Rozas, L. P. (2002). Nekton in gulf coast wetlands: fine-scale distributions, landscape patterns, and restoration implications. Ecological Applications, 12, 441-455.

Minello, T. J. & Webb, Jr., J. W. (1997). Use of natural and created *Spartina alterniflora* salt marshes by fishery species and other aquatic fauna in Galveston Bay, Texas, USA. Marine Ecology Progress Series, 151, 165-179.

Minello, T. J., Webb, J. W., Zimmerman, R. J., Wooten, R. B., Martinez, J. L., Baumer, T. J., & Pattillo. M. C. (1991). Habitat availability and utilization by benthos and nekton in Hall's Lake and West Galveston Bay. National Oceanic and Atmospheric Administration Technical Memorandum, NMFS-SEFC-275. National Oceanic and Atmospheric Administration, Washington, DC.

Moulton, D. L., Dance, M. A., Williams, J. A., Sluis, M. Z, Stunz, G. W., & Rooker, J. R. (2017). Habitat partitioning and seasonal movement of red drum and spotted seatrout. Estuaries and Coasts, 40, 905-916.

Nevins, J. A., Pollack, J. B., & Stunz, G. W. (2014). Characterizing nekton use of the largest unfished oyster reef in the United States compared with adjacent estuarine habitats. Journal of Shellfish Research, 33, 227-238.

Perret, W. S., Weaver, J. E., Williams, R. O., Johansen, P. L., McIlwain, T. D., Raulerson, R. C., & Tatum, W. M. (1980). Fishery profiles of red drum and spotted seatrout. Gulf States Marine Fisheries Commission Report 6.

Plunket, J. & La Peyre, M. K. (2005). Oyster beds as fish and macroinvertebrate habitat in Barataria Bay, Louisiana. Bulletin of Marine Science, 77, 155-164.

Robillard, M. M. R., Stunz, G. W., & Simons, J. (2010). Relative value of deep subtidal oyster reefs to other estuarine habitat types using a novel sampling method. Journal of Shellfish Research, 29, 291-302.

Rozas, L. P. & Minello, T. J. (1998). Nekton use of salt marsh, seagrass, and nonvegetated habitats in a south Texas (USA) estuary. Bulletin of Marine Science, 63, 481-501.

Rozas, L. P. & Minello, T. J. (2001). Marsh terracing as a wetland restoration tool for creating fishery habitat. Wetlands, 21, 327-341.

Rozas, L.P. & Minello, T. J. (2006). Nekton use of *Vallisneria americana* Michx.(wild celery) beds and adjacent habitats in coastal Louisiana. Estuaries and Coasts, 29, 297–310.

Rozas, L. P. & Minello, T. J. (2015). Small-scale nekton density and growth patterns across a saltmarsh landscape in Barataria Bay, Louisiana. Estuaries and Coasts, 38, 2000-2018.

Rozas, L. P., Minello, T. J., & Dantin, D. D. (2012). Use of shallow lagoon habitats by nekton of the northeastern Gulf of Mexico. Estuaries and Coasts, 35, 572-586.

Rozas, L. P. & Zimmerman, R. J. (2000). Small-scale patterns of nekton use among marsh and adjacent shallow nonvegetated areas of the Galveston Bay Estuary, Texas (USA). Marine Ecology Progress Series, 193, 217-239.

Rozas, L. P., Minello, T. J., Zimmerman, R. J., & Caldwell, P. (2007). Nekton populations, long-term wetland loss, and the effect of recent habitat restoration in Galveston Bay, Texas, USA. Marine Ecology Progress Series, 344, 119-130.

Sable, S. E., Lindquist, D. C., D'Acunto, L., Hijuelos, A.C., La Peyre, M. K., O'Connell, A. M., & Robinson, E. M. (2019). 2023 Coastal Master Plan Habitat Suitability Index Model Improvement Recommendations. Coastal Protection and Restoration Authority, Baton Rouge, Louisiana.

Shervette, V. R. & Gelwick, F. (2008). Seasonal and spatial variations in fish and macroinvertebrate communities of oyster and adjacent habitats in a Mississippi estuary. Estuaries and Coasts, 31, 584-596.

Stunz, G. W., Minello, T. J., & Rozas, L. P. (2010). Relative value of oyster reef as habitat for estuarine nekton in Galveston Bay, Texas. Marine Ecology Progress Series, 406, 147-159.

Tolley, S. G. & Volety, A. K. (2005). The role of oysters in habitat use of oyster reefs by resident fishes and decapod crustaceans. Journal of Shellfish Research, 24, 1007-1012.

Wilson, K. A., Able, K. W., & Heck, Jr., K. L. (1990). Habitat use by juvenile blue crabs: a comparison among habitats in southern New Jersey. Bulletin of Marine Science, 46, 105-114.

Zimmerman, R. J. & Minello, T. J. (1984). Densities of *Penaeus aztecus*, *Penaeus setiferus*, and other natant macrofauna in a Texas salt marsh. Estuaries, 7, 421-433.

Zimmerman, R. J., Minello, T. J., Baumer, T. J., & Castiglione, M. C. (1989). Oyster reef as habitat for estuarine macrofauna. et al. (1989). Oyster reef as habitat for estuarine macrofauna. National Oceanic and Atmospheric Administration Technical Memorandum, NMFS-SEFC-249. National Oceanic and Atmospheric Administration, Washington, DC.

Zimmerman, R. J., Minello, T. J., Castiglione, M. C., & Smith, D. L. (1990a). The use of Juncus and Spartina marshes by fisheries species in Lavaca Bay, Texas, with reference to effects of floods. National Oceanic and Atmospheric Administration Technical Memorandum, NMFS-SEFC-251. National Oceanic and Atmospheric Administration, Washington, DC.

Zimmerman, R. J., Minello, T. J., Castiglione, M. C., & Smith, D. L. (1990b). Utilization of marsh and associated habitats along a salinity gradient in Galveston Bay. National Oceanic and Atmospheric Administration Technical Memorandum, NMFS-SEFC-250. National Oceanic and Atmospheric Administration, Washington, DC.

Zimmerman, R. J., Minello, T. J., & Zamora, G. (1984). Selection of vegetated habitat by brown shrimp, *Penaeus aztecus*, in a Galveston Bay salt marsh. Fishery Bulletin, 82, 325-336.